

Numerical and Analytical Investigation into the Plastic Buckling Paradox for Metal Cylinders

A thesis submitted for the degree of Doctor of Philosophy

By

Rabee Shamass

School of Engineering, Design and Physical Sciences

Brunel University London

March 2016

Declaration

This thesis entitled “Numerical and Analytical Investigation into the Plastic Buckling Paradox of Metal Cylinder”, is submitted to the Department of Mechanical, Aerospace and Civil Engineering, School of Engineering, Design and Physical Sciences, Brunel University of London, Kingston Lane, Uxbridge, UB8 3PH, UK, for the degree of Doctor of Philosophy. The research has not formed the basis of a submission for any other degree.

Publications based on this thesis:

Conference papers

Shamass, R., Alfano, G. and Guarracino, F. (2013) ‘A numerical investigation into the plastic buckling of circular cylinders’. *Shell Structures: Theory and Application*, 3, pp.441-444.

Journal articles

Shamass, R., Alfano, G. and Guarracino, F. (2014) ‘A numerical investigation into the plastic buckling paradox for circular cylindrical shells under axial compression’ *Engineering Structures*, 75, 429-447.

Shamass, R., Alfano, G. and Guarracino, F. (2015) ‘An analytical insight into the buckling paradox for circular cylindrical shells under axial and lateral loading’, *Mathematical problems in engineering*, ID 514267:1-11.

Shamass, R., Alfano, G. and Guarracino, F. (2015) ‘An investigation into the plastic buckling paradox for circular cylindrical shells under non-proportional loading’, *Thin-Walled Structures*, 95, 347-362.

Shamass, R. Alfano, G. and Guarracino, F. (2016) ‘On the Elastoplastic Buckling Analysis of Cylinders under Non-proportional Loading via the Differential Quadrature Method’, *International journal of Structural Stability and Dynamics*, (online ready).

Book Chapter

Shamass, R., Alfano, G. and Guarracino, F. (2016). Investigation on the plastic buckling paradox for metal cylinders. In: B.G. Falzon et al., ed., *Buckling and Postbuckling Structures II: Experimental, Analytical and Numerical Studies*. Imperial College Press/World Scientific, Accepted.

Rabee Shamass

Date

Abstract

It is widely accepted that, for many buckling problems of plates and shells in the plastic range, the flow theory of plasticity either fails to predict buckling or significantly overestimates buckling stresses and strains, while the deformation theory, which fails to capture important aspects of the underlying physics of plastic deformation, provides results that are more in line with experimental findings and is therefore generally recommended for use in practical applications. This thesis aims to contribute further understanding of the reasons behind the seeming differences between the predictions provided by these two theories, and therefore provide some explanation of this so-called 'plastic buckling paradox'.

The study focuses on circular cylindrical shells subjected to either axial compression or non-proportional loading, the latter consisting of combined axial tensile stress and increasing external pressure. In these two cases, geometrically nonlinear finite-element (FE) analyses for perfect and imperfect cylinders are conducted using both the flow and the deformation theories of plasticity, and the numerical results are compared with data from widely cited physical tests and with analytical results. The plastic buckling pressures for cylinders subjected to non-proportional loading, with various combinations of boundary conditions, tensile stresses, material properties and cylinder's geometries, are also obtained with the help of the differential quadrature method (DQM). These results are compared with those obtained using the code BOSOR5 and with nonlinear FE results obtained using both the flow and deformation theories of plasticity.

It is found that, contrary to common belief, by using a geometrically nonlinear FE formulation with carefully determined and validated constitutive laws, very good agreement between numerical and test results can be obtained in the case of the physically more sound flow theory of plasticity. The reason for the 'plastic buckling paradox' appears to be the over-constrained kinematics assumed in many analytical and numerical treatments, such as BOSOR5 and NAPAS, whereby a harmonic buckling shape in the circumferential direction is prescribed.

Acknowledgment

I am very grateful to Dr. Giulio Alfano, my supervisor from Brunel University London, and to Dr. Federico Guarracino, my supervisor from University of Naples in Italy, for their continued encouragement and their helpful guidance in doing this research. Their patience, understanding, and immense knowledge helped me in all the time of research. Without their timely advices, my thesis work would not be finished. I owe Dr. Giulio Alfano a debt of gratitude for their careful reading of this thesis and the corrections and suggestions he has made.

I would like to express my warm appreciation for Dr. Mustafa Batikha, my teacher from Damascus University in Syria, who is always encouraging me through the difficult times.

Finally, truly unbounded thanks are due to Imane, my dear wife, who with her love, understanding and patience supported me in finishing this research.

Table of Contents

Chapter 1	1
Introduction	1
1.1 What is buckling?	1
1.2 Plastic buckling and its importance in engineering applications	2
1.3 Plastic-buckling paradox	5
1.4 Aims and objectives	7
1.5 Summary of methodology	7
1.6 Outline of the thesis	8
Chapter 2	10
Literature Review	10
2.1 The equilibrium differential equations	10
2.2 Nonlinear equilibrium paths	12
2.2.1 The adjacent equilibrium criterion	14
2.2.2 The Trefftz criterion	15
2.3 Elastic versus plastic buckling	16
2.3.1 Elastic Buckling	17
2.3.1.1. Stable symmetric buckling	17
2.3.1.2. Unstable symmetric buckling	18
2.3.1.3. Asymmetric buckling	19
2.3.2 Plastic Buckling	20
2.4 Key milestones in the development of buckling theories	21
2.4.1 Elastic buckling	21
2.4.2 Post-buckling behaviour	23
2.4.3 Inelastic buckling	24
2.5 Early development in Plasticity	27
2.6 Computational Plasticity	30
2.7 Inelastic material behaviour –Elasto-plasticity based on the flow theory 31	
2.7.1 Plastic stress-strain relations	31
2.7.2 Classical yield surfaces	33
2.7.3 The Prandtl-Reuss equations for plane stress assumption	38
2.8 Inelastic material behaviour –Elasto-plasticity based on the deformation theory	39
2.8.1 The Hencky equations for plane stress assumption	41
2.9 Plastic buckling paradox	44

2.10	A brief overview of the underlying methods of BOSOR5	52
Chapter 3		55
A Detailed Numerical Investigation into the Plastic Buckling Paradox for Circular Cylindrical Shells under Axial Compression		55
3.1.	Introduction	55
3.2.	Test samples and finite-element modelling	56
3.2.1	Geometry and elements	56
3.2.2	Constitutive relationship and material constants.....	59
3.2.3	Large displacement formulation.....	65
3.2.4	Solution strategy.....	65
3.2.5	Imperfection sensitivity analysis	66
3.3.	FEA results for Lee's specimens.....	67
3.4.	FEA results for Batterman's experiments.....	76
3.5.	Discussion and interpretation of FEA results in the context of the plastic buckling paradox.....	83
3.5.1	Robustness of the FE model	84
3.5.2	Influence of initial imperfections.....	84
3.5.3	Buckling shapes and over-constraint of analytical models	85
3.5.4	Effects of unloading: analysis through a semi-analytical model... ..	88
3.6.	Conclusions	96
Chapter 4		98
A Numerical and Analytical Investigation into the Plastic Buckling Paradox for Circular Cylindrical Shells under Non-Proportional Loading		98
4.1.	Introduction	98
4.2.	Test samples and finite-element modelling	100
4.2.1.	Geometry and elements	100
4.2.1.1	Modelling of tests made by Blachut et al. (1996)	100
4.2.1.2	Modelling of tests made by Giezen et al. (1991)	103
4.2.2.	Material parameters.....	104
4.2.3.	Large displacement formulation and solution procedure	107
4.2.4.	Description of imperfections	108
4.3.	Finite-element results for the experiments in Blachut et al. (1996) ..	111
4.3.1.	Comparison of the numerical results with experimental results .	111
4.3.2.	Comparison of the FE results with the numerical results by Blachut et al. (1996)	117
4.4.	Comparison of FE results with results by Giezen et al. (1991).....	121
4.5.	Imperfection sensitivity analysis	127

4.5.1. Imperfections generated by different eigenmodes.....	127
4.5.2. Imperfections generated by a linear combination of different eigenmodes.....	129
4.5.3. Bifurcation analysis for a perfect model using BOSOR5 and an asymptotic approach in ABAQUS.....	132
4.6. Analytical treatment.....	137
4.7. Results and discussion	141
4.8. Interpretation of FEA results in the context of the plastic buckling paradox.....	146
4.9. Conclusions	148
Chapter 5	149
On the Elastoplastic Buckling Analysis of Cylinders under Non-proportional Loadings via the Differential Quadrature Method.....	149
5.1. Introduction	149
5.2. Flugge's differential equations for cylinders under combined loading	152
5.2.1. Strain-displacement relations	153
5.2.2. Stress-strain relations in plastic range.....	154
5.2.3. Governing differential equations.....	155
5.2.4. The rate of displacement function.....	157
5.3. Solution via the differential quadrature method.....	159
5.3.1. DQ approximation of the differential equations and solution procedure	161
5.3.2. Verification with known solutions	164
5.3.3. Effect of thickness ratio on the buckling pressure.....	169
5.3.4. Effect of tensile stress and E/σ_y ratio on the buckling pressure	172
5.3.5. Effect of boundary conditions on the buckling pressure	173
5.3.6. Effects of L/D ratio on the buckling pressure	178
5.4. Effect of shear stiffness proposed by Becque (2010).....	179
5.5. Finite-element modelling	183
5.6. Comparison between the DQ and the FEA results.....	185
5.5.1. Interpretation of the presented and FE results in the context of the plastic buckling paradox	189
5.7. Conclusions	199
Chapter 6	202
Conclusions and Recommendations.....	202
6.1. Conclusions	202
6.2. Recommendations for further work	205

References.....	207
Appendix.....	215
A1. Equations used for the flow theory of plasticity employed in ABAQUS 215	
A2. Analytically derived buckling formulas derived by Batterman	216
A3. FORTRAN code for the semi-analytical model in Chapter 3.....	217
A4. Matlab code for determining the plastic buckling pressure and buckling mode using the DQ method based on both the flow and deformation theories of plasticity	221

Chapter 1

Introduction

1.1 What is buckling?

Buckling is a physical phenomenon occurring when the deformed configuration of a structure, under a given load, undergoes a relatively sudden variation in shape, typically with large or relatively large increase in displacements and strains. The most famous case, for most engineers, is that of a reasonably straight and slender body bending laterally and abruptly from its longitudinal position due to compression stresses, leading to the catastrophic collapse of the structure under compressive loads, often with very large deformations. However, from an engineering and scientific view point, the important phase of buckling generally occur before deformations become very large, when the structure appear to the naked eye to be undeformed or only slightly deformed (Bushnell, 1982).

Buckling is inherently a nonlinear problem, certainly from a geometrical point of view and often from a material point of view. The material nonlinearity is due to nonlinear relationships between stresses and strains, as it is the case in plasticity. The geometrical nonlinearity is related to the nonlinearity of the kinematic relations which represent the influence of large displacements and rotations of structural elements on the behaviour of the structure (Brush and Almroth, 1975). Some form of geometric nonlinearity must be included in order to derive buckling equations and identify the equilibrium paths, whose points represent configurations of equilibrium.

To predict buckling two types of analyses can normally be conducted, sometimes in combination: a bifurcation analysis and a nonlinear collapse analysis (Bushnell, 1981).

A bifurcation, or eigenvalue, buckling analysis, searches for the point of intersection between the primary equilibrium path (pre-buckling path) and a secondary equilibrium path (post-buckling path), called a bifurcation point, or also a 'bifurcation buckling' point. At this point, the deformation can start to grow in a new pattern which is different but energetically 'orthogonal' to the pre-buckling deformation pattern (Bushnell, 1981). In this analysis, geometric nonlinearity should be considered. Bifurcation buckling is purely conceptual, as it occurs only in a 'perfect' structure, subject to loads that do not perform any first-order work for any incremental deformation along the secondary equilibrium path. A typical example is a column subjected to axial compressive loading which must pass through the centre of mass of the cross-section.

In a nonlinear collapse analysis, the slope of the load-deflection curve decreases by increasing the load and becomes zero at the collapse load (Jones, 2006; Bushnell, 1981). If the load is prescribed as the structure deforms, the structure becomes unstable and further deformation can only be captured in the analysis with a path-following technique, such as an arc-length method, or through a dynamic analysis (Falzon and Aliabadi, 2008). This type of behaviour is called snap-through buckling and, from a mathematical point of view, is an instability problem. In order for a nonlinear collapse analysis to be effective in capturing buckling, either the structure has to be characterised by some geometric 'imperfection', or the applied load must perform some positive first-order work for the incremental deformation at collapse. Furthermore, geometrical nonlinearity must be accounted for in the analysis.

1.2 Plastic buckling and its importance in engineering applications

Shell structures are widely used in many branches of engineering such as, spacecrafts, aircrafts, cooling nuclear reactors, towers, steel silos and tanks for storage of bulk solids and liquids, pressure vessels, pipelines and offshore platforms.

Several examples of catastrophic failure of expensive shell structures due to buckling are described in the literature. A steel water tank can collapse

because of unexpected buckling of the bottom part of the conical portion of the tank, a region subjected to meridional compressive stress combined with circumferential tension from the fluid pressure inside the tank (Bushnell and Bushnell, 2005). Cooling towers structures of nuclear reactors can buckle locally near the base due to axial compression. Moreover, wind can also cause overall buckling in an ovalisation mode in which the maximum buckling displacement occurs near the open top of the tower. The wind load and its combination with self-weight of the cooling tower can cause catastrophic failure due to the buckling instability (Asadzadeh and Alam, 2014). For aerospace applications, rocket boosters consist of segmented shell structures, which can buckle during launch (NASA, 2013). In aircraft applications, due to hard landing of a flight vehicle, the inner cylinder of the landing gear can axially buckle (Boeing, 2014). Some offshore oil platforms have supporting structures that consist of cylindrical shells with impressively large diameters. If large very powerful sea waves hit the platforms, these supporting structures can buckle (Bushnell and Bushnell, 2005).

All the very important engineering problems mentioned above involve cylindrical shell structures subjected to compressive stresses which can be either uniform or varying throughout the cylinder. The buckling load of a thin cylindrical shell under axial compression is very sensitive to imperfections, and the buckling load and mode of thin/thick cylinders depend on the geometry, loading and boundary conditions. Therefore, the axially compressed cylinder has been the most broadly studied of all shell buckling problems, giving a wealth of results from both experimental and theoretical work (Teng and Rotter, 2004). This problem will be studied in Chapter 3 of this thesis.

Another important area of engineering where buckling and often plastic buckling pose significant concern is the design and analysis of pipelines, which are the ideal means of transportation for gas and liquids such as oil, water or sewage. Often they are exposed to extreme environments such as arctic cold, desert heat or underwater environments. Smaller diameter pipelines buried in relatively shallow channels may buckle like beams under compressive axial forces. For example, the compressive stresses caused by

ground motion can cause an entire section of the pipeline to move out of the ground and bend up in the air. Pipelines with large diameter buried in relatively deep channels are constrained from lateral movement by the soil cover and can buckle and collapse like shells if any ground motion is caused by fault movements, landslides, permafrost melting and soil liquefaction that results in axial compression in the pipeline (Yun and Kyriakides, 1990).

In buried pipelines used to transfer hot oil, the internal temperature and pressure can rise. The pipeline will expand as a result of temperature increase. If such expansion is restrained due to soil friction, axial compressive stresses will set up in the pipe-wall. As a result, global vertical buckling of a pipeline may occur, which is called upheaval buckling (Maltby and Calladine, 1995).

In all the above cases, pipelines are again cylinders mainly subject to axial compression. However, important problems where different types of loading can occur in pipes involve submarine pipelines, which play an important role in offshore oil and gas exploitation projects. The installation of pipelines in deep water indeed can induce loads to the structure, which will lead to the risk of buckling. The most commonly used installation methods are the S-Lay and the J-Lay (Kashani and Young, 2005; Kyriakides and Corona, 2007). The pipeline in the S-Lay installation method starts in horizontal position on the vessel and produces an S-shape on the way to the seabed. The tensioners and the lay-vessel at the top provide the required tensile load to hold the suspended pipeline and control its shape. Therefore, the upper and lower curved parts of the pipeline, which are called over-bend and the sag-bend regions, respectively, suffer from combined tensile load, bending and external pressure (Kyriakides and Corona, 2007). The pipeline between these two regions has to withstand combined tensile load and external pressure. If the seabed is relatively flat, the part of the empty pipeline lying on the seabed can be considered to be under hydrostatic external pressure loading.

As the water depth increase, the tension load required to suspend the S-lay pipeline increases. Therefore, the J-lay installation method is used as

alternative method in which the pipeline leave the vessel from a nearly vertical position (Kashani and Young, 2005). The pipeline then has to sustain high tension and relatively small external pressure close to the surface of the sea, increasing external pressure and decreasing tension further down the long suspending section, high external pressure, bending and tension in the sag-bend and essentially hydrostatic pressure on a flat seabed (Kyriakides and Corona, 2007). All these cases show the importance of studying buckling of cylinders subject to combined loading consisting of axial tension and external pressure, which is covered in Chapters 4 and 5.

1.3 Plastic-buckling paradox

The plasticity models that have been proposed for metals in the strain hardening range for the study of plastic buckling can be divided into two groups: the 'deformation theory' of plasticity and the 'flow theory' of plasticity. In both of these theories the plastic deformations do not allow volume changes as plastic yielding is governed by the second invariant J_2 of the deviatoric part of the stress tensor, whereby in this respect they are both called J_2 theories. The main difference between these two theories lays in the fact that the deformation theory of plasticity is based on the assumption that, at any point of the solid body considered, the state of stress at any time is uniquely determined by the current state of strain and, therefore, it is a special class of path-independent nonlinear elastic constitutive laws, while the flow theory of plasticity assumes that the stress at any point and time is a function not only of the current strain but also of the strain history at the same point. In the deformation theory of plasticity, after a strain reversal in the plastic range, the initial loading curve is followed. On the contrary, in the flow theory of plasticity after a strain reversal in the plastic range the unloading takes place according to the initial elastic stiffness, as it is found experimentally in physical tests, and when the loading is totally removed, it leaves a permanent plastic strain. This makes the constitutive relationship path-dependent.

There is a general agreement among engineers and researchers that the deformation theory of plasticity lacks physical rigour in comparison to the flow theory (Hill, 1950; Mendelson, 1968). However, it has been found by many

authors (Durban and Zuckerman, 1999; Mao and Lu, 1999; Lee, 1962; Ore and Durban, 1992; Blachut et al., 1996; Giezen et al., 1991; Galletly et al., 1990) that the deformation theory predicts buckling loads that are in closer, and in some cases much closer, agreement with experiments than those predicted by the flow theory of plasticity.

This ‘plastic buckling paradox’ has been observed in a wide range of shell structures such as cruciform columns, plates, torispherical domes and circular cylinders under different loading conditions and using different boundary conditions. Among these, the problem of relatively thick cylindrical shell structures subject to either axial compression or combined axial tension and external pressure has attracted significant interest due to their significant importance in engineering applications, which led to a rich literature, with classic benchmark tests and results available for further investigation.

In the early and mid-90s, the plastic buckling paradox was considered still “unresolved” by Yun and Kyriakides (1990) and proposed explanations judged still “inconclusive” by Teng (1996), who quoted results, recent at that time, “which once again confirm the better agreement between deformation theory and experiment”, these results being those by Ore and Durban (1989, 1992), Galletly et al. (1990), Giezen et al., (1991). Blachut et al. (1996) “hoped that the paradox will be resolved in the near future”.

Since then, however, Bardi and Kyriakides (2006) reported that the flow theory significantly over-estimates buckling stresses, strains and wavelength of wrinkles while the deformation theory provides results in good agreement with experimental ones. Wange and Huang (2009) concluded that the possible reason for the large discrepancy in the results between the flow and the deformation theories is the small deformation assumption used to establish the governing differential equation. Zhang and Wang (2011) provided that another explanation of the results obtained by both theories may be that the deformation theory predicts an increasingly lower in-plane shear modulus as the level of plasticity increases, which results in lower calculated buckling-stress values. Other researchers, such as Mao and Lu (2002) and Zhang et al. (2015), accept the fact that the

deformation theory provides plastic buckling results that are in better agreement with the experimental results than those predicted by the flow theory. Therefore, they employed only the deformation theory in their analytical analysis.

1.4 Aims and objectives

The present thesis aims to shed light on the plastic buckling of cylinders subjected to proportional and non-proportional loading, i.e. simple axial compression or combined axial tensile load and external lateral pressure.

Specific objectives of the thesis are the following:

- a clarification about the actual existence of the paradox for cylindrical shells subjected to axial compression or combined axial tension and external pressure;
- a possible explanation of the plastic buckling paradox and a critical revision of the results obtained by many authors in the literature, which led to the definition of the paradox;
- an assessment of the imperfection sensitivity of shells buckling in the plastic domain;
- the establishment of new analytical solutions for plastic buckling of cylindrical shells in order to investigate the effect the boundary conditions, material parameters and geometry of the cylinders on the discrepancies in the results obtained using the flow and deformation theories.

1.5 Summary of methodology

Nonlinear finite-element (FE) analyses for perfect and imperfect cylinders subjected to either axial compression or combined axial tension and external pressure have been carefully conducted using both the flow and deformation theories of plasticity in order to identify the discrepancies in the results obtained and, therefore, to check whether the paradox really exists. The analyses included an investigation of the imperfection sensitivity of the cylinders as they buckle in the plastic domain. The FE results were compared with experimental, numerical and analytical results available in the literature.

Analytical approaches for the considered case studies were also pursued in order to provide a possible explanation of the plastic buckling paradox and investigate the effect of the simplified assumptions used in many analytical treatments on the discrepancy between the flow and deformation theories. The obtained analytical results have been compared with experimental and numerical results obtained by other authors using the code BOSOR5 (Bushnell, 1986) and with the FE results presented in this thesis.

A semi-analytical model was developed using a simplified formulation proposed by Hutchinson (1972) to qualitatively investigate the effect of the imperfections and of the unloading law in the constitutive relationships on the calculated plastic buckling load and on the post-buckling behaviour, using the flow and deformation theories.

A differential-quadrature (DQ) method has been finally employed to obtain, for the first time, the critical loads leading to elasto-plastic buckling of cylinders under combined axial tension and external pressure, for various geometries, material parameters and boundary conditions, again using both the deformation and the flow theory of plasticity. The DQ results are discussed and analysed also via a comparison with FE results.

1.6 Outline of the thesis

The thesis is divided into six chapters. A brief description for each chapter is presented below:

This first chapter has introduced the problem of plastic buckling, its importance in engineering applications, and discussed the unresolved plastic buckling paradox. Furthermore, it set the aims and objectives and provided a brief summary of the methodology used in this research.

Chapter 2 reviews the mathematical concepts in buckling analysis and what distinguishes elastic buckling from plastic buckling. It provides a historical background of buckling theories and of the development of the plasticity theories. In this chapter, the explicit expressions of stress-strain relations in the plastic range are derived based on the Prandtl-Ruess and the Hencky

equations. Finally, the literature related to the plastic buckling paradox is reviewed.

Chapter 3 presents geometrically nonlinear finite-element analyses of cylinders subjected to axial compression by using the code ABAQUS. The numerical results are then compared with accurate experimental and analytical results. A semi-analytical model is used to investigate the effect of imperfections and of the plasticity law on the buckling load. In this chapter, the reasons underlying the buckling paradox are discussed in detail.

Chapter 4 presents in detail the finite-element (FE) modelling of selected cylindrical shells, subject to combined axial tension and external pressure, again by using the code ABAQUS. The comparison of the FE results with the experimental and numerical results conducted by other authors using the code BOSOR5 is also presented. This chapter contains a comprehensive discussion of the results in order to provide an insight into the underpinning causes of the discrepancy between the present predictions, test data, and results by other authors. Moreover, analytical results are discussed and compared with experimental and numerical findings.

In Chapter 5, the differential quadrature (DQ) method is used to obtain the elastic-plastic buckling pressures of cylinders under combined loading, again consisting of tensile stress and increasing external pressure. A parametric study was then performed to characterize the effect of the thickness-to-radius, t/R , length-to-diameter, L/D , and material stiffness-to-strength, E/σ_y , ratios, as well as the influence of the tensile stress and various boundary conditions on the discrepancies between the predictions of the flow and deformation theories. Nonlinear FE analyses of cylindrical shells are then conducted using both the flow theory and the deformation theory of plasticity, whose results are compared with the present DQ results and discussed again within the framework of the plastic buckling paradox.

Chapter 6 presents the conclusions drawn from the previous chapters. Recommendations for further research are also made.

Chapter 2

Literature Review

2.1 The equilibrium differential equations

The behaviour of structures under an applied load can be described by a set of differential equations and associated boundary conditions that identify the interaction between forces (internal and external) and corresponding deformations. The complexity of these differential equations depends on the shape and geometries of the problem and on the structural model used, so that they may be derived in terms of simplifying assumptions.

To obtain the differential equations two methods are normally described in the literature (Brush and Almroth, 1975; Yoo and Lee, 2011); the method of equilibrium and the principle of stationary potential energy.

For the first method, differential equations can be derived by summation of forces and moments to ensure static equilibrium of an infinitesimal element of structure. Kinematic differential equations can then be written to relate displacement and strain fields, and constitutive relationships are written to relate stresses and strains. Overall, all these equations govern the equilibrium of the structure and therefore, in the following, they will be called equilibrium differential equations.

To capture buckling, the equilibrium equations must be written in the deformed configuration. In the case of the Cauchy three-dimensional continuum model, fifteen unknowns exist in the resulting equations: six internal stresses, six strains and three displacements at every point.

Therefore, fifteen equations are required to find these unknown fields, which are three equilibrium differential equations, six constitutive equations and six strain-displacement relations. The number of unknowns can be reduced according to assumptions related to 1D or 2D problems.

The second method can be used when the total potential energy can be defined for the problem under examination. In such a case, let denote by U and V the strain energy density and the loss of potential energy of applied loads, respectively. Thus, the total potential energy of the mechanical system is:

$$\Pi = U + V \quad (2.1)$$

It was proven that minimizing the total potential energy Π governs the stable equilibrium of the structure, see (Yoo and Lee, 2011 ; Brush and Almroth, 1975) among many others.

Consider, for instance, a thin enough cylinder modelled with the Kirchhoff-Love thin-shell theory in which each material point is identified by the axial coordinate x and its circumferential coordinate y , and has three degrees of freedom, u, v, w , representing the displacement in the axial, circumferential and radial direction, respectively. If the system is given infinitesimal virtual displacements $\delta u, \delta v, \delta w$ about u, v, w , the total potential energy in Taylor series expansion about u, v, w is:

$$\begin{aligned} \Pi(u + \delta u, v + \delta v, w + \delta w) = & \Pi(u, v, w) + \frac{\partial \Pi}{\partial u} \delta u + \frac{\partial \Pi}{\partial v} \delta v + \frac{\partial \Pi}{\partial w} \delta w + \\ & \frac{1}{2!} \left[\frac{\partial^2 \Pi}{\partial u^2} (\delta u)^2 + \frac{\partial^2 \Pi}{\partial v^2} (\delta v)^2 + \frac{\partial^2 \Pi}{\partial w^2} (\delta w)^2 + 2 \frac{\partial^2 \Pi}{\partial u \partial v} \delta u \delta v + 2 \frac{\partial^2 \Pi}{\partial u \partial w} \delta u \delta w + \right. \\ & \left. 2 \frac{\partial^2 \Pi}{\partial v \partial w} \delta v \delta w \right] + \dots \dots \dots \end{aligned} \quad (2.2)$$

The change in the total potential energy can then be written:

$$\Delta \Pi = \Pi(u + \delta u, v + \delta v, w + \delta w) - \Pi(u, v, w) = \delta \Pi + \frac{1}{2!} \delta^2 \Pi + \frac{1}{3!} \delta^3 \Pi \dots \quad (2.3)$$

Because the virtual displacements, $\delta u, \delta v, \delta w$, are infinitesimal, each non-zero term is much larger than the sum of succeeding terms. Therefore, $|\delta \Pi| > |\delta^2 \Pi|$. Hence, the necessary and sufficient condition for the total potential energy Π to be stationary is that $\delta \Pi$ vanishes: $\delta \Pi = 0$.

The total potential energy Π can be written in the form:

$$\Pi = \int_V F(x, y, u, v, w, u_{,x}, u_{,y}, v_{,x}, v_{,y}, w_{,x}, w_{,y}, w_{,xx}, w_{,xy}, w_{,yy}) dV \quad (2.4)$$

where function F is called the integrand of Π , x, y are the independent variables, and $u, v, w, u_{,x}, u_{,y}, v_{,x}, v_{,y}, w_{,x}, w_{,y}, w_{,xx}, w_{,xy}, w_{,yy}$ are dependent variables as they are all function of x, y . Here the notations $\blacksquare_{,x}$ and $\blacksquare_{,y}$ indicate partial differentiation of \blacksquare with respect to x and y , respectively, so the highest-order derivatives are of first order in u and v and second order in w . The equilibrium is achieved when $\delta \Pi = 0$. Accordingly, the integrand F must satisfy the Euler-Lagrange equations with respect to arbitrary variation of u, v and w (Brush and Almroth, 1975):

$$\begin{aligned} \frac{\partial F}{\partial u} - \frac{\partial}{\partial x} \frac{\partial F}{\partial u_{,x}} - \frac{\partial}{\partial y} \frac{\partial F}{\partial u_{,y}} &= 0 \\ \frac{\partial F}{\partial v} - \frac{\partial}{\partial x} \frac{\partial F}{\partial v_{,x}} - \frac{\partial}{\partial y} \frac{\partial F}{\partial v_{,y}} &= 0 \\ \frac{\partial F}{\partial w} - \frac{\partial}{\partial x} \frac{\partial F}{\partial w_{,x}} - \frac{\partial}{\partial y} \frac{\partial F}{\partial w_{,y}} + \frac{\partial^2}{\partial x^2} \frac{\partial F}{\partial w_{,xx}} + \frac{\partial^2}{\partial x \partial y} \frac{\partial F}{\partial w_{,xy}} + \frac{\partial^2}{\partial y^2} \frac{\partial F}{\partial w_{,yy}} &= 0 \end{aligned} \quad (2.5)$$

2.2 Nonlinear equilibrium paths

The simplifying assumptions considered in the derivation of the equilibrium differential equations play an important role in the investigation of the behaviour of structures under applied loads. One of the main assumptions is whether the deformations are infinitesimal (geometrically linear, or first-order, theory), moderate or finite. The equilibrium differential equations written on the undeformed configuration and in the assumption of infinitesimal deformations are linear, and do not allow capturing any aspect of buckling. By approximating the deformation fields by a second-order Taylor expansion, or writing the equilibrium equations on the deformed configuration, for a structure with perfect geometry and in absence of first-order terms of the external work, the resulting equations are homogeneous and define a generalised eigenvalue problem, which only allow the determination of the bifurcation loads, the eigenvectors being the buckling modes. In presence of geometrical imperfections, or in the case of non-zero first-order terms of the external work done for the first buckling mode, the equations become non-

homogenous and a nonlinear solution is found, with no bifurcation. In the assumption of finite deformations, the differential equations are nonlinear because they contain linear, quadratic and, for shell models, cubic terms in the derivatives of u, v, w .

The equilibrium paths are here defined as the plots reporting the applied load versus a given measure of the deformation of the structure, which can be found by the solution of the equilibrium differential equations.

Consider the case of a cylinder subjected to axial compressive load and without geometrical imperfections. Figure 2.1 represents a schematic plot of the load versus the axial displacement if rotations are neglected in the pre-buckling phase. Two equilibrium paths can be observed: the primary and secondary paths. The linear equilibrium differential equations govern the primary path OA, called also pre-buckling path, and nonlinear equilibrium differential equations govern the secondary path AB, called the post-buckling. The intersection between the primary and secondary paths represents the bifurcation point.

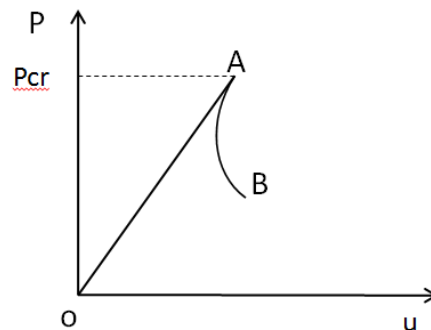


Figure 2. 1: Equilibrium paths for cylinder subjected to axial compressive loading

As rotations in the above example are neglected in the pre-buckling path, this is obtained by neglecting the nonlinear terms in the equilibrium equations. However, in many shell structures, the deformations in the pre-buckling are not rotation-free and must be taken into account to obtain an accurate bifurcation point. Therefore, the pre-buckling path determined with the second-order theory becomes nonlinear and iterative methods are needed to solve such nonlinear equations (See Figure 2. 2).

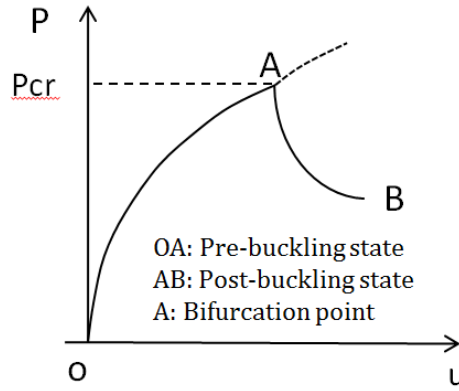


Figure 2. 2: Equilibrium paths with nonlinear pre-buckling state

For simplicity, in the analytical treatments, the bifurcation point can be obtained by solution of linearized differential equations and neglecting the influence of pre-buckling rotations. These equations are derived from nonlinear differential equations using the adjacent equilibrium criterion or the Trefftz criterion methods (Brush and Almroth, 1975; Yoo and Lee, 2011). The linearized differential equations are called the stability equations.

The solution of the stability equations provides the bifurcation point but no information is obtained about the initial slope or the shape of the secondary equilibrium path because the incremental displacements are infinitesimally small and linearization is an approximation that is only valid around a region close to the bifurcation point. Sometimes the behaviour of some structures (e.g. plate and shells) can be understood only if the shape of the secondary path is known. Moreover, the shape of secondary path governs the sensitivity of structure to the initial imperfections.

2.2.1 The adjacent equilibrium criterion

The stability equations can be derived from the nonlinear equilibrium differential equations by use of a perturbation technique, in which the displacement field of the problem \bar{u} is replaced by $\bar{u}_0 + \bar{u}_1$ in the nonlinear equilibrium differential equations, where \bar{u}_0 is the displacement field at the bifurcation point in the primary path and \bar{u}_1 is an arbitrary incremental displacement field. The resulting equations contain linear, quadratic and cubic terms in \bar{u}_0 and \bar{u}_1 , in general. All terms containing only \bar{u}_0 are equal to zero because \bar{u}_0 is in equilibrium configuration and terms which are quadratic

and cubic in \bar{u}_1 are dropped out because the incremental displacements are very small. The final equations are homogeneous and linear in \bar{u}_1 with variable coefficients in \bar{u}_0 . These coefficients can be identified by the solution of original nonlinear equilibrium equations. However, it is desirable in the analytical analysis to limit the range of applicability of the linearized equations by requiring that \bar{u}_0 be restricted to configuration governed by linear differential equilibrium equations.

2.2.2 The Trefftz criterion

As is illustrated in Section 2.1, the change of total potential energy can be written in the form:

$$\Delta\Pi = \delta\Pi + \frac{1}{2!}\delta^2\Pi + \frac{1}{3!}\delta^3\Pi \dots \dots \quad (2.6)$$

The term $\delta\Pi$ vanishes by use of the principle of stationarity of the potential energy. Each nonzero term in this expression is much larger than the sum of the succeeding term. Therefore, the sign of $\Delta\Pi$ is determined by the sign of second variation of Π that is the $\delta^2\Pi$, if this is non zero. A sufficient condition for Π to be a local minimum is that the second variation is positive definite. Therefore, the critical load of a structural system is the lowest load for which $\delta^2\Pi$ is no longer positive definite. At this load the equilibrium changes from stable to unstable. This leads $\delta^2\Pi$ to be stationary:

$$\delta(\delta^2\Pi) = 0 \quad (2.7)$$

i.e. the derivative with respect to \bar{u}_1 of the integrand in $\delta^2\Pi$ must be equal to zero (Brush and Almroth, 1975).

In order to obtain the second variation, the displacement field \bar{u} is replaced again by $\bar{u}_0 + \bar{u}_1$ in the total potential energy. In components it results:

$$\begin{aligned} u &\rightarrow u_0 + u_1 \\ v &\rightarrow v_0 + v_1 \\ w &\rightarrow w_0 + w_1 \end{aligned} \quad (2.8)$$

The total potential energy can be expressed in Taylor series expansion:

$$\begin{aligned} \Pi(u_0 + u_1, v_0 + v_1, w_0 + w_1) &= \Pi(u_0, v_0, w_0) + \left.\frac{\partial\Pi}{\partial u}\right|_0 u_1 + \left.\frac{\partial\Pi}{\partial v}\right|_0 v_1 + \\ &\left.\frac{\partial\Pi}{\partial w}\right|_0 w_1 + \frac{1}{2}\left[\left.\frac{\partial^2\Pi}{\partial u^2}\right|_0 (u_1)^2 + \left.\frac{\partial^2\Pi}{\partial v^2}\right|_0 (v_1)^2 + \left.\frac{\partial^2\Pi}{\partial w^2}\right|_0 (w_1)^2 + 2\left.\frac{\partial^2\Pi}{\partial u\partial v}\right|_0 u_1 v_1 + \right. \end{aligned} \quad (2.9)$$

$$2 \frac{\partial^2 \Pi}{\partial u \partial w} \Big|_0 u_1 w_1 + 2 \frac{\partial^2 \Pi}{\partial v \partial w} \Big|_0 v_1 w_1 \Big] + \dots$$

where the notation $\Big|_0$ indicates that Π is to be computed for $u = u_0$, $v = v_0$ and $w = w_0$. The second variation is defined as:

$$\begin{aligned} \frac{1}{2} \delta^2 \Pi = & \frac{1}{2} \left[\frac{\partial^2 \Pi}{\partial u^2} \Big|_0 (u_1)^2 + \frac{\partial^2 \Pi}{\partial v^2} \Big|_0 (v_1)^2 + \frac{\partial^2 \Pi}{\partial w^2} \Big|_0 (w_1)^2 + 2 \frac{\partial^2 \Pi}{\partial u \partial v} \Big|_0 u_1 v_1 + \right. \\ & \left. 2 \frac{\partial^2 \Pi}{\partial u \partial w} \Big|_0 u_1 w_1 + 2 \frac{\partial^2 \Pi}{\partial v \partial w} \Big|_0 v_1 w_1 \right] \end{aligned} \quad (2.10)$$

In the resulting expression, one collects all second-order terms in u_1, v_1, w_1 . Hence, the second variation in Π is found to be:

$$\frac{1}{2} \delta^2 \Pi = \int_V H(x, y, u_1, v_1, w_1) dV \quad (2.11)$$

Eq. (2.7) implies that the integrand H in $\frac{1}{2} \delta^2 \Pi$ should satisfy the Euler-Lagrange equations. Since the integrand of second variation is a homogeneous quadratic function, the resulting expressions by use of Euler-Lagrange equations are linear homogeneous differential equations.

2.3 Elastic versus plastic buckling

An elastic buckling analysis is based on the assumption that the stresses in the structure are below the yield stress of the material and, therefore, that buckling occurs in the elastic range. This assumption may be correct for slender structural member but it is not valid for thicker and/or shorter members in which the internal stresses exceed the yield stress before buckling. In such cases, buckling occurs in the plastic range and must be determined by taking the inelastic behaviour of the material into account.

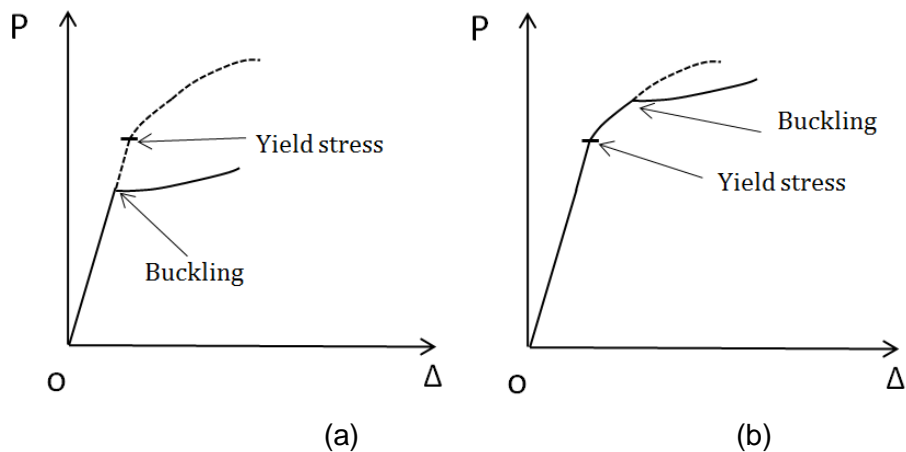


Figure 2.3: (a) elastic buckling versus (b) plastic buckling

2.3.1 Elastic Buckling

Classical analysis of stability of perfect structures takes the form of a generalized eigenvalue problem. The smallest buckling load defined from the solution of eigenvalue problem is called bifurcation load P_c . However, classical analysis does not give any indication of the character of the post-buckling behaviour or the behaviour of imperfect structure. The following are three typical cases of possible load–deflection curves describing the static equilibrium configurations (Falzon and Hitchings, 2006).

2.3.1.1. Stable symmetric buckling

Stable symmetric buckling occurs when the structure has no preference for the direction of the deformed shape and when the secondary path is stable. This type of post-buckling occurs for example for a simply supported perfect plate subjected to compressive edge loads. Increasing the load up to the buckling load P_c never causes lateral deflection. At this load level, the primary stable equilibrium path becomes unstable and the plate begins to deform perpendicularly to its un-deformed configuration. By increasing the load beyond the critical load with appropriate boundary conditions, the behaviour follows the secondary equilibrium path and the plate is able to support more load than the critical buckling load (Figure 2.4). The secondary path displays as a stiffening effect with increasing loads.

In reality, the plate has initial imperfections causing a smooth transition in the response of structure from pre-buckling to post-buckling curve and the bifurcation point disappears. Large amount of imperfections reduces moderately the collapse load. Therefore, this type of structure is termed imperfection insensitive.

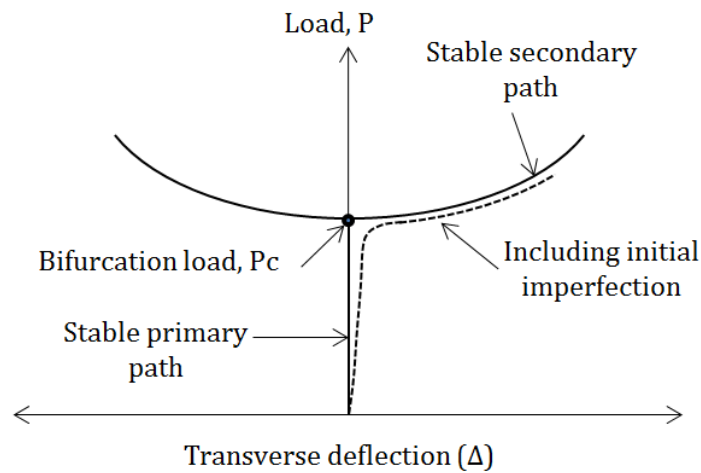


Figure 2.4: Stable symmetric buckling (Falzon and Hitchings, 2006)

2.3.1.2. Unstable symmetric buckling

In this type of buckling, the post-buckling path is unstable (Figure 2.5). The structure exhibits imperfection sensitivity for which a small amount of imperfections can reduce the buckling load significantly. An example of such structures is a circular cylindrical shell subjected to axial compressive loads. Numerous experimental studies showed that the observed buckling loads were significantly lower than those predicted by the classical analysis. This fact was interpreted by the presence of inevitable small imperfections in the specimens which, due to inherent imperfection sensitivity, reduce the experimental buckling loads (Falzon and Hitchings, 2006).

Koiter evaluated that, for small imperfections, the reduction in critical load for unstable response was proportional to the imperfection parameter raised to the power $2/3$ (Hutchinson and Koiter, 1970).

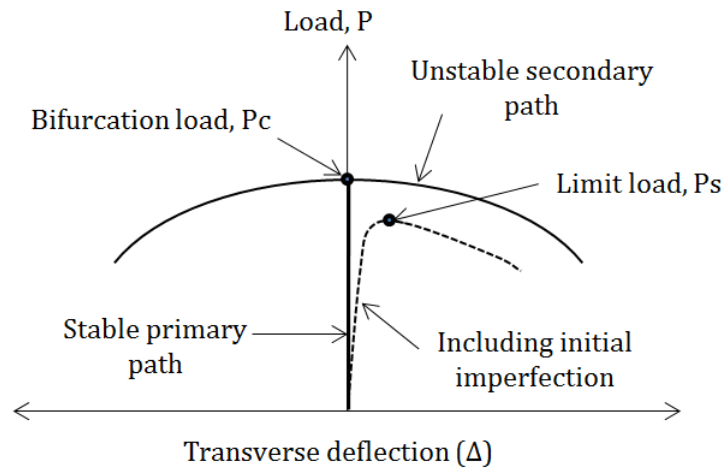


Figure 2.5: Unstable symmetric buckling (Falzon and Hitchings, 2006)

2.3.1.3. Asymmetric buckling

This response is caused due to asymmetries in loading or geometry of the shell. It is characterized by a secondary path which could be stable for some imperfections or unstable negative for others (Figure 2.6).

Koiter evaluated that the reduction in critical load identified by the limit point for unstable response for these type of structures was proportional to the imperfection parameter raised to the power $\frac{1}{2}$ (Hutchinson and Koiter, 1970). Therefore, asymmetric buckling displays higher imperfection sensitivity than the unstable symmetric buckling.

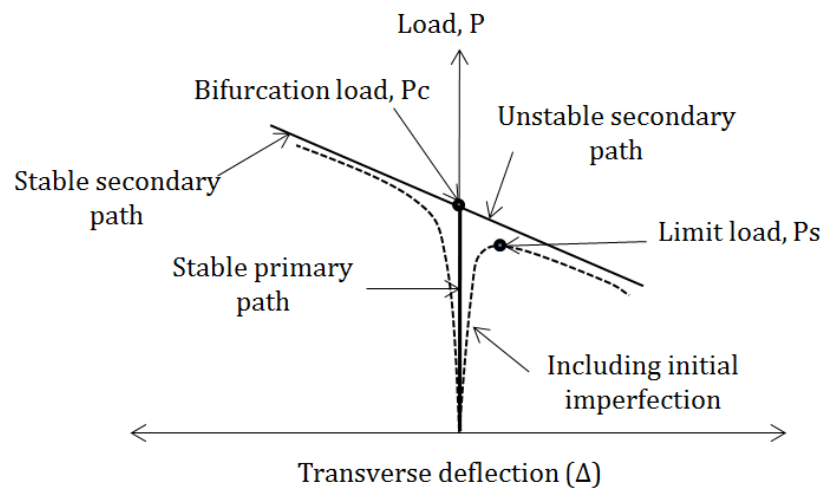


Figure 2.6: Asymmetric buckling (Falzon and Hitchings, 2006)

2.3.2 Plastic Buckling

The phenomenon of plastic buckling was firstly found in the behaviour of thick cylindrical shells which deform at first axisymmetrically and then non-axisymmetrically under axial compressive load (Bushnell, 1982). Accurate prediction of the critical loads in plastic range requires accounting not only for moderate large deflection but also for nonlinear material behaviour (Bushnell, 1982).

The elastic buckling in shells usually occurs catastrophically and suddenly, while the plastic buckling failure of shells experience cascade of events. Figure 2.7 shows two points on the load-deflection curve, the limit point at A and the bifurcation point at B. The cylinder experiences gradual growing of axisymmetric wrinkles at path OA, in which the cylinder fails at the limit load at point A, followed by the path ABC or ABD. The axisymmetric wrinkles develop along the path ABC while non-axisymmetric wrinkles develop along the path BD. The equilibrium path OABC is called fundamental path while the post-bifurcation equilibrium path BD, corresponding to the non-axisymmetrical mode of deformation, is called secondary path. The unusual point in this example is that the bifurcation point B occurs after the collapse point. In this case, the bifurcation load is of less engineering interest than the collapse load (Bushnell, 1982).

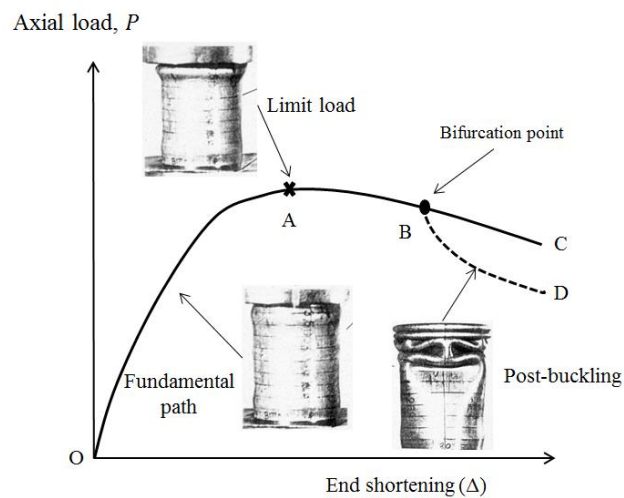


Figure 2.7: the stress-shortening response of long perfect circular cylinder subjected to axial compression (Bushnell, 1982).

Another commonly occurring situation, particularly for axisymmetric shells, is that bifurcation point B frequently occurs at load levels below the limit load A (Hutchinson and Koiter, 1970), as shown in Figure 2.8. Paths OAC and BD are again related to the axisymmetric and non-axisymmetric deformations, respectively. In this case the initial failure of the structure could be described by rapidly growing of non-axisymmetric deformation. The collapse load P_L is of less engineering interest than the bifurcation point P_c (Bushnell, 1982). For real structures which contain unavoidable imperfections, the buckling behaviour will follow the fundamental path OEF and collapse at the point E.

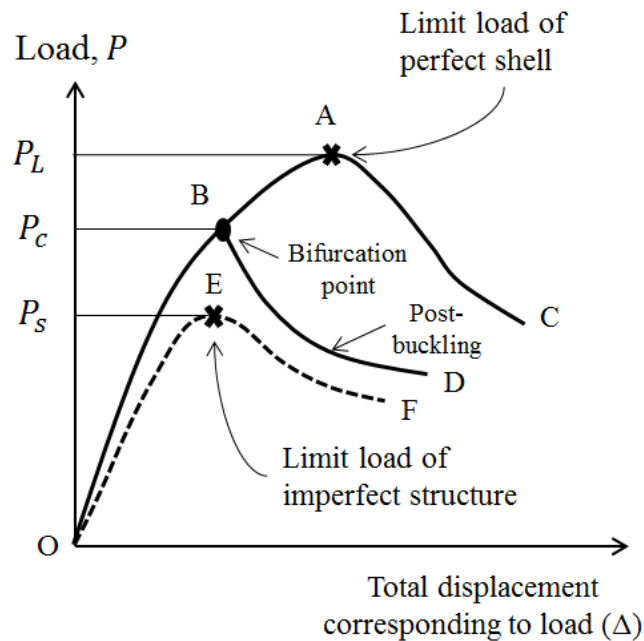


Figure 2.8: Load deflection curves in general nonlinear analysis (Bushnell, 1982).

2.4 Key milestones in the development of buckling theories

2.4.1 Elastic buckling

Euler (1757) established the principle of elastic stability. He used the differential equation governing the deflection of a beam, written though in the deformed configuration, to derive a simple formula for the critical load of a slender ideal column with simply supported ends and subjected to a centred axial compressive force. Furthermore he extended his analysis to cover columns with variable cross section and treated the problem of buckling of columns with axial load distributed along its length. However, his calculations

to find the correct solution for these complicated problems were incomplete (Timoshenko, 1983).

Bryan (1890) was the first to use the so-called energy criterion of stability to study the stability of plane rectangular or circular plates. He showed that for the stability of equilibrium of a given configuration the total potential energy should be minimum in that configuration. Bryan studied an elastic plate subjected to compressive load in its own plane. He described a displacement field which was normal to the middle surface of the plate and should satisfy the boundary conditions. He identified the work done by the applied compressive loads and the bending strain energy of the plate. He concluded that if the work done by the applied loads (V) for a small variation in displacements is greater than the corresponding change of bending strain energy U_b , the change of the total potential energy of the system ($U_b - V$) will be negative and consequently there will be a form of unstable equilibrium, which results in the plate to buckle.

Southwell (1913) derived general “equations of neutral equilibrium”. The most important advantage of the Southwell’s theory was its accuracy in following the actual stress history in a body which fails by instability under increasing stresses.

Biezeno and Hencky (1928) deduced differential equations for the general case of elastic stability. They considered an elastic body that satisfies the equilibrium equations under the action of volumetric forces and surface-tractions. Consider a body which undergoes a known state of stress and strain, indicated by I . Another state of strain, indicated by II , is defined by adding infinitesimal displacement to the considered body. They attempted to find the stresses which must be added on the faces of the infinitesimal cube cut from the body in state I to bring it into state II .

Trefftz (1933) used the energy stability criterion to develop a stability theory based on the theory of elasticity for finite deformations. He indicated that the adequate condition for stability was that the second variation of the total potential energy should be positive for all possible variations of displacements, which is the condition for the total potential energy to be a

relative minimum. Denoting by Π the total potential energy, the critical load of a structural system then is the lowest load for which $\delta^2\Pi$ is no longer positive. At this load the equilibrium changes from stable to unstable.

In classical theory of elasticity in the assumption of infinitesimal deformations, the strain components ε_{xx} , ε_{yy} and γ_{xy} and the rotation ω of a point of the two-dimensional elastic body, with respect to the original coordinate system x, y , are:

$$\begin{aligned}\varepsilon_{xx} &= \frac{\partial u}{\partial x}, \quad \varepsilon_{yy} = \frac{\partial v}{\partial y}, \quad \gamma_{xy} = \frac{1}{2} \left(\frac{\partial u}{\partial y} + \frac{\partial v}{\partial x} \right) \\ \omega &= \frac{1}{2} \left(\frac{\partial v}{\partial x} - \frac{\partial u}{\partial y} \right)\end{aligned}\tag{2.12}$$

Boit (1938) determined the terms which must be added to the classical equations of elasticity when there is a possibility of large rotation and small strains. He used a stiff string with fixed ends or thin clamped plate for which the nonlinear effects are not neglected. By proposing a new way to describe the deformed state, he succeeded in obtaining the stability equations in such a form that it is possible to provide a physical meaning of the various terms in the equations.

2.4.2 Post-buckling behaviour

The theories illustrated above have been limited to the analysis of neutral equilibrium. They aimed at determining the stability limit or the bifurcation point while the post-buckling response occurring possibly after overcoming this limit was left out of account. There were two reasons for this restriction. Firstly, there were great mathematical difficulties to treat the theoretical elastic behaviour after overcoming the stability limit. The linear differential equations can describe the neutral equilibrium whereas the equations which described the behaviour after the limit point were no longer linear. Secondly, engineers were satisfied with calculating the critical or buckling loads. However, it is now known, for long time, that some structures like flat plate supported along its edges and subjected to compressive loads in its plane are capable to resist more loads than the buckling load without exceeding the

elastic limit at any point (Koiter, 1945). This phenomenon is important in modern engineering, for example in the aerospace industry which requires light structures. Moreover, some shells structures such as axially compressed thin-walled cylinders experience significant scatter in the experimentally measured values of the buckling load, which lie considerably below the theoretical limit (Koiter, 1945).

The post-buckling behaviour of thin shell structures came into the light in 1940's when von Karman and Tsien (1939) showed that the large differences between the theoretical and experimental buckling behaviour of thin shells were due to the unstable post-buckling behaviour of these structures. Almost at the same time Koiter (1945) established a general theory of elastic stability valid for structures subjected to conservative loading. Furthermore, he succeeded in describing the elastic post-buckling behaviour of thin shell structures using an asymptotic power expansion. At the same time, he studied the imperfection sensitivity of an elastic buckled beam. His research explained the reasons why some structures, such as a flat plate supported along its edges and subjected to compressive loads in its plane, are capable to carry more loads above the buckling load, while other structures, such as axially compressed cylindrical shells, experimentally collapse at loads far below the buckling load found theoretically.

2.4.3 Inelastic buckling

In 1889, Engesser extended the elastic buckling of a compressed column to the case of inelastic buckling (Hutchinson, 1974). Engesser's theory assumes that, during loading, the column remains straight up to the critical buckling load, which is the compressive force at which equilibrium can be maintained also when slightly deflecting the column from the straight form of equilibrium. This small deflection causes a slightly increasing compressive stress on the concave side and a slightly decreasing compressive stress on the convex side. If point C in Figure 2.9 represents the stress-strain point that corresponds to the critical load of the column, the changes in stress and strain on the concave side of the column follow the tangent CC' , which is the tangent modulus of the material E_t , while, on the convex side, the changes in

stress and strain follow the slope line CC'' , which is the initial modulus of elasticity E or the elastic unloading.

One simplified way to apply Engesser's 'tangent-modulus theory' was to just replace the elastic modulus E with tangent modulus E_t in the Euler's columns formula (Timoshenko and Gere, 1961).

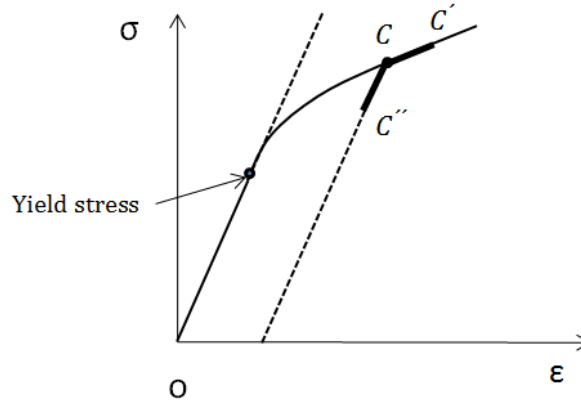


Figure 2.9: Stress-strain relation for material in compression (Timoshenko and Gere, 1961).

In 1898, Engesser corrected his original simplified theory by accounting for the different tangent modulus of the tensioned side of the cross section. He assumed that the cross section remained plane during bending and therefore the strains along the cross section of the column were distributed linearly. The position of the neutral axis was identified from the condition that the resultant of the compressive and tensile stresses must be equal (Timoshenko and Gere, 1961). To obtain the buckling load of such a column, the elastic modulus should be replaced with a reduced modulus of elasticity \bar{E} in Euler's column formula, which takes the form

$$\bar{E} = E \frac{I_1}{I_x} + E_t \frac{I_2}{I_x} \quad (2.13)$$

where I_1 is the second moment of inertia of the tension side of the cross section about the neutral axis and I_2 is the second moment of inertia of the compression side of the cross section.

For 50 years, engineers faced the dilemma that the reduced modulus was expected to be the correct theory but the experimental data were closer to those predicted by the tangent-modulus theory. Shanley (1947) resolved this

dilemma by conducting very careful experiments on small aluminum columns in conjunction with theoretical treatments. The importance of his work is still recognized now by using the term 'Shanley's column' to refer to his theory. In his analysis, he considered a discrete model of a rigid rod with two degrees of freedom. Two elastoplastic springs supported the model at the bottom, and an axial compressive force was applied at the top. He noted that the lateral deflection started very near to the theoretical load predicted by the tangent-modulus theory and that the load capacity increased with increasing lateral deflections. Therefore, during the buckling process, the mean stress on the buckled column might exceed the tangent-modulus stress but it would never exceed the reduced-modulus stress. The maximum value of the axial load lies somewhere between the tangent-modulus load and the reduced-modulus load. Moreover, he pointed out that the column would begin to buckle while the axial compressive load was still increasing which made possible for the stress on the convex side of the column to continue to increase, during the early stage of buckling (Allen and Bulson, 1980).

Duberg and Wilder (1952) studied theoretically the post-buckling behaviour of a column accounting for its inelastic behaviour. They showed that if the initial imperfection of the column vanished, the critical load of the column was the tangent-modulus load at which the bending started. They pointed out that the behaviour of the perfect column at loads beyond the tangent-modulus load depended on the stress-strain curve of the material. If the Ramberg-Osgood law was used in the analysis, the ratio between the maximum load of the column and the tangent-modulus load increased by decreasing the exponent n of the law.

Numerous tests of plates and shells were carried out in the late 1940s and early 1950s and solutions for the bifurcation load were obtained for many cases of interest. However, researches faced a major obstacle which was known as 'plasticity paradox' or 'plastic buckling paradox'. Many studies reported that plastic bifurcation loads of shells and plates based on the deformation theory of plasticity, which is clearly less approximate, are

reasonably in good agreement with test results, while calculations based on the flow theory of plasticity consistently overestimate plastic bifurcation load.

Hill (1956, 1958) identified the buckling criterion for elastic-plastic solids mathematically modelled using smooth or cornered yield surfaces. His plasticity formulation could be applied not only to find the bifurcation under compressive loading, but also to solve problems involving bifurcation in tension such as necking (Hutchinson, 1974). He established uniqueness and stability criteria, and pointed out the difference between bifurcation and stability.

The reasons which led researchers to study the post-buckling analysis of continuous solids and structures in the plastic range are that, in many cases of compressive loading, the lowest buckling load in plastic range of the material occurs under increasing load as it was illustrated by Shanley theory. Moreover, the material nonlinearity with a high hardening parameter, which reflects decreasing stiffness with increasing deformation or strain, adds additional destabilization to the geometric nonlinearity included already in the pre-buckling analysis (Hutchinson, 1974). Hutchinson (1974) studied the post-buckling behaviour and the imperfection-sensitivity aspects of plastic buckling for several plate and shell structures. He examined a simple discrete model, which was similar to Shanley's model for plastic buckling of columns, to illustrate its post-buckling behaviour. He then used a simple continuous model to bring out some features of the behaviour of a continuous solid. He applied Hill's bifurcation criteria for three dimensions solid to the widely used theory for plates and shells, the Donnell-Mushtari-Vlasov (DMV) theory.

2.5 Early development in Plasticity

Criteria for plastic yielding of solids, such as soils, had been proposed by different researchers, for example Coulomb in 1773. In his first paper on the fracture of sandstone, he concluded that the fracture of sandstone occurs when the shear stress reaches a certain value (Bell, 1984). His criterion was used by Poncelet in 1840 and Rankine in 1853. However, it appeared that

there were not as important investigations conducted on metals at the same time (Hill, 1950).

In 1864, Tresca carried out experiments on metal forming problems such as punching and extrusion, which led him to state that the metal yields plastically when the maximum shear stress attained a critical value (Bell, 1984).

Tresca's yield criterion was employed in 1870 and 1872 by Saint-Venant to identify the stresses in partly plastic cylinders subjected to torsion or rectangular beam subjected to bending and pressurized hollow cylinders. He constructed a system of equations relating the stresses and strains in two dimensional problems and found that there was no one-to-one relation between stress and total plastic strain (Hill, 1950). These equations were based on the assumptions that the volume of material did not change during plastic deformation, the direction of principal strains coincided with the direction of the principal stresses and the maximum shear stress at each point was equal to a specific constant in the plastic region (Jones, 2009; Osakada, 2010).

In 1871, Maurice Levy used Saint-Venant's assumptions except that Levy postulated the direction of the increments of the principal strains, and not the total principal strains, coincided with the direction of principle stresses (Timoshenko, 1953). This was the first attempt to use the incremental flow rule. Moreover, he proposed three-dimensional relations between stress and rate of plastic strain (Hill, 1950).

In 1885, Bauschinger carried out tests to identify stress-strain relations of different metallic materials using a tension-compression testing machine. He found that the yield stress in compression after plastic tensile deformation was significantly lower than the yield stress in tension (Timoshenko, 1953).

In 1882, Otto Mohr presented a graphical representation of stress at a point of a body by plotting circles, known as Mohr's circles, for states of stress at failure in the plane of the maximum and minimum principle stresses. He suggested that the envelope of the circles was a fracture limit (Osakada, 2010).

After Levy, it seemed no further significant studies were conducted before the end of the century but further experiments results, such as by Guest in 1900, were obtained and agreed with Tresca's criterion (Hill, 1950).

In 1904 Huber proposed that the total strain energy was composed of a dilatational (volumetric) component, which depends on the hydrostatic stress, and a distortional (shear) component, which depends on the deviatoric components of stress (Rees, 2006). Moreover, he addressed the failure of brittle material.

Maxwell showed that the hydrostatic stress plays no part upon yielding. In his letter to his friend William Thomson in 1856, he suggested the distortional energy could be used as a yield criterion. He proposed that yielding occurred when the shear strain energy component of the total energy reached a critical value (Rees, 2006).

In 1913, von Mises proposed his famous criterion of plastic yielding, which was physically interpreted by Hencky by stating that plastic yielding occurs when the elastic shear strain energy attains a critical value. Von Mises independently proposed similar equations to Levy's equations (Hill, 1950). He considered the increments of plastic strains components were proportional to the deviatoric stress components.

In 1920 and 1921, Prandtl calculated the loads required to notch a plane surface and a trimmed wedge by a flat die. Nadai conducted experiments and his results were in good agreement with Prandtl's calculations (Hill, 1950).

In 1923 Hencky proposed a general theory underlying the special solutions of Prandtl. Moreover, he established the concept of deformation theory of plasticity. His equations lead to approximately correct results for proportional loading paths without unloading (Hencky, 1924), but do not capture the physics correctly for non-proportional loading or in case of unloading, as will be discussed extensively later and in the following chapters of this thesis.

The applications of plasticity theories to technological processes began in 1925 when von Karman analyzed the state of stresses in rolling of sheet

metal (von Karman, 1925). He presented in his paper the fundamental differential equations, pressure acting on the roll surface and the energy efficiency. Similar studies were made in 1927 by Sachs and Siebel for wire-drawing.

In 1926, Lode measured the deformation of metallic tubes subjected to combined tension and internal pressure. His experimental results validated the Levy-Mises equations with some approximation (Hill, 1950).

The theory of plasticity then was generalized into two ways. The first one, based on assumptions confirmed by experiments made by Homhenemser in 1931, was suggested by Reuss who made allowance for the elastic components of strain, following an early suggestion by Prandtl. The second one was proposed by Schmidt in 1932 and Odquist in 1933, who showed how work hardening could be brought within the framework of Levy-Mises equations (Hill, 1950). In 1932, following all the above-mentioned key contributions, a theory of plasticity for isotropic metals was constructed and validated with experimental observations. Hill (1950) used such theory to solve various metal forming problems using plasticity theory.

2.6 Computational Plasticity

The finite element method (FEM) was developed in the 1950s to study the elastic behaviour of airplane structures. The elastic-plastic FEM was developed as an extension of the elastic FEM. Marca and King (1967) studied elastic-plastic analysis of two-dimensional problem. The incremental stress-strain relationship was derived based on Prandtl-Reuss equations and von Mises yield criterion. Their numerical results for an infinitely long thick cylinder subjected to internal pressure and for plate with a hole subject to tensile stress reasonably agree with test results. In the next year, Yamada et al. (1968) constructed the stress-strain matrix for an elastic-plastic analysis. The FEM motivated researchers in the field of plasticity and numerous papers on metal forming problems began to be published, which required the study of large elastic-plastic deformations (McMeeking and Rice, 1975). From 1980s until now, commercial software for elastic-plastic analysis appeared

and the FE method began to be used in the industry. Many researchers, such as J.C Simo, K.J Bathe , O.C. Zienkiewicz, R.L. Taylor and T.J.R. Hughes and others, published various papers and books in finite element analysis in the field of plasticity, creep and viscoplasticity. Their significant contributions have been implemented in a number of commercial software such as ABAQUS and ADINA.

2.7 Inelastic material behaviour –Elasto-plasticity based on the flow theory

2.7.1 Plastic stress-strain relations

In this section, assuming the elastoplastic response of the material is governed by the classical incremental theory of plasticity, called the flow theory, we will construct the stress-strain matrix in elasto-plasticity for three-dimensional and plane-stress problems. With this approach, in addition to the elastic stress-strain relations, the following three properties characterize the material behaviour:

- the yield criterion is used to identify stress combinations which will initiate the plastic response and to identify initial yield surface;
- the flow rule is used to relate the plastic strain increments to the current stress level and stress increments;
- The hardening rule is employed to identify the evolution of the yield surface as a function of stresses, strains and other parameters.

The yield condition or the yield surface at time t is:

$${}^tF({}^t\sigma_{ij}, {}^t\kappa) = 0 \quad (2.14)$$

where ${}^t\kappa$ is a state variable which depends on the plastic strains ${}^t\varepsilon_{ij}^p$

The flow rule is assumed in the form (Bathe, 1982):

$$d\varepsilon_{ij}^p = {}^t\lambda \frac{\partial {}^tF}{\partial {}^t\sigma_{ij}} = {}^t\lambda q_{ij} \quad (2.15)$$

where ${}^t\lambda$ is a positive scalar at time t . This equation means that the increment of plastic deformation is a vector normal to the yield surface tF .

Using matrix notation

$$\begin{aligned} d\sigma &= \{d\sigma_{11} \quad d\sigma_{22} \quad d\sigma_{33} \quad d\sigma_{12} \quad d\sigma_{23} \quad d\sigma_{31}\}^T \\ d\varepsilon^p &= \{d\varepsilon_{11}^p \quad d\varepsilon_{22}^p \quad d\varepsilon_{33}^p \quad d\varepsilon_{21}^p + d\varepsilon_{12}^p \quad d\varepsilon_{23}^p + d\varepsilon_{32}^p \quad d\varepsilon_{13}^p + d\varepsilon_{31}^p\}^T \end{aligned} \quad (2.16)$$

$${}^t q = \left\{ \frac{\partial {}^t F}{\partial {}^t \sigma_{11}} \quad \frac{\partial {}^t F}{\partial {}^t \sigma_{22}} \quad \frac{\partial {}^t F}{\partial {}^t \sigma_{33}} \quad 2 \frac{\partial {}^t F}{\partial {}^t \sigma_{12}} \quad 2 \frac{\partial {}^t F}{\partial {}^t \sigma_{23}} \quad 2 \frac{\partial {}^t F}{\partial {}^t \sigma_{31}} \right\}^T \quad (2.17)$$

The factor 2 shown in Eq. (2.17) is due to the fact that, in the plastic strain vector shown in Eq. (2.16), the total plastic shear strains increments are the sum of two shear plastic strain increment components.

The total differentiation of the function ${}^t F$ is

$$d {}^t F = \frac{\partial {}^t F}{\partial {}^t \sigma_{ij}} d\sigma_{ij} + \frac{\partial {}^t F}{\partial {}^t \varepsilon_{ij}^p} d\varepsilon_{ij}^p \quad (2.18)$$

By defining

$${}^t \underline{p} = - \left\{ \frac{\partial {}^t F}{\partial {}^t \varepsilon_{11}^p} \quad \frac{\partial {}^t F}{\partial {}^t \varepsilon_{22}^p} \quad \frac{\partial {}^t F}{\partial {}^t \varepsilon_{33}^p} \quad \frac{\partial {}^t F}{\partial {}^t \varepsilon_{12}^p} \quad \frac{\partial {}^t F}{\partial {}^t \varepsilon_{23}^p} \quad \frac{\partial {}^t F}{\partial {}^t \varepsilon_{31}^p} \right\}^T \quad (2.19)$$

then ${}^t F$ can be written

$$d {}^t F = {}^t \underline{q}^T d\sigma - {}^t \underline{p}^T d\varepsilon^p$$

Since, during plastic deformation, ${}^t F = 0$ (Bathe, 1982), we also have

$$d {}^t F = 0$$

$${}^t \underline{q}^T d\sigma - {}^t \underline{p}^T d\varepsilon^p = 0 \quad (2.20)$$

The total rate of strain is assumed to be split into an additive sum of the elastic part and the plastic part

$$d\varepsilon = d\varepsilon^e + d\varepsilon^p \quad (2.21)$$

Then

$$d\varepsilon^e = d\varepsilon - d\varepsilon^p$$

The stress increment is obtained by

$$d\sigma = \underline{\underline{D}}^e d\varepsilon^e = \underline{\underline{D}}^e (d\varepsilon - d\varepsilon^p) \quad (2.22)$$

where $\underline{\underline{D}}^e$ is the matrix of elastic moduli.

Substituting Eq. (2.22) and (2.15) into the first term of Eq. (2.20), we will have

$${}^t \underline{q}^T d\sigma = {}^t \underline{q}^T \left(\underline{\underline{D}}^e (d\varepsilon - d\varepsilon^p) \right) = {}^t \underline{q}^T \left(\underline{\underline{D}}^e (d\varepsilon - {}^t \lambda {}^t \underline{q}) \right)$$

Eq. (2.20) then is

$${}^t\mathbf{q}^T \left(\mathbf{D}^e \left(d\mathbf{\underline{\underline{\varepsilon}}} - {}^t\lambda \mathbf{q}^T \right) \right) = {}^t\mathbf{P}^T {}^t\lambda \mathbf{q}^T$$

Finally

$${}^t\lambda = \frac{{}^t\mathbf{q}^T \mathbf{D}^e d\mathbf{\underline{\underline{\varepsilon}}}}{{}^t\mathbf{q}^T \mathbf{D}^e \mathbf{q} + {}^t\mathbf{P}^T \mathbf{q}} \quad (2.23)$$

Substituting ${}^t\lambda$ from Eq. (2.23) into Eq. (2.15) and then into Eq. (2.22), we get the stress increment as a function of total strain increment

$$d\mathbf{\underline{\underline{\sigma}}} = \mathbf{D}^{ep} d\mathbf{\underline{\underline{\varepsilon}}} \quad (2.24)$$

where \mathbf{D}^{ep} is the instantaneous elastic-plastic stress-strain (tangent) matrix:

$$\mathbf{D}^{ep} = \mathbf{D}^e - \frac{\mathbf{D}^e \mathbf{q} \left(\mathbf{D}^e \mathbf{q} \right)^T}{{}^t\mathbf{P}^T \mathbf{q} + {}^t\mathbf{q}^T \mathbf{D}^e \mathbf{q}} \quad (2.25)$$

The above stress-strain matrix depends on the yield function tF , the current stress and on the plastic strains, which are related to the history of strains.

The matrix enters in the evaluation of the stress increment from time t to time $t + \Delta t$. If the stress at time t is known, then the stress corresponding to time $t + \Delta t$ is calculated using (Bathe, 1982)

$${}^{t+\Delta t}\mathbf{\underline{\underline{\sigma}}} = {}^t\mathbf{\underline{\underline{\sigma}}} + \int_t^{t+\Delta t} d\mathbf{\underline{\underline{\sigma}}} = {}^t\mathbf{\underline{\underline{\sigma}}} + \int_{{}^t\mathbf{\underline{\underline{\varepsilon}}}}^{t+\Delta t} \mathbf{D}^{ep} d\mathbf{\underline{\underline{\varepsilon}}} \quad (2.26)$$

Various well-known schemes for integration of Eq. (2.26) have been proposed in the literature and can be classified into explicit and implicit categories (Zienkiewicz and Taylor, 2005) and (Bathe, 1982).

2.7.2 Classical yield surfaces

The general procedure outlined in the previous section allows us to determine the elastic-plastic matrix for any yield surface employed in practice.

The three deviatoric stress invariants at time t are:

$$\begin{aligned} {}^tI_1 &= {}^t\sigma_{ii} \\ {}^tJ_2 &= \frac{1}{2} {}^t s_{ij} {}^t s_{ij} \end{aligned} \quad (2.27)$$

$${}^tJ_3 = \frac{1}{3} {}^t\sigma_{ij} {}^t\sigma_{jk} {}^t\sigma_{ki}$$

in which $\underline{{}^t\sigma}$ is the deviatoric stress

$$\begin{aligned} {}^t\sigma_{ij} &= {}^t\sigma_{ij} - \delta_{ij} {}^t\sigma_m \\ {}^t\sigma_m &= \frac{1}{3} {}^tI_1 = \frac{1}{3} ({}^t\sigma_{11} + {}^t\sigma_{22} + {}^t\sigma_{33}) \end{aligned} \quad (2.28)$$

where δ_{ij} is the Kronecker delta

$$\delta_{ij} = \begin{cases} 0; i \neq j \\ 1; i = j \end{cases} \quad (2.29)$$

Useful form of these invariants for use in yield conditions is (Zienkiewicz and Taylor, 2005):

$$\begin{aligned} {}^t\sigma_m &= \frac{1}{3} {}^tI_1 \\ {}^t\sigma_f &= \sqrt{{}^tJ_2} \\ {}^t\theta &= \frac{1}{3} \sin^{-1} \left(-\frac{3\sqrt{3} {}^tJ_3^{\frac{1}{3}}}{2 {}^t\sigma_f} \right) \quad \text{with} \quad -\frac{\pi}{6} \leq \theta \leq \frac{\pi}{6} \end{aligned} \quad (2.30)$$

Using these definitions and stress invariants, several yield conditions can be given:

1. Tresca yield condition (Zienkiewicz and Taylor, 2005):

$${}^tF = 2 {}^t\sigma_f \cos {}^t\theta - {}^tY(\kappa) \quad (2.31)$$

where ${}^tY(\kappa)$ is function of the isotropic hardening parameter κ .

2. Von Mises yield condition (Bathe, 1982):

$${}^tF = {}^tJ_2 - {}^t\kappa \quad (2.32)$$

where ${}^t\kappa$ at time t is (Bathe, 1982)

$${}^t\kappa = \frac{1}{3} {}^t\sigma_y^2 \quad (2.33)$$

${}^t\sigma_y$ is the yield stress at time t . In the case of von Mises theory, the yield condition only depends on the value of the second invariant of the deviatoric stress, J_2 . For this reason this theory is also known as a J_2 theory.

Conditions 1 and 2 are widely used in metal plasticity. For soils, concrete and other 'frictional' materials the Mohr-Coulomb or Drucker-Prager surfaces are used.

3. The Mohr-Coulomb yield function is (Zienkiewicz and Taylor, 2005):

$${}^tF = {}^t\sigma_m \sin \phi + {}^t\sigma_f \left(\cos {}^t\theta - \frac{1}{\sqrt{3}} \sin \phi \sin {}^t\theta \right) - c \cos \phi \quad (2.34)$$

where c and ϕ are the cohesive strength and the angle of friction of the material, respectively. They are function of the isotropic hardening parameter or constant for the case of perfect plasticity.

4. The Drucker-Prager yield function is (Zienkiewicz and Taylor, 2005):

$${}^tF = 3\alpha {}^t\sigma_m + {}^t\sigma_f - k \quad (2.35)$$

where α and k are material property parameters.

$$\alpha = \frac{2 \sin \phi}{\sqrt{3} (3 - \sin \phi)}$$

$$k = \frac{6 \cos \phi}{\sqrt{3} (3 - \sin \phi)} \quad (2.36)$$

Next we consider the von Mises yield condition with isotropic hardening to construct the elastic-plastic matrix.

We have from Eq. (2.32)

$${}^tF = {}^tJ_2 - \frac{1}{3} {}^t\sigma_y^2$$

$${}^tJ_2 = \frac{1}{2} {}^t s_{ij} {}^t s_{ij} = \frac{1}{2} ({}^t s_{11}^2 + {}^t s_{22}^2 + {}^t s_{33}^2 + 2 {}^t s_{12}^2 + 2 {}^t s_{23}^2 + 2 {}^t s_{31}^2)$$

To obtain $\underline{\underline{D}}^{ep}$ from Eq. (2.25), we need to find ${}^t\underline{q}$ and ${}^t\underline{p}$.

To find ${}^t\underline{p}$:

$${}^t\underline{p} = \frac{\partial {}^tF}{\partial {}^t\varepsilon_{ij}^p} = \frac{\partial {}^tF}{\partial {}^t\sigma_y} \frac{\partial {}^t\sigma_y}{\partial {}^t\varepsilon_{ij}^p} = -\frac{2}{3} {}^t\sigma_y \frac{\partial {}^t\sigma_y}{\partial {}^t\varepsilon_{ij}^p} \quad (2.37)$$

Thus we need to find the relation between ${}^t\sigma_y$ and the plastic strains

One way to formulate this equation is to assume hardening is a function of the plastic work, which takes the form

$${}^tW_P = \int_0^{t\varepsilon_{ij}^p} {}^t\sigma_{ij} d\varepsilon_{ij}^p \quad (2.38)$$

Therefore

$$\frac{\partial {}^t W_P}{\partial {}^t \varepsilon_{ij}^p} = {}^t \sigma_{ij}$$

Substituting into Eq. (2.37), one can find

$$\frac{\partial {}^t F}{\partial {}^t \varepsilon_{ij}^p} = -\frac{2}{3} {}^t \sigma_y \frac{\partial {}^t \sigma_y}{\partial {}^t W_P} \frac{\partial {}^t W_P}{\partial {}^t \varepsilon_{ij}^p} = -\frac{2}{3} {}^t \sigma_y \frac{\partial {}^t \sigma_y}{\partial {}^t W_P} {}^t \sigma_{ij} = -A {}^t \sigma_{ij} \quad (2.39)$$

where

$${}^t A = \frac{2}{3} {}^t \sigma_y \frac{\partial {}^t \sigma_y}{\partial {}^t W_P} \quad (2.40)$$

The variable ${}^t A$ is zero in perfect plasticity.

Considering 1-D test result and linear hardening, the current yield stress can be written in term of the plastic work from time 0 to t (Figure 2.10):

$${}^t W_P = \frac{1}{2} \left(\frac{1}{E_t} - \frac{1}{E} \right) ({}^t \sigma_y^2 - {}^0 \sigma_y^2)$$

where E is the elastic modulus and E_t is tangent modulus or strain hardening modulus of the material.

By differentiation of both side of this equation, one can obtain

$$\frac{\partial {}^t \sigma_y}{\partial {}^t W_P} = \frac{E E_t}{E - E_t} \frac{1}{{}^t \sigma_y} \quad (2.41)$$

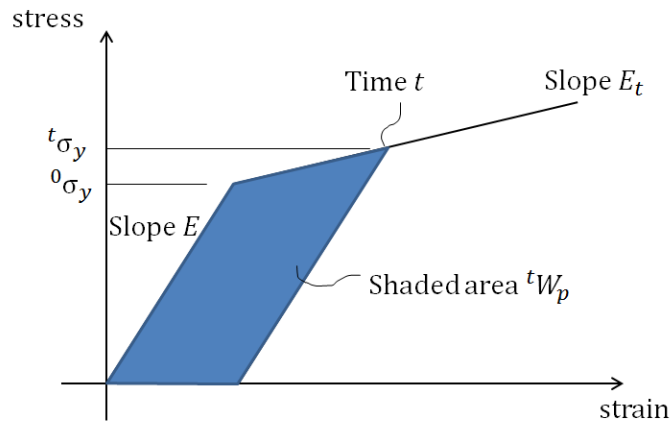


Figure 2.10: the stress-strain of a material for 1-D test

Substituting into Eq. (2.41) into Eq. (2.40)

$${}^tA = \frac{2}{3} {}^t\sigma_y \frac{E E_t}{E - E_t} \frac{1}{{}^t\sigma_y} = \frac{2}{3} \frac{E E_t}{E - E_t} \quad (2.42)$$

Finally

$$\underline{{}^tP} = -\frac{\partial {}^tF}{\partial \underline{{}^t\varepsilon^p}} = {}^tA \{ {}^t\sigma_{11} \quad {}^t\sigma_{22} \quad {}^t\sigma_{33} \quad {}^t\sigma_{12} \quad {}^t\sigma_{23} \quad {}^t\sigma_{31} \}^T \quad (2.43)$$

It is proven from Bathe (1982) that the matrix $\underline{{}^tq}$ is

$$\underline{{}^tq} = \{ {}^tS_{11} \quad {}^tS_{22} \quad {}^tS_{33} \quad 2 {}^tS_{12} \quad 2 {}^tS_{23} \quad 2 {}^tS_{31} \}^T \quad (2.44)$$

By setting

$$\begin{aligned} a &= \underline{{}^tP}^T \underline{{}^tq} \\ \underline{b} &= \underline{\underline{D}}^e \underline{{}^tq} \\ c &= \underline{{}^tq}^T \underline{\underline{D}}^e \underline{{}^tq} = \underline{{}^tq}^T \underline{b} \end{aligned} \quad (2.45)$$

we can now evaluate $\underline{\underline{D}}^{ep}$:

$$\underline{\underline{D}}^{ep} = \underline{\underline{D}}^e - \frac{\underline{b} \underline{b}^T}{a + c} \quad (2.46)$$

The stress-strain increments are therefore related as follows:

$$d\underline{\underline{\sigma}} = \underline{\underline{D}}^{ep} d\underline{\underline{\varepsilon}}$$

Using the rate form of the stresses and strains in which $d\underline{\underline{\sigma}} = \underline{\dot{\underline{\sigma}}} dt$

$$\underline{\dot{\underline{\sigma}}} = \underline{\underline{D}}^{ep} \underline{\dot{\underline{\varepsilon}}}$$

$\underline{\underline{D}}^e$ is the 6×6 matrix of elastic. Using the index notation

$$D_{ijkl}^e = \lambda \delta_{ij} \delta_{kl} + G (\delta_{ik} \delta_{jl} + \delta_{il} \delta_{jk}) \quad (2.47)$$

where λ is Lamé's elastic constant and G is the shear modulus

$$\lambda = \frac{\nu E}{(1 + \nu)(1 - 2\nu)} \quad , \quad G = \frac{E}{2(1 + \nu)} \quad (2.48)$$

$\underline{\underline{D}}^{ep}$ is a 6×6 matrix too and represents the instantaneous tangent elastic-plastic stress-strain matrix. Using the index notation, the stress rate is

$$\dot{\sigma}_{ij} = D_{ijkl}^{ep} \dot{\varepsilon}_{kl} \quad (2.49)$$

and the von Mises effective stress is

$${}^t\bar{\sigma} = \sqrt{3 {}^tJ_2}$$

2.7.3 The Prandtl-Reuss equations for plane stress assumption

Let consider a point of a plate or a shell, whose mid plane is plane 1-2, and let assume they are in a state of plane stress, so that we have $\dot{\epsilon}_{23} = \dot{\epsilon}_{31} = \dot{\sigma}_{33} = 0$. Thus the constitutive equation in rate form (Eq. (2.49)) is reduced to the form

$$\dot{\sigma}_{\alpha\beta} = \overline{D}_{\alpha\beta\kappa\gamma}^{ep} \dot{\epsilon}_{\kappa\gamma} \quad (2.50)$$

$\overline{D}_{\alpha\beta\kappa\gamma}^{ep}$ is the plane-stress moduli which is given in term of the three dimensional quantities by (Hutchinson, 1974)

$$\overline{D}_{\alpha\beta\kappa\gamma}^{ep} = D_{\alpha\beta\kappa\gamma}^{ep} - \frac{D_{\alpha\beta 33}^{ep} D_{33\kappa\gamma}^{ep}}{D_{3333}^{ep}} \quad (2.51)$$

where α, β, κ and γ range from 1 to 2. Thus $\underline{\underline{\overline{D}}}^{ep}$ is 2×2 matrix.

For the case of cylindrical shells subjected to non-proportional loading, which are the external pressure and the axial load, assuming 1 and 2 are the axial and hoop directions, the applied stresses ${}^t\sigma_{12} = {}^t\sigma_{23} = {}^t\sigma_{31} = {}^t\sigma_{33} = 0$ and ${}^t\sigma_{11} \neq 0, {}^t\sigma_{22} \neq 0$

Let denote by x the axis of the shell and by r an axis orthogonal to x on a reference cross section, defining a radial direction. Introducing an angle $\theta \in [0, 2\pi]$, (x, θ, r) defines a set of cylindrical coordinates for the cylindrical shell. Using the this alternative notation, the applied stresses are ${}^t\sigma_{11} = \sigma_{xx}$ and ${}^t\sigma_{22} = \sigma_{\theta\theta}$.

Substituting into Eqs. (2.43), (2.44) and (2.45), the rate form of the constitutive Eq. (2.50) is

$$\begin{bmatrix} \dot{\sigma}_{xx} \\ \dot{\sigma}_{\theta\theta} \\ \dot{\tau}_{x\theta} \end{bmatrix} = \frac{E}{1+\nu} \begin{bmatrix} \alpha & \beta & 0 \\ \beta & \gamma & 0 \\ 0 & 0 & \frac{2+2\nu}{E} G \end{bmatrix} \begin{bmatrix} \dot{\epsilon}_{xx} \\ \dot{\epsilon}_{\theta\theta} \\ \dot{\epsilon}_{x\theta} \end{bmatrix} \quad (2.52)$$

The expressions of α, β and γ are

$$\alpha = \frac{1+\nu}{\rho} \left[4 - 3 \left(1 - \frac{E_t}{E} \right) \frac{\sigma_{xx}^2}{\bar{\sigma}^2} \right] \quad (2.53)$$

$$\beta = \frac{1+\nu}{\rho} \left[2 - 2(1-2\nu) \frac{E_t}{E} - 3 \left(1 - \frac{E_t}{E} \right) \frac{\sigma_{xx}\sigma_{\theta\theta}}{\bar{\sigma}^2} \right]$$

$$\gamma = \frac{1+\nu}{\rho} \left[4 - 3 \left(1 - \frac{E_t}{E} \right) \frac{\sigma_{\theta\theta}^2}{\bar{\sigma}^2} \right]$$

$$\rho = (5-4\nu) - (1-2\nu)^2 \frac{E_t}{E} - 3(1-2\nu) \left(1 - \frac{E_t}{E} \right) \frac{\sigma_{xx}\sigma_{\theta\theta}}{\bar{\sigma}^2}$$

$$G = \frac{E}{2(1+\nu)}$$

The effective stress $\bar{\sigma}$ is written with the assumption of plane stress as follows

$$\bar{\sigma}^2 = \sigma_{xx}^2 - \sigma_{xx}\sigma_{\theta\theta} + \sigma_{\theta\theta}^2 \quad (2.54)$$

2.8 Inelastic material behaviour –Elasto-plasticity based on the deformation theory

Hencky (1947) proposed total stress-strain relations in which the total strain components are related directly to the total current stress components. The total plastic strain is (Mendelson, 1968) (Jahed et al., 1998)

$$\varepsilon_{ij}^p = \frac{3}{2} \frac{\bar{\varepsilon}^p}{\bar{\sigma}} s_{ij} \quad (2.55)$$

where s_{ij} , $\bar{\sigma}$ and $\bar{\varepsilon}^p$ are the deviatoric stress, the effective stress and the effective plastic strain, respectively.

The above equation shows that the plastic strains are functions of the current state of the stress and independent from the loading history. This assumption significantly simplifies the plastic problem with respect to the actual physical behaviour, since experimental evidence shows that the plastic strain is generally dependent of the loading path. Therefore, the deformation theory generally cannot provide correct results (Mendelson, 1968; Hill, 1950). However, for the case of proportional and monotonic loading, in which all stress components monotonically increase with a constant ratio between each other, the flow theory and the deformation theory are identical. Moreover, Budiansky (1959) proposed that the deformation theory of plasticity can be employed for a range of loading paths other than proportional loading when the deformation theory satisfies postulates and

assumptions proposed by Drucker to develop the general incremental theory of plasticity.

To derive the specific expression of Eq. (2.55), it is observed that, in the assumption of small strains, the total strain can still be written in terms of elastic and plastic strain parts as

$$\varepsilon_{ij} = \varepsilon_{ij}^e + \varepsilon_{ij}^p \quad (2.56)$$

According to the generalized Hooke's law; the elastic strain is given by

$$\varepsilon_{ij}^e = \frac{1 + \nu}{E} s_{ij} + \frac{1 - 2\nu}{E} \delta_{ij} \sigma_m \quad (2.57)$$

Replacing into Eq. (2.56)

$$E \varepsilon_{ij} = (1 + \nu) s_{ij} + (1 - 2\nu) \delta_{ij} \sigma_m + \frac{3}{2} E \frac{\bar{\varepsilon}^p}{\bar{\sigma}} s_{ij} \quad (2.58)$$

This relation is used in the commercial code ABAQUS (Simulia, 2011) in combination with Ramberg-Osgood formula.

The plastic strain part of the Ramberg-Osgood for a multi-axial stress state is

$$E \bar{\varepsilon}^p = \alpha \left(\frac{\bar{\sigma}}{\sigma_y} \right)^{n-1} \bar{\sigma} \quad (2.59)$$

where E and ν are Young's modulus and Poisson's ratio, respectively, σ_y is the nominal yield strength (sometimes called 'proof stress' and denoted by $\sigma_{0.2\%}$, as it is the yield strength corresponding to an effective plastic strain of 0.2%), α is the 'yield offset' and n is the strain hardening parameter.

Substituting Eq. (2.59) into Eq. (2.58), one can obtain

$$E \varepsilon_{ij} = (1 + \nu) s_{ij} + (1 - 2\nu) \delta_{ij} \sigma_m + \frac{3}{2} \alpha \left(\frac{\bar{\sigma}}{\sigma_y} \right)^{n-1} s_{ij} \quad (2.60)$$

Eq. (2.60) is the constitutive model employed in ABAQUS using the deformation theory of plasticity (Simulia, 2011).

2.8.1 The Hencky equations for plane stress assumption

For an isotropic material, the J_2 deformation theory depends on the effective stress $\bar{\sigma}$ and strain $\bar{\varepsilon}$. The effective stress is given as a function of the multi-axial stress by

$$\bar{\sigma} = \sqrt{3 J_2} \quad (2.61)$$

in which the second invariant of the deviatoric stress J_2 can be written in term of the stress invariants I_1 and I_2 (Jones, 2009)

$$J_2 = \frac{1}{2} s_{ij} s_{ij} = \frac{1}{3} I_1^2 - I_2$$

where

$$I_1 = \sigma_{ij}$$

$$I_2 = \frac{1}{2} (\sigma_{ii} \sigma_{jj} - \sigma_{ij} \sigma_{ij})$$

The effective strain is given as

$$\bar{\varepsilon} = \sqrt{\frac{2}{3} \varepsilon_{ij} \varepsilon_{ij}}$$

Those quantities relate together by

$$\bar{\sigma} = E_s \bar{\varepsilon}$$

The incremental form of the those quantities relate together as follows

$$d\bar{\sigma} = E_t d\bar{\varepsilon}$$

where $d\bar{\sigma}$ and $d\bar{\varepsilon}$ are the effective stress and the total effective strain increments, respectively.

During buckling, the stresses, strains and secant modulus E_s vary from their pre-buckling value. Let the variation be denoted by d . Then the variation of the Eq. (2.55) is

$$\begin{aligned} d\varepsilon_{ij}^p &= \frac{3}{2} \left(\frac{d\bar{\varepsilon}^p \bar{\sigma} - d\bar{\sigma} \bar{\varepsilon}^p}{\bar{\sigma}^2} \right) s_{ij} + \frac{3}{2} \frac{\bar{\varepsilon}^p}{\bar{\sigma}} ds_{ij} \\ d\varepsilon_{ij}^p &= \frac{3}{2} \frac{d\bar{\sigma}}{\bar{\sigma}} \left(\frac{d\bar{\varepsilon}^p}{d\bar{\sigma}} - \frac{\bar{\varepsilon}^p}{\bar{\sigma}} \right) s_{ij} + \frac{3}{2} \frac{\bar{\varepsilon}^p}{\bar{\sigma}} ds_{ij} \end{aligned} \quad (2.62)$$

We have the following relations

$$\frac{\bar{\varepsilon}^p}{\bar{\sigma}} = \frac{\bar{\varepsilon} - \bar{\varepsilon}^e}{\bar{\sigma}} = \frac{1}{E_s} - \frac{1}{E}$$

$$\frac{d\bar{\varepsilon}^p}{d\bar{\sigma}} = \frac{d\bar{\varepsilon} - d\bar{\varepsilon}^e}{d\bar{\sigma}} = \frac{1}{E_t} - \frac{1}{E}$$

Substituting them into Eq. (2.62), one obtains

$$d\varepsilon_{ij}^p = \frac{3}{2} \frac{d\bar{\sigma}}{\bar{\sigma}} \left(\frac{1}{E_t} - \frac{1}{E_s} \right) s_{ij} + \frac{3}{2} \left(\frac{1}{E_s} - \frac{1}{E} \right) ds_{ij} \quad (2.63)$$

$d\bar{\varepsilon}^p$ and $d\bar{\varepsilon}^e$ are the effective plastic and elastic strain increment, respectively.

From Eq. (2.56), the incremental form of the total strain is

$$d\varepsilon_{ij} = d\varepsilon_{ij}^e + d\varepsilon_{ij}^p \quad (2.64)$$

where $d\varepsilon_{ij}^e$ is the elastic strain increment. Computing the variation of Eq. (2.57), one has

$$d\varepsilon_{ij}^e = \frac{1+\nu}{E} ds_{ij} + \frac{1-2\nu}{E} \delta_{ij} d\sigma_m \quad (2.65)$$

Substituting Eqs. (2.63) and (2.65) into (2.64), one has

$$d\varepsilon_{ij} = \frac{1+\nu}{E} ds_{ij} + \frac{1-2\nu}{E} \delta_{ij} d\sigma_m + \frac{3}{2} \frac{d\bar{\sigma}}{\bar{\sigma}} \left(\frac{1}{E_t} - \frac{1}{E_s} \right) s_{ij} + \frac{3}{2} \left(\frac{1}{E_s} - \frac{1}{E} \right) ds_{ij}$$

or

$$d\varepsilon_{ij} = \left(\frac{3}{2E_s} - \frac{1-2\nu}{2E} \right) ds_{ij} + \frac{1-2\nu}{E} \delta_{ij} d\sigma_m + \frac{3}{2} \frac{d\bar{\sigma}}{\bar{\sigma}} \left(\frac{1}{E_t} - \frac{1}{E_s} \right) s_{ij}$$

Using the rate form of the stresses and strains

$$\dot{\varepsilon}_{ij} = \left(\frac{3}{2E_s} - \frac{1-2\nu}{2E} \right) \dot{s}_{ij} + \frac{1-2\nu}{E} \delta_{ij} \dot{\sigma}_m + \frac{3}{2} \frac{\dot{\bar{\sigma}}}{\bar{\sigma}} \left(\frac{1}{E_t} - \frac{1}{E_s} \right) s_{ij} \quad (2.66)$$

Assuming that the plate and shell problems are in a state of approximate plane stress, one can assume $\dot{\varepsilon}_{23} = \dot{\varepsilon}_{31} = \dot{\varepsilon}_{33} = 0$. Thus the constitutive equation in rate form Eq. (2.66) is reduced to the form

$$\dot{\varepsilon}_{\alpha\beta} = \left(\frac{3}{2E_s} - \frac{1-2\nu}{2E} \right) \dot{s}_{\alpha\beta} + \frac{1-2\nu}{E} \delta_{\alpha\beta} \dot{\sigma}_m + \frac{3}{2} \frac{\dot{\bar{\sigma}}}{\bar{\sigma}} \left(\frac{1}{E_t} - \frac{1}{E_s} \right) s_{\alpha\beta} \quad (2.67)$$

where α and β range from 1 to 2

For cylindrical shells subjected to non-proportional loading, let σ_{xx} and $\sigma_{\theta\theta}$ denote the non-zero applied stresses, again with x and θ coinciding with axes 1 and 2, respectively. The effective stress (Eq. (2.61)) is

$$\bar{\sigma}^2 = \sigma_{xx}^2 - \sigma_{xx} \sigma_{\theta\theta} + \sigma_{\theta\theta}^2 \quad (2.68)$$

A straightforward differentiation of Eq. (2.68) gives

$$\frac{d\bar{\sigma}}{\bar{\sigma}} = \frac{(2\sigma_{xx} - \sigma_{\theta\theta}) d\sigma_{xx} + (2\sigma_{\theta\theta} - \sigma_{xx}) d\sigma_{\theta\theta}}{2 \bar{\sigma}^2}$$

The constitutive Eq. (2.67) therefore furnishes

$$\begin{aligned} \dot{\varepsilon}_{xx} &= \frac{1}{2} \left(\frac{1}{E_s} - \frac{1-2\nu}{3E} \right) (2\dot{\sigma}_{xx} - \dot{\sigma}_{\theta\theta}) + \frac{1-2\nu}{3E} (\dot{\sigma}_{xx} + \dot{\sigma}_{\theta\theta}) + \frac{(2\sigma_{xx} - \sigma_{\theta\theta})}{4\bar{\sigma}^2} \left(\frac{1}{E_t} - \frac{1}{E_s} \right) ((2\sigma_{xx} - \sigma_{\theta\theta}) \dot{\sigma}_{xx} + (2\sigma_{\theta\theta} - \sigma_{xx}) \dot{\sigma}_{\theta\theta}) \\ \dot{\varepsilon}_{\theta\theta} &= \frac{1}{2} \left(\frac{1}{E_s} - \frac{1-2\nu}{3E} \right) (2\dot{\sigma}_{\theta\theta} - \dot{\sigma}_{xx}) + \frac{1-2\nu}{3E} (\dot{\sigma}_{xx} + \dot{\sigma}_{\theta\theta}) + \frac{(2\sigma_{\theta\theta} - \sigma_{xx})}{4\bar{\sigma}^2} \left(\frac{1}{E_t} - \frac{1}{E_s} \right) ((2\sigma_{xx} - \sigma_{\theta\theta}) \dot{\sigma}_{xx} + (2\sigma_{\theta\theta} - \sigma_{xx}) \dot{\sigma}_{\theta\theta}) \\ \dot{\varepsilon}_{x\theta} &= \frac{1}{2} \left(\frac{3}{E_s} - \frac{1-2\nu}{E} \right) \dot{\tau}_{x\theta} \end{aligned}$$

After some algebraic manipulations, the above equations are reduced to

$$\begin{aligned} E_t \dot{\varepsilon}_{xx} &= \left(1 - \left(1 - \frac{E_t}{E_s} \right) \frac{3\sigma_{\theta\theta}^2}{4\bar{\sigma}^2} \right) \dot{\sigma}_{xx} - \left\{ \frac{1}{2} \left[1 - (1-2\nu) \frac{E_t}{E} - 3 \left(1 - \frac{E_t}{E_s} \right) \left(\frac{\sigma_{xx}\sigma_{\theta\theta}}{2\bar{\sigma}^2} \right) \right] \right\} \dot{\sigma}_{\theta\theta} \\ E_t \dot{\varepsilon}_{\theta\theta} &= \left\{ \frac{1}{2} \left[1 - (1-2\nu) \frac{E_t}{E} - 3 \left(1 - \frac{E_t}{E_s} \right) \left(\frac{\sigma_{xx}\sigma_{\theta\theta}}{2\bar{\sigma}^2} \right) \right] \right\} \dot{\sigma}_{xx} + \left(1 - 3 \left(1 - \frac{E_t}{E_s} \right) \frac{\sigma_{xx}^2}{4\bar{\sigma}^2} \right) \dot{\sigma}_{\theta\theta} \\ E_t \dot{\varepsilon}_{x\theta} &= \frac{1}{2} \left(\frac{3E_t}{E_s} - (1-2\nu) \frac{E_t}{E} \right) \dot{\tau}_{x\theta} \end{aligned}$$

The above relations can be inverted to give the constitutive relations in the form

$$\begin{aligned} \dot{\sigma}_{xx} &= \frac{E}{1+\nu} (\alpha \dot{\varepsilon}_{xx} + \beta \dot{\varepsilon}_{\theta\theta}) \\ \dot{\sigma}_{\theta\theta} &= \frac{E}{1+\nu} (\beta \dot{\varepsilon}_{xx} + \gamma \dot{\varepsilon}_{\theta\theta}) \\ \dot{\tau}_{x\theta} &= \frac{E}{1+\nu} \left(\frac{2+2\nu}{E} G \dot{\varepsilon}_{x\theta} \right) \end{aligned} \quad (2.69)$$

The expressions of α , β and γ are

$$\begin{aligned}
\alpha &= \frac{1+\nu}{\rho} \left[4 - 3 \left(1 - \frac{E_t}{E_s} \right) \frac{\sigma_{xx}^2}{\bar{\sigma}^2} \right] \\
\beta &= \frac{1+\nu}{\rho} \left[2 - 2(1-2\nu) \frac{E_t}{E} - 3 \left(1 - \frac{E_t}{E_s} \right) \frac{\sigma_{xx}\sigma_{\theta\theta}}{\bar{\sigma}^2} \right] \\
\gamma &= \frac{1+\nu}{\rho} \left[4 - 3 \left(1 - \frac{E_t}{E_s} \right) \frac{\sigma_{\theta\theta}^2}{\bar{\sigma}^2} \right] \\
\rho &= 3 \frac{E}{E_s} + (1-2\nu) \left[2 - (1-2\nu) \frac{E_t}{E} - 3 \left(1 - \frac{E_t}{E_s} \right) \frac{\sigma_{xx}\sigma_{\theta\theta}}{\bar{\sigma}^2} \right] \\
G &= \frac{E}{2(1+\nu) + 3 \left(\frac{E}{E_s} - 1 \right)}
\end{aligned} \tag{2.70}$$

2.9 Plastic buckling paradox

During investigations of plastic buckling of plates and shells subjected to uniform stresses, the plastic paradox appeared. Use of the deformation theory of plasticity predicts buckling loads that are smaller than those obtained with the incremental (or flow) theory, and physical evidence obtained by comparing measured and calculated buckling loads points in favour of the results predicted by the deformation theory. This discrepancy was pronounced in the case of axially compressed cruciform column in which the test results seem to be in better agreement with the deformation theory than the flow theory. Onat and Drucker (1953) pointed out through an approximate analysis that cruciform columns with very small initial twist and modelled using the flow theory were predicted to collapse at loads which were slightly above the bifurcation loads predicted by deformation theory. Apparently, a small amount of shear strains in the pre-bifurcation analysis was enough to reduce the effective shear modulus of the flow theory from the elastic value G to the value near the effective shear modulus predicted by deformation theory (Bushnell, 1982). The extreme sensitivity of shear modulus in a cruciform column to small imperfections-related shearing forces applied, while the material is stressed into plastic range, led to use the effective shear modulus predicted by the deformation theory in the bifurcation analyses. Therefore, Bushnell (1982) suggested using the flow theory with the shear modulus predicted by the deformation theory. The purpose of this

strategy is to eliminate much of the discrepancy in buckling predictions between the flow theory and the deformation theory (Bushnell, 1982).

There have been many other attempts to explain this so called “plastic buckling paradox” and to formulate accurate methods based on the flow theory of plasticity, that typically differ from each other on account of the choice and formulation of the constitutive equations and of the associated factors. For instance, Drucker (1949) pointed out that if a small initial imperfection or twist in a compressed plate is taken into account, the shear modulus predicted by the flow theory will greatly reduce and may well provide the reason of the paradox. Batdorf and Budiansky (1949) suggested using the slip theory in plastic buckling analysis. Sewell (1973) proposed the use of Tresca yield surface in the flow theory of plasticity which led to significant reductions in the buckling loads. Lay (1965) proposed that the effective shear modulus should be employed when using the flow theory, whereas Ambartsumjan (1963) recommended considering the transverse shear deformation.

Hutchinson and Budiansky (1976) showed again that more accurate results can be obtained in the case of the flow theory if extremely small imperfections on axially compressed cruciform columns are taken into account. Furthermore, in another paper, Hutchinson (1972) investigated the post-buckling behaviour of perfect and imperfect spherical shells under external pressure, in order to study the imperfection sensitivity of structures in the plastic range. He found, as is typical for plates and shells, that the bifurcation pressures predicted by the deformation theory were lower than those predicted by the flow theory. However, plastic buckling pressures predicted by the flow theory tend to those predicted by the deformation theory if small but unavoidable imperfections were taken into account. Moreover, he found that the imperfections had strong effect on the bifurcation pressures: the more the imperfections, the lower the bifurcation pressures in plastic range. This indicated that the imperfection-sensitivity was potentially important in the plastic range for spherical shells. However, the imperfection sensitivity in the plastic range is not as severe a problem as it is for elastic

range of the structures because the plastic buckling of structure requires high thickness-to-radius ratio, whereby it is less difficult to manufacture shells or panels with relatively very small imperfections.

Durban and Zuckerman (1999) examined analytically the elastoplastic bifurcation of rectangular plate subjected to simultaneous biaxial loads (uniform compressive load $\sigma_2 = -\sigma$ and tensile or compressive load $\sigma_1 = \xi\sigma$ in the perpendicular direction, where ξ is the 'biaxial loading ratio' or also, the 'loading path'). Different thickness ratios, aspect ratios, loading parameters and boundary conditions were considered and studied in the analyses. They observed, for all sets of boundary conditions, the plastic buckling stress σ_{cr} predicted by the flow theory were consistently higher than those predicted by the deformation theory. They found that the flow theory is more sensitive to the stabilizing tensile load than the deformation theory, which can considerably delay buckling. The authors clarified that, for all sets of considered boundary conditions, the deformation theory predicted an optimal loading path ξ , at which the compressive buckling load reached a maximum (see Figure 2.11, curve (a)), while the flow theory never detected such an optimal path loading over all range of the parameters investigated (Figure 2.11, curve (b)). However, in certain cases, with the flow theory a local minimum of the $\sigma_{cr} - \xi$ curve could be detected, as shown in Figure 2.11, curve (c).

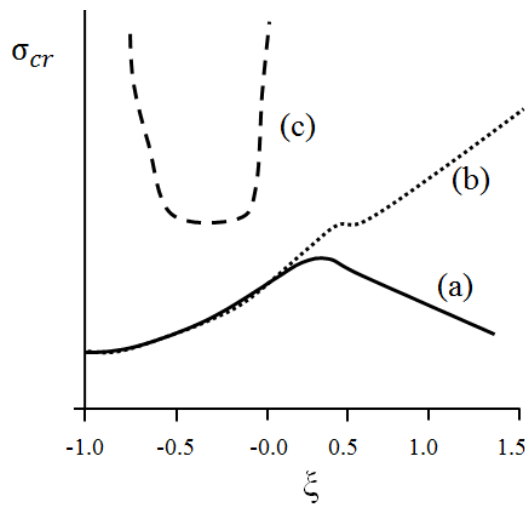


Figure 2.11: variation of buckling stress over a range of loading parameter ξ (qualitatively adopted from Durban and Zuckerman (1999))

In order to consider the effect of the transverse shear deformation, Wang et al. (2001) employed the Mindlin thick plate theory in the analytical study of the elastic-plastic buckling of rectangular plates subjected to uniaxial or equibiaxial loading and circular plates subjected to uniform radial load. As expected, they found that the buckling stresses predicted by the deformation theory were lower than the corresponding results predicted by the flow theory. Moreover, they showed that, for simply supported circular plates, both theories predicted almost similar buckling stresses while for clamped plates, the buckling stresses differed significantly using the flow and deformation theories.

More recently, Kadkhodayan and Maarefdoust (2014) investigated analytically the plastic buckling of thin rectangular plate under various boundary conditions and loads. The in-plane loads were applied either uniformly or linearly varying. Both the flow and deformation theories of plasticity were considered in their analysis and the differential quadrature method (DQM) was employed to solve the stability equations. It was found that the discrepancies between the results of the flow and deformation theories increase by applying boundary conditions closer to fully clamped and by increasing thickness-to-length ratio, biaxial loading parameter and linear loading parameter in linearly varying in-plane loading. Moreover, agreement between the flow theory and the deformation theory results were found more in the case of equibiaxial loading rather than for uniaxial loading.

In another recent paper, Wang and Huang (2009) examined analytically the elastoplastic buckling of a rectangular plate made of alloy Al 7075 T6, typically used in the aerospace industry, subjected to biaxial loading (again with $\sigma_2 = -\sigma$ and tension or compression load $\sigma_1 = \xi\sigma$ in the perpendicular direction). A detailed parametric study was made using the differential quadrature method (DQ) and the authors concluded that the small deformation assumption used to establish the governing differential equation could possibly be the reason for the large discrepancy between the results obtained using either deformation or flow theory. In a later paper, Zhang and Wang (2011) used the DQ method to obtain the analytically elastoplastic

buckling stresses for thick rectangular plates with various values of the thickness-to-side-length ratio, and for various material properties and boundary conditions. They found that the discrepancy in the calculated buckling stresses between the two theories of plasticity gets larger with increasing plate thickness, the ratio E/σ_y and exponent n in the Ramberg–Osgood expression, where E and σ_y are the Young's modulus and yield strength. Similarly to the previously mentioned argument by Bushnell (1982), they suggested that another explanation of the discrepancies in the results using the two theories for thick plates could be that the deformation theory predicts an increasingly lower in-plane shear modulus as the level of plasticity increases, which results in lower calculated buckling-stress values. Becque (2010) presented a theory describing the inelastic buckling of perfect plates. The formulation was based on the flow theory and avoids the plastic buckling paradox by establishing an equation for the shear stiffness which is based on second order considerations. The governing equation of buckling of a plate was solved analytically for the case of a plate simply supported along three edges and with one longitudinal edge free. He found out that the proposed relation between the shear stresses and the shear strains at the onset of plastic buckling effectively overcomes the plastic buckling paradox. This relation is tested in Chapter 5 of this thesis.

Restricting attention to the plastic buckling of circular cylindrical shells, Mao and Lu (1999) analytically examined simply supported cylinders made of aluminium alloy subjected to axial compression load. They compared the buckling stresses predicted by their analytical formula with the experimental results obtained by Lee (1962) and found that the deformation theory provides closer results with the tests while the flow theory significantly over-predicts the critical loads.

Ore and Durban (1992) analytically investigated the buckling of axially compressed circular cylindrical shells in the plastic range for various boundary conditions. Similar to Mao and Lu (1999), they concluded that the buckling compression stresses predicted by the deformation theory appeared to be in good agreement with measured test results, while those provided by

the flow theory overestimated the measured test values. Moreover, the authors observed that the differences between the theoretical results predicted by the flow and deformation theory reduced with increasing value of the strain hardening parameter in the Ramberg–Osgood expression.

Bardi and Kyriakides (2006) tested fifteen cylindrical stainless steel tubes, with diameter-to-thickness ranging between 23 and 52, under axial compression and determined the critical stresses and strains at the onset of wrinkling. They reported the buckling modes, including the number and the size of waves. They also calculated the same quantities analytically using the deformation or the flow plasticity theory. The calculations included the effects of assuming both isotropic and anisotropic material behaviour. They concluded that the flow theory significantly over-predicts the critical stresses and strains while the deformation theory leads to critical stress and strain in better agreement with the experimental results. Moreover, the flow theory grossly over-predicted the wavelength of wrinkles while the deformation theory was in better agreement with the wavelengths measured in the tests.

In the case of axially loaded cylinders, at least during the elastic phase, the walls are subjected to proportional loading, and in many points during plastic yielding, the deviation from the loading path is relatively limited. Nevertheless, the flow and deformation theories seem to provide quite different results.

It is therefore not surprising that similar or even more significant discrepancies have been reported between the results from the flow and deformation theory in the case of non-proportional loading even in the elastic phase.

Blachut et al. (1996) conducted experimental and numerical analyses of 30 mild-steel machined cylinders, of different dimensions, subject to axial tension and increasing external pressure. They showed that agreement between the buckling pressures calculated using the code BOSOR5 (Bushnell, 1986) and employing both plasticity theories was strongly dependent on the ratio of the length L of the cylindrical shell to its outer diameter D . For short cylinders ($L/D \leq 1$) the plastic buckling pressure

predicted by the flow or deformation theory coincided only when the tensile axial load vanished. By increasing the axial tensile load, the plastic buckling pressure predicted by the flow theory of plasticity quickly diverged from corresponding values calculated using the deformation theory, which were closer to the experimental values. For specimens with L/D ranging from 1.5 to 2 the results predicted by both theories were very similar for a certain range of combined loading, beyond which the values calculated using the flow theory began to deviate from the corresponding results using the deformation theory and became unrealistic in correspondence of large plastic strains.

Giezen et al. (1991) conducted experiments and numerical analyses on two sets of tubes made of aluminium alloy 6061-T4 and subjected to combined axial tension and external pressure, making resort to the code BOSOR5 (Bushnell, 1986). The tubes were characterised by a L/D ratio equal to one and two loading paths were considered. In the first one the axial tensile load was held constant and the external pressure was increased. In the second one, the external pressure was held constant and the axial tensile load was increased. The numerical studies showed that the buckling pressure predicted by the flow theory increases with increasing applied tensile load while the experimental tests revealed a reduction in buckling resistance with increasing axial tension. Thus, the discrepancy between the test results and the numerical results predicted by the flow theory increased significantly with the rise of the axial tension. On the other hand, the results by the deformation theory displayed the same trend of the test results. However, the deformation theory significantly under-predicted the buckling pressure observed experimentally for some load paths. Therefore, Giezen (1988) concluded that both plasticity theories were unsuccessful in predicting buckling load. Interestingly enough, Giezen (1988) showed in his thesis that, when reversing the load path, the deformation theory was able to predict buckling while the flow theory failed to do so.

Tuğcu (1998) investigated analytically the effect of the axial loads, applied at both edges of infinitely long simply-supported panels, on the critical shear

stress applied at the short edge of the plate (Figure 2.12). The applied tensile or compressive load was considered proportional to the shear traction stress. He revealed that the critical shear stresses predicted by the flow theory were more sensitive with respect to axial load than those predicted by the deformation theory. Therefore, he suggested that the details of the experimental set-up and boundary conditions which cause secondary stresses should be carefully accounted for to obtain reliable predictions. He assumed that some anisotropy could be present in the material, possibly as a result of manufacturing. He then added that, although the estimation of the material anisotropy was not expected to play a vital rule in reducing the flow theory predictions because of the limited range of buckling strains, the existence of the initial anisotropy could be a factor when the shear was involved as a critical buckling mode such as torsion buckling of cylinders or shear buckling of panels.

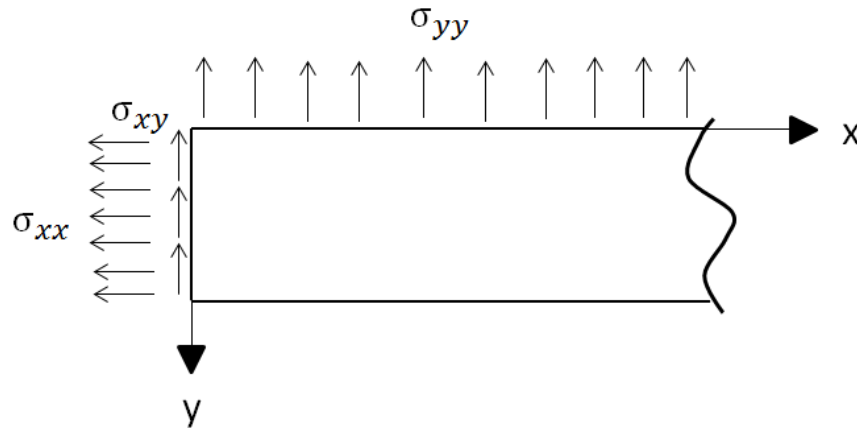


Figure 2.12: Schematic representation of shear panel

In another paper, the same author (Tuğcu, 1991a) analytically studied a thin rectangular plate under biaxial loading conditions. He examined the sensitivity of the buckling stresses predicted by the flow and deformation theories to the inclusion of small amounts of in-plane shear stress. For the case of pure biaxial loading (shear stress $\sigma_{xy} = 0$), the buckling stresses based on the flow theory (σ_{xx}) were very sensitive with respect to σ_{yy} , while those predicted by the deformation theory showed little to no sensitivity. He concluded that a considerable reduction in the predictions of the flow theory

can be achieved when a small non-zero in-plane shear stress exists in the analysis.

The same author, (Tuğcu, 1991b) investigated analytically the buckling of cylinders under combined axial load and torque and combined external pressure and torque. Again he found that the predictions of the flow theory were more sensitive to the non-proportionality of loading than those of the deformation theory although the predictions of both theories were similar in some region of a particular interaction.

Overall, the above mentioned literature indicates that the flow theory has been generally found to be more sensitive with respect to non-proportional loading than the deformation theory.

The plastic paradox does not seem to be limited to the buckling of plates and cylinders. For example, Galletly et al. (1990) investigated the plastic buckling of six machined steel torispherical domes of different geometries and subjected to internal pressure. The tests were carried out to highlight the differences in buckling stresses calculated, using the code BOSOR5 (Bushnell, 1986), with either the flow or the deformation theory. They measured low-amplitude waves in the knuckle of the torispherical domes by probes allocated at the knuckle region for all six specimens. These waves grew with the increasing internal pressure in four test specimens and became visible to the naked eye while in other two specimens the waves could not be visually detected but could be felt by finger-tip contact. In their analysis they found that, for all the tests, the buckling mode failure and the internal pressure predicted by the deformation theory was in good agreement with the experimental results, the difference varying between 6% and 29%. On the other hand, the flow theory did not predict a buckling failure mode for any of the four test specimens.

2.10 A brief overview of the underlying methods of BOSOR5

The bifurcation load and the corresponding buckling mode are determined in BOSOR5 through a sequence of two subsequent analyses (Bushnell, 1986). The first one is a nonlinear pre-buckling analysis which is valid for small

strains and moderately large rotations and accounts for material nonlinearity. This nonlinear problem is solved using a strategy in which a nested iteration loop is applied at each load level. The inner loop is used to analyse the nonlinear behaviour caused by the moderately large displacements using the Newton-Raphson method. The outer loop is used to evaluate the constitutive matrix and the plastic strain components, and to test loading and unloading condition in the material by means of a sub-incremental strategy (Bushnell, 1982). The results from this analysis are used in the following analysis, which is an eigenvalue analysis which yields the bifurcation load and the corresponding axisymmetric or non-symmetric buckling mode, respectively (Bushnell, 1982). At the bifurcation load, the infinitesimal displacement field has components in the axial, circumferential and radial direction denoted as $\delta u, \delta v$ and δw . They are assumed to vary harmonically around the circumference as follows (Bushnell, 1984)

$$\begin{cases} \delta u = u_n(s) \sin(n\theta) \\ \delta v = v_n(s) \cos(n\theta) \\ \delta w = w_n(s) \sin(n\theta) \end{cases} \quad (2.71)$$

where n is the number of circumferential waves, s and θ are the arc length of the shell measured along the reference surface and the circumferential coordinate, respectively.

BOSOR5 users are asked to specify the range of circumferential wave numbers (n_{min} and n_{max}), and the starting wave number, n_o , which might correspond, in the user's judgment, to the minimum bifurcation load. BOSOR5 calculates the determinant of the global stability stiffness matrix (K_{1n_o}) for the chosen n_o at each time increment until the determinant changes sign. If the determinant of the stiffness matrix changes sign, BOSOR5 sets up, for all the values of n ranged between n_{min} and n_{max} , a series of eigenvalue problems of the form illustrated in the equations (Bushnell, 1982)

$$(K_{1n} + \lambda_n K_{2n})(q_n) = 0 \quad (2.72)$$

where K_{1n} and K_{2n} are the stiffness matrix and load-geometric matrix corresponding to n circumferential waves, respectively, and λ_n and q_n are the eigenvalues and eigenvectors for the numbers of wave n , respectively.

The critical wave number n_{cr} corresponds to the minimum value of λ_n . The strategy used to identify buckling load is explained in detail in Bushnell (1982).

It is important to note that the discretisation in BOSOR5 is only performed in the meridian direction because the resulting displacements are axisymmetric in the pre-buckling phase.

Chapter 3

A Detailed Numerical Investigation into the Plastic Buckling Paradox for Circular Cylindrical Shells under Axial Compression

3.1. Introduction

In the framework provided by the cited publications in Section 2.9, the work presented in this chapter aims to shed light on the plastic buckling paradox by conducting accurate linear and nonlinear finite-element modelling of buckling of cylindrical shells using the flow theory and the deformation theory of plasticity, as well as using simplified semi-analytical models.

Attention is focused on cylindrical shells subject to axial compression with outer-radius-to-thickness ratio R/t ranging between 9 and 120, because of the great significance of this geometry and loading conditions for engineering application. The predictions have been compared with widely recognised experimental results reported in the literature by Lee (1962) and Batterman (1965) and with the analytical results reported by Mao and Lu (1999) and Ore and Durban (1992).

It is found that, in contrast to common understanding, by using carefully developed geometrically nonlinear finite element (FE) models a very good agreement between numerical and experimental results can be obtained in the case of the physically sound flow theory of plasticity. The reasons

underlying the apparent buckling paradox are then investigated and discussed in detail.

3.2. Test samples and finite-element modelling

3.2.1 Geometry and elements

The plastic buckling of perfect and imperfect cylinders subjected to axial compression has been numerically simulated using nonlinear FE analyses using both the flow and the deformation theory of plasticity, adopting the FE code ABAQUS, version 6.11-1. Specific attention has been paid to adopt model parameters which, in the case of proportional monotonic (increasing) loading, result in the same stress-strain curve in both theories, to within a negligible numerical error. The FE simulations were conducted for aluminium cylinders tested by Lee (1962) and Batterman (1965). Out of the ten cylinders tested by Lee and of the thirty cylinders tested by Batterman, eight and nine of them, respectively, were chosen for the numerical investigation. The criterion used for the selection of these tests was to account for a wide range of R/t . The results of the analysis are compared with the corresponding test results reported by the above authors and with analytical results derived by Ore and Durban (1992) and Mao and Lu (1999).

In Lee's experiments, the specimens were made of cylinders of aluminium alloy 3003-0, which were reported to be free of residual stresses. The compression pad used to transfer the axial force and the base block had annular recesses in which the specimens were inserted. Lee tested 10 cylinders with an outer diameter of 101.6 mm and radius-thickness ratios R/t varying between 9.36 and 46.06. He pointed out that the imperfections in general were irregular such that the cross sections had somewhat oval shapes. Eight cylindrical shells were chosen for the present numerical analysis, as illustrated in Table 3.1.

The end sections during the test were neither perfectly hinged nor perfectly clamped. Therefore, the two idealised boundary conditions, hinged and clamped, were modelled separately. For the case of clamped ends, the bottom edge of the shell was considered as fully fixed, i.e. with no allowed

translations and rotations for all degrees of freedom; the other edge was also considered fully restrained, except for the displacement in the axial direction which was prescribed to increase monotonically downward. In the case of hinged ends, the rotations normal to the cylinder wall were fully allowed.

The cylindrical specimens were modelled using a general purpose 4-noded shell element which has six degrees of freedom at each node. This element is named “S4” in the commercial software ABAQUS and is based on a thick shell theory. The shell formulation accounts for finite membrane strains, therefore this element can be used to perform large strain analyses. The element is widely used for industrial applications because it is suitable for both thin and thick shells. The S4 element uses a normal integration rule with four integration points. The enhanced-strains approach is employed to prevent shear and membrane locking. Among the ABAQUS elements, S4 outperforms S4R as the former evaluates more accurately the membrane strains, which play a key role in the problem at hand (Simulia, 2011).

Spec.	R (mm)	R/t	L/R	t (mm)	L (mm)	Imperfection ratio δ/t
A330	50.8	9.36	4.21	5.43	213.87	0.012
A230	50.8	9.38	6.32	5.42	321.01	0.012
A130	50.8	9.39	10.5	5.41	533.40	0.012
A320	50.8	19.38	4.1	2.62	208.28	0.03
A220	50.8	19.4	6.15	2.62	321.10	0.05
A310	50.8	29.16	4.06	1.74	206.25	0.045
A110	50.8	29.22	10.16	1.74	516.13	0.033
A300	50.8	46.06	4.04	1.1	205.23	0.105

Table 3.1: Geometry and imperfection ratio of the aluminium cylinders tested by Lee (1962).

A structured mesh was used, made from a number of divisions along the circumference and longitudinal direction reported in Table 3.2 for each specimen.

Number of elements	Specimens							
	A330	A230	A130	A320	A220	A310	A110	A300
- around the circumference	150	150	150	150	150	150	150	150
- along the length	100	150	250	98	150	97	242	96

Table 3.2: FE mesh discretisation adopted for the FE analyses of the cylinders tested by Lee.

In the tests carried out and reported by Batterman (1965), the specimens were made of cylinders of aluminium alloy 2024-T4. The ends of the specimens were restrained such as to be considered clamped. Batterman tested 30 cylinders with radius-thickness ratio R/t varying between 9.7 and 121.25. Nine cylindrical shells were chosen for the present numerical analysis, as presented in Table 3.3.

Spec.	R (mm)	R/t	L/R	t (mm)	L (mm)
12	34.79	9.7	2.92	3.586	101.6
18	34.8	9.76	2.92	3.566	101.6
22	35.56	13.93	0.72	2.553	25.4
5	33.42	25.94	0.76	1.297	25.4
15	34.72	44.69	1.47	0.777	50.8
16	34.59	56.52	0.73	0.612	25.4
26	34.49	85.95	0.74	0.4013	25.4
8	33.2	114.56	1.53	0.29	50.8
9	33.12	116.61	0.77	0.284	25.4

Table 3.3: Geometries of aluminium cylinders tested by Batterman (1965).

Again 4-noded shell (S4) elements were used in the FE modelling with a structured mesh with numbers of elements along circumference and length shown in Table 3.4 for each specimen.

Number elements of	Specimens								
	12	18	22	5	15	16	26	8	9
- around the circumference	150	150	250	250	150	250	250	250	250
- along the length	70	70	28	30	35	29	29	61	31

Table 3.4: FE mesh discretisation adopted for the analyses of the cylinders tested by Batterman.

3.2.2 Constitutive relationship and material constants

The uniaxial stress-strain relationship of the material under monotonic loading was characterised by the Ramberg-Osgood relationship:

$$E\varepsilon = \sigma + \alpha \left(\frac{\sigma}{\sigma_y} \right)^{n_p - 1} \sigma \quad (3.1)$$

where ε and σ denotes uniaxial strain and stress, E and ν are Young's modulus and Poisson's ratio, respectively, σ_y is the nominal yield strength, sometimes called 'proof stress' and denoted by $\sigma_{0.2\%}$ (see Figure 3.2), α is the 'yield offset' and n_p is the strain hardening parameter.

The Ramberg-Osgood input parameters used in the numerical simulations are reported in Table 3.5.

	E [GPa]	σ_y [MPa]	ν	n_p	α
Lee's tests	70	23.62	0.32	4.1	0.429
Batterman's tests	74.5	389.6	0.32	14.45	0.382

Table 3.5: Ramberg-Osgood constants used in the numerical analyses.

For the cylinders tested by Lee (1962), the parameters used for the FE modelling are those reported by Mau and Lu (1999), Mau and Lu (2001) and Ore and Durban (1992), which in turn were based on the properties given by Lee (1962). Notice that σ_y does not represent the classically defined proof stress, nominally corresponding to a plastic strain of 0.2%, because of the nature of Equation (3.1). The actual proof stress at 0.2% of plastic strain is equal to 41.2. Furthermore, the relatively low value of the hardening

exponent results in a gradual hardening and values of the stresses higher than 100 MPa at a strain of 0.1%, as shown in the stress-strain curve reported in Figure 3.1.

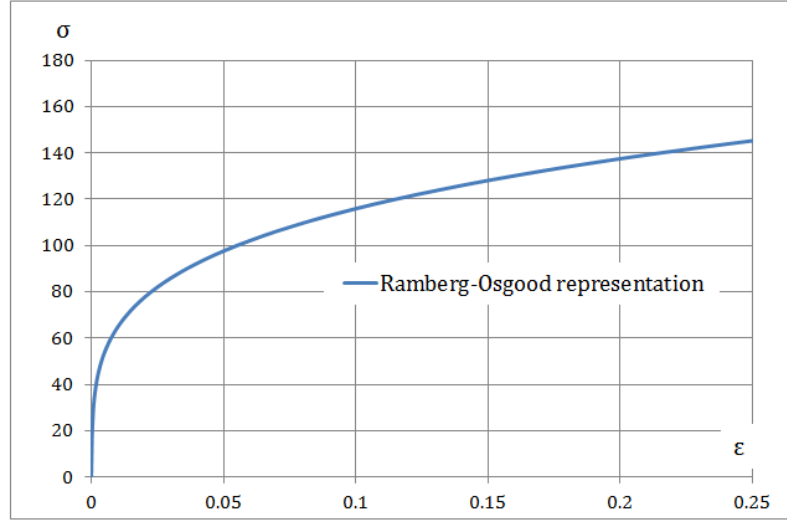


Figure 3.1: Stress-strain curve for Lee's tests

For Batterman's tests two sets of experimental data from tensile and compression tests were reported by the author and fitted with the Ramberg-Osgood relationship. In particular, two values of the yield strength, $\sigma_{0.2\%}$ and $\sigma_{0.5\%}$, corresponding to strains of 0.2% and 0.5%, respectively, measured in tensile and compression tests were reported by Batterman (1965) and were used to calculate the values of α and n_p reported in Table 3.6. In particular, since $\sigma_y = \sigma_{0.2\%}$, from Eq. (3.1) one has:

$$\alpha = 0.002 \frac{E}{\sigma_y} \quad (3.2)$$

and n_p is obtained from the relationship:

$$n_p = \frac{\ln\left(\frac{0.005 E}{\alpha \sigma_y}\right)}{\ln\left(\frac{\sigma_{0.5\%}}{\sigma_y}\right)} \quad (3.3)$$

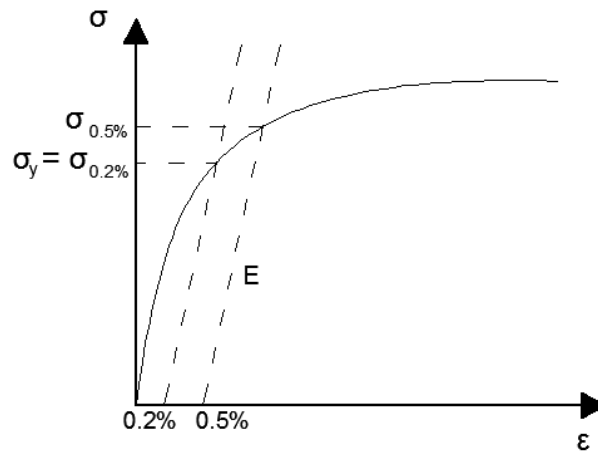


Figure 3.2: Illustration of $\sigma_{0.2\%}$ and $\sigma_{0.5\%}$ on the stress-strain curve.

Data from	Compression tests	Tension tests
E [GPa]	74.46	73.57
$\sigma_{0.2\%}$ [MPa]	389.6	408.9
$\sigma_{0.5\%}$ [MPa]	415.1	419.2
α	0.382	0.36
n_p	14.45	36.68

Table 3.6: Material constants from tensile and compression tests (Batterman, 1965).

Figure 3.3 shows a comparison between the experimental uniaxial stress-strain curves reported by Batterman and those obtained using the Ramberg-Osgood relationship with the parameters in Table 3.6. It can be seen that the Ramberg-Osgood constants calculated using the compression tests lead to a very good agreement with the experimental compression data, such that they have been used for the numerical analyses.

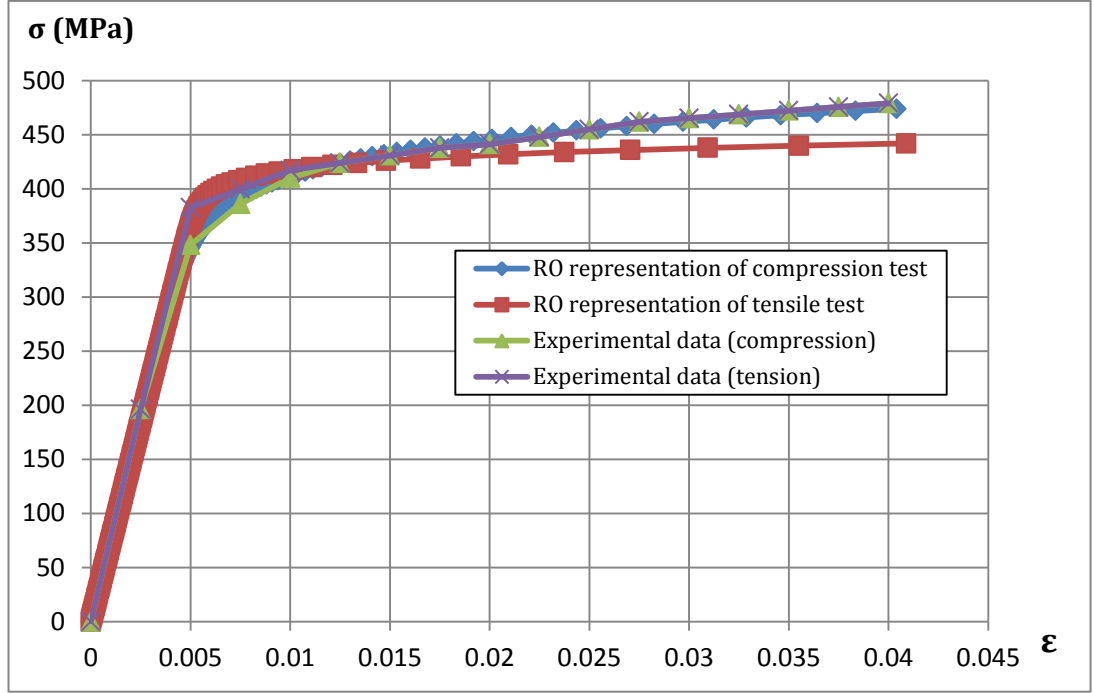


Figure 3.3: Comparison between experimental and formula curves

The deformation theory of plasticity used in the numerical simulations is obtained by extending the Ramberg-Osgood law to the case of a multi-axial stress state using the von Mises formulation (J_2 theory) and results in a path-independent relationship (Simulia, 2011). The resulting equations are reported in Section 2.8.

The flow theory used in the numerical simulations was the classical J_2 flow theory of plasticity, with nonlinear isotropic hardening and in the small-strain regime (Simo and Hughes, 1998; Simulia, 2011). Such theory is implemented in a model available in ABAQUS. For the sake of completeness the equations governing the theory are those reported in Appendix A1. On the other hand, it is important to underline here that the input data for the flow theory were obtained in such a way that the same stress-strain curve as in the case of the deformation theory is obtained for the case of uniaxial stress and monotonic loading, to within a negligibly small numerical tolerance.

It is worth recalling that the Ramberg-Osgood relationship does not account for any initial linearly elastic behaviour but represents a nonlinear material response for any value of the stress, even if for relatively small stress values the deviation from linearity is quite small. Hence, the function $\bar{\sigma}$ in Eq. (A.7)

should be such that $\bar{\sigma}(0) = 0$, i.e. the initial yield stress in the flow theory should be taken as zero. However, the numerical implementation of the J_2 flow theory requires the use of the well-known radial-return algorithm (see Simo and Hughes, (1998) among many others) which, in turn, requires the calculation of the unit normal vector to the yield surface. The unit normal vector is undefined if the yield surface degenerates to a point, which is why, using the J_2 flow theory implemented in ABAQUS, a zero value of $\bar{\sigma}(0)$ leads to lack of convergence in the first increment. Hence, the value $\bar{\sigma}(0) = 10^{-5}$ MPa was assumed. Furthermore, a tabulated approximation of $\bar{\sigma}(\varepsilon_p^{eq})$ was obtained by considering $\bar{\sigma}$ increments of 2 MPa; for each value of the stress $\bar{\sigma}$ the corresponding equivalent plastic strain value ε_p^{eq} was obtained from Eq. (3.1) as follows

$$\varepsilon_p^{eq} = \alpha \left(\frac{\bar{\sigma}}{\sigma_y} \right)^{n_p-1} \frac{\bar{\sigma}}{E} \quad (3.4)$$

Figure 3.5 illustrates the load-displacement curves obtained for the numerical tensile test of a square rod of $10 \times 10 \text{ mm}^2$ subject to homogeneous uniaxial stress using both plasticity theories in conjunction with the material parameters used for the simulation of Lee's tests (Figure 3.4). It can be appreciated that the load-deflection curves are identical during the loading process. Upon unloading, in the case of the deformation theory the same loading curve is followed, whereas in the case of the flow theory, the unloading is elastic. In the case of the flow theory, in order to restore the value of deflection to zero, a compressive load is applied and the load-deflection path proceeds as shown in Figure 3.5. The same procedure has been followed for the material models used to simulate Batterman's tests, which led to a perfectly analogous graph as in Figure 3.5.

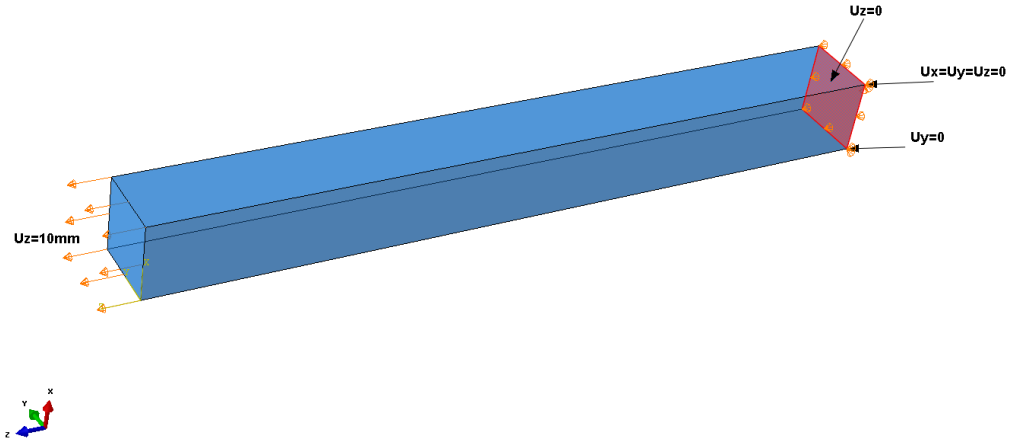


Figure 3.4: Regular prism of section 10x10 mm with boundary conditions

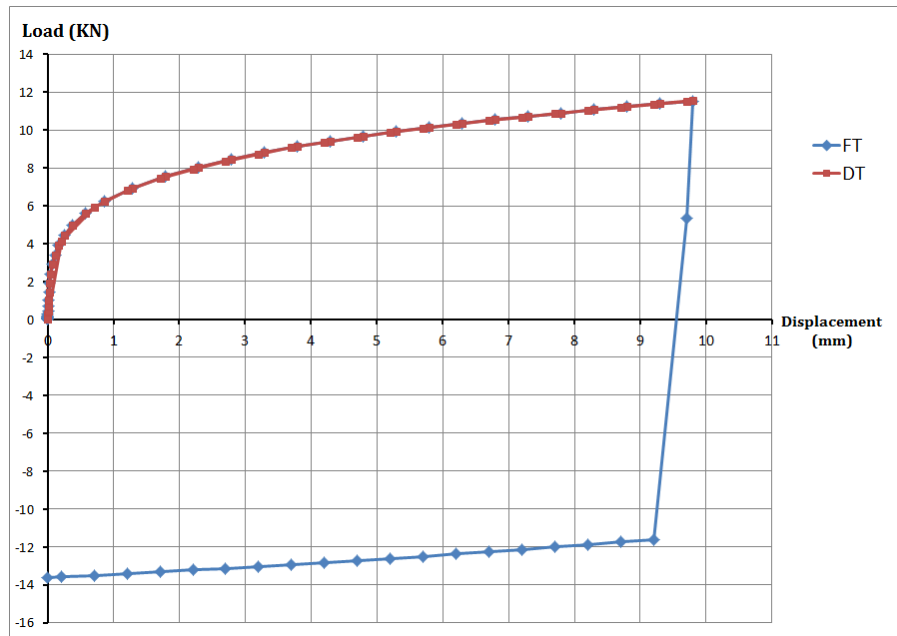


Figure 3.5: Load-displacement relation for a 10x10 mm² square rod of aluminium alloy 3003-0 subjected to homogeneous uniaxial stress.

It is worth remarking that the nonlinear isotropic model used for the flow theory of plasticity obviously does not account for the Baushinger effect, but plastic strain reversal always occurred in the simulations considered here after the maximum (buckling) load had been reached, so that ignoring the Baushinger effect does not affect the buckling predictions for the problems under analysis.

3.2.3 Large displacement formulation

The above constitutive relationships are extended to the large-strain regime by using spatial co-rotational stress and strain measures and a hypo-elastic relation between the rates of stress and elastic strain (Simulia, 2011). This has been the subject of controversial debate because hypo-elastic laws lead to fictitious numerical dissipation (Simo and Hughes, 1998). However, this large-strain formulation is widely implemented in many commercial codes, including ABAQUS, and it is generally accepted that the hypo-elasticity of the formulation has limited influence on the results because, even when strains are large, the elastic part of the strain is typically still very small and therefore close to the limit where hypo-elastic and hyper-elastic formulations coincide (Simo and Hughes, 1998).

3.2.4 Solution strategy

The nonlinear analysis was conducted using the modified Riks' approach (Riks, 1979) to trace the nonlinear response. Riks' method was the first of the so-called "arc-length" techniques, which provide an incremental approach to the solution of problems involving limit points in the equilibrium path. In this technique, both the vector of displacement increments $\Delta \mathbf{u}$ and the increment $\Delta \lambda$ of the scalar multiplier of the applied loads or displacements are unknown variables in the incremental/iteration scheme. The Riks' formulation iterates along a hyper plane orthogonal to the tangent of the arc-length from a previously converged point on the equilibrium path (Falzon, 2006). The iterations within each increment are performed using the Newton–Raphson method; therefore, at any time there will be a finite radius of convergence (Simulia, 2011).

In this analysis, the displacement at the top edge of the cylinder is prescribed to be equal to $\lambda \mathbf{u}_0$, where \mathbf{u}_0 denotes a reference downward vertical displacement and λ is the scalar multiplier. The analysis accounts for geometrical nonlinearity as discussed in Sections 3.2.1 and 3.2.3. The critical load is determined by the point at which the load-shortening curve reaches a maximum.

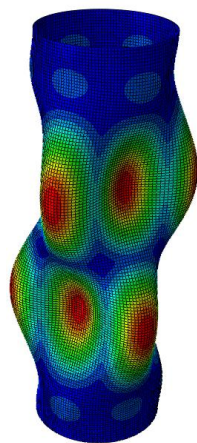
The machine compliance was not included in the analyses reported because it does not affect the computed buckling stresses and only results in a rightward shift of the load-shortening curves. This was confirmed by additional analyses, not reported here, in which the compliance was introduced with suitably inserted springs at the top edge.

3.2.5 Imperfection sensitivity analysis

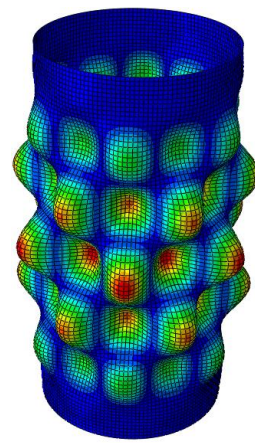
In order to study the imperfection sensitivity of the cylinders, in the case of Lee's tests the analysis was carried out both for perfect cylinders and for two reference values of maximum imperfection amplitude, equal to 10% and 20% of the thickness. Moreover, the analysis was also conducted for the imperfection amplitudes presented in Table 3.1, experimentally measured by Lee (1962).

In the case of Batterman's tests, the analysis was carried out both for perfect cylinders and for two reference values of imperfection amplitude, i.e. 5% and 10% of the thickness.

In both cases, imperfections were modelled by scaling the first eigenmode of linear buckling analysis and adding it to the perfect cylinder (see Figure 3.6 and Figure 3.7). The linear buckling analysis has been conducted assuming linear elastic material behaviour and small displacements.

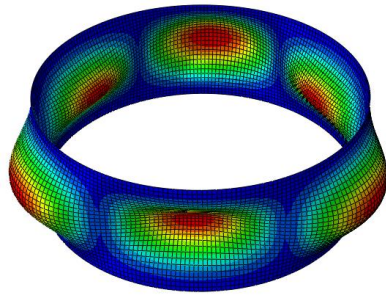


First eigenmode for A220 cylinder

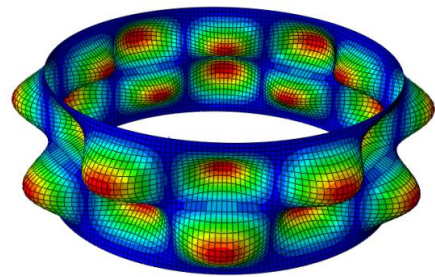


First eigenmode for A300 cylinder

Figure 3.6: Buckling eigenmodes used in the simulation of Lee's tests to account for imperfections.



First eigenmode for sp.22 cylinder



First eigenmode for sp.16 cylinder

Figure 3.7: Buckling eigenmodes used in the simulation of Batterman's tests to account for imperfections.

3.3. FEA results for Lee's specimens

As mentioned earlier, due to the uncertainty regarding the actual boundary conditions, both perfectly hinged and perfectly clamped conditions were considered at the ends of the specimens. With hinged boundary conditions applied to the perfect model, wrinkles developed in an axisymmetric fashion as shown in the Figure 3.9. However, for clamped edges Figure 3.8 and Figure 3.10 show that the deformed shapes of model appear to correspond well with the test results. Moreover, Table 3.7 shows that, for the flow and deformation theories, the clamped boundary conditions resulted in a closer agreement between numerically calculated and experimentally measured plastic buckling stresses than in the case of hinged boundary conditions. This suggests that the actual test arrangement by Lee should be considered to prevent radial displacements and rotations at both ends of the specimens

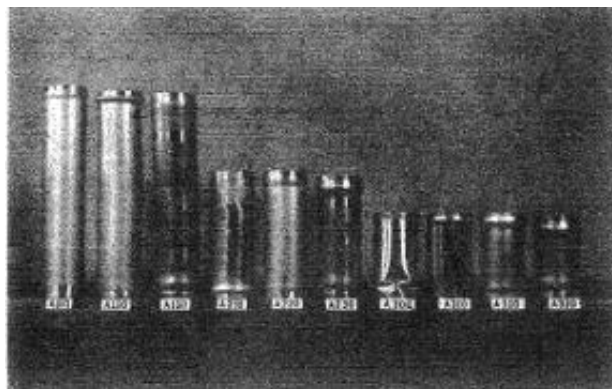


Figure 3.8: Buckling mode failure predicted experimentally (Lee, 1962) (reprinted by kind permission of the American Institute of Aeronautics and Astronautics, Inc.)

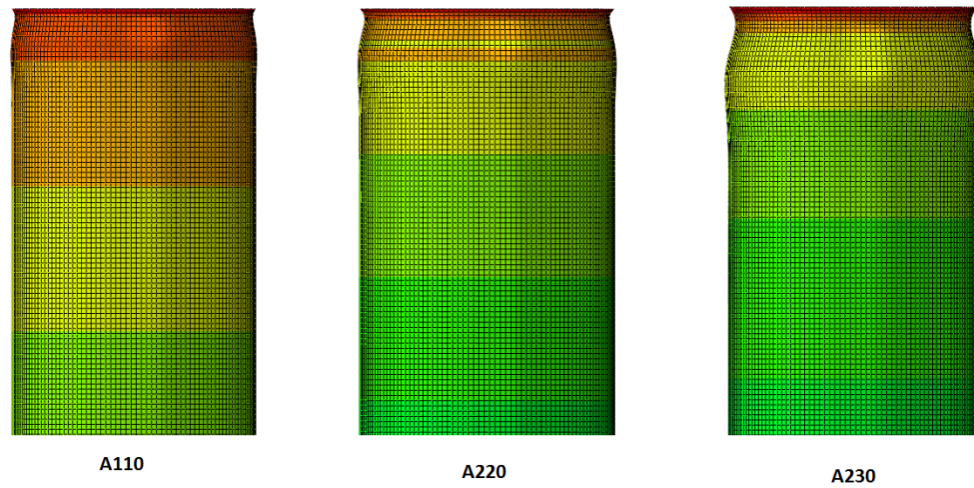


Figure 3.9: Axisymmetric deformation of axial compression shells with hinged boundary conditions and without initial imperfection

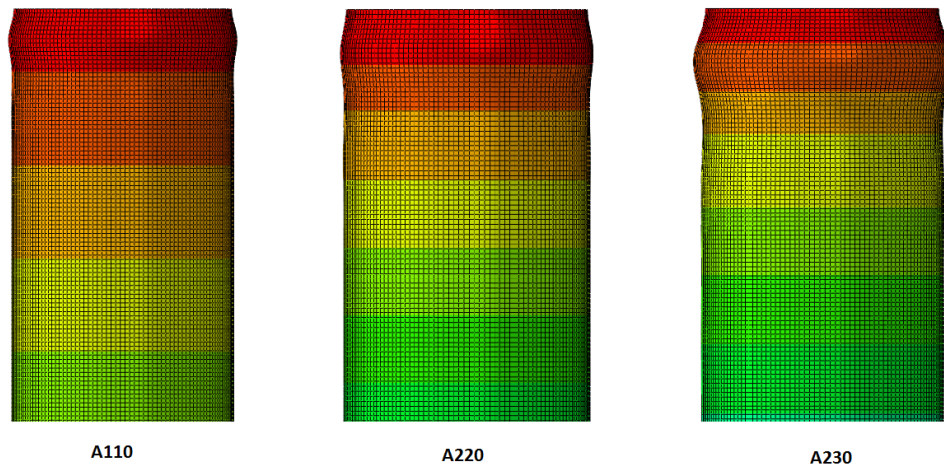


Figure 3.10: Axisymmetric deformation of axial compression shells with clamped boundary conditions and without initial imperfection.

Figure 3.11 and Figure 3.12 show that the buckling stresses calculated using the flow and the deformation theory in the simulation of Lee's tests have a low sensitivity to the imperfection amplitude for moderately thick shells. However, both theories show an increase in the imperfection sensitivity with increasing R/t ratios. It should be noted that the failure mode, which is obtained using a non-axisymmetric shape of imperfections (see Figure 3.6), highly depends on the slenderness of the cylinder (R/t ratios) and the reference value of maximum imperfection amplitude, as seen in Table 3.8. For instance, the failure mode obtained numerically using the flow theory for specimen A330, which has the smallest R/t among the specimens, is

axisymmetric with ring-shaped near the edges when the reference value of maximum imperfection amplitude is 10% of thickness although the shape of imperfection is non-axisymmetric. However, its failure mode becomes ring-shaped near the edges with gentle diamond shaped bucking wave pattern in the central region when imperfection amplitude is 20% of thickness.

Moreover, the failure mode obtained numerically using the flow theory of specimen A300, which has the highest R/t among the specimens, is ring-shaped near the edges with gentle diamond shaped bucking wave pattern in the central region when the reference value of maximum imperfection amplitude is 10% of thickness. However, when the imperfection amplitude is 20% of thickness, the ring-shaped deformation near the edges disappears and only a gentle diamond shaped buckling wave pattern in the central region dominates the failure mode.

Table 3.9 shows that the results calculated using the flow theory are in better agreement with the measured test results than those using the deformation theory. In fact, the buckling stresses calculated using the deformation theory tend to fall below the experimental values for all specimens except A310. In the case of the flow theory, on the contrary, numerical and experimental values generally are within a 3% discrepancy, with no clear pattern. The only cases in which the buckling stresses are under-estimated by the flow theory are for specimens A110 and A300, and in such cases the difference with the experiments were 2% and 9% respectively, generally well below the 9% and 21% differences which occurred for the same cases when the deformation theory was used.

Figure 3.13 and Figure 3.14 show the load-displacement curves resulting from flow and deformation plasticity for specimens A230 and A300, respectively. It can be seen that the curve predicted by flow theory is always above the curve predicted by deformation theory for all cases. Moreover, it can be noticed that both curves are identical up to specific point then they diverge. Therefore, the buckling loads found by the flow theory more than those found by the deformation theory but in line with experimental predictions for most cases. The load-displacement curves obtained for all

other specimens are very similar to those in Figure 3.13 and Figure 3.14 and therefore have not been reported.

Spec.	Experimental Buckling Stress (Lee , 1962)	Numerical Analysis (ABAQUS)-simply supported edges				Numerical Analysis (ABAQUS)-clamped edges			
		Flow Plasticity		Deformation Plasticity		Flow Plasticity		Deformation Plasticity	
		Buckling Stress (Mpa)	P_{expt}/P_{ABAQUS}	Buckling Stress (Mpa)	P_{expt}/P_{ABAQUS}	Buckling Stress (Mpa)	P_{expt}/P_{ABAQUS}	Buckling Stress (Mpa)	P_{expt}/P_{ABAQUS}
A330	96.87	81.64	1.19	75.52	1.28	98.58	0.98	88.82	1.09
A230	97.22	81.40	1.19	75.43	1.29	97.84	0.99	88.74	1.10
A130	94.6	81.3491	1.16	75.47	1.25	97.83	0.97	88.89	1.06
A320	78.6	62.30	1.26	59.94	1.31	80.48	0.98	74.10	1.06
A220	81.15	62.30	1.30	60.27	1.35	80.85	1.00	73.90	1.10
A310	64.74	54.79	1.18	53.31	1.21	72.47	0.89	66.84	0.97
A110	74.12	54.81	1.35	53.16	1.39	72.94	1.02	66.84	1.11
A300	69.71	47.64	1.46	47.11	1.48	64.25	1.08	59.16	1.18

Table 3.7: Results obtained with hinged and clamped boundary conditions for both deformation and flow theory of plasticity, in comparison with the corresponding test results by Lee (1962) (for perfect cylinders).

Spec.	Mode of failure predicted Numerically (Abaqus)					
	Flow Plasticity			Deformation Plasticity		
	perfect	10% imperfection	20% imperfection	perfect	10% imperfection	20% imperfection
A330	AX, Ring-Shaped near the edges	AX, Ring-Shaped near the edges	Ring-Shaped near the edges and gentle DM pattern in the central region	AX, 4LW	AS, 4LW	AS, 4LW
A230	AX, Ring-Shaped near the edges	AX, Ring-Shaped near the edges	AX, Ring-Shaped near the edges	AX, 6LW	AX, 6LW	AS, 6LW
A130	AX, Ring-Shaped near the edges	Ring-Shaped near the edges and local buckling in the central region	Ring-Shaped near the edges and local buckling in the central region	AX, 6LW near the edges	Ring-Shaped near the edges and local buckling in the central region	Ring-Shaped near the edges and local buckling in the central region
A320	AX, Ring-Shaped near the edges	AX, Ring-Shaped near the edges	Ring-Shaped near the edges and gentle DM pattern in the central region	AX, 5LW	Ring-Shaped near the edges and gentle DM pattern in the central region	Ring-Shaped near the edges and gentle DM pattern in the central region
A220	AX, Ring-Shaped near the edges	Ring-Shaped near the edges and gentle DM pattern in the central region	Ring-Shaped near the edges and gentle DM pattern in the central region	AX, 8LW	Ring-Shaped near the edges and gentle DM pattern in the central region	Ring-Shaped near the edges and gentle DM pattern in the central region
A310	AX, Ring-Shaped near the edges	Ring-Shaped near the edges and gentle DM pattern in the central region	Ring-Shaped near the edges and DM patterns in the central region	AX, 6LW	Ring-Shaped near the edges and gentle DM pattern in the central region	DM patterns in the central region
A110	AX, Ring-Shaped near the edges	Ring-Shaped near the edges and gentle DM pattern in the central region	Ring-Shaped near the edges and gentle DM pattern in the central region	AX, 6LW near the edges	Ring-Shaped near the edges and gentle DM pattern in the central region	Ring-Shaped near the edges and gentle DM pattern in the central region
A300	AX, Ring-Shaped near the edges	Ring-Shaped near the edges and gentle DM pattern in the central region	DM patterns in the central region	AX, 8LW	Ring-Shaped near the edges and gentle DM pattern in the central region	DM patterns in the central region

* AX-Axisymmetric buckling wave * AS- Almost axisymmetric buckling wave * DM-Diamond shaped buckling wave * LW- number of longitudinal waves

Table 3.8: Comparison between modes of failure numerically calculated for perfect and imperfect cylinders (Cylinders tested by Lee (1962))

Spec.	Experimental Buckling Stress (Lee , 1962)	Imperfection ratio δ/t	Numerical Analysis (ABAQUS)					
			Flow Plasticity			Deformation Plasticity		
			Buckling Stress (Mpa)	P_{expt}/P_{ABAQUS}	Mode of failure	Buckling Stress (Mpa)	P_{expt}/P_{ABAQUS}	Mode of failure
A330	96.87	0.012	98.54	0.98	AX, Ring-Shaped near the edges	89.05	1.09	*AX, 4* LW
A230	97.22	0.01	97.84	0.99	AX, Ring-Shaped near the edges	88.74	1.10	AX, 6LW
A130	94.6	0.01	97.82	0.97	AS, Ring-Shaped near the edges	88.32	1.07	*AS, 6LW near the edges
A320	78.6	0.03	80.48	0.98	AX, Ring-Shaped near the edges	74.10	1.06	AX, 5LW
A220	81.15	0.05	80.84	1.00	AX, Ring-Shaped near the edges	73.90	1.10	AS, 8LW
A310	64.74	0.05	71.54	0.90	AS, Ring-Shaped near the edges	66.59	0.97	AS, 6LW
A110	74.12	0.03	72.94	1.02	AS, Ring-Shaped near the edges	66.84	1.11	AS, 6LW near the edges
A300	69.71	0.11	64.16	1.09	Ring-Shaped near the edges and gentle DM pattern in the central region	57.44	1.21	Ring-Shaped near the edges and gentle DM pattern in the central region

Table 3.9: Comparison between test and numerical results for both flow and deformation theory of plasticity (imperfections identified by Lee (1962))

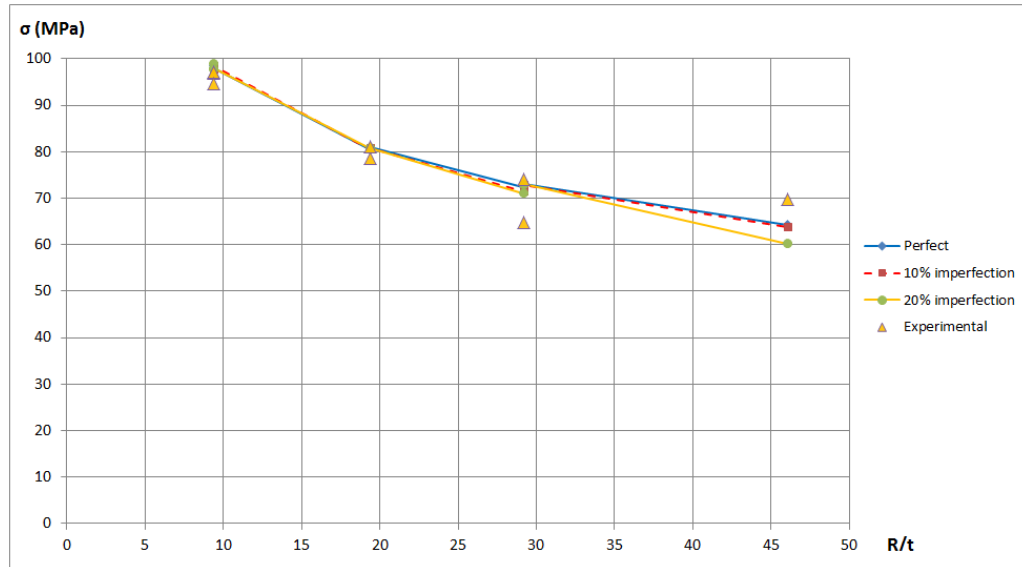


Figure 3.11: Effect of imperfections on the buckling load calculated using the flow theory of plasticity

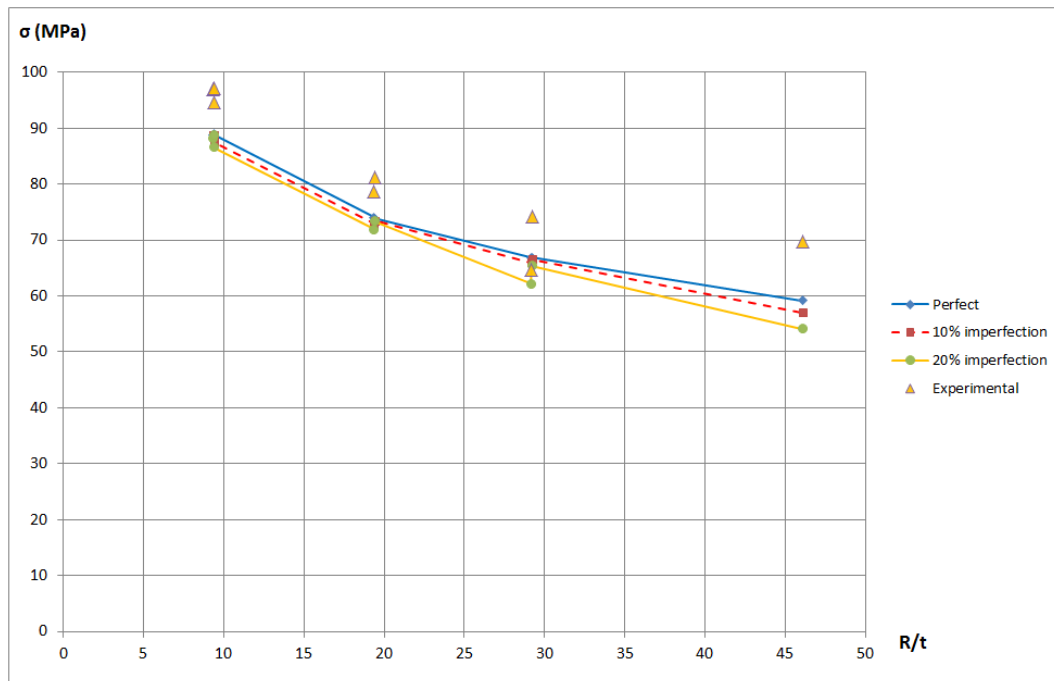


Figure 3.12: Effect of imperfections on the buckling load calculated using the deformation theory of plasticity

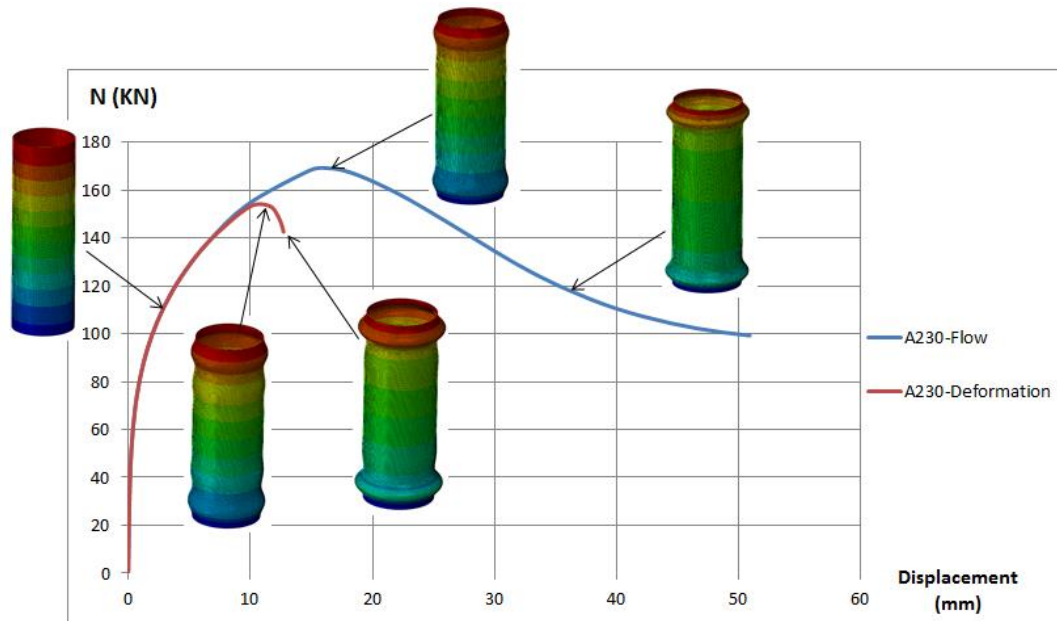


Figure 3.13: Axial load vs. prescribed displacement for specimen A230 for flow and deformation theories.

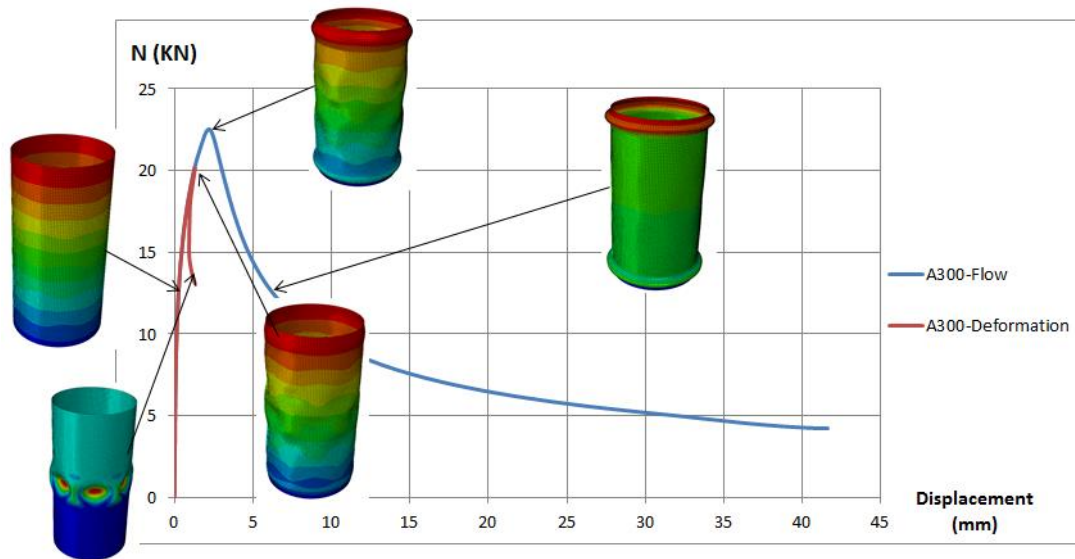


Figure 3.14: Axial load vs. prescribed displacement for specimen A300 for flow and deformation theories.

Lee's tests were studied analytically by Ore and Durban (1992) and Mao and Lu (1999) under the assumption of axisymmetric buckling. The results of their calculations, illustrated in Table 3.10 and Table 3.11, show that the deformation theory results in better agreement with the findings by Lee (1962) and that the flow theory predictions systematically overestimate the buckling stresses. This is in contrast with the results of the present study,

which show that, if appropriately applied, the flow theory accurately estimates the experimental buckling stress.

Spec.	Experimental Buckling Stress (Mpa)	Analytical (Mao and Lu, 1999)		Numerical Analysis (ABAQUS)	
	(Lee , 1962)	Flow	Deformation	Flow	Deformation
A330	96.87	165.46	89.71	98.58	88.82
A320	78.60	124.25	74.87	80.48	74.10
A310	64.74	106.00	67.70	72.47	66.84

Table 3.10: Comparison between results Mao and Lu (1999) and present numerical results for both flow and deformation theories of plasticity

Spec.	Experimental Buckling Stress (Mpa)	Analytical (Ore and Durban, 1992)		Numerical Analysis (ABAQUS)	
	(Lee , 1962)	Flow	Deformation	Flow	Deformation
A330	96.87	162.32	88.34	98.58	88.82
A230	97.22	162.32	88.34	97.84	88.74
A130	94.6	161.59	87.81	97.83	88.89
A320	78.6	121.74	73.26	80.48	74.10
A220	81.15	121.51	72.80	80.85	73.90
A310	64.74	107.73	66.79	72.47	66.84
A110	74.12	107.64	66.52	72.94	66.84
A300	69.71	87.26	59.25	64.25	59.16

Table 3.11: Comparison between results by Ore and Durban (1992) and present numerical results for both flow and deformation theories of plasticity

3.4. FEA results for Batterman's experiments

Figure 3.15 and Figure 3.16 show that the buckling stresses calculated using the flow and deformation theories in the simulation of Batterman's tests display a low sensitivity to the imperfection amplitude for shells with $10 \leq R/t \leq 45$. However, both theories show an increase in the imperfection sensitivity for R/t ratios above 45. In particular, the flow and deformation theories of plasticity both overestimate the ultimate load for shells with $45 \leq R/t \leq 120$ if imperfections in the shells are not accounted for. On the other hand, both theories provide good agreement with experimental results if a 5% imperfection is included in the analysis.

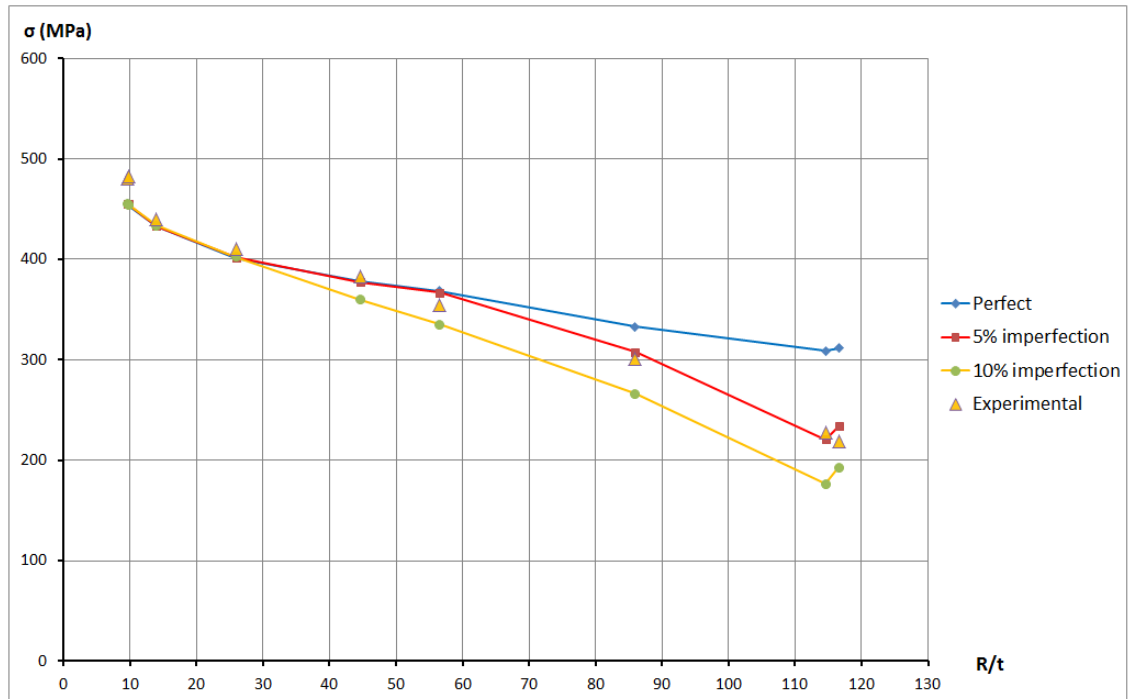


Figure 3.15: Imperfection sensitivity of buckling stress computed using the flow theory of plasticity.

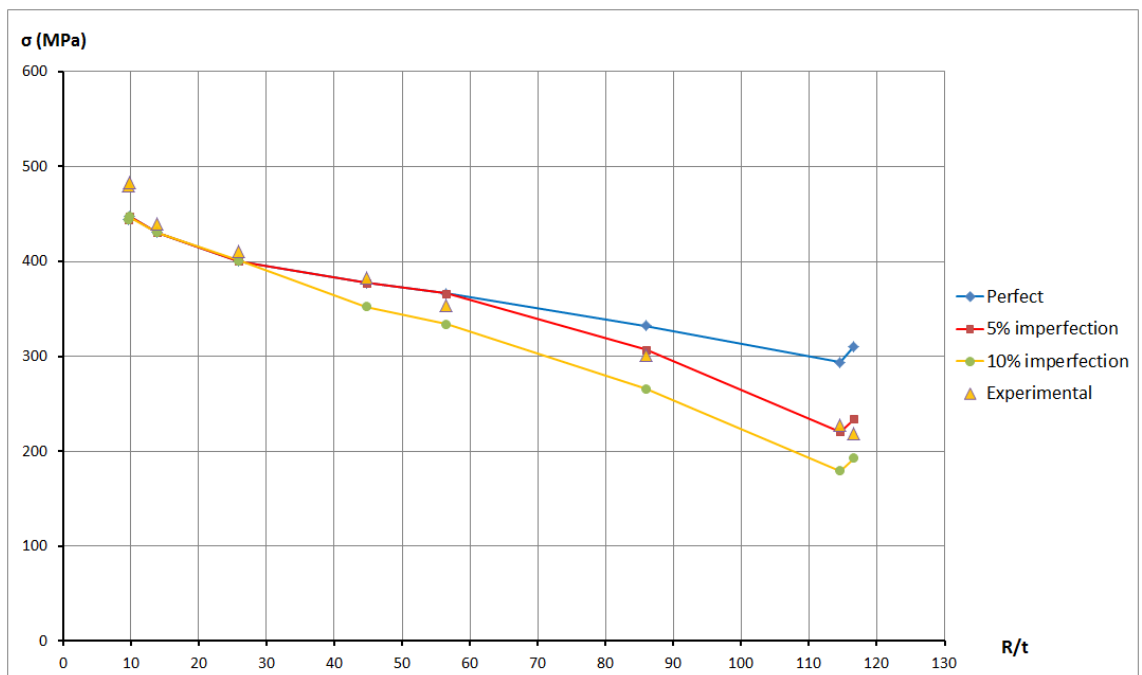


Figure 3.16: Imperfection sensitivity of buckling stresses computed using the deformation theory of plasticity.

It can be also noticed in Tables 3.12- 3.14 that the differences between the calculations of buckling stresses using flow and deformation theories for perfect and imperfect cylinders are quite small both for thick and thin shells.

Spec.	Experimental Buckling Stress (Batterman, 1965)	Numerical Analysis (ABAQUS)					
		Flow Plasticity			Deformation Plasticity		
		Buckling Stress (Mpa)	P_{expt}/P_{ABAQUS}	Mode of failure	Buckling Stress (Mpa)	P_{expt}/P_{ABAQUS}	Mode of failure
12	480.08	455.632	1.05	AX, Ring-Shaped near the edges	444.198	1.08	AX, 3LW
18	482.63	453.912	1.06	AX, Ring-Shaped near the edges	447.863	1.08	AX, 3LW
22	439.8	433.111	1.02	AX, Ring-shaped at the central region	430.336	1.02	AX, Ring-shaped at the central region
5	410.72	401.427	1.02	AX, Ring-shaped at the central region	400.203	1.03	AX, Ring-shaped at the central region
15	382.6	377.503	1.01	AX, 3LW	377.429	1.01	AX, 3LW
16	354.25	368.405	0.96	AX, Ring-Shaped near the edges	366.162	0.97	AX, Ring-Shaped near the edges
26	301.23	333.042	0.90	AX, Ring-Shaped near the edges	332.445	0.91	AX, Ring-Shaped near the edges
8	227.73	308.725	0.74	AX, Ring-Shaped near the edges	296.1	0.78	AX, 5LW
9	219.05	311.703	0.70	AX, Ring-Shaped near the edges	310.609	0.71	AX, Ring-shaped at the central region

* AX-Axisymmetric buckling wave * LW- number of longitudinal waves

Table 3.12: Comparison between measured test results and corresponding numerical results for both flow and deformation theories of plasticity for perfect cylinders

Spec.	Experimental Buckling Stress (Batterman, 1965)	Numerical Analysis (ABAQUS)					
		Flow Plasticity			Deformation Plasticity		
		Buckling Stress (Mpa)	P_{expt}/P_{ABAQUS}	Mode of failure	Buckling Stress (Mpa)	P_{expt}/P_{ABAQUS}	Mode of failure
12	480.08	455.57	1.05	AX, Ring-Shaped near the edges	444.13	1.08	AX, 3LW
18	482.63	454.87	1.06	AX, Ring-Shaped near the edges	447.70	1.08	AX, 3LW
22	439.8	433.18	1.02	AX, Ring-shaped at the central region	430.38	1.02	AX, Ring-shaped at the central region
5	410.72	401.56	1.02	AX, Ring-shaped at the central region	400.36	1.03	AX, Ring-shaped at the central region
15	382.6	377.44	1.01	AX near the ends, gentle DM pattern in the central region	377.40	1.01	Ring-Shaped near the edges and DM pattern in the central region
16	354.25	366.92	0.97	DM pattern	366.25	0.97	DM pattern
26	301.23	307.92	0.98	DM pattern	306.92	0.98	DM pattern
8	227.73	220.93	1.03	DM pattern	220.84	1.03	DM pattern
9	219.05	234.04	0.94	DM pattern	234.03	0.94	DM pattern

* AX-Axisymmetric buckling wave * DM-Diamond shaped buckling wave * LW- number of longitudinal waves

Table 3.13: Comparison between measured test results and numerical results for both flow and deformation theories of plasticity (5% imperfections)

Spec.	Experimental Buckling Stress (Batterman, 1965)	Numerical Analysis (ABAQUS)					
		Flow Plasticity			Deformation Plasticity		
		Buckling Stress (Mpa)	P_{expt}/P_{ABAQUS}	Mode of failure	Buckling Stress (Mpa)	P_{expt}/P_{ABAQUS}	Mode of failure
12	480.08	455.385	1.05	AX, Ring-Shaped near the edges	443.92	1.08	AS, 3LW
18	482.63	454.604	1.06	AX, Ring-Shaped near the edges	447.40	1.08	AS, 3LW
22	439.8	433.366	1.01	AX, Ring-shaped at the central region	430.51	1.02	AX, Ring-shaped at the central region
5	410.72	402.334	1.02	AX, Ring-shaped at the central region	400.83	1.02	AX, Ring-shaped at the central region
15	382.6	359.507	1.06	DM pattern in the central region	352.59	1.09	DM pattern in the central region
16	354.25	334.873	1.06	DM pattern	333.85	1.06	DM pattern
26	301.23	266.18	1.13	DM pattern	266.02	1.13	DM pattern
8	227.73	176.401	1.29	DM pattern	179.52	1.27	DM pattern
9	219.05	192.924	1.14	DM pattern	192.83	1.14	DM pattern

Table 3.14: Comparison between measured test results and numerical results for both flow and deformation theories of plasticity (10% imperfections)

Spec.	Experimental Buckling Stress (Batterman, 1965)		Mode of failure predicted Numerically (Abaqus)					
	Buckling Stress (Mpa)	Mode of Failure	Flow Plasticity			Deformation Plasticity		
			perfect	5%	10%	perfect	5%	10%
12	480.08	AX Mode	AX, Ring-Shaped near the edges	AX, Ring-Shaped near the edges	AX, Ring-Shaped near the edges	AX, 3LW	AX, 3LW	AS, 3LW
18	482.63	AX Mode	AX, Ring-Shaped near the edges	AX, Ring-Shaped near the edges	AX, Ring-Shaped near the edges	AX, 3LW	AX, 3LW	AS, 3LW
22	439.8	AX Mode	AX, Ring-shaped at the central region	AX, Ring-shaped at the central region	AX, Ring-shaped at the central region	AX, Ring-shaped at the central region	AX, Ring-shaped at the central region	AX, Ring-shaped at the central region
5	410.72	AX Mode	AX, Ring-shaped at the central region	AX, Ring-shaped at the central region	AX, Ring-shaped at the central region	AX, Ring-shaped at the central region	AX, Ring-shaped at the central region	AX, Ring-shaped at the central region
15	382.6	AX Mode near ends, gentle DM pattern in central region	AX, 3LW	AX near the ends, gentle DM pattern in the central region	DM pattern in the central region	AX, 3LW	Ring-Shaped near the edges and DM pattern in the central region	DM pattern in the central region
16	354.25	DM pattern	AX, Ring-Shaped near the edges	DM pattern	DM pattern	AX, Ring-Shaped near the edges	DM pattern	DM pattern
26	301.23	DM pattern	AX, Ring-Shaped near the edges	DM pattern	DM pattern	AX, Ring-Shaped near the edges	DM pattern	DM pattern
8	227.73	DM pattern	AX, Ring-Shaped near the edges	DM pattern	DM pattern	AX, 5LW	DM pattern	DM pattern
9	219.05	DM pattern	AX, Ring-Shaped near the edges	DM pattern	DM pattern	AX, Ring-shaped at the central region	DM pattern	DM pattern

Table 3.15: Comparison between modes of failure numerically calculated and those experimentally observed by Batterman (1965).

Error! Reference source not found. shows that the presence of initial imperfections also affects the failure modes bringing them into closer agreement with the failure mode predicted experimentally.

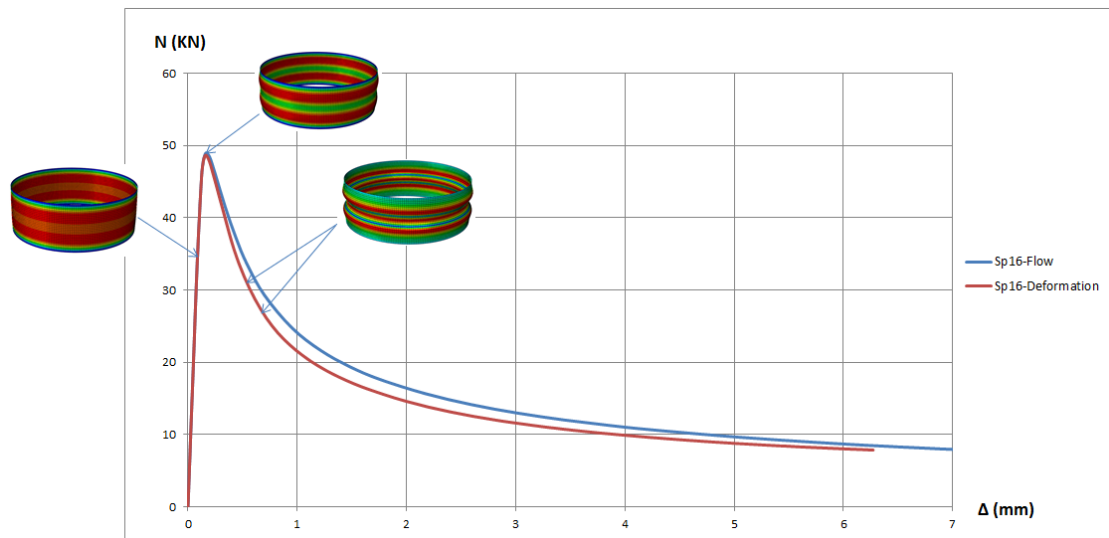


Figure 3.17: Axial load vs. prescribed displacement numerically predicted for specimen 16 for flow and deformation theory in the case of perfect geometry.

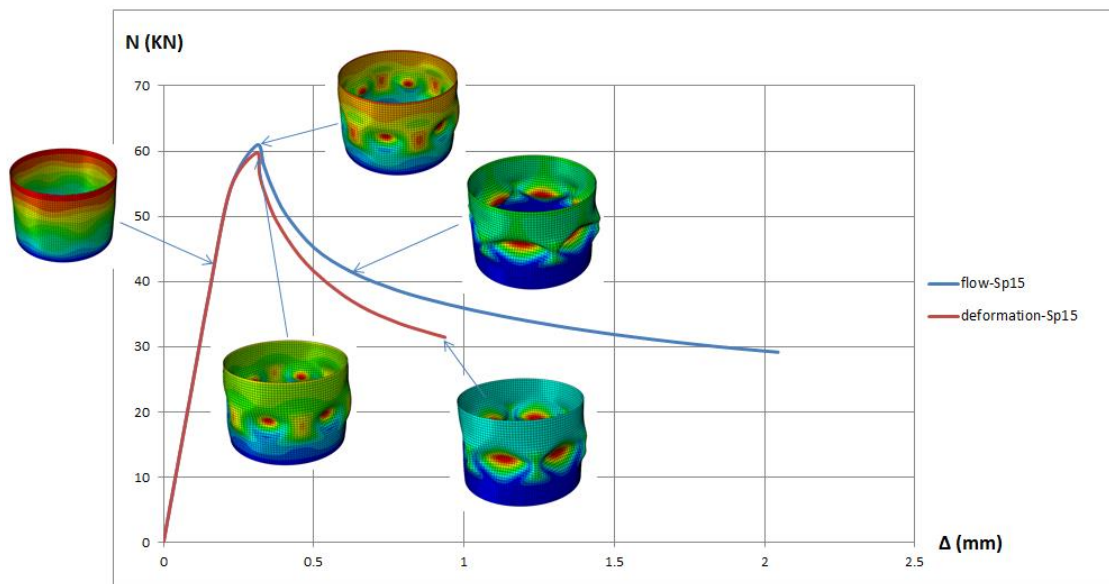


Figure 3.18: Axial load vs. prescribed displacement numerically predicted for specimen 15 for flow and deformation theory with an amplitude of initial imperfection equal to 10% of the thickness.

Figure 3.17 and Figure 3.18 show the relation between axial loads and corresponding end shortening for specimens 15 and 16. The load-displacement curves obtained for all other specimens are very similar to

those in Figure 3.17 and Figure 3.18 and therefore have not been reported. Again, it can be observed that for the various geometries and imperfections considered the curves predicted by the flow theory are always above those provided by the deformation theory.

3.5. Discussion and interpretation of FEA results in the context of the plastic buckling paradox

The main findings from the numerical results presented in Sections 3.3 and 3.4 are that:

- (i) when correctly and accurately incorporated in accurate FE modelling, the deformation and flow theories of plasticity provide results which in general, and in particular in terms of buckling stresses, are similar and only occasionally differ more than 10%;
- (ii) the flow theory of plasticity consistently provides results which are in closer agreement with the experimental data;
- (iii) following the first part of the load-displacement curve, in which the two theories essentially provide the same results, with increasing applied displacements the loads calculated using the flow theory become systematically larger than those obtained using by the deformation theory for all cases analysed.

The first two findings are in clear contrast with the conclusions of many authors, as discussed in Section 2.9. In particular, Table 3.10 and Table 3.11 show very large discrepancies between the buckling stresses calculated using the present numerical simulations and those calculated analytically by Ore and Durban (1992) and Mao and Lu (1999).

The following sections present a comprehensive discussion on the possible causes for such discrepancy.

First a mesh-convergence analysis and the effects of the initial imperfections are examined and it is concluded that both have negligible effect on the findings. Second, it is shown that the analytical approaches provide, by their own nature, solutions that are kinematically over constrained and that, for this reason, lead to an over stiffened model both in the case of the flow and

deformation theories of plasticity. Third, the influence of using the flow or the deformation theory of plasticity from the material standpoint is analysed with the help of a simplified model in the fashion of that proposed by Hutchinson (1972). This elementary model highlights in a very direct manner the influence of the different unloading paths on the results provided by the deformation and the flow theories of plasticity and it qualitatively shows why the loads-displacement curves found numerically by the flow theory always above those provided by the deformation theory. Moreover, it clearly shows why the deformation theory underestimates buckling loads calculated numerically in comparison to the flow theory.

3.5.1 Robustness of the FE model

A mesh-convergence analysis performed showed negligible changes in results by employing either coarser or and more refined meshes than those used to produce the presented results; additionally, a sensitivity analysis revealed that the results are not affected by the small numerical difference in the monotonic uniaxial stress-strain curve between the flow and the deformation theory of plasticity on account of setting $\bar{\sigma}(0) = 10^{-5}$ MPa instead of $\bar{\sigma}(0) = 0$ (see Section 3.2.2). Hence, it is concluded that there seems to be no particular issue with the accuracy of the FE modelling used here.

3.5.2 Influence of initial imperfections

With respect to the influence of initial imperfections, some authors recently suggested that, at least in the case of the analysis of lined pipes under compression, the overestimation of the buckling stress predicted by the flow theory can be reduced by giving the initial imperfections a certain amplitude (Hilberink et al., 2010). However, the results of the sensitivity analysis to imperfections reported in Sections 3.3 and 3.4 clearly show that not accounting for imperfections leads to an overestimation of the buckling stress which is very similar for both the flow and the deformation theory. In other words, for both sets of tests simulated in the present analyses erroneous consideration of imperfections would not lead to a larger overestimation of

the buckling stress when using the flow theory than using the deformation theory of plasticity.

3.5.3 Buckling shapes and over-constraint of analytical models

The implicit kinematic constraint in assuming a certain buckling shape as the basis of analytical models seems to be the main reason for the discrepancy between the presented numerical results and the analytical findings which have suggested the existence of a plastic buckling paradox. Actually, it is on the basis of the results from several analytical calculations that it is widely accepted that the flow theory leads to a significant overestimation of the buckling stress while the deformation theory provides much more accurate prediction and is therefore recommended for use in practical applications (see, for example, Mao and Lu (2001, 2002)).

Actually, the buckling shapes determined by the inherent simplifications of the analytical treatments result in kinematic constraints which yield a stiffer structural response and, as a consequence, an overestimation of the buckling stress.

Batterman (1965) derived analytical equations to define the buckling stress and corresponding number of half wave (m) for flow and deformation theories of plasticity.

He assumed simply supported boundary conditions and the stress-strain relationship of the material was represented by the Ramberg-Osgood expression. The expressions of the buckling stresses obtained in the case of the flow and deformation theories are reported in Appendix A2. They were derived from an axisymmetric buckling shape in the form

$$v_n = A \sin(m\pi x / L) \quad (3.5)$$

Table 3.16 shows the maximum buckling stress for each specimen of Lee's cylindrical shells and its corresponding number of half waves m . It can be seen that the corresponding number of half waves predicted by the flow theory of plasticity is very different from that predicted by the deformation theory of plasticity and therefore the maximum buckling stress predicted also

differs sensibly. Further validation of these results is given by the fact that the maximum buckling stresses are almost equal to the buckling stresses calculated by Ore and Durban (1992) (Table 3.11).

Spec.	Experimental buckling stress (MPa)	Analytical predictions			
		m (Flow)	σ (Flow)	m (Def.)	σ (Def.)
A330	96.87	3	165.6	7	89.85
A320	78.6	5	124.2	11	74.63
A220	81.15	7	125.05	17	74.63
A310	64.74	7	105.74	13	67.23
A110	74.12	17	105.75	33	67.23
A300	69.71	9	88.75	17	59.78

Table 3.16: The maximum buckling stress and corresponding number of half-waves obtained analytically

To investigate this hypothesis further, cylindrical test specimens have been modelled here using finite-element modelling based on a 2-node linear axisymmetric shell element (named SAX1 in ABAQUS), with a uniform mesh. In order to reproduce the shape from the analytical solution presented in Table 3.16, the cylinders were partitioned into an appropriate number of parts, corresponding to the number of half waves yielded by the analytical solution, by using the edge partition tool in ABAQUS. Each part was meshed into ten elements. Linear constraint equations were used to ensure that the radial displacements of the nodes replicated the desired number of half-waves.

This is shown, for example, in Figure 3.19.

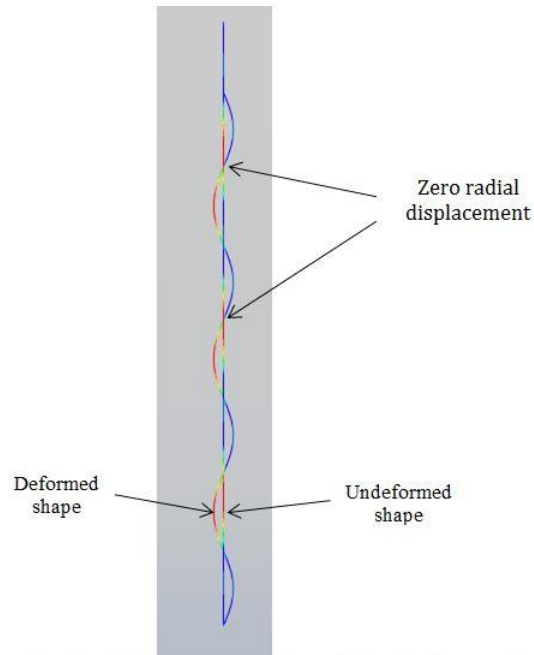


Figure 3.19: Deformed and undeformed shape of the cylinder for the case of $m=7$

Table 3.17 shows the comparison between the maximum buckling stresses obtained analytically and numerically with and without the use of equation constraints for a number of specimens.

It is evident that imposing constraint equations on the FE model in order to reproduce the shape of the analytical solution makes the buckling stresses predicted by the flow theory of plasticity well in excess of those predicted by the deformation theory of plasticity. The latter coincidentally seem therefore to be in better agreement with the experimental results.

Spec.	Experi- mental buckling stress (MPa)	Analytical predictions				Numerical (FE+ kinematical constraints)		Numerical using S4 element (Without kinematical constraints)		Numerical using SAX1 element (Without kinematical constraints)	
		m (Flow)	σ (Flow)	m (Def.)	σ (Def.)	σ (Flow)	σ (Def.)	σ (Flow)	σ (Def.)	σ (Flow)	σ (Def.)
A330	96.87	3	165.6	7	89.85	151.77	101.3	98.58	88.82	92.64	85.20
A320	78.6	5	124.2	11	74.63	121.9	83.4	80.48	74.10	74.72	69.58
A220	81.15	7	125.05	17	74.63	136.67	84.42	80.85	73.90	74.74	69.57
A310	64.74	7	105.74	13	67.23	106.13	75.28	72.47	66.84	66.59	62.29
A110	74.12	17	105.75	33	67.23	121.23	76.78	72.94	66.84	66.63	62.29
A300	69.71	9	88.75	17	59.78	94.95	66.66	64.25	59.16	58.55	55.03

Table 3.17: Comparison between the buckling stresses obtained analytically and numerically with and without the use of equation constraints

On the other hand, without any constraints on the displacements the results from using the flow theory of plasticity in the S4 elements are, as pointed out in the previous sections, in much better agreement with the experimental results than those by use of the deformation theory. Using SAX1 axisymmetric elements without kinematic constraints confirms this fact, but in such a case the results from the deformation theory tend to underestimate the buckling stresses even more than in the case of the S4 elements.

Overall, it can be concluded that the use of the deformation theory tends to underestimate the buckling load and this fact, in the case of the analytical solution proposed by Batterman, compensates the over stiffened kinematics from the simplified analytical equations.

3.5.4 Effects of unloading: analysis through a semi-analytical model

It is worth recalling that the fundamental differences between flow and deformation theories lie in the stress-strain responses (i) during non-proportional loading and (ii) during unloading.

Plastic buckling does indeed lead to non-proportional loading because, before the onset of plasticity, strains are elastic whereas, once the stress reaches and exceeds the yield strength, plastic strains gradually become

predominant. Since the rate of plastic strain is normal to the yield domain, typically the strain path deviates significantly from the initial straight line followed during elastic loading. This aspect is captured in the same manner by the constitutive relationships used in the performed numerical FE analyses and in the analytical formulations.

Unloading is correctly represented by the use of the flow theory in the present numerical calculations, but it is physically misrepresented in the numerical calculations based on the deformation theory as well as in the analytical investigations. As for the latter, it is worth clarifying that unloading is not considered in analytical models using either the deformation theory or the flow theory. Therefore, the consideration of unloading does not offer insight into why analytical models based on the deformation theory provide lower buckling predictions compared to models based on the flow theory. Instead, considering the different ways unloading is treated in the numerical calculations can explain why the deformation theory intrinsically tends to under predict the buckling load in the numerical simulations.

In order to isolate the role played by the different stress responses resulting from the use of the flow or the deformation theory after strain reversal, i.e. material unloading, a simplified model conceptually similar to the one proposed by Hutchinson (1972) is considered. The model qualitatively reproduces the geometrically nonlinear response of a cylinder in compression and is modelled by uniaxial stress-strain relationships, leading by definition to proportional (material) loading. The model is described in Figure 3.20: it consists of two rigid bars connected by two pin-ended short struts. Suffixes 1 and 2 are used to denote the lower and upper central struts. Each rigid bar has length equal to $a - h$ and a rectangular cross section of depth d and width c , whereby the cross section area is $A = c d$. The short struts have length $2h$ and cross sectional areas equal to $A_1 = A_2 = A/2$.

The structure is axisymmetrically supported and subjected to an end-load P with an eccentricity e . Moreover, nonlinear elastic ‘unstable’ springs are assumed to act orthogonally to the rigid bars. They are introduced to account for geometric nonlinearity effects and are characterized by a nonlinear and

de-stabilizing response. The responses of the springs are unstable in the sense that the force transmitted is in the same direction as the spring deformation rather than opposite to it, i.e. tensile for spring elongation and compressive for spring shortening, in accordance with the following formula

$$Q = c \beta \Delta^2 \text{sign}(\Delta) \quad (3.6)$$

where Q is the force, Δ is the lateral displacement (spring elongation) and β is the material constant of the spring.

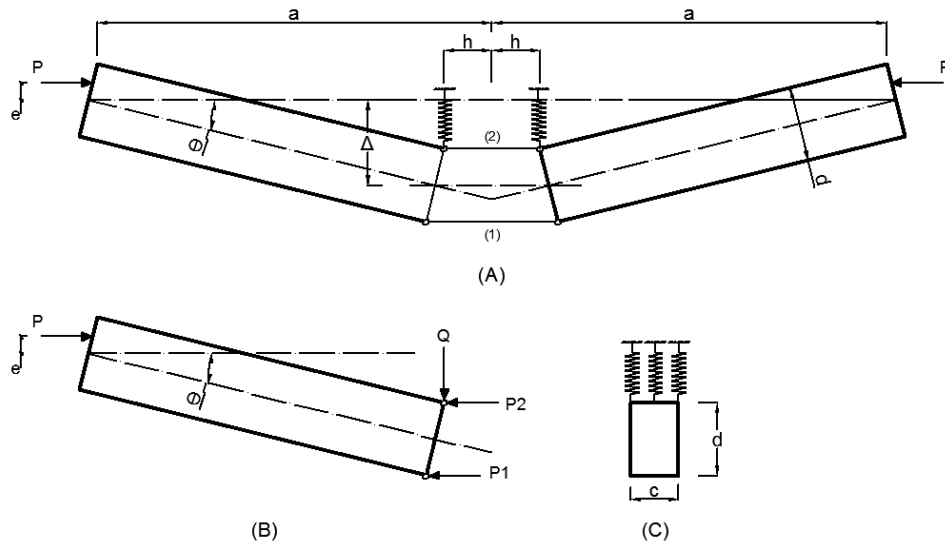


Figure 3.20: A simplified model after Hutchinson (1972)

Essentially, the presence of these nonlinear and unstable springs qualitatively reproduces the unstable post-buckling responses due to the peculiar geometrically nonlinear nature of structures, such as cylinders in compression, via the introduction of material nonlinearity and unstable structural components. Geometrical nonlinearity is translated into material nonlinearity, which enables a study of the pre- and post-buckling response of the structure with a simple second-order approach, resulting in relatively easy analytical computations.

The stresses and strains in the struts are taken as positive when compressive. Denoting the strain in the struts by ε_1 and ε_2 , the rotation of the left hand bar is given by

$$\theta = \frac{h(\varepsilon_2 - \varepsilon_1)}{d} \quad (3.7)$$

From Figure 3.20, the lateral displacement Δ is:

$$\Delta = (a - h) \theta = (a - h) \frac{h(\varepsilon_2 - \varepsilon_1)}{d} \quad (3.8)$$

The stress-strain relation is in the form of a bilinear elastic-plastic behaviour with isotropic hardening which can be expressed as

$$\begin{cases} \sigma_1 = a_1 + b_1 \varepsilon_1 \\ \sigma_2 = a_2 + b_2 \varepsilon_2 \end{cases} \quad (3.9)$$

where a_i and b_i , $i = 1, 2$, are material constants that depend on the (linear) branch of the stress-strain curve and on whether the deformation or the flow theory of plasticity is used, as shown in Figure 3.21.

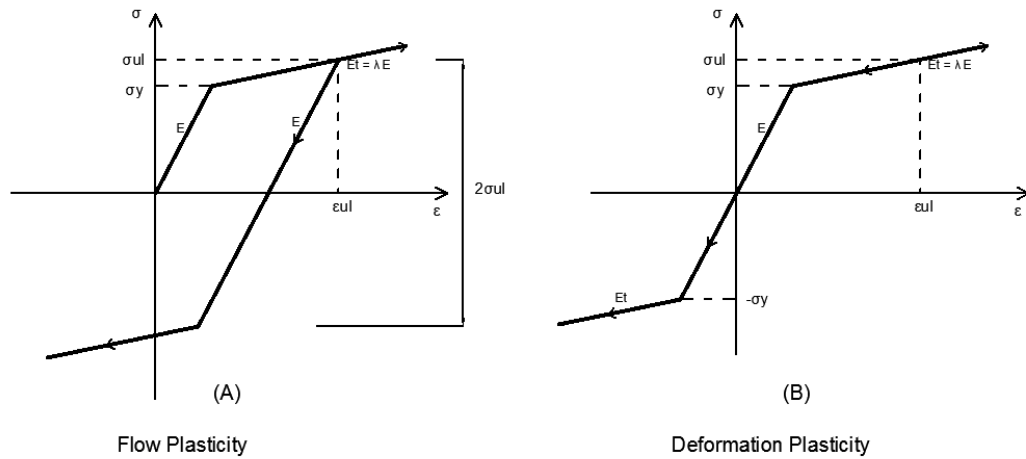


Figure 3.21: Bilinear stress-strain curves used for the flow and deformation theory.

Equilibrium requires that

$$P_1 + P_2 = P \quad (3.10)$$

where

$$\begin{cases} P_1 = A_1 \sigma_1 = \frac{1}{2} A \sigma_1 = \frac{1}{2} d c \sigma_1 \\ P_2 = A_2 \sigma_2 = \frac{1}{2} A \sigma_2 = \frac{1}{2} d c \sigma_2 \end{cases} \quad (3.11)$$

Equilibrium about any point along the line of action of P yields

$$P_1(\Delta + e + d/2) + P_2(\Delta + e - d/2) + (a - h) c \beta \Delta^2 = 0 \quad (3.12)$$

And from Eq. (3.8), one has

$$\varepsilon_2 - \varepsilon_1 = \frac{\Delta}{a-h} \frac{d}{h} \quad (3.13)$$

By defining

$$x = \varepsilon_2 - \varepsilon_1 \quad \text{and} \quad \sigma = (\sigma_1 + \sigma_2)/2 \quad (3.14)$$

and solving for σ leads to:

$$\sigma = \frac{a_2 b_1 d^2 - a_1 b_2 d^2 + b_1 b_2 d^2 x + 2 a b_1 \beta \Delta^2 + 2 a b_2 \beta \Delta^2 - 2 b_1 h \beta \Delta^2 - 2 b_2 h \beta \Delta^2}{d(b_2(-d+2(e+\Delta)) + b_1(d+2(e+\Delta)))} \quad (3.15)$$

The horizontal deflection of the point where the load P is applied can be calculated:

$$u = \frac{(\varepsilon_1 + \varepsilon_2)h}{2} + a e \theta + a(1 - \cos\theta) \quad (3.16)$$

In order to determine the relation between stress σ and the deflection Δ or the longitudinal displacement u the following procedure is used.

The value of deflection Δ is incrementally increased and σ and x are calculated from Eqs. (3.13) and (3.15). The strains $\varepsilon_1, \varepsilon_2$, stresses σ_1, σ_2 and the horizontal deflection u are then evaluated. At each increment, the loading stage of each strut on the stresses-strain curve (Figure 3.21) is determined based on its stresses σ_1, σ_2 . The coefficients a_1, a_2, b_1, b_2 are then calculated according to the current loading stage and to the plasticity theory adopted in accordance with Table 3.18 and Table 3.19.

Loading stage		Strut 1	Strut 2
1	Both struts are elastic	$a_1 = 0$ $b_1 = E$	$a_2 = 0$ $b_2 = E$
2	Strut 2 plastic, strut 1 elastic	$a_1 = 0$ $b_1 = E$	$a_2 = \sigma_y(1 - \lambda)$ $b_2 = \lambda E$
3	Both struts plastic	$a_1 = \sigma_y(1 - \lambda)$ $b_1 = \lambda E$	$a_2 = \sigma_y(1 - \lambda)$ $b_2 = \lambda E$
4	Strut 1 elastic unloading, Strut 2 plastic loading	$a_1 = \sigma_{ul} - E \varepsilon_{ul}$ $b_1 = E$	$a_2 = \sigma_y(1 - \lambda)$ $b_2 = \lambda E$

5	Strut 1 plastic reloading, Strut 2 plastic loading	$a_1 = \sigma_{ul}(2\lambda - 1)$ $\quad - \lambda E \varepsilon_{ul}$ $b_1 = \lambda E$	$a_2 = \sigma_y(1 - \lambda)$ $b_2 = \lambda E$
----------	---	--	--

Table 3.18: loading stages in the case of flow plasticity.

Loading stage		Strut 1	Strut 2
1	Both struts are elastic	$a_1 = 0$ $b_1 = E$	$a_2 = 0$ $b_2 = E$
2	Strut 2 plastic, strut1 elastic	$a_1 = 0$ $b_1 = E$	$a_2 = \sigma_y(1 - \lambda)$ $b_2 = \lambda E$
3	Both struts plastic	$a_1 = \sigma_y(1 - \lambda)$ $b_1 = \lambda E$	$a_2 = \sigma_y(1 - \lambda)$ $b_2 = \lambda E$
4	Strut 1 plastic unloading, strut 2 plastic loading	$a_1 = \sigma_{ul} - \lambda E \varepsilon_{ul}$ $b_1 = \lambda E$	$a_2 = \sigma_y(1 - \lambda)$ $b_2 = \lambda E$
5	Strut 1 elastic unloading, strut 2 plastic loading	$a_1 = 0$ $b_1 = E$	$a_2 = \sigma_y(1 - \lambda)$ $b_2 = \lambda E$
6	Strut 1 plastic reloading, strut 2 plastic loading	$a_1 = \sigma_y(\lambda - 1)$ $b_1 = \lambda E$	$a_2 = \sigma_y(1 - \lambda)$ $b_2 = \lambda E$

Table 3.19: loading stages in the case of deformation plasticity.

The procedure was implemented in a FORTRAN code and analyses were conducted assuming $a = 250$ mm , $d = 15$ mm, $h = 5$ mm (Appendix A3). The cross section of the rigid bar was assumed to be square. The material properties for the struts were assumed to be $\sigma_y = 100$ MPa, $E = 70000$ MPa and $\lambda = 0.5$. The nonlinear spring constant was assumed equal to $\beta = 10$ Nmm⁻³ and two values of load eccentricity considered in the calculations were, $e = 0.5$ mm , $e = 2$ mm. The results are reported in Figure 3.22 to Figure 3.25.

It is evident from the $P - u$ and $P - \Delta$ plots that both theories of plasticity provide the same results up to the onset of stage 3 (i.e. start of unloading in one strut). From that point onwards, the deformation theory of plasticity underestimates the carried load by up to 20% with respect to the corresponding load calculated using the flow theory, depending on the value of the assumed imperfection.

This fact provides a direct and physical explanation to the findings of FE analyses in which the load-displacement curves provided by the flow and deformation theories are identical up to the point of unloading then the flow theory tends to be stiffer than deformation theory and thus provide higher buckling loads but more in line with the experimental findings than the deformation theory findings.

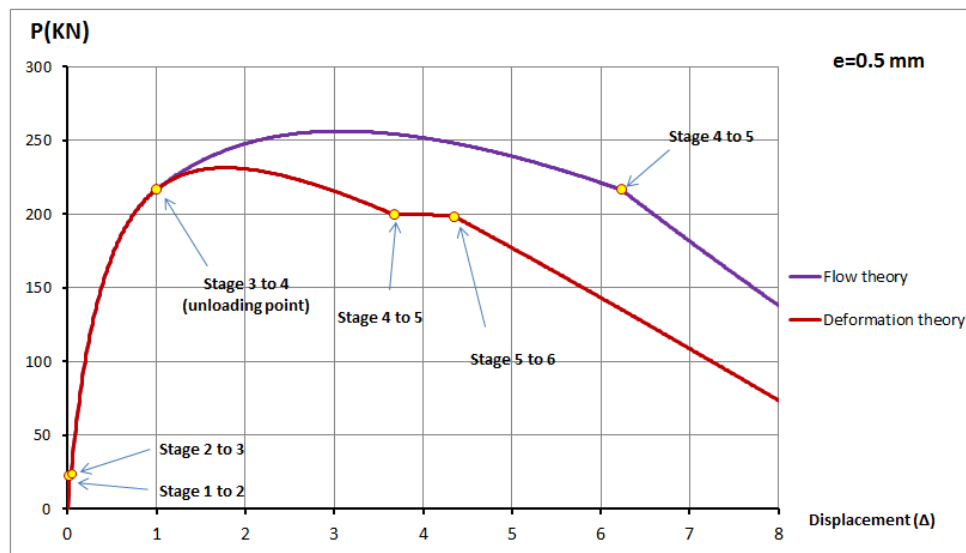


Figure 3.22: $P - \Delta$ plot from the simplified model: comparison between flow and deformation theory, $e = 0.5$ mm.

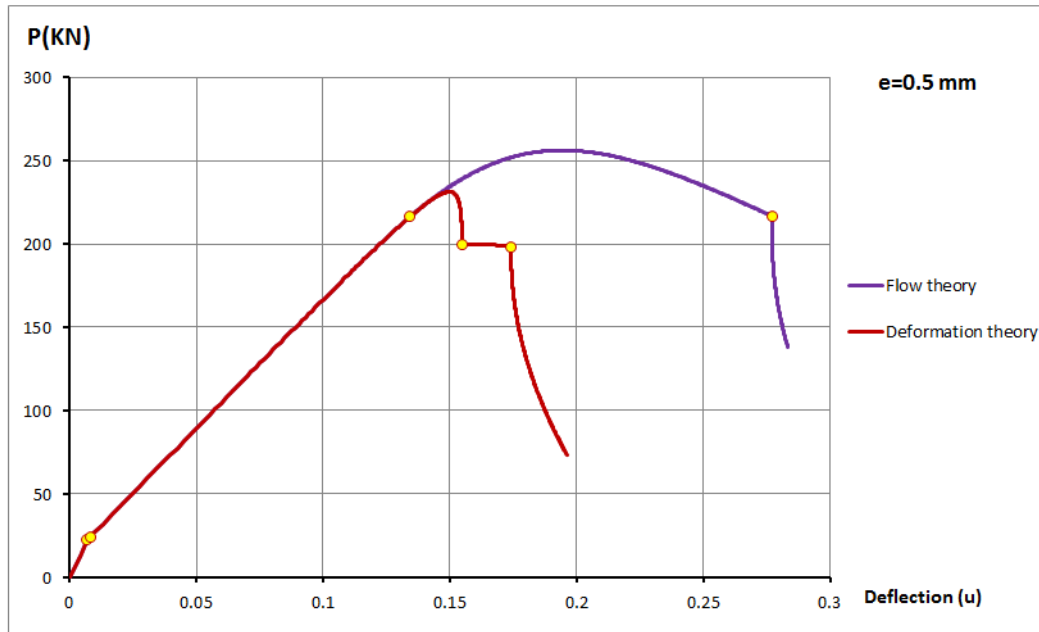


Figure 3.23: $P - u$ plot from the simplified model: comparison between flow and deformation theory, $e = 0.5$ mm.

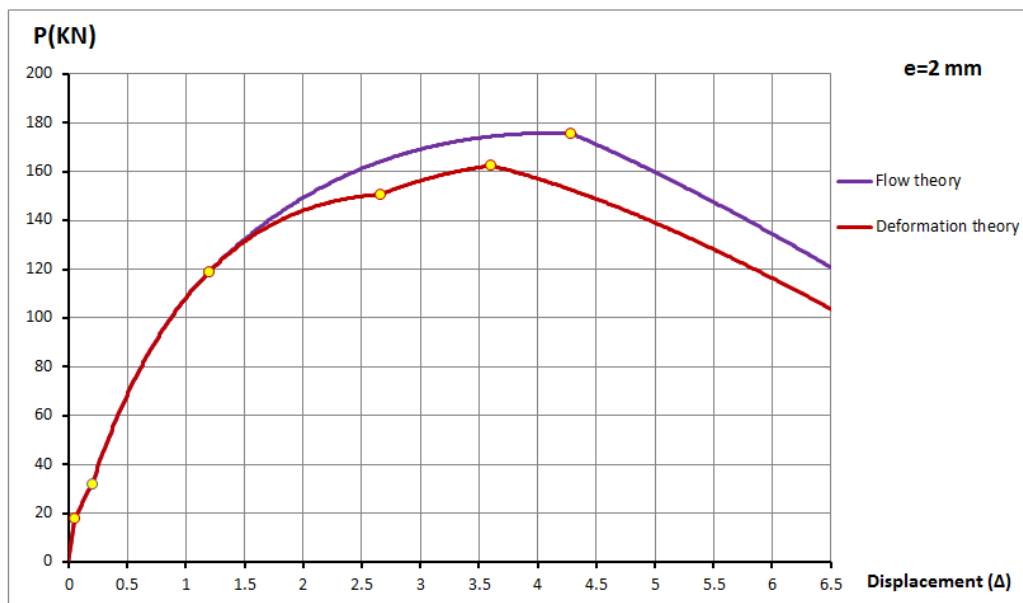


Figure 3.24: $P - \Delta$ plot from the simplified model: comparison between flow and deformation theory, $e = 2$ mm.

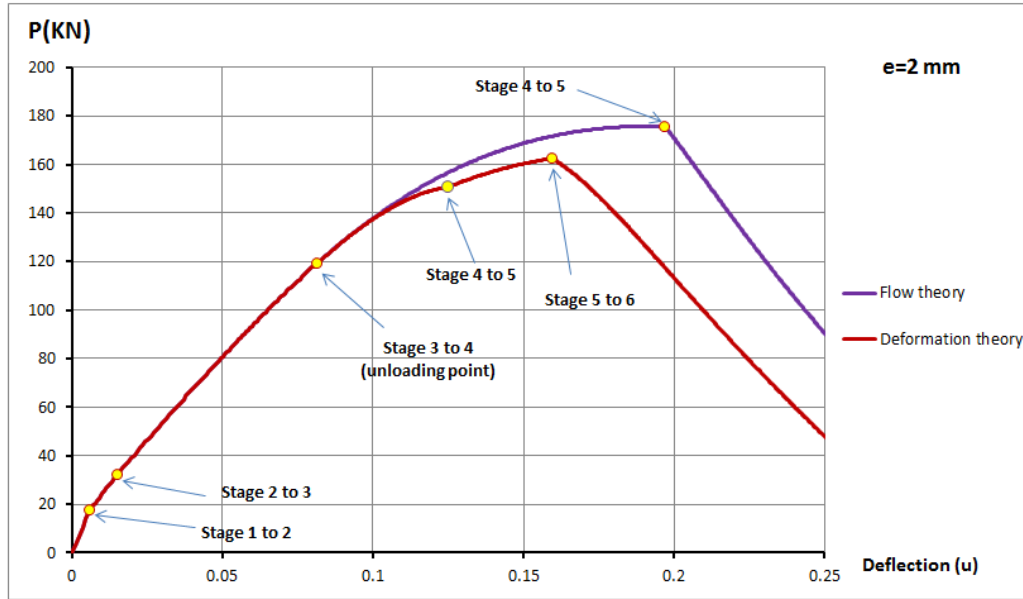


Figure 3.25: $P - u$ plot from the simplified model: comparison between flow and deformation theory, $e = 2$ mm.

3.6. Conclusions

The discrepancy between the presented results and those in the literature by many other authors can be summarised by stating that, according to the performed numerical investigations in the cases under consideration here there is actually no plastic buckling paradox. In fact, the flow theory of plasticity, which provides a physically sound description of the behaviour of metals, leads to predictions of the buckling stress which are in better agreement with the corresponding test results than those provided by use of the deformation theory.

This is in contrast to the conclusions by other authors and with the widely accepted belief that the flow theory leads to a significant overestimation of the buckling stress while the deformation theory leads to much more accurate predictions and, therefore, is the recommended choice for use in practical applications. The reason for these different conclusions has been carefully investigated from different standpoints and with the help of simplified models.

The roots of the discrepancy, according to present results, may be found in the simplifying assumptions with regards to assumed buckling modes used as the basis of many analytical investigations and essentially in the fact that

adopting the deformation theory of plasticity contributes to counterbalance the excessive stiffness induced by kinematically constraining the cylinders to follow predefined buckling modes, thus providing results that are only apparently more in line with the experimental findings. Furthermore, additional analytical investigations could be carried out by taking into consideration buckling modes different from the harmonic one and evaluate if this can deliver any improvement in the predictions based on the flow theory of plasticity.

Chapter 4

A Numerical and Analytical Investigation into the Plastic Buckling Paradox for Circular Cylindrical Shells under Non-Proportional Loading

4.1. Introduction

In Chapter 3 the so-called “plastic buckling paradox” of cylinders subjected to axial compression was investigated by conducting accurate finite-element modelling of the buckling of cylindrical shells using both the flow theory and the deformation theory of plasticity. It was found that, in contrast to common understanding, a very good agreement between numerical and experimental results can be obtained in the case of the physically sound flow theory of plasticity. The discrepancy between the presented results and those in the literature by many other authors can be summarised by stating that, according to the performed numerical investigations in the cases under consideration, no plastic buckling paradox actually exists. In fact, the flow theory of plasticity, which provides a physically sound description of the behaviour of metals, leads to predictions of the buckling stress which are in better agreement with the corresponding test results than those provided by use of the deformation theory.

The roots of the discrepancy may be in the simplifying assumptions with regard to assumed buckling modes used as the basis of many analytical investigations and essentially in the fact that adopting the deformation theory of plasticity contributes to counterbalance the enhanced stiffness induced by kinematically constraining the cylinders to follow predefined buckling modes.

In the case of axially loaded cylinders studied in Chapter 3, material points are generally subjected to proportional loading in the elastic range, and this remains relatively true also in the initial phase of plastic buckling. Nevertheless, the flow and deformation theory seem to provide quite different results. It is, therefore, not surprising that similar or even more significant discrepancies have been reported between the results from the flow and deformation theory in the case of non-proportional loading.

It was noted in Section 2.9 that, for the case of cylinders subjected to axial tensile load and external pressure, Blachut et al. (1996) and Giezen et al. (1991) concluded that the flow theory significantly over predicts the plastic strains and buckling loads for high tensile loads while the deformation theory leads to acceptable plastic strains and buckling loads that are more in line with experimental observations in most cases. In many practical applications the deformation capacity is the main concern rather than buckling load. For instance for reeling of pipelines, one is interested in how far one can bend a pipe without wrinkling it and incorrect prediction of strains calculated using the flow plasticity are not acceptable (Peek, 2000). Additionally, one cannot use the deformation theory in the post-buckling analysis of shells because it does not account for elastic unloading after bifurcation. This led the prudent designer not to rely only on the flow theory, and moved researchers to attempt a revised deformation theory by including unloading (Peek, 2000) or propose a total deformation theory applicable for non-proportional loading defined as a sequence of linear loadings (Jahed et al., 1998).

This chapter aims to shed further light on the plastic buckling paradox by means of carefully conducted finite-element (FE) analyses of cylindrical shells using both the flow theory and the deformation theory of plasticity. Results are compared with the experimental and the numerical results

obtained by Blachut et al. (1996) and Giezen et al. (1991) using the code BOSOR5. The study also aims to examine the sensitivity of the predicted critical strains and buckling pressures with respect to the applied tensile load. Moreover, it attempts to provide further understanding of the apparent discrepancy between the predictions of the flow and deformation theories of plasticity by means of a straightforward analytical approach, which moves from the formulation presented by Chakrabarty (2010) and employs both the flow and deformation theories. The obtained analytical results are again compared with the experimental and numerical results obtained in Blachut et al. (1996) and Giezen et al. (1991) using the code BOSOR5 and with the present numerical ones.

The analysis is focused on machined short cylindrical shells subjected to non-proportional loading consisting of axial tension and increasing external pressure, with length-to-outer diameter ratio L/D ranging between 1 and 2 because this allowed us to compare our numerical results with the classical experimental results reported in the literature by Blachut et al. (1996) and Giezen et al. (1991).

4.2. Test samples and finite-element modelling

4.2.1. Geometry and elements

The plastic buckling of selected imperfect cylinders tested by Blachut et al. (1996) and Giezen et al. (1991), subjected to uniform external pressure and axial tensile load, has been numerically simulated using nonlinear FE analyses using both the flow theory and the deformation theory of plasticity, adopting the FE code ABAQUS, version 6.11-1 (Simulia, 2011).

4.2.1.1 Modelling of tests made by Blachut et al. (1996)

Blachut et al. (1996) conducted tests on 30 machined cylinders made of mild steel with outer diameter 34 mm and length-diameter ratio (L/D) of 1.0, 1.5 and 2.0. In the experimental setting, one flange of the specimen was rigidly attached to the end flange of the pressure chamber and the other flange was bolted to a coupling device which in turn was bolted to the load cell, see

Figure 4.1. The load cell was centred with respect to the test chamber in order to prevent any eccentricity of the axial load exerted on the specimen. The authors reported that the maximum initial radial imperfection measured at the mid-length of the specimens was about 1% of the wall thickness.

In the present investigation, in order to keep the numerical analyses at a reasonable number, twelve cylinders were chosen, as illustrated in Table 4.1, in such a way that (a) a significant range of L/D is covered in the study and (b) for all the selected cases, except S2 and L4, the flow theory of plasticity failed to predict buckling numerically according to Blachut et al. (1996).

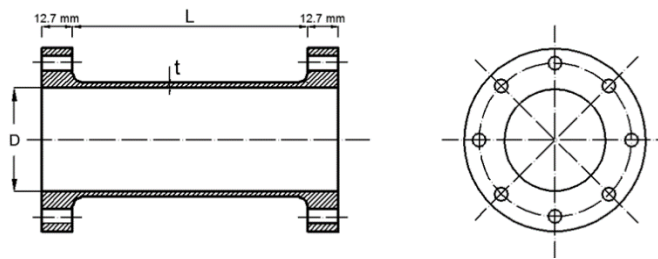


Figure 4.1: Experimental setting (Blachut et al., 1996).

Spec.	Geometry of the cylinders		
	D (mm)	t (mm)	L/D
S1	34.01	0.685	0.982
S2	33.98	0.688	0.983
S3	34.05	0.667	0.982
S4	34.07	0.667	0.982
S5	33.98	0.679	0.981
S6	34.06	0.704	0.979
S7	33.97	0.675	0.982
M2	34	0.616	1.47
M12	33.59	0.669	1.474
M7	33.97	0.63	1.473
L4	34	0.669	1.961
L8	33.96	0.693	1.964

Table 4.1: Geometry of tested cylinders.

In the FE modelling one reference point has been located at the centre of the top end of the cylinder and the axial displacements of all the nodes at the top edge of the cylinder have been constrained to the axial displacement of this reference point. The axial tensile load has been applied directly to the reference point. All the other degrees of freedom of the nodes at the top edge

have been restrained. The bottom edge of the shell has been considered fully fixed, i.e. with no allowed translation or rotations at any node.

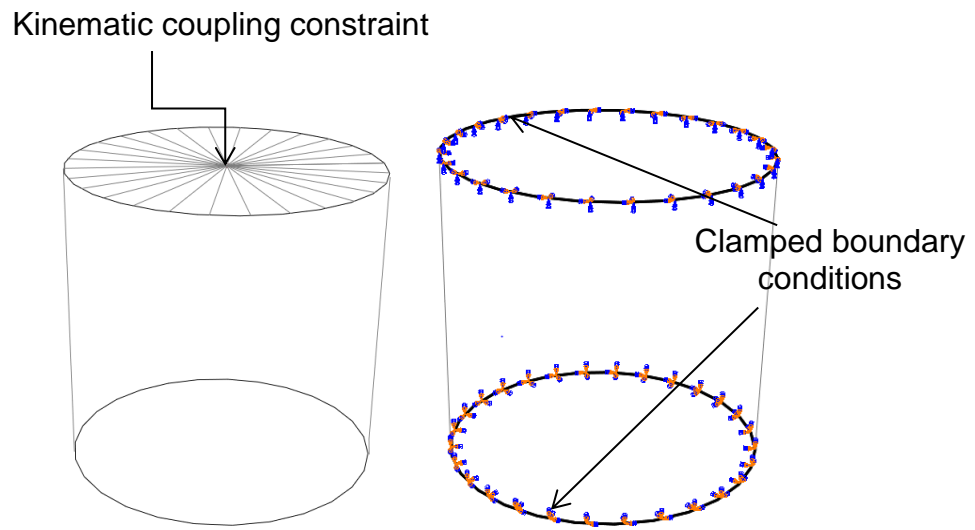


Figure 4.2: Boundary conditions.

In order to simulate the experimental settings, two types of loading have been considered: axial tensile load in the longitudinal direction and external pressure applied normally to the surface of the shell elements (Table 4.2). First the tensile load has been applied and held constant. Successively, an increasing lateral pressure has been applied.

Specimen	S1	S2	S3	S4	S5	S6	S7
Axial tension (N)	17960	0	18000	3990	12010	15030	7970

Specimen	M2	M12	M7	L4	L8
Axial tension (N)	10670	18530	15060	8210	16490

Table 4.2: Axial tension values for the selected cylinders.

The cylinders have been modelled by means of the general-purpose 4-noded fully-integrated shell element, “S4” (Simulia, 2011), whose features have already been discussed in Section 3.2.1.

A structured mesh was used, made from a number of divisions along the circumference and longitudinal direction, as reported in Table 4.3 for each specimen.

	Specimens						
Number of elements	S1	S2	S3	S4	S5	S6	S7
- around the circumference	200	200	200	200	200	200	200
- along the length	63	63	63	63	63	63	63

	Specimens				
Number of elements	M2	M12	M7	L4	L8
- around the circumference	200	200	200	200	200
- along the length	94	94	94	125	125

Table 4.3: FE mesh discretisation adopted for the analyses of the cylinders tested by Blachut et al. (1996).

4.2.1.2 Modelling of tests made by Giezen et al. (1991)

In the test carried out by Giezen et al. (1991), the cylindrical specimens were made of aluminium alloy 6061-T4. Two sets of specimens were tested, namely Set A and Set B. The average wall-thickness values of the first and second set were 0.76 and 0.71 mm, respectively, and the length-to-diameter ratio (L/D) was equal to one. The maximum initial imperfections were found to be about 0.076mm (10% of the thickness) (Giezen et al., 1991).

For the present numerical analysis only specimens subjected to constant axial tensile load and increasing external pressure have been chosen, as shown in Table 4.4 and Table 4.5.

Specimen	SP.1	SP.2	SP.3	SP.4	SP.5	SP.6	SP.7
Axial tension (N)	0	1254.4	2508.8	4076.8	5205.8	6021.2	6522.9
n. of buckling waves	5	5	5	5	4	4	4

Specimen	SP.8	SP.9	SP.10	SP.11	SP.12	SP.13
Axial tension (N)	6899.2	7902.8	9408.1	11666	12920.4	14613.80
n. of buckling waves	4	4	4	4	4	4

Table 4.4: Axial tensile load and observed number of buckling waves (in the circumferential direction) for Set A specimens

Specimen	SP.1	SP.2	SP.3	SP.4	SP.5	SP.6	SP.7
Axial tension (N)	0	2343.76	4793	7089.9	9375	11777.4	14062.6
n. of buckling waves	4	4	4	4	4	4	4

Table 4.5: Axial tensile load and observed number of buckling waves (in the circumferential direction) for Set B specimens.

Again, a 4-noded shell elements (S4) has been used with a structured mesh and a division of 210 and 67 elements along the circumference and the length, respectively. The same boundary conditions used to simulate Blachut's experiments have been adopted.

4.2.2. Material parameters

The uniaxial stress-strain relationship of the material under monotonic loading has been characterised by means of the Ramberg-Osgood law, i.e Eq. (3.1).

The Ramberg-Osgood input parameters used in the numerical simulations are reported in Table 4.6.

	E [MPa]	σ_y [MPa]	ν	n_p	α
Blachut's test	212000	328 or 290	0.31	300	0.428
Giezen's test-Set A	65129.73	177.75	0.3	16	0.733
Giezen's test-Set B	60986.34	165.37	0.3	11.76	0.738

Table 4.6: Ramberg-Osgood constants used in the numerical analyses.

Blachut et al. (1996) conducted longitudinal tensile tests on a number of coupons to determine the mechanical properties of the cylindrical specimens. They reported that the yield plateau in the stress-strain relationship of the material appears to be extended to a strain value of almost 3%, see Figure 4.3. Moreover, they observed that the upper yield stress of the tested coupons, cut along the longitudinal direction of the cylinders, varied from 280 to 360 MPa, with an average value of 328 MPa, and the lower yield stress from 275 to 305 MPa, with an average value of 290 MPa (Blachut et al., 1996). In the present numerical analysis both the average upper yield stress,

$\sigma_y^u = 328\text{MPa}$, and the average lower yield stress, $\sigma_y^l = 290\text{ MPa}$, were employed in order to perform meaningful comparisons.

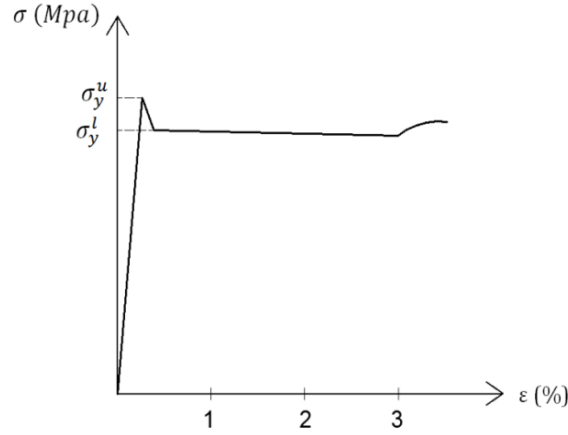


Figure 4.3: Typical stress-strain curve of the mild steel.

With respect to Blachut's examples, two approaches have been used in the present numerical analyses. In the first use has been made of an elastic-perfectly plastic flow theory (EPP flow theory). In the second recourse has been made to an isotropic nonlinear hardening material model with an initial yield stress close to zero and a hardening curve based on the Ramberg-Osgood law (NLH flow theory). A detailed description of this implementation in the case of the flow theory of plasticity is given in Section 3.2.2.

It is worth noticing that, despite the very high value of the hardening parameter, the NLH flow theory cannot reproduce the elastic-perfectly plastic behaviour of the material undergoing monotonic loading, see Figure 4.4.

In order to compare the results from the flow theory with those from the deformation theory, the input parameters of the flow theory in the numerical analyses have been tuned so that the same stress-strain curve of the material as in the case of the deformation theory is obtained for the case of uniaxial stress and monotonic loading, to within a negligible numerical tolerance.

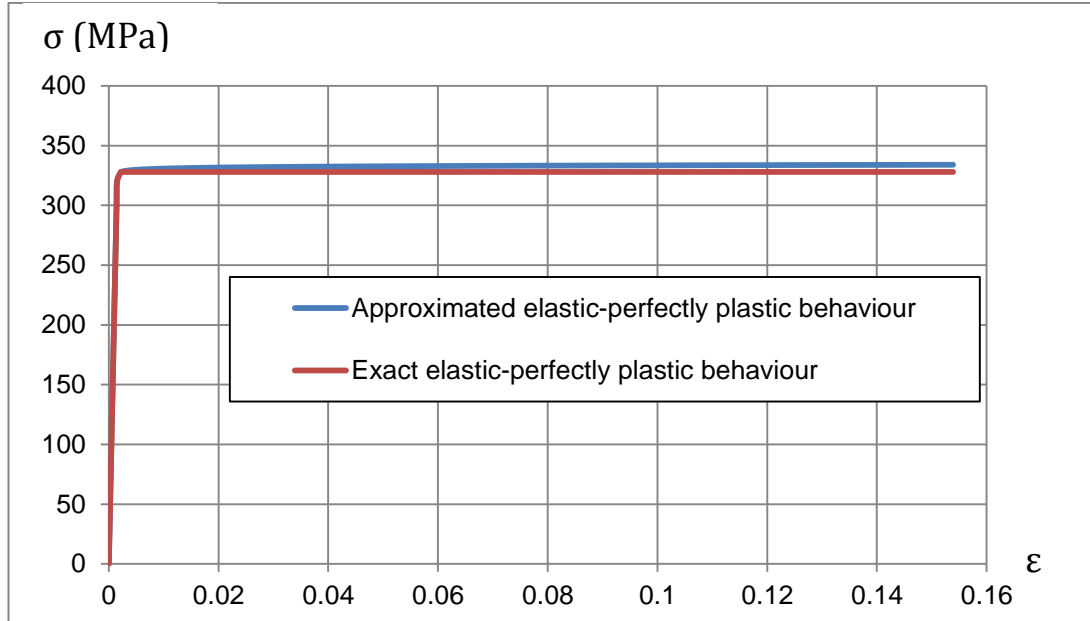


Figure 4.4: Comparison between the approximated and the exact elastic-perfect plastic material behaviour.

Giezen et al. (1991) reported stress-strain data recorded from material tests on a number of strips machined from the original tubes of the sets A and B to evaluate the material properties of the cylindrical specimen.

With respect to Giezen 's examples, in the present study the material behaviour has been simply determined by fitting the Ramberg-Osgood relation to the available data set, as shown in Figure 4.5 and Figure 4.6.

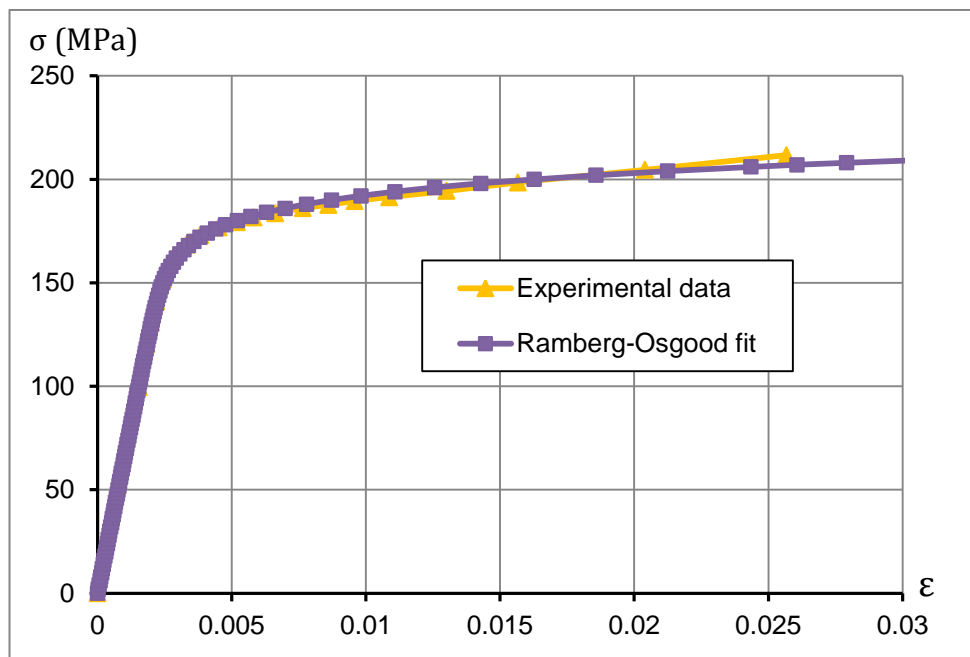


Figure 4.5: Ramberg-Osgood fit (Set A).

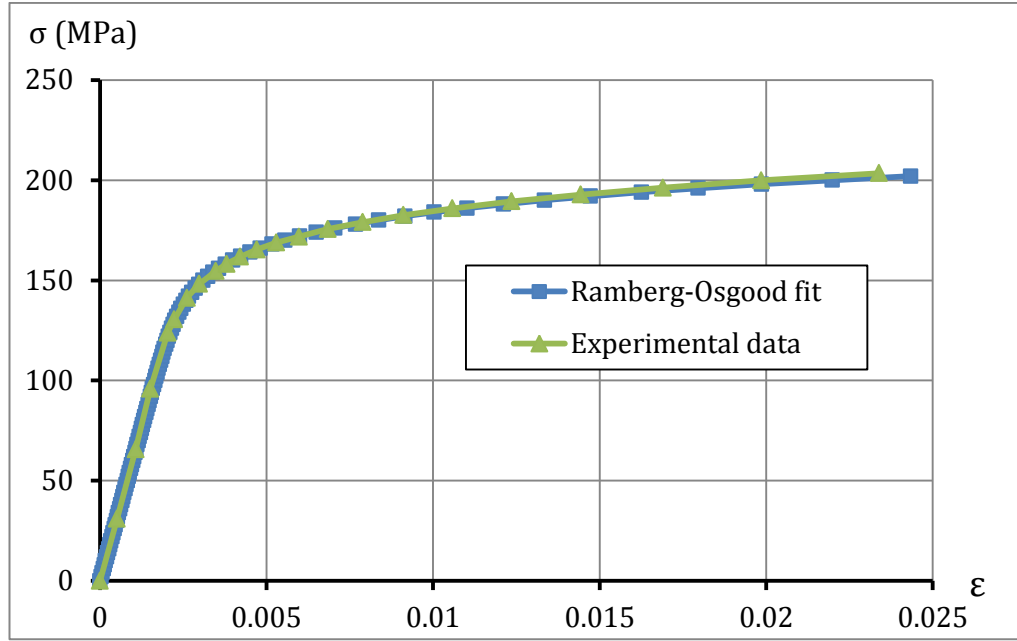


Figure 4.6: Ramberg-Osgood fit (Set B).

The formulations of the flow and deformation theories of plasticity adopted in the numerical simulations are reported in Appendix A1 and Section and 2.8, respectively.

4.2.3. Large displacement formulation and solution procedure

The numerical analyses have been performed accounting for large deformations by using spatial co-rotational stress and strain measures and a hypo-elastic relation between the rates of stress and elastic strain (Simulia, 2011). As discussed in Section 3.2.3, this approach can be considered sufficiently accurate for the purposes of these analyses, because, the elastic part of the strain is typically still very small and close enough to the limit where hypo-elastic and hyper-elastic formulations coincide (Simo and Hughes, 1998).

As for the analyses discussed in Chapter 3, the Riks arc-length method (Riks, 1979) has been used in the version implemented in ABAQUS (Simulia, 2011), whose main features have been already discussed in Section 3.2.4.

For the analyses presented in this chapter, the external pressure is set as λP_0 , where P_0 denotes a reference inward external pressure and λ is a scalar

multiplier. The critical load is determined by the point at which the load-arc length curve reaches a maximum.

The bifurcation point is the intersection of secondary and primary paths, which are the pre-buckling and post buckling paths, respectively. To avoid such discontinuous response at bifurcation, it is common to introduce geometric imperfections in order to remove bifurcation points (Falzon, 2006; Simulia, 2011). In this way, the post-buckling problem analysed using Riks method will turn into a problem with a continuous response. The critical point determined on the equilibrium path is the limit point and there is no bifurcation prior to collapse. The choice of the size of the imperfection and its shape is discussed in later sections. Furthermore, if analyses are conducted with progressively reduced size of the imperfection, the limit point found in those with the smallest amount of imperfections; say 0.05% or 0.1% of the thickness turns out to be a good approximation of the bifurcation load (Bushnell, private communication). This method is used later in Section 4.5.3.

4.2.4. Description of imperfections

Accounting for imperfections has been achieved by scaling and adding buckling eigenmodes to a perfect geometry in order to create a perturbed initial geometry. The scaling factor has been set as a percentage of the shell thickness, t . The analyses have been conducted for an imperfection amplitude equal to 1% of the thickness, as experimentally measured by Blachut et al. (1996).

The choice of linear elastic eigenmodes used to generate the imperfect models was made with the aim of choosing those with the same number of circumferential waves that were found experimentally in the post-buckling path. Except for specimen M2, for which a buckling mode with 3 waves was reported, Blachut et al. (1996) did not report the observed failure modes of the other cylinders. However, they did report that the number of circumferential waves observed from the test varied from 3 waves for high values of axial tensile load to 6 waves for pure applied external pressure. Therefore, for very small values of the axial load such as in specimen S2, the fifth eigenmode with 6 waves was used; for specimen M2 and for the others

which were tested with very high tensile loads, the eigenmode corresponding to 3 waves was used; for the other specimens subject to intermediate smaller or larger tensile loads, the eigenmodes with 5 or 4 waves were used, respectively. This is summarised in Table 4.7, which shows the eigenmode number used to generate the shape of imperfection in the FE models for each specimen together with the associated number of circumferential waves (see Figure 4.7).

On the other hand, Giezen et al. (1991) reported the buckling failure modes found experimentally, as illustrated in Table 4.4 and Table 4.5. Hence, for these cases the eigenmodes used to generate the imperfections are those with the same number of waves found experimentally, with a single wave in the longitudinal direction. Accordingly, the eigenmodes with five circumferential waves have been chosen to generate initial imperfection's shape for specimens SP.1 to SP.4 in Set A and those with four waves have been chosen for the rest of the specimens (see Figure 4.8). The analyses have been conducted for an imperfection amplitude equal to 10% of the thickness for both Set A and B, as experimentally measured by Giezen et al. (1991).

In all the cases the linear buckling analysis has been conducted assuming linear elastic material behaviour and small displacements, under constant axial tensile loading.

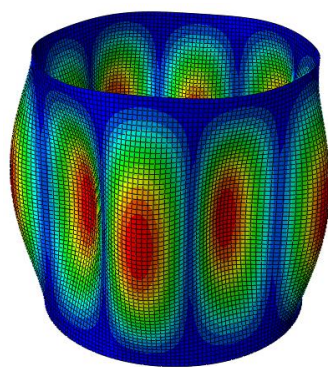
It is worth pointing out that existing results show that it is not universally true for geometrically imperfect structures to fail by collapse at a reduced magnitude of load. In fact, Blachut and Galletly (1993) observed that the elastic buckling load of externally pressurized torispheres was not affected by local flattening with small amplitudes and this fact was verified experimentally. Actually, the limit carrying load of shells of revolution is known to exhibit complex phenomena including mode switching and interaction and many analyses of the non-axisymmetric buckling deformation of spherical domes suggest that the observed deformation at collapse is mostly determined by the form of the imperfections, rather than by their magnitude.

This seems to be hardly the case with the circular cylindrical shells object of the present study, especially in the case of non-proportional loading. In fact, apart from the observation that the behaviour described by Blachut and Galletly tends to depend on the rise of the torispheres, a geometric characteristic which does not pertain to cylinders, in the performed numerical analyses, the R/t ratio of the cylinders was about 25, placing the buckling in a substantially pure plastic range, where imperfect shells are prone to show a reduced collapse load with respect to perfect ones. As an additional point, Figure 4.23 and Figure 4.25 show that the plastic buckling resistances of the cylinders under analysis are actually sensitive to imperfection amplitudes.

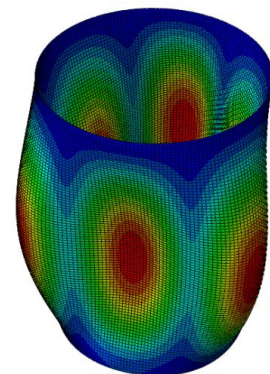
Specimens	S1	S2	S3	S4	S5	S6	S7
Eigenmode number	3	5	3	1	3	3	1
Number of circumferential waves	4	6	4	5	4	3	5

Specimens	M2	M12	M7	L4	L8
Eigenmode number	7	7	7	1	3
Number of circumferential waves	3	3	3	4	3

Table 4.7: Number of circumferential waves used to generate imperfections in the FE modelling for the specimens tested by Blachut et al. (1996).

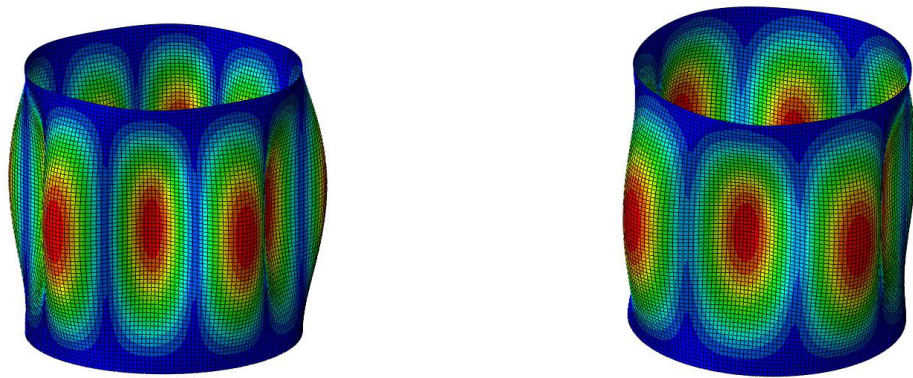


First eigenmode for S4 cylinder



Seventh eigenmode for M2 cylinder

Figure 4.7: Buckling eigenmodes used in the simulation of Blachut's tests to account for initial imperfections.



First eigenmode for SP.1 (Set A) cylinder Fifth eigenmode for SP.1 (Set B) cylinder

Figure 4.8: Buckling eigenmodes used in the simulation of Giezen's tests to account for initial imperfections.

4.3. Finite-element results for the experiments in Blachut et al. (1996)

4.3.1. Comparison of the numerical results with experimental results

The plastic buckling pressures, based on the deformation theory, the EPP flow theory and the NLH flow theory of plasticity, have been calculated for different specimen geometries, axial tensions and both values of the average yield stress. The results are illustrated in Figure 4.9 and show that the buckling pressure results predicted by the NLH flow theory and the deformation theory of plasticity are extremely close to each other.

The calculated buckling pressures based on the flow theory and the deformation theory in conjunction with the upper value of the yield stress are in better agreement with experimental results for the specimens S2, S3, S5, S7, M2, M12, M7, and L4. The calculated buckling pressures based on the flow theory and the deformation theory in conjunction with the lower value of the yield stress are in better agreement with experimental results for the specimens S1, S4, S6, and L8.

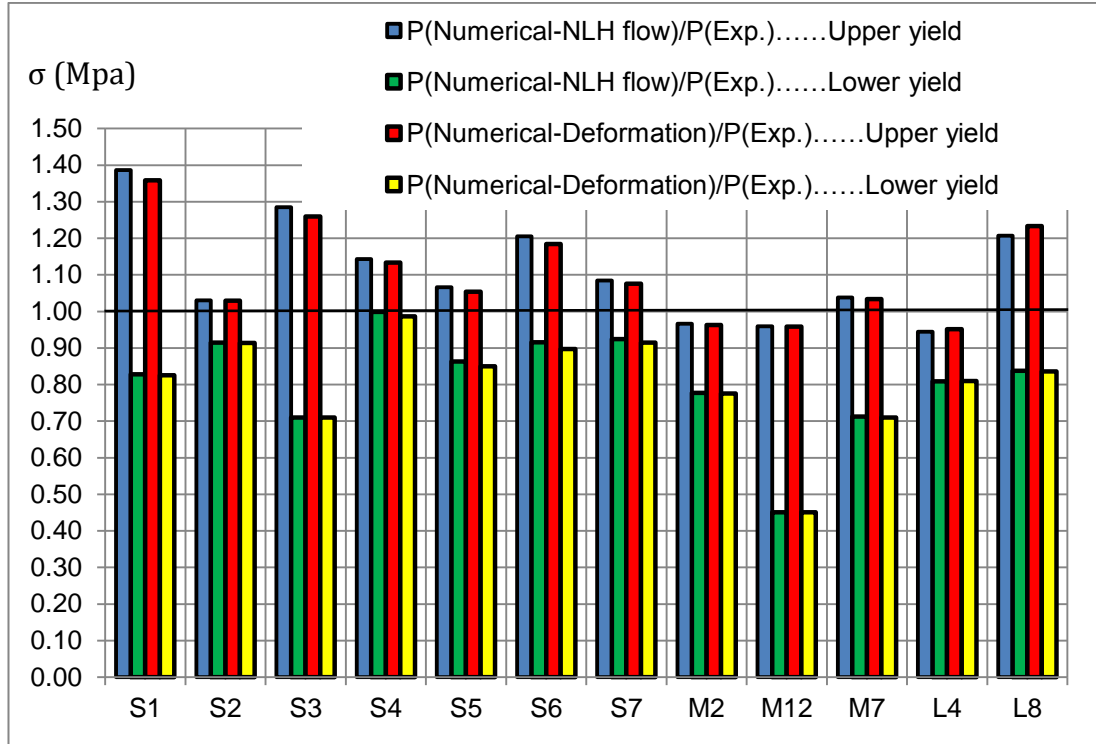


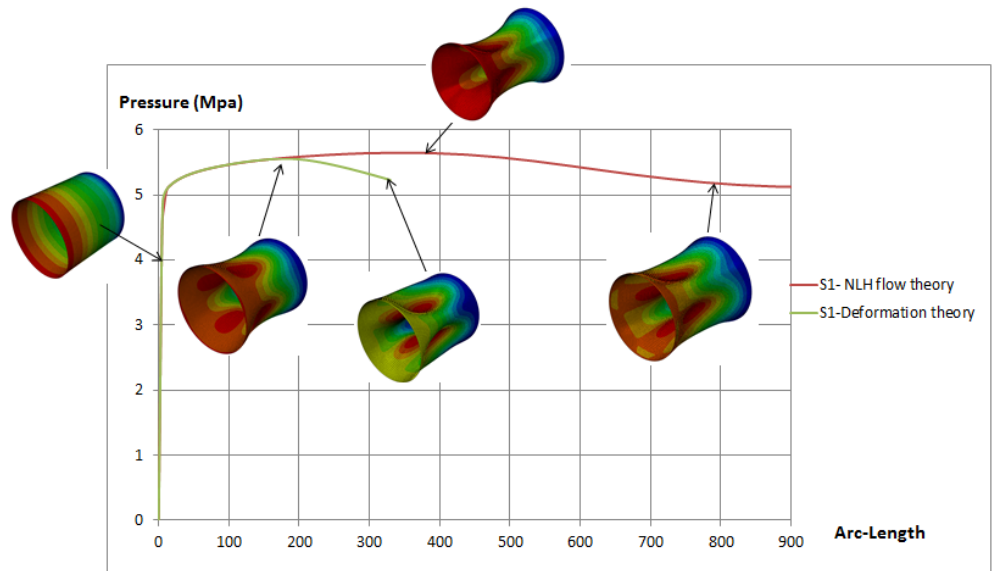
Figure 4.9: Comparison between experimental and numerical results for both the deformation theory and the NLH flow theory of plasticity.

Figure 4.10 shows the external pressure vs arc length plots resulting from flow and deformation plasticity for different specimens. It can be noticed that the curve predicted by the flow theory lays above the curve predicted by the deformation theory for most cases.

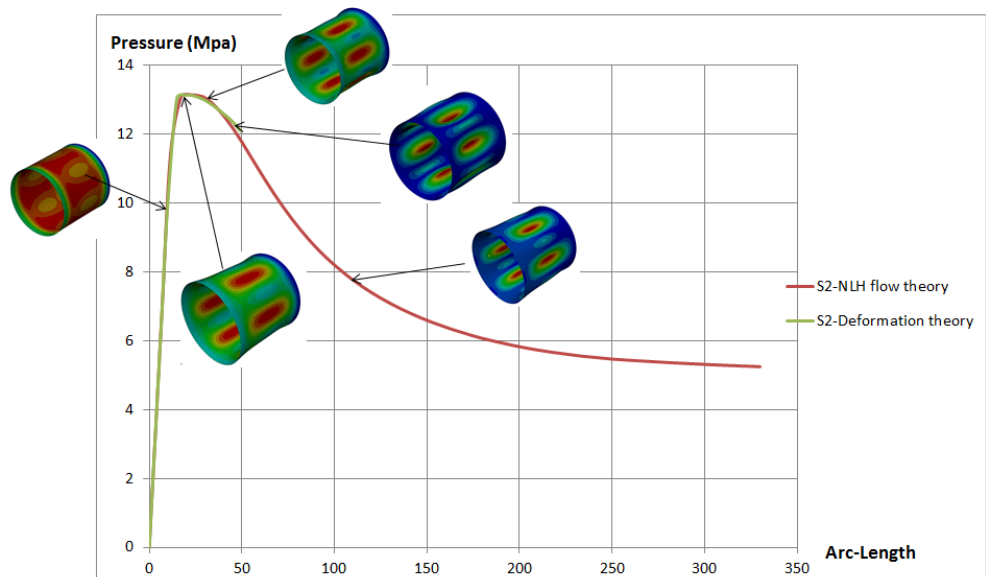
Figure 4.11 and Figure 4.12 show the predicted circumferential and meridian plastic strains at the onset of buckling according to the flow and deformation theory of plasticity. It can be observed that the differences in the predictions increase with the intensification of the applied tensile load.

Figure 4.11 and Figure 4.12 show that both plasticity theories succeed in predicting buckling with physically acceptable plastic strains for all specimens. In fact, although the maximum plastic strains calculated at the buckling pressure in meridian and circumferential directions and predicted by the NLH flow theory of plasticity are larger than those predicted by the deformation theory, the result still acceptable for all specimens with $L/D \approx 1$. Additionally, Table 4.8 to Table 4.10 show that meridian and circumferential plastic strains predicted using the flow theory of plasticity are physically realistic, being smaller than 1.5%, with the exception of specimens S1, S3

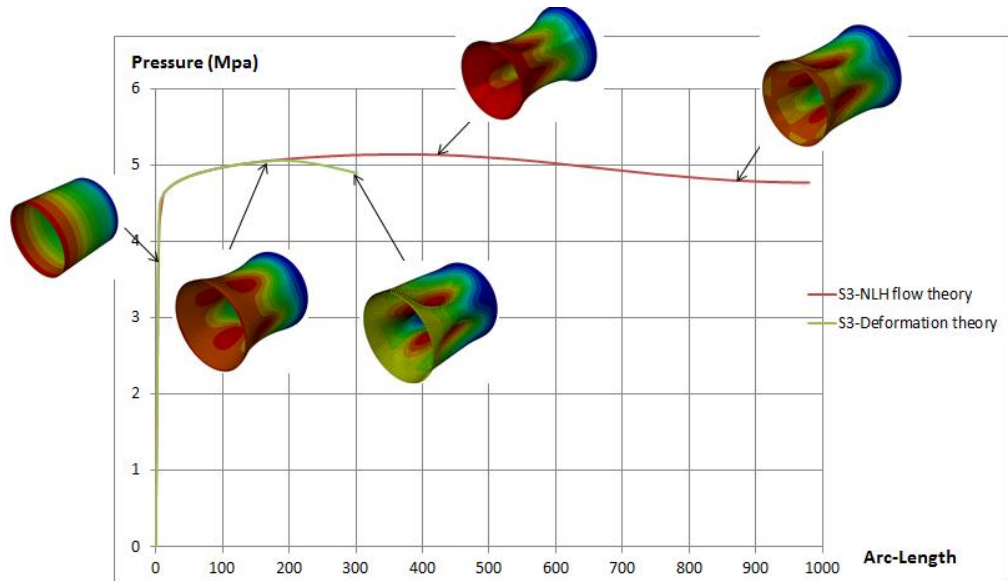
and S6 in Table 4.10, albeit with values still largely below 5%. The plastic buckling pressures presented in Figure 4.9 and calculated using the flow theory can be thus considered all physically acceptable.



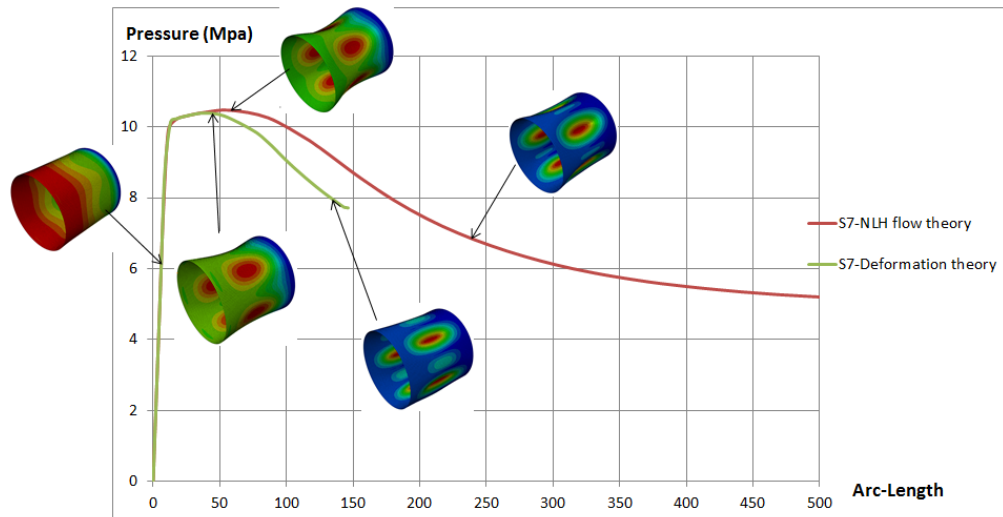
(a) External pressure versus arc-length for specimen S1



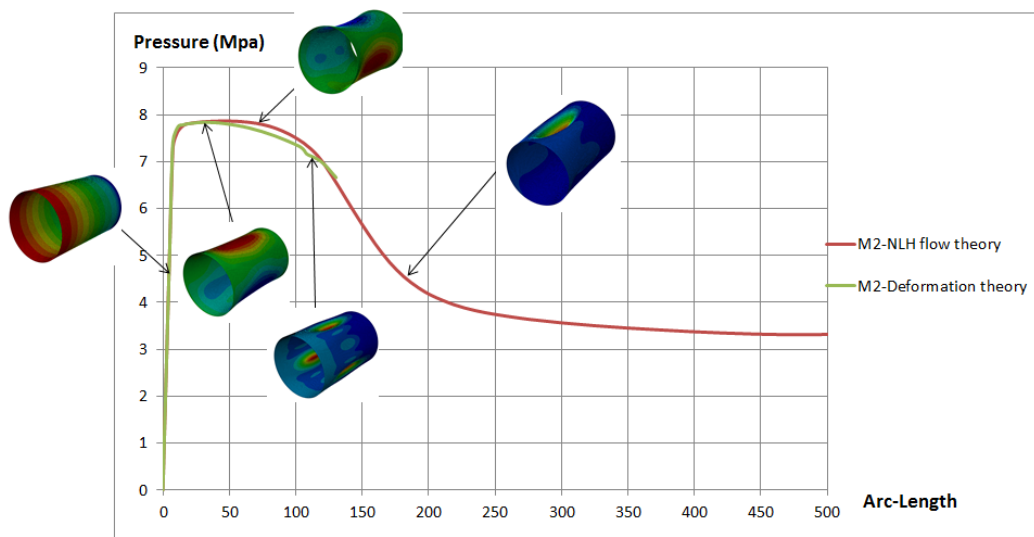
(b) External pressure versus arc-length for specimen S2



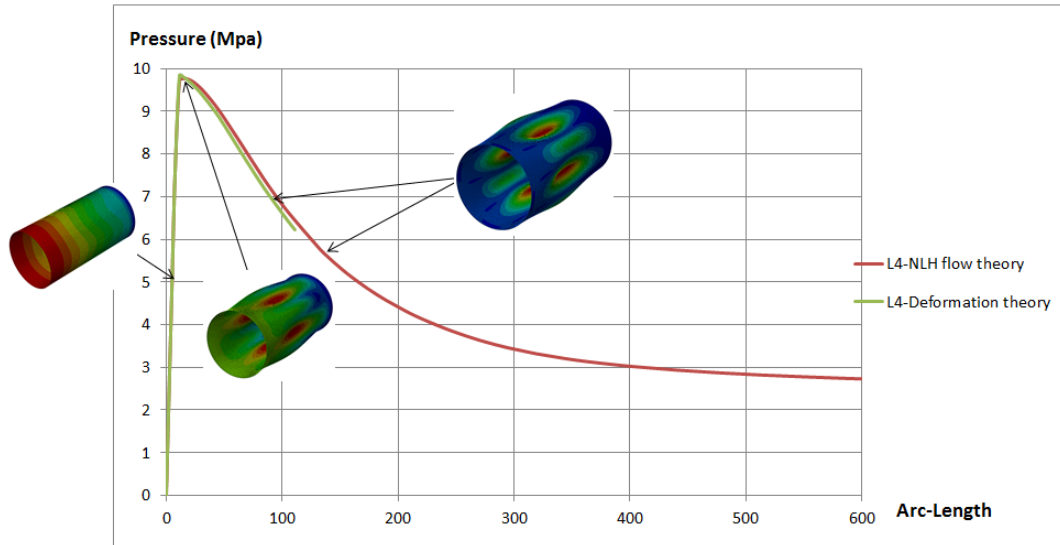
(c) External pressure versus arc-length for specimen S3



(d) External pressure versus arc-length for specimen S7



(e) External pressure versus arc-length for specimen M2



(f) External pressure versus arc-length for specimen L4

Figure 4.10: External pressure vs. arc-length curves for specimens (a) S1, (b) S2, (c) S3, (d) S7, (e) M2 and (f) L4 (upper value of the yield stress) showing the buckling response, ultimate external pressure and deformation modes before, after and at the limit pressure load (colour indicating the total deformation).

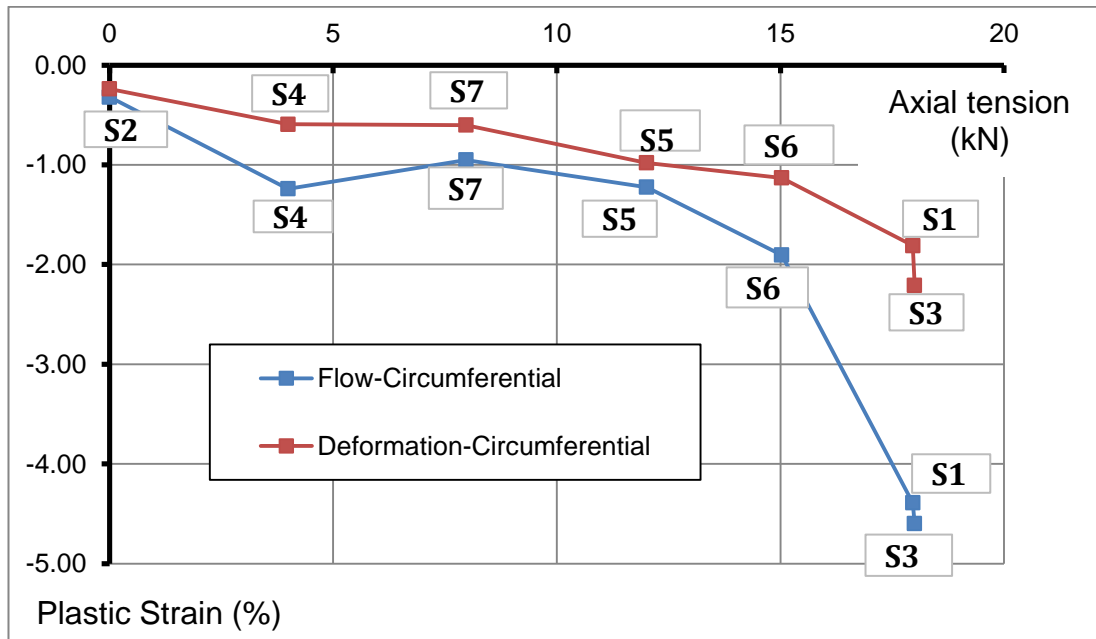


Figure 4.11: Maximum circumferential plastic strains at the mid-section of the cylinders under combined loading ($L/D \cong 1$), calculated using the upper value of the yield stress.

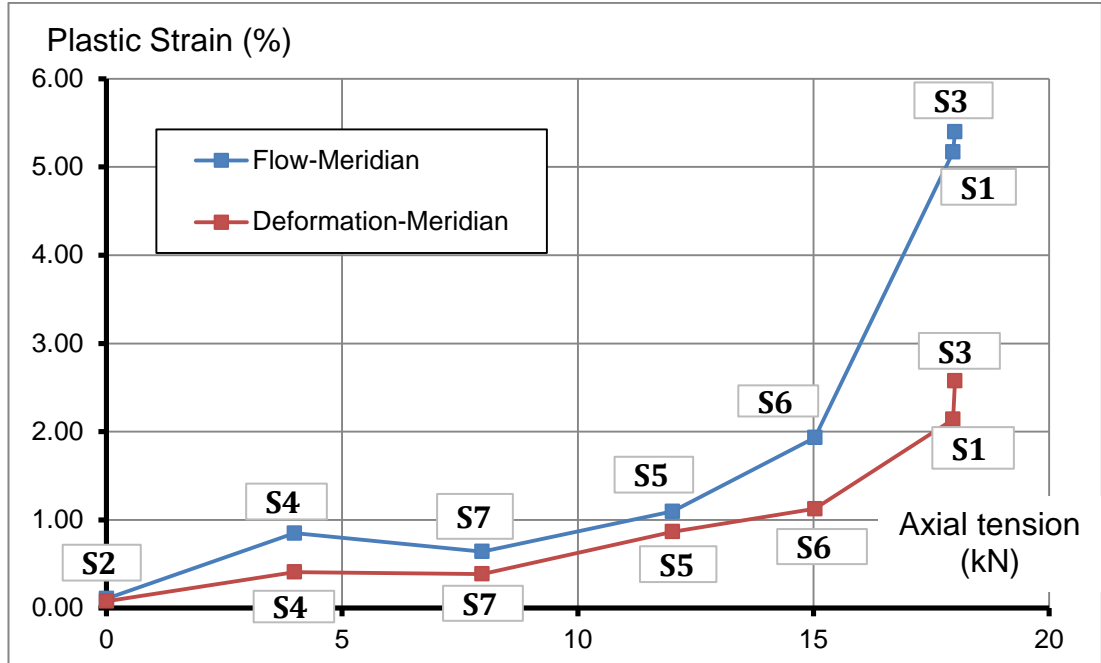


Figure 4.12: Maximum meridian plastic strains at the mid-section of the cylinders under combine loading ($L/D \cong 1$), calculated using the upper value of the yield stress.

Spec	M2		M12		M7		L4		L8	
	C	M	C	M	C	M	C	M	C	M
S=0	-0.028	0.320	-0.030	0.320	-0.027	0.242	-0.021	0.176	-0.0245	0.205
S=0.25	-0.453	0.403	-0.580	0.750	-0.380	0.404	-0.065	0.044	-0.210	0.231
S=0.5	-0.679	0.603	-0.960	1.250	-0.638	0.660	-0.151	0.087	-0.309	0.318
S=0.75	-0.453	0.403	-0.640	0.866	-0.380	0.404	-0.065	0.037	-0.210	0.223
S=1	-0.028	0.320	-0.030	0.320	-0.027	0.242	-0.021	0.176	-0.0245	0.205

Table 4.8: Maximum plastic strains (%) at the buckling at different sections of the cylinders ($S=x/L$), according to the NLH flow theory of plasticity and using the upper value of the yield stress (C-circumferential direction; M-meridian direction).

Spec	M2		M12		M7		L4		L8	
	C	M	C	M	C	M	C	M	C	M
S=0	-0.023	0.266	-0.026	0.454	-0.207	0.220	0.018	0.160	-0.020	0.190
S=0.25	-0.330	0.298	-0.734	0.961	-0.261	0.273	-0.047	0.032	-0.138	0.150
S=0.5	-0.480	0.420	-1.268	1.656	-0.417	0.421	-0.127	0.071	-0.179	0.182
S=0.75	-0.330	0.298	-0.734	0.961	-0.261	0.273	-0.047	0.032	-0.138	0.150
S=1	-0.023	0.266	-0.026	0.454	-0.207	0.220	0.018	0.160	-0.020	0.190

Table 4.9: Maximum plastic strains (%) at the buckling at different sections of the cylinders ($S=x/L$), according to the deformation theory of plasticity and using the upper value of the yield stress.

Spec.	NLH flow theory		Deformation plasticity	
	Circumferential	Meridian	Circumferential	Meridian
S1	-2.66	4.00	-2.96	4.52
S2	-0.36	0.13	-0.28	0.09
S3	-2.63	4.14	-2.06	3.30
S4	-1.25	0.88	-0.49	0.34
S5	-1.80	1.54	-0.91	0.88
S6	-2.60	2.93	-1.66	1.77
S7	-1.00	0.77	-0.67	0.51
M2	-0.94	0.89	-0.56	0.53
M12	-0.52	0.84	-0.62	1.00
M7	-0.83	1.02	-0.83	0.94
L4	-0.13	0.08	-0.86	0.14
L8	-0.57	0.69	-0.37	0.44

Table 4.10: Maximum plastic strains (%) at the buckling pressure based on the flow theory and the deformation theory of plasticity, calculated using lower value of yield stress.

4.3.2. Comparison of the FE results with the numerical results by Blachut et al. (1996)

Blachut et al. (1996) conducted numerical analyses of their experimental tests using the code BOSOR5. In their investigation they looked for the plastic buckling pressure and investigated which plasticity theory used in BOSOR5 seemed to better agree with the test results. The most significant finding was that the maximum plastic strains for most of numerically tested cylinders as predicted by the flow theory were an order of magnitude greater than those predicted by the deformation theory of plasticity. As a

consequence, they concluded that the flow theory predictions (including buckling pressures) were physically unrealistic and incorrect, particularly when $D/L \approx 1$.

This finding is in contrast with the numerical results from the present study, as shown in Table 4.8 to Table 4.10 and Figure 4.11 and Figure 4.12. In fact, the presented numerical findings show that the flow theory can predict buckling within physically acceptable plastic strains.

Figure 4.13 shows that although the flow theory used by Blachut et al. (1996) using BOSOR5 and the upper yield material stress failed to predict buckling for all selected specimens except for S2 and L4, the present numerical investigation based on the flow theory succeeds in predicting buckling for all specimens with physically acceptable plastic strains. Therefore, according to the presented results both plasticity theories can reasonably predict plastic buckling pressure values. Moreover, the plastic buckling pressures calculated in the FE analyses using the deformation theory are extremely close to those calculated by Blachut et al. (1996).

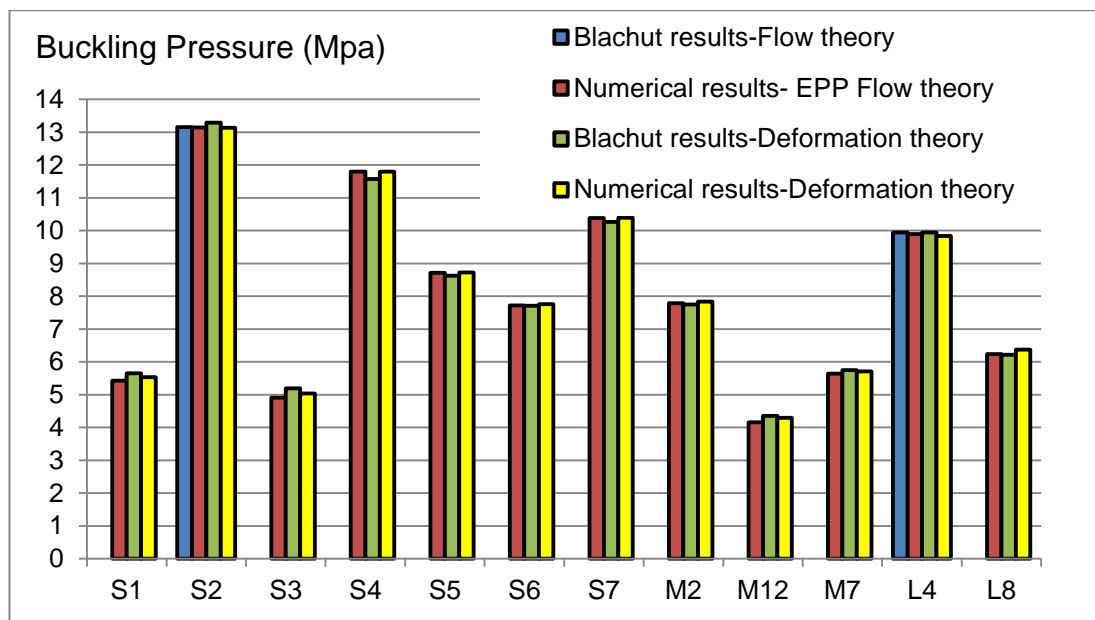


Figure 4.13: Comparison of Blachut et al. (1996) with present numerical predictions for both the flow and deformation theories of plasticity, using the upper yield stress.

Blachut et al. (1996) also reported the plastic strains obtained by means of the flow and deformation theory of plasticity for an axial tensile load of 10 kN

on the basis of the upper yield stress ($\sigma_{yp}^u = 328$ MPa), for specimens with average geometry $D/L = 0.98$ and $D/L = 1.47$. The comparison with the present numerical analyses, presented in Table 4.11(a), shows that plastic buckling pressure predicted by Blachut et al. (1996) and based on the flow theory is larger than the one predicted by the deformation theory by about 34%. Moreover, the maximum predicted plastic strains seem unacceptable and this fact led the authors to agree only with the predictions from the deformation theory. However, the present numerical investigations show that the plastic buckling pressures predicted by the flow theory are close to those by the deformation plasticity, see Table 4.11(a) and Table 4.11(b). Moreover, the maximum plastic strains resulting from the FE analyses using the flow theory and the deformation theory result different from those reported in Blachut et al. (1996) and physically acceptable. For instance, the maximum plastic strains in meridian and circumferential directions, shown in Table 4.11(a), according to the flow theory are 63% and -19.42%, respectively, while the maximum plastic strains given by the present study are 0.7% and -0.85%.

(a) $L/D = 0.98$

	Flow theory (Blachut et al.,1996)		Deformation theory (Blachut et al., 1996)	
Buckling pressure (MPa)	12.7		9.52	
Maximum plastic strains (%)	Meridian	Circumferential	Meridian	Circumferential
S=0	63.08	-0.049	1.273	-0.034
S=0.25	13.11	-13.652	0.193	-0.213
S=0.5	18.57	-19.42	0.390	-0.439
S=0.75	13.11	-13.652	0.193	-0.213
S=1	63.08	-0.049	1.273	-0.034

Plastic strains results obtained by Blachut et al. (1996) using the flow theory and the deformation theory of plasticity, $L/D=0.98$

	EPP flow theory Our numerical analysis		Deformation theory Our numerical analysis	
Buckling pressure (MPa)	9.53		9.38	
Maximum plastic strains (%)	Meridian	Circumferential	Meridian	Circumferential
S=0	0.330	-0.029	0.30	-0.0233
S=0.25	0.327	-0.423	0.249	-0.34
S=0.5	0.700	-0.85	0.54	-0.675
S=0.75	0.327	-0.423	0.249	-0.34
S=1	0.330	-0.029	0.30	-0.0233

Plastic strains results obtained by present numerical analysis using the flow theory and the deformation theory of plasticity, $L/D=0.98$

(b) $L/D = 1.47$

	Flow theory (Blachut et al.,1996)		Deformation theory (Blachutetal.,1996)	
Buckling pressure (MPa)	8.92		8.8	
Maximum plastic strains (%)	Meridian	Circumferential	Meridian	Circumferential
S=0	1.667	-0.034	0.406	-0.032
S=0.25	0.462	-0.523	0.047	-0.054
S=0.5	0.785	-0.888	0.005	-0.005
S=0.75	0.462	-0.523	0.047	-0.054
S=1	1.677	-0.034	0.406	-0.032

Plastic strains results obtained by Blachut et al. (1996) using the flow theory and the deformation theory of plasticity, $L/D=1.47$

	EPP flow theory Our numerical analysis		Deformation theory Our numerical analysis	
Buckling pressure (MPa)	8.077		8.079	
Maximum plastic strains (%)	Meridian	Circumferential	Meridian	Circumferential
S=0	0.1700	-0.0212	0.1750	-0.0188
S=0.25	0.0900	-0.1160	0.0880	-0.1150
S=0.5	0.1130	-0.1550	0.1100	-0.1500
S=0.75	0.0900	-0.1160	0.0880	-0.1150
S=1	0.1700	-0.0212	0.1750	-0.0188

Plastic strains obtained by present numerical analysis using the flow theory and the deformation theory of plasticity, $L/D=1.47$

Table 4.11: Comparison between plastic strains obtained by Blachut et al. (1996) and those by the present numerical analysis using the flow theory and the deformation theory of plasticity.

4.4. Comparison of FE results with results by Giezen et al. (1991)

Giezen et al. (1991) conducted numerical analyses on the set of cylindrical specimens tested by means of the code BOSOR5 and an axisymmetric shell formulation. They observed that the results from the deformation theory results were in better agreement with the experimental ones than those predicted by the flow theory. Moreover, the flow theory seemed to display a stiffening character, in the sense that the buckling load increased with the axial tensile load. This was in contrast with their experimental findings.

The present numerical analyses show that both the flow and the deformation theory display a softening character with the increase in the axial tensile load (Figure 4.14 and Figure 4.15). Furthermore, Figure 4.14 and Figure 4.15 show that the difference between the flow and the deformation theory predictions increases with the intensification of the non-proportionality of the load while become almost negligible when the loading tends to be proportional (i.e. when the tensile load tend to become negligible). It can be noticed that addition of axial tensile load reduces the buckling pressure. This can be explained by the fact that the axial tension is materially destabilizing because it moves the material further into the plastic region and reduce the stiffness of structure (material instability).

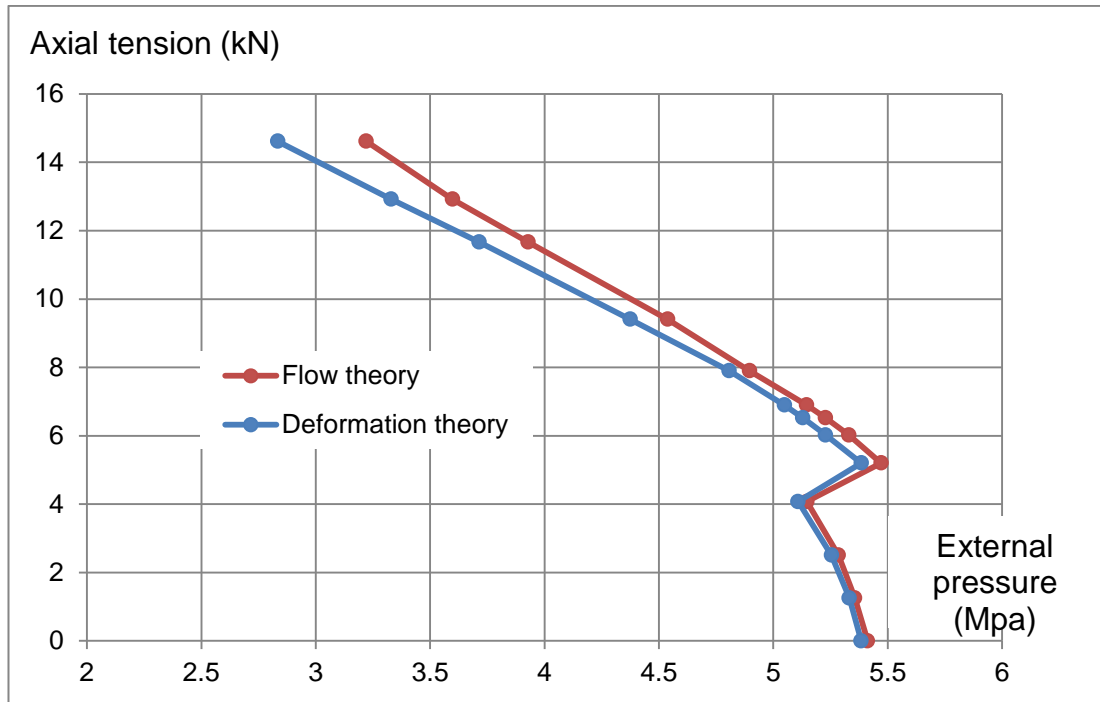


Figure 4.14: External pressure vs axial load – present numerical results (Set A)

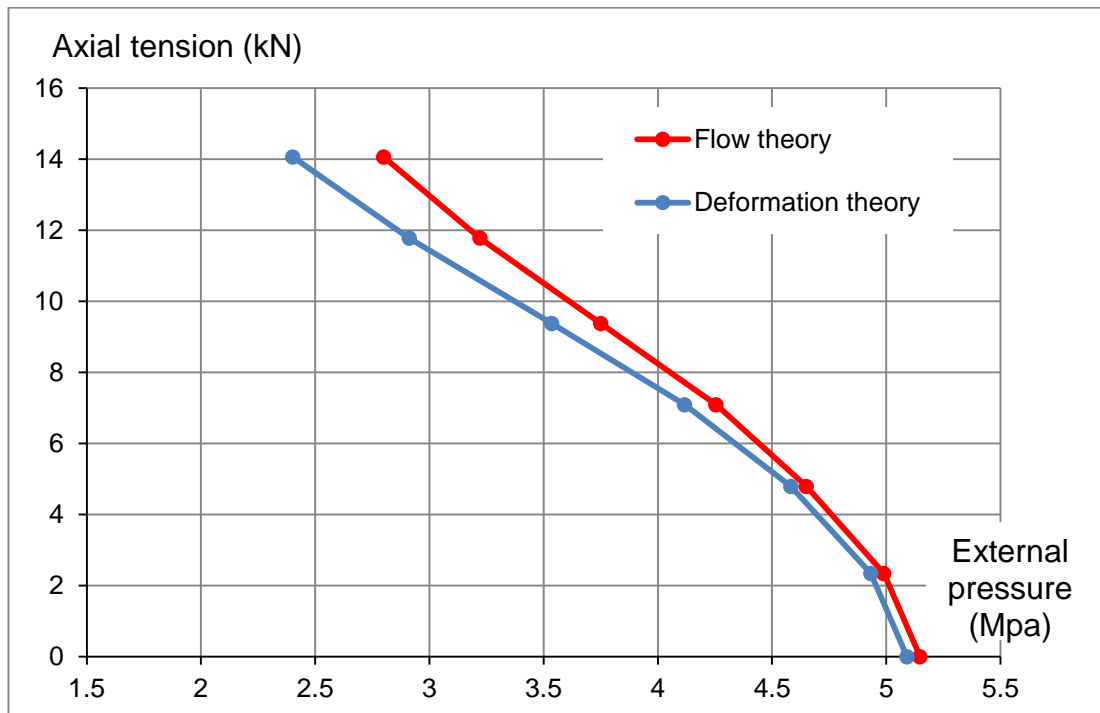


Figure 4.15: External pressure vs axial load – present numerical results (Set B).

Figure 4.16 and Figure 4.17 show that the results calculated using the flow theory are in better agreement with the test results than those using the deformation theory for all specimens except SP.7 in set B, for which the flow theory and the deformation theory over-predict the buckling pressure by 37%

and 18%, respectively. Figure 4.16 shows that the buckling pressures calculated using both the flow and deformation theories tend to fall short of the experimental values. In the case of the flow theory, the discrepancy between the numerical and experimental values ranges between 4% and 20% while in the case of the deformation theory the discrepancy ranges between 6% and 30%. On the other hand, Figure 4.17 shows that the differences with the experiment in the case of the flow theory range between 0.2% and 7.5%, with the exception of SP.7, while in the case of the deformation theory the differences range between 1.2% and 7.2%. Overall, it can be concluded that the flow theory succeeds in predicting buckling pressure in all cases except one, with a deviation from the test results which is generally below 20% and in many cases below 10%.

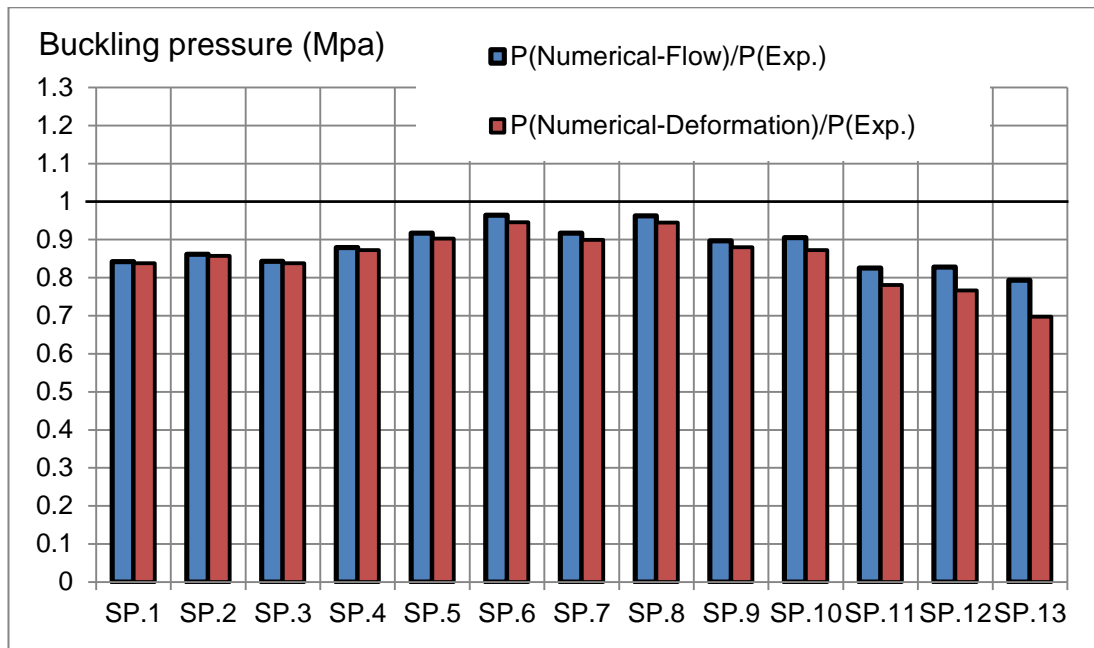


Figure 4.16: Comparison between numerical and test results (Set A).

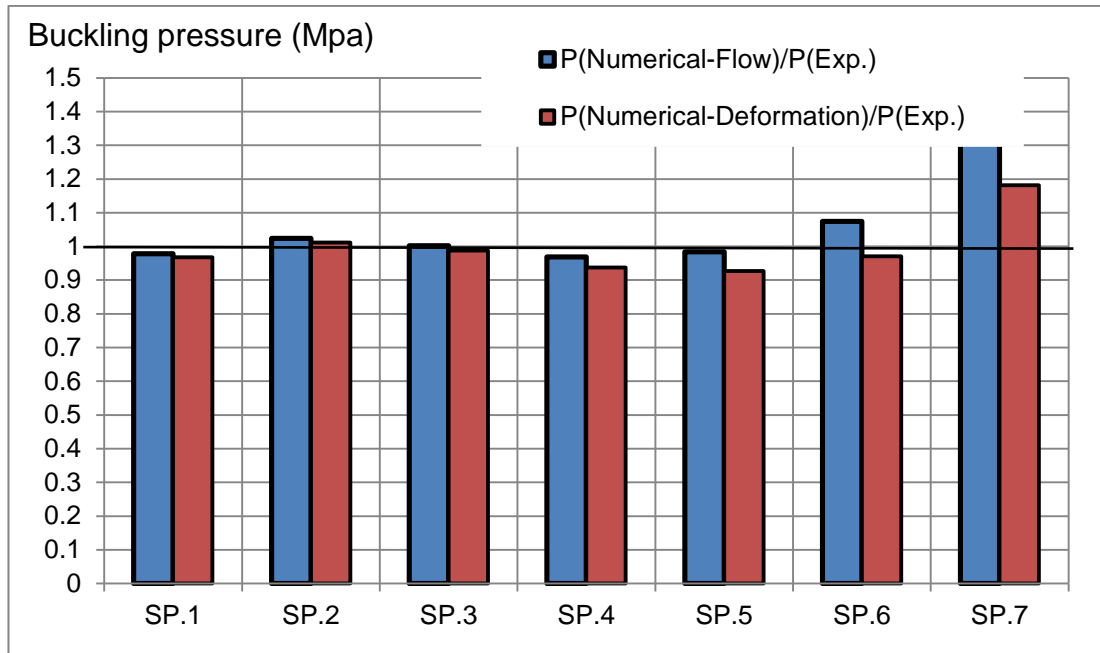


Figure 4.17: Comparison between numerical and test results (Set B).

A comparison between the flow and the deformation theory predictions in terms of plastic strains at the onset of buckling is also interesting. The plastic strains from the deformation theory seem generally less sensitive to the non-proportionality of loading than those predicted by the flow theory for moderate values of axial tension, as shown in Figure 4.18 to Figure 4.21. The plastic strains calculated using the flow and deformation theory are very close for low values of the tensile load but the discrepancies increase with the biaxial loading.

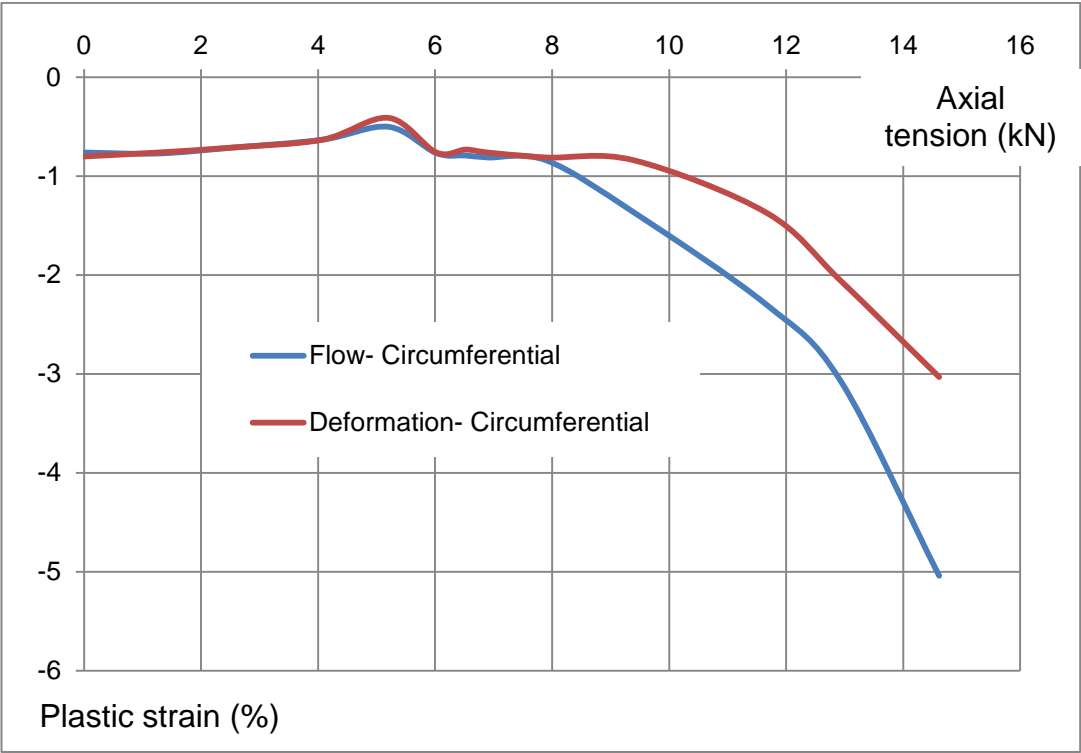


Figure 4.18: Maximum circumferential plastic strains (Set A).

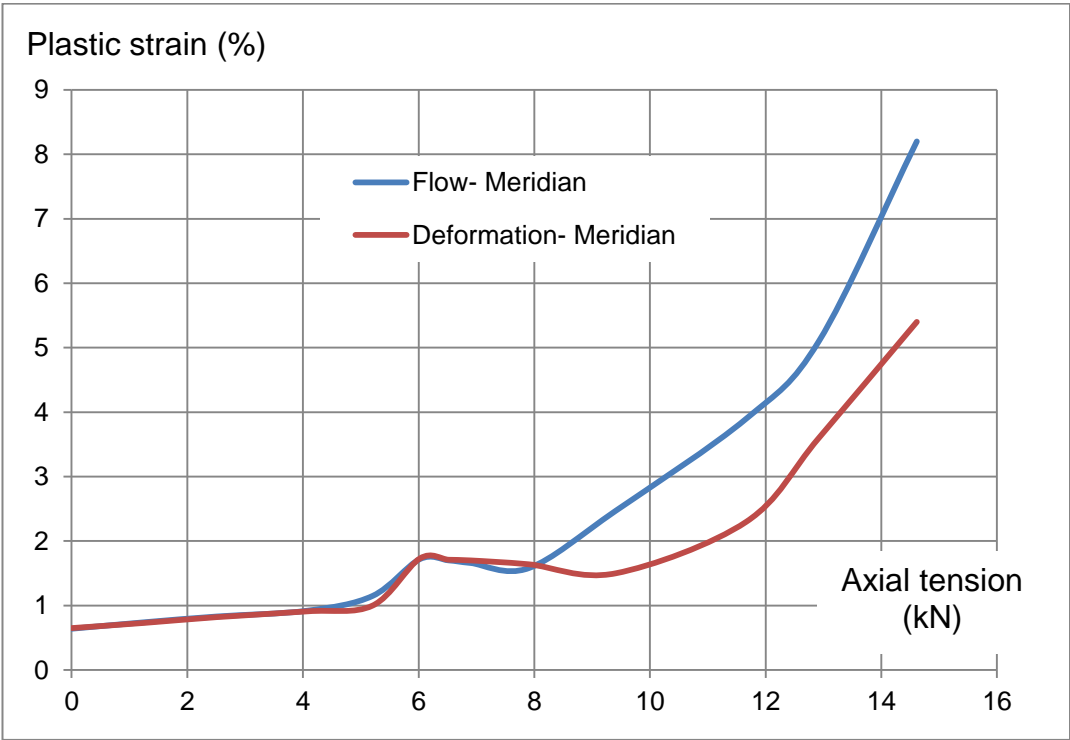


Figure 4.19: Maximum meridian plastic strains (Set A).

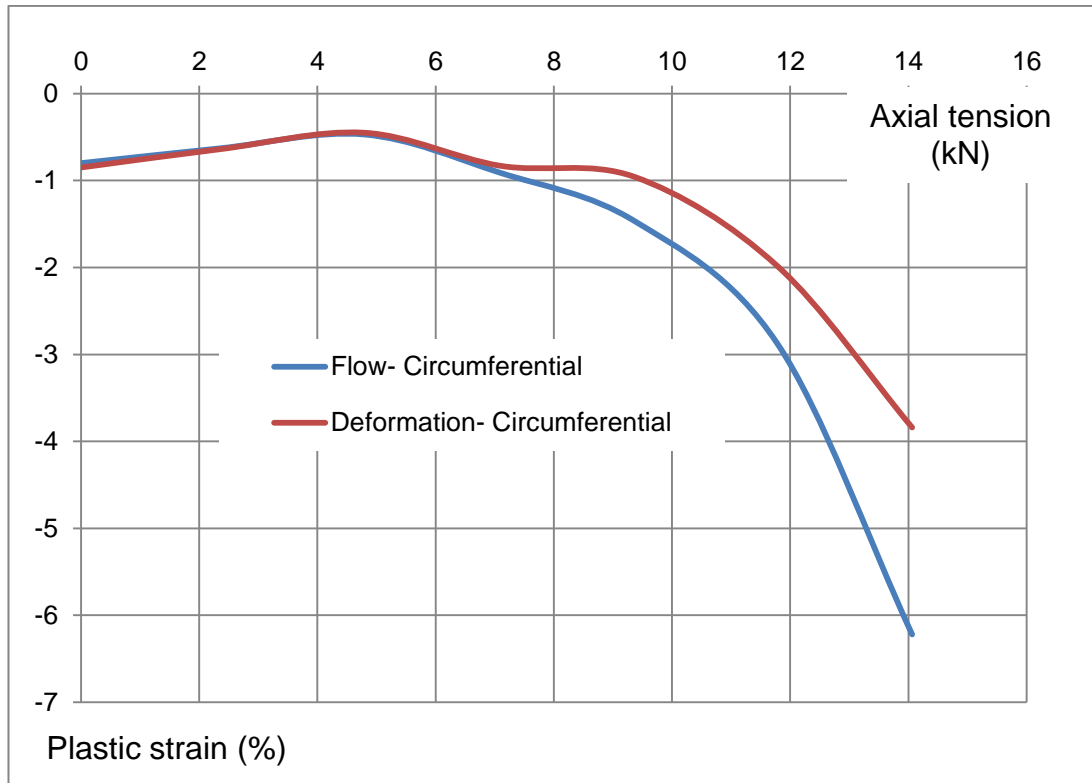


Figure 4.20: Maximum circumferential plastic strains (Set B).

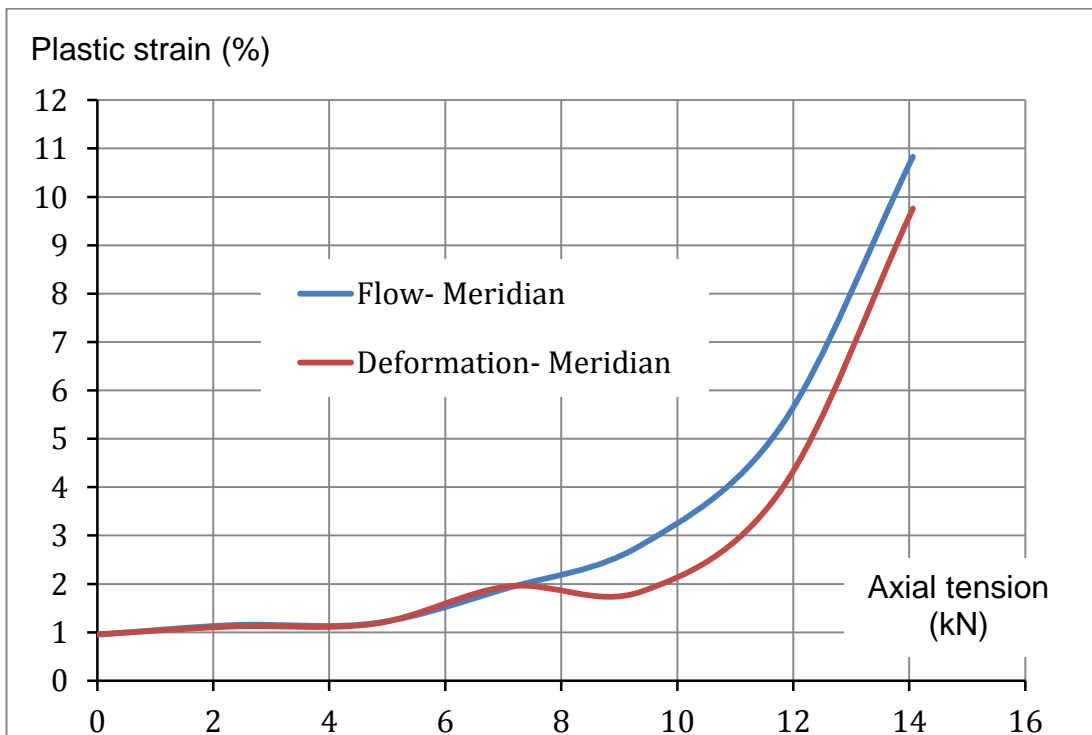


Figure 4.21: Maximum meridian plastic strains (Set B).

4.5. Imperfection sensitivity analysis

All the presented plastic buckling pressures have been obtained by assuming imperfections based on the experimentally observed buckling modes. Since this might appear a key point in obtaining a very good agreement with experimental results, in this section the influence of the choice of the eigenmode used to generate the imperfect initial shape will be investigated in depth. To this purpose the results of additional numerical analyses conducted for specimens SP.6-Set B and SP.10-Set A, studied by Giezen et al. (1991) are presented.

In a first set of analyses, reported in Section 4.5.1, 3 separate cases are considered in which the initial imperfection, of varying size, is generated by three different eigenmodes. For the same specimens a second set of analyses, reported in Section 4.5.2, have also been conducted, in which the imperfection was generated as a linear combination of the same three eigenmodes considered in Section 4.5.1.

Furthermore, in Section 4.5.3 the analyses for the same specimens were performed again using BOSOR5, combining a nonlinear analysis of the axisymmetric perfect cylinder with an eigenvalue analysis based on harmonic variation of radial displacements in the circumferential direction.

4.5.1. Imperfections generated by different eigenmodes

The results reported in this section are relative to specimens SP.6-Set B and SP.10-Set A, which were studied by means of a nonlinear analysis of the imperfect cylinders with imperfection sizes varying from 1% to 14% of the thickness, and the imperfection shapes based on the first, third and fifth elastic eigenmodes, which correspond to a number n of circumferential waves equal to five, four and six, as shown in Figure 4.22.

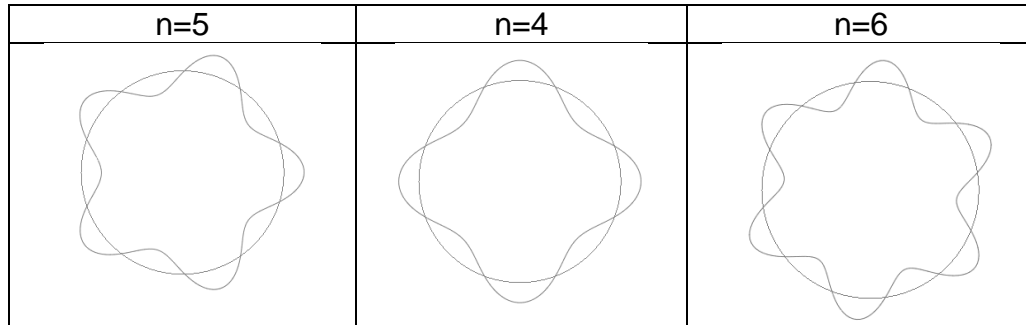
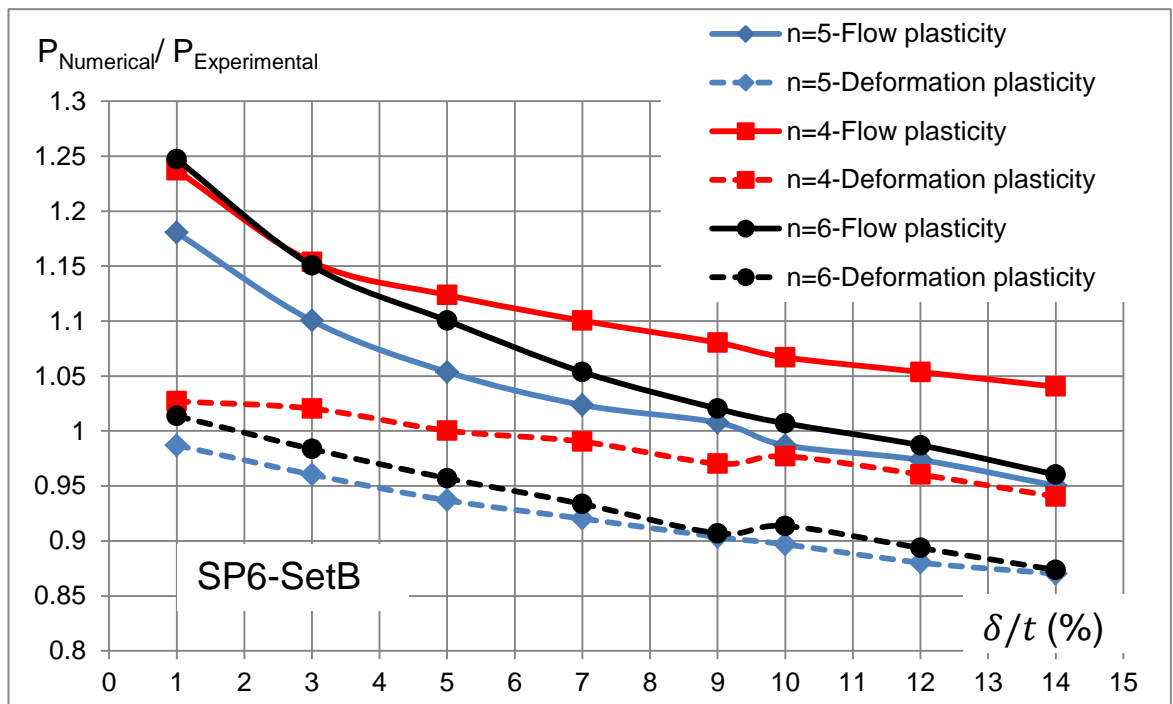


Figure 4.22: Imperfection distribution considered in this analysis

Figure 4.23 shows, as it was expected, that the buckling pressures are sensitive to the size and shape of imperfection. The imperfection shape based on the linear elastic eigenmodes with 5 waves, which provides the lowest elastic buckling pressure, also provides the lowest plastic buckling pressure. Moreover, the buckling pressure values predicted by the deformation theory are lower than those predicted by the flow theory. The discrepancies between the flow and deformation theories results vary from 18.7% to 8.5% for the case of SP.6-Set B and from 8% to 2% for the case of SP.10-Set A. It can be also noticed that the discrepancies between both plasticity theories decrease with increasing imperfection ratios.



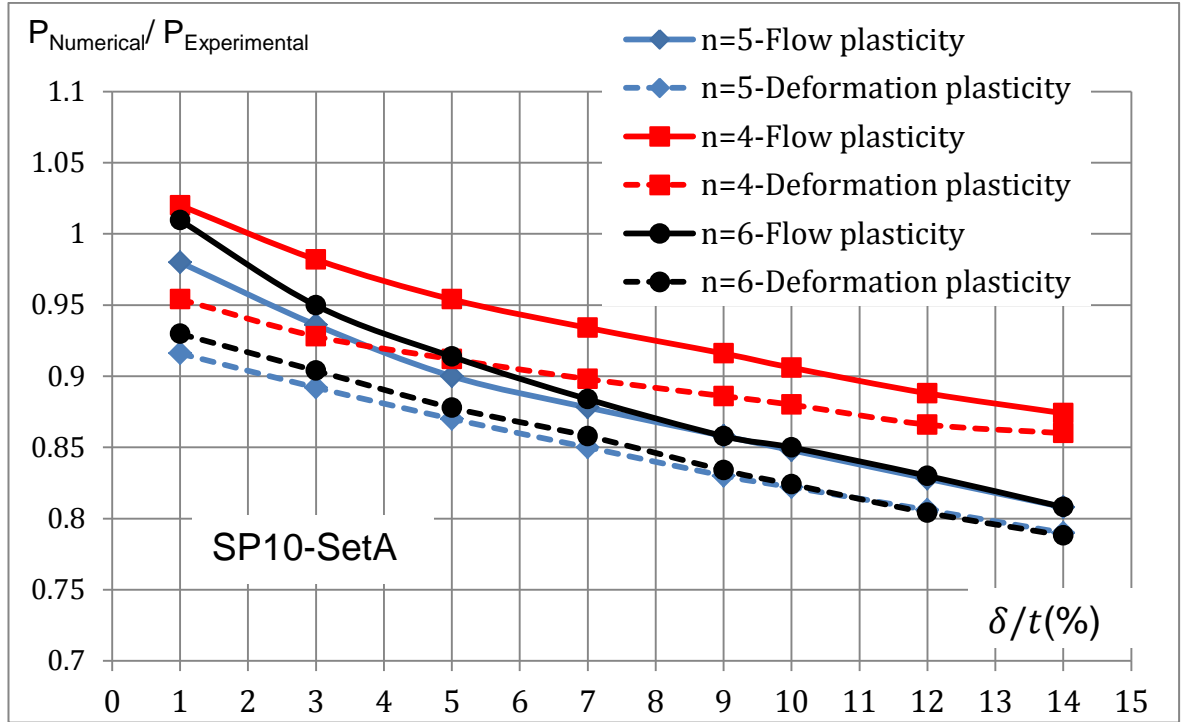


Figure 4.23: Effect of imperfections size and shapes on the buckling pressure (P) calculated using the flow and deformation theories of plasticity.

4.5.2. Imperfections generated by a linear combination of different eigenmodes

The nonlinear analyses reported in this section, again with reference to specimens SP.6-Set B and SP.10-Set A, were based on imperfections generated from a linear combination of the same three eigenmodes considered in section 4.5.1. The largest contribution within the linear combination was assigned to the fifth eigenmode, because four waves were observed experimentally at failure.

Table 4.12 and Table 4.13 show that both the flow and the deformation theory provide results that are in overall in good agreement with the test results and that the deformation theory provides buckling pressures slightly lower than the flow theory. For both theories, the results are influenced by all the modes considered in the combination. For example, the addition of 2% of the 5- and 6-wave mode to a 3% 4-wave mode results in a change of the ratio $P_{\text{Flow}} / P_{\text{Experimental}}$ from 1.15 to 1.09. The fact that all the considered eigenshapes contribute to the failure mode can be seen in Table 4.14 where, for two cases, the undeformed and deformed shape at the middle cross

section of the cylinder is shown, before and after buckling and using both theories. This result is in good agreement with the experimental finding reported by Giezen (1988), for instance in Figures 3.13 and 3.21 of his work, where the radial displacements present a rather irregular profile, which cannot be easily identified with a particular one of the eigenmode shapes.

	n. of waves	Imperfection amplitude (% of shell's thickness)	$P_{\text{Flow}} / P_{\text{Experimental}}$	$P_{\text{Deformation}} / P_{\text{Experimental}}$
Case 1	4	2	1.15	0.98
	5	1		
	6	1		
Case 2	4	3	1.09	0.96
	5	2		
	6	2		
Case 3	4	6	1.06	0.94
	5	2		
	6	2		
Case 4	4	10	1.04	0.93
	5	2		
	6	2		
Case 5	4	10	0.97	0.89
	5	5		
	6	5		
Case 6	4	10	0.9	0.83
	5	10		
	6	10		

Table 4.12: Buckling pressures for specimen SP.6-Set B obtained from our numerical analysis (ABAQUS) based on the flow and deformation theories. 4, 5 and 6 waves are used to seed the imperfection (P is the plastic buckling pressure).

	n. of waves	Imperfection amplitude (% of shell's thickness)	$P_{Flow} / P_{Experimental}$	$P_{Deformation} / P_{Experimental}$
Case 1	4	2	0.96	0.91
	5	1		
	6	1		
Case 2	4	3	0.92	0.87
	5	2		
	6	2		
Case 3	4	6	0.91	0.86
	5	2		
	6	2		
Case 4	4	10	0.88	0.86
	5	2		
	6	2		
Case 5	4	10	0.83	0.82
	5	5		
	6	5		
Case 6	4	10	0.77	0.77
	5	10		
	6	10		

Table 4.13: Buckling pressures for specimen SP.10-Set A obtained from our numerical analysis (ABAQUS) based on the flow and deformation theories and using a combination of imperfections generated with 4, 5 and 6 waves.

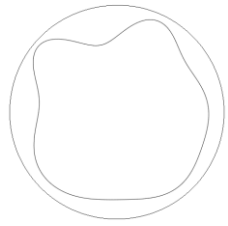
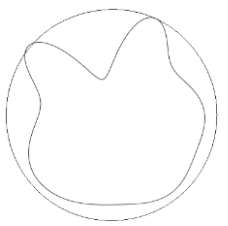
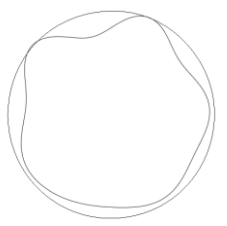
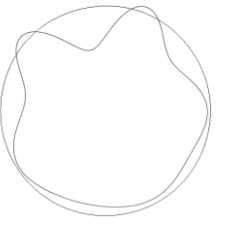
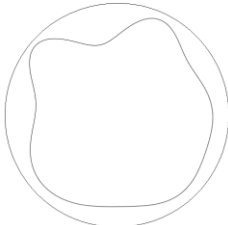

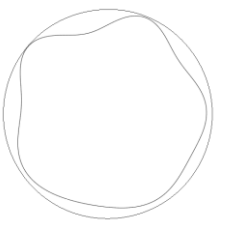
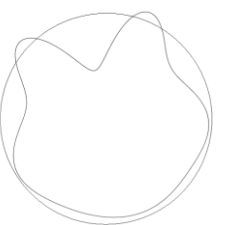
	Flow theory		Deformation theory	
	Buckling pressure	After buckling pressure	Buckling pressure	After Buckling pressure
Case1				
Case2				

Table 4.14: The deformed shape at the mid-section of the SP.6-Set B cylinder at the buckling pressure and after buckling pressure (the deformation is 10 times enlarged and the outer circle of each picture represents the un-deformed shape of the cylinder).

4.5.3. Bifurcation analysis for a perfect model using BOSOR5 and an asymptotic approach in ABAQUS

While the results of the nonlinear analyses conducted using the flow theory in ABAQUS are in good agreement with the test results, similar analyses conducted in BOSOR5 tend to strongly over-predict plastic buckling pressures, by about 100% and 29% for SP.6-Set B and SP.10-Set A cylinders, respectively, as reported in Table 4.15. The procedure used in BOSOR5 is discussed in detail in Section 4.7, but here it is worth noticing that no imperfections are introduced and that bifurcations are searched by means of an eigenvalue analysis using a tangent stiffness matrix that accounts for the elastoplastic material stiffness and is computed assuming a harmonic variation of the radial displacement with a predefined number n of circumferential waves.

Spec	P_{Exp} (MPa)	Flow theory-BOSOR5			Deformation theory-BOSOR5		
		P(MPa)	P/ P_{Exp} .	Number of waves	P(MPa)	P/ P_{Exp} .	Number of waves
SP.6-Set B	2.99	6.12	2.04	3	3.20	1.1	5
SP.10-Set A	5.02	6.5	1.29	4	4.83	0.97	5
S5	8.25	NB	NB	NB	8.71	1.05	5

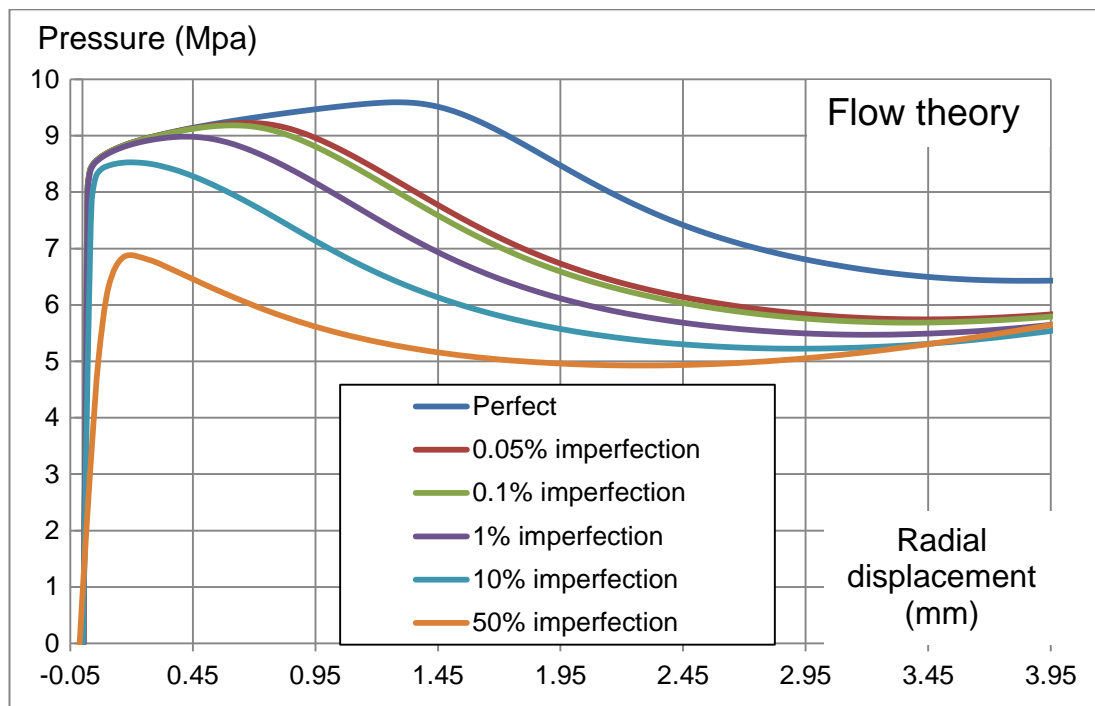
Table 4.15: Buckling pressures and corresponding buckling modes obtained from BOSOR5 code based on the flow and deformation theories.

In ABAQUS it is not possible to compute the bifurcation loads with a similar procedure, that is using a geometrically perfect model in the elastoplastic range. This is because, even if an eigenvalue buckling analysis can be conducted starting from a “base state geometry” equal to “the deformed geometry at the end of the last general analysis step, ... during an eigenvalue buckling analysis, the model's response is defined by its linear elastic stiffness in the base state. All nonlinear and/or inelastic material properties, as well as effects involving time or strain rate, are ignored” (Simulia, 2011).

Therefore, in order to estimate the bifurcation load for a perfect model, an asymptotic procedure was used in ABAQUS for the two specimens S5 and SP.6-Set B, using six different values for imperfection amplitudes. The values of the imperfection amplitudes were 0%-0.05%-0.1%-1%-10% -50%. Four circumferential waves were chosen to generate the initial imperfection as this was the number of waves observed experimentally.

It is worth noting that if the imperfection was made even smaller than the smallest one considered, it could become less important than the numerical errors due to FEA approximation, the convergence tolerances used in the iterative solution procedure, and ultimately machine precision.

Figure 4.24 and Figure 4.25 show the equilibrium curves of the external pressure versus the radial displacement. It can be appreciated that, with a progressively decreasing amount of imperfection, the load-displacement curve tends towards a limit curve, which however does not coincide with the curve obtained for a perfect cylinder. The point where these deviate is the bifurcation point for the perfect model.



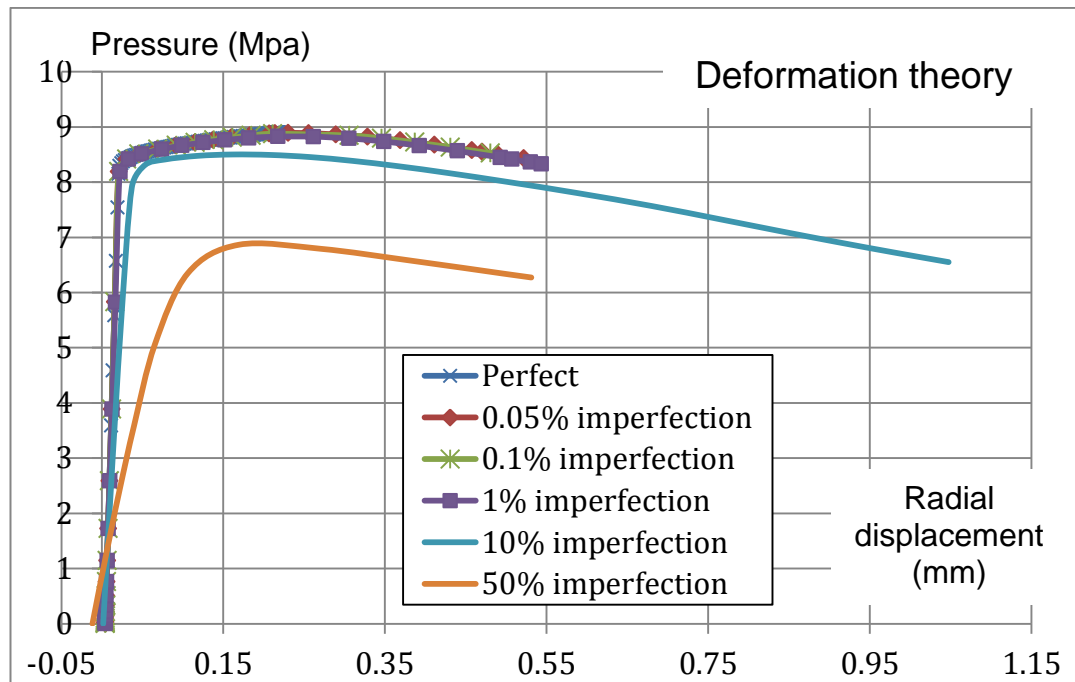
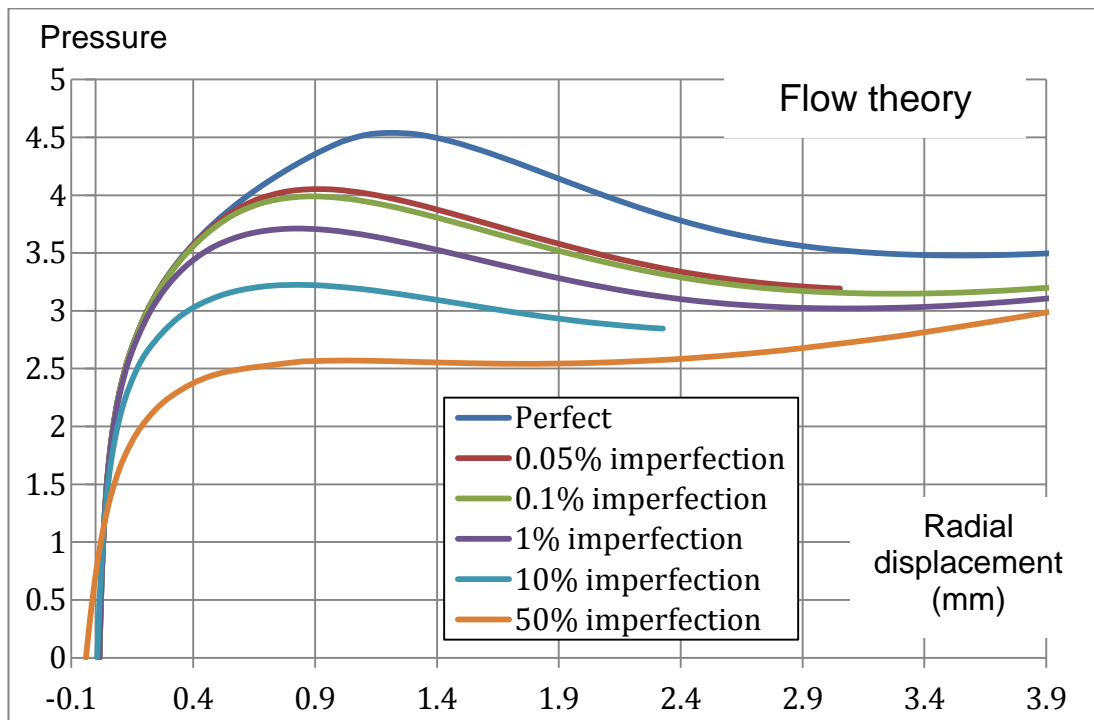


Figure 4.24: External pressure vs. radial displacement curves for specimens S5 (upper value of the yield stress) for different imperfection amplitudes

	Flow theory		Deformation theory	
	At the onset of buckling pressure	Post buckling path	At the onset of buckling pressure	Post buckling path
Perfect				
0.05% imperf- ection				
0.1% imperf- ection				

Table 4.16: The deformed shape at the mid-section of the S5 cylinder at the buckling pressure and after buckling pressure (Deformation is 10 times enlarged)

The buckling pressure for the cylinder S5 calculated in the present numerical analysis using the flow theory with 0.05% imperfection is equal to 9.23 MPa while the flow theory employed in BOSOR5 code fail to predict plastic buckling pressure, as shown in Table 4.15. Moreover, the buckling pressure of the cylinder SP.6-Set B calculated in the present numerical analysis using the flow theory with 0.05% imperfection is equal to 4.05 MPa while the flow theory employed in BOSOR5 code over-predicts plastic buckling pressure.



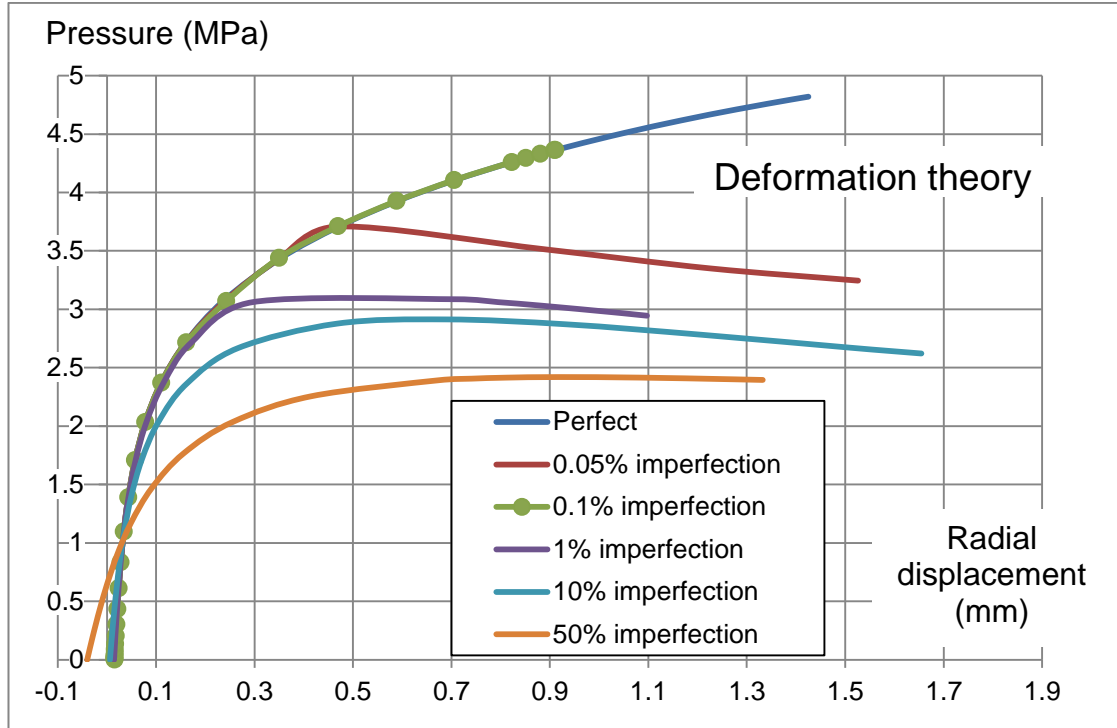


Figure 4.25: External pressure vs. radial displacement curves for specimens SP.6-Set B (upper value of the yield stress) for different imperfection amplitudes

Overall, the performed sensitivity imperfection analyses confirm the fact that, according to the present numerical studies, the flow and the deformation theories of plasticity tend to yield very similar results when the predominant imperfection coincides with the experimentally observed buckling mode. At the same time they show that for progressively different imperfection modes, the difference between the results from the flow and deformation theory tend to increase but significantly less than observed in other previous numerical treatments.

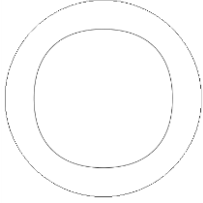
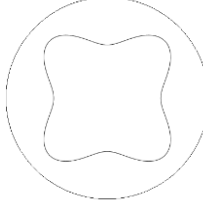
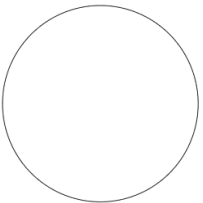

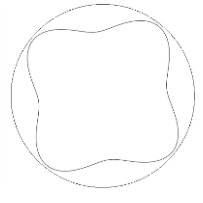
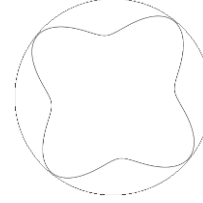
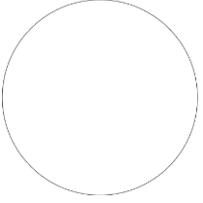
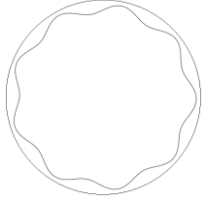
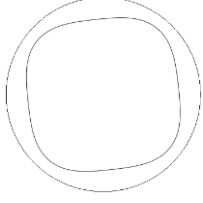
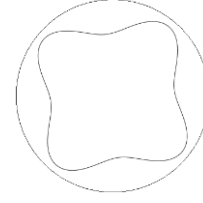
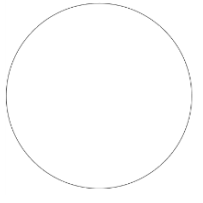

	Flow theory		Deformation theory	
	At the onset of buckling pressure	Post buckling path	At the onset of buckling pressure	Post buckling path
Perfect				
0.05% imperfection				
0.1% imperfection				

Table 4.17: The deformed shape at the mid-section of the SP.6-Set B cylinder at the buckling pressure and after buckling pressure (Deformation is 10 times enlarged)

4.6. Analytical treatment

In order to get further insight in to the root causes of the differences between present numerical results and those obtained by Blachut et al. (1996) and Giezen et al. (1991), an analytical treatment of the buckling of a circular cylindrical shell under combined axial tensile load and lateral pressure has been developed on the basis of the approach presented Chakrabarty (2010). The analytical treatment has been extended to cover both the use of deformation and flow theory of plasticity. The obtained analytical results are compared with the experimental and numerical results obtained in Blachut et al. (1996) and Giezen et al. (1991) using the code BOSOR5 and with the numerical ones obtained by ABAQUS.

To determine the bifurcation load for a circular cylindrical shell with mean radius R , length L and uniform thickness t , subject to combined axial

tension and uniform external pressure, let x be the axis of the shell and r the radial direction. Then, the angle $\theta \in [0, 2\pi]$ defines a set of cylindrical coordinates for the shell, see Figure 4.26.

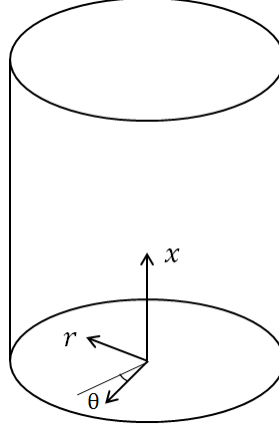


Figure 4.26: The cylindrical reference system.

At any point within the shell z is the distance of the point from the middle surface of the shell, which is taken positive if the point is on the outer side of the middle surface. The components of the velocity with respect to the above cylindrical coordinates at the considered point may be written as follows

$$\begin{cases} v_x = u + z \omega_\theta \\ v_\theta = v - z \omega_x \\ v_r = w \end{cases} \quad (4.1)$$

where u, v and w denote the velocities at the middle surface in the x, θ and radial directions r , respectively, while ω_x and ω_θ indicate the rotational velocities of the normal to the middle surface about the positive x - and θ -axes, respectively.

In the realm of the thin-shell theory, ω_x and ω_θ are related to the mid-surface velocities components as follows

$$\begin{aligned} \omega_x &= \frac{1}{R} \left(\frac{\partial w}{\partial \theta} - v \right) \\ \omega_\theta &= - \frac{\partial w}{\partial x} \end{aligned} \quad (4.2)$$

At the onset of bifurcation different modes of deformation can be found as a solution of the rate problem. A key assumption is to characterise such modes of deformation with the following harmonic expressions for u, v and w

$$\begin{aligned}
u(\xi, \theta) &= U \cos \mu \xi \sin (n\theta) \\
v(\xi, \theta) &= V \sin \mu \xi \cos (n\theta) \\
w(\xi, \theta) &= W \sin \mu \xi \sin (n\theta)
\end{aligned} \tag{4.3}$$

where U, V and W are arbitrary constants, $\mu = m\pi R/L$, $\xi = x/R$ and m and n are two positive integers. m represents the number of half waves along the generator of the cylinder and n denotes the number of waves in the circumferential direction.

The constitutive equations of the flow and deformation theories used in present analytical analysis are shown in Eq.(2.52) and Eq.(2.69), respectively.

Since the material obeys the von-Mises yield criterion, the effective stress $\bar{\sigma}$ is written, under the assumption of plane stress (i.e. $\sigma_{rr} = \tau_{zr} = \tau_{z\theta} = 0$) as follows (Eq. (2.54))

$$\bar{\sigma}^2 = \sigma_{xx}^2 - \sigma_{xx}\sigma_{\theta\theta} + \sigma_{\theta\theta}^2$$

Setting $\sigma_{xx} = \sigma_t$ and $\sigma_{\theta\theta} = -P R/t$ at the point of bifurcation, it is

$$\bar{\sigma}^2 = \sigma_t^2 + \sigma_t \frac{P R}{t} + \left(\frac{P R}{t}\right)^2 \tag{4.4}$$

The ratios of the elastic modulus E to the tangent modulus, E_t , and to the secant modulus, E_s , are expressed by the Ramberg and Osgood relationship as

$$\frac{E}{E_t} = 1 + \frac{\alpha n_p \bar{\sigma}^{n_p-1}}{\sigma_y^{n_p-1}} \tag{4.5}$$

$$\frac{E}{E_s} = 1 + \frac{\alpha}{\sigma_y^{n_p-1}} \bar{\sigma}^{n_p-1} \tag{4.6}$$

Under the assumption that the cylinders are simply supported at both ends and following the same line of reasoning as in Chakrabarty (2010), the equilibrium equations at the bifurcation point lead to the following set of buckling equations in the unknown constants U, V , and W

$$\begin{aligned}
&\left[\alpha \mu^2 + \left(\frac{1+\nu}{E} G - q \right) n^2 \right] U - \left(\frac{1+\nu}{E} G + \beta \right) \mu n V - (\beta + q) \mu W = 0 \\
&- \left(\frac{1+\nu}{E} G + \beta \right) \mu n U + \left[\left(\frac{1+\nu}{E} G \mu^2 + \gamma n^2 + \mu^2 s \right) + k \left(\frac{4+4\nu}{E} G \mu^2 + \right. \right. \\
&\left. \left. \gamma n^2 \right) \right] V + \left[\gamma n + k n \left\{ \left(\frac{4+4\nu}{E} G + \beta \right) \mu^2 + \gamma n^2 \right\} \right] W = 0
\end{aligned} \tag{4.7}$$

$$-(\beta + q) \mu U + \left[\gamma n + k n \left\{ \left(\frac{4+4\nu}{E} G + \beta \right) \mu^2 + \gamma n^2 \right\} \right] V + \left[\gamma + \mu^2 s - (n^2 - 1)q + k \left\{ \alpha \mu^4 + \left(\frac{4+4\nu}{E} G + 2\beta \right) \mu^2 n^2 + \gamma n^4 \right\} \right] W = 0$$

and a sufficient condition for bifurcation to take place is that the following characteristic equation is satisfied

$$A + Bk = Cs + Dq \quad (4.8)$$

where s and q are related to the applied average axial stress and external pressure, respectively, and k is a geometry dependent parameter, as follows

$$s = (1 + \nu) \frac{\sigma_t}{E} \quad q = (1 + \nu) \frac{PR}{Et} \quad k = \frac{t^2}{12R^2} \quad (4.9)$$

It is worth noticing that Eq. (4.8) is obtained by neglecting the higher-order terms which involve the square and products of s , q and k . A , B , C and D are obtained in such a way that the Eq. (4.8) is valid for the case of combined axial tensile stress and external pressure, and the use of both flow and deformation theory of plasticity.

It is

$$\begin{aligned} A &= \frac{G \mu^4}{E} (-\beta^2 + \alpha\gamma - \beta^2\nu + \alpha\gamma\nu) \\ B &= \frac{1}{E^2} \left[-E^2 n^2 (\beta^2 - \alpha\gamma) \mu^2 \{ (-1 + n^2)^2 \gamma + 2(-1 + n^2) \beta \mu^2 + \alpha \mu^4 \} + \right. \\ &\quad E G (1 + \nu) \{ n^4 (-1 + n^2)^2 \gamma^2 + 2((-2 + 5n^2 - 4n^4) \beta^2 + (2 - 4n^2 + 3n^4) \alpha\gamma) \mu^4 + \alpha^2 \mu^8 \} \\ &\quad \left. + 4G^2 n^2 \mu^2 (1 + \nu)^2 \{ (-1 + n^2)^2 \gamma - 2(-1 + n^2) \beta \mu^2 + \alpha \mu^4 \} \right] \end{aligned} \quad (4.10)$$

$$C = -\frac{\mu^2}{E} [-E (1 + n^2) (\beta^2 - \alpha\gamma) \mu^2 + G (1 + \nu) \{ n^4 \gamma + \alpha \mu^4 + n^2 (\gamma - 2\beta \mu^2) \}]$$

$$D = -\frac{1}{E} [E n^2 (-1 + n^2) (\beta^2 - \alpha\gamma) \mu^2 - G (1 + \nu) \{ n^6 \gamma - (\alpha - 2\beta) \mu^4 + n^2 \mu^2 (2\beta - \gamma + \alpha \mu^2) - n^4 (\gamma + 2\beta \mu^2) \}]$$

From Eq. (4.8) it follows

$$q = \frac{(A + Bk - Cs)}{D} \quad (4.11)$$

Consequently, for sequential values of m and n a series of corresponding values of the external pressure P can be obtained. The smallest value of P and the corresponding determinations of m and n provide the buckling pressure and the corresponding buckling mode.

4.7. Results and discussion

Using the Ramberg-Osgood input parameters reported in Table 4.6, the buckling pressures and corresponding buckling modes have been analytically calculated using Eq. (4.11) and reported in Table 4.18, using both the flow and deformation theories. The smallest eigenvalue in all the examined cases corresponds to $m = 1$, which means that only one half wave is formed in the longitudinal direction of the cylinder axis.

Table 4.18 collects the results from a subset of experimental tests and BOSOR5 numerical analyses (Blachut et al., 1996; Giezen et al., 1991). The results have been chosen to represent cases in which the flow theory of plasticity, according to BOSOR5, does not provide a buckling load or strongly overestimates the ones from tests, and cases in which there is agreement between the flow and deformation theory of plasticity.

Table 4.19, along with the analytical results from the presented treatment, shows the results from nonlinear FE analyses obtained by means of the commercial package ABAQUS (Sections 4.3.1 and 4.4).

Sp.	Experimental results			BOSOR5 results: Deformation theory		BOSOR5 results: Flow theory	
	Number of waves	Axial tension (N)	External pressure (MPa)	Number of waves	Buckling pressure (MPa)	Number of waves	Buckling pressure (MPa)
S1	NA	17960	4.07	NA	5.65	NA	NA
S2	NA	0	12.76	NA	13.29	NA	13.15
S3	NA	18000	4	NA	5.2	NA	NA
S5	NA	12010	8.28	NA	8.63	NA	NA
M2	NA	10670	8.14	NA	7.75	NA	NA
L4	NA	8210	10.34	NA	9.84	NA	9.85
SP.1-Set B	4	0	5.26	5	5.98	5	6.22
SP.6-Set B	4	11771	3.00	5	3.32	4	6.20
SP.3-Set A	5	2341	6.27	5	6.25	4	6.49

Table 4.18: Experimental vs BOSOR5 results (NA=Not Available)

Sp.	Numerical results (ABAQUS): Deformation theory		Numerical results (ABAQUS): Flow theory		Analytical results: Deformation Theory		Analytical results: Flow Theory	
	Number of waves	Buckling pressure (MPa)	Number of waves	Buckling pressure (MPa)	Number of waves	Buckling pressure (MPa)	Number of waves	Buckling pressure (MPa)
S1	4	5.53	4	5.64	4	5.29	2	16.24
S2	6	13.14	6	13.15	4	13.24	4	13.28
S3	4	5.04	4	5.14	4	4.81	2	16.22
S5	4	8.73	4	8.83	4	8.56	2	11.02
M2	3	7.84	3	7.87	4	7.75	4	7.91
L4	3	9.76	3	9.84	3	9.87	3	9.87
SP.1-Set B	4	5.09	4	5.15	5	5.32	5	5.44
SP.6-Set B	4	2.91	4	3.22	4	2.75	3	5.36
SP.3-Set A	5	5.25	5	5.28	4	6.00	4	6.27

Table 4.19: Numerical vs analytical.

It is found that the plastic buckling results calculated analytically using both the flow and deformation theories closely match those, when available, obtained numerically by using the code BOSOR5. The analytical results thus confirm that the flow theory seems to over-predict buckling pressures for high values of applied tensile load while the deformation theory predictions appear in better agreement with experimental results.

It is immediate to notice that the analytical treatment, differently from BOSOR5, always provides a value of the buckling pressure, albeit sometimes very different from the experimental results.

This is not surprising, given that the difference between the two theories lies, in the proposed procedure, only in the adoption of different values for the expressions of α, β, γ and G , Eq. (2.53) and Eq. (2.70), respectively.

Furthermore, the buckling mode is assumed in BOSOR5 to vary harmonically in the circumferential direction in the bifurcation buckling analysis, as seen in Eq. (2.71). As a result, using the flow theory, the stiffening effect due to the constrained kinematics is so large that BOSOR5 fails to compute a buckling load in the cases of specimens S1, S3, S5 and M2 tested by Blachut et al. (1996), as shown in Table 4.18.

The numerical analyses conducted by means of the nonlinear FE code ABAQUS, instead, lead to the correct determination of the buckling loads, in accordance with the experimental results, both for the deformation and the flow theory of plasticity.

The main finding from the presented analytical treatment is that when the buckling modes coincide using either the deformation or the flow theory, i.e. in the case of specimens S2, M2, L4, SP1-Set B and SP3-Set A, the buckling loads result the same and in line with the experimental and FE results. When the buckling modes do not coincide in the case of the deformation or of the flow theory of plasticity, then the buckling loads provided by the flow theory of plasticity result much higher than those provided by the deformation theory, see specimens S1, S3, S5 and SP6-Set B.

It is worth pointing out that the buckling modes yielded by the presented analytical analysis do not need to coincide with those by the FE analyses or by the experimental results in order to lead to the same value of the buckling pressure. This is the case, for example of specimens S2 and SP.3-Set A, as shown in Figure 4.27 and Figure 4.28. Figure 4.29 shows the 3D isometric views of the deformed shapes for specimens S2 and SP.3-Set A with the von Mises stress as contour plot.

Also, this is not surprising, given that the kinematics in the FE approach is far less constrained than that in the analytical one, as discussed in Section 3.5.3

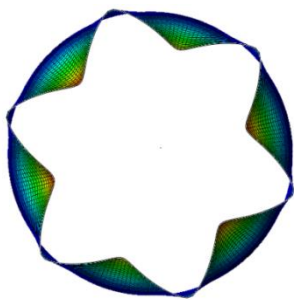
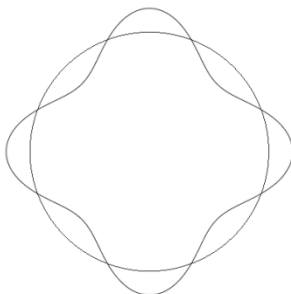
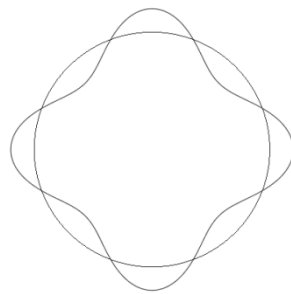
Specimen S2		
Buckling shape by FE (ABAQUS) using either the Flow or Deformation theory	Buckling shape by the analytical treatment Flow theory	Buckling shape by the analytical treatment Deformation theory
		

Figure 4.27: Specimen S2 (Blachut et al., 1996), Comparison between buckling shapes from different methods.

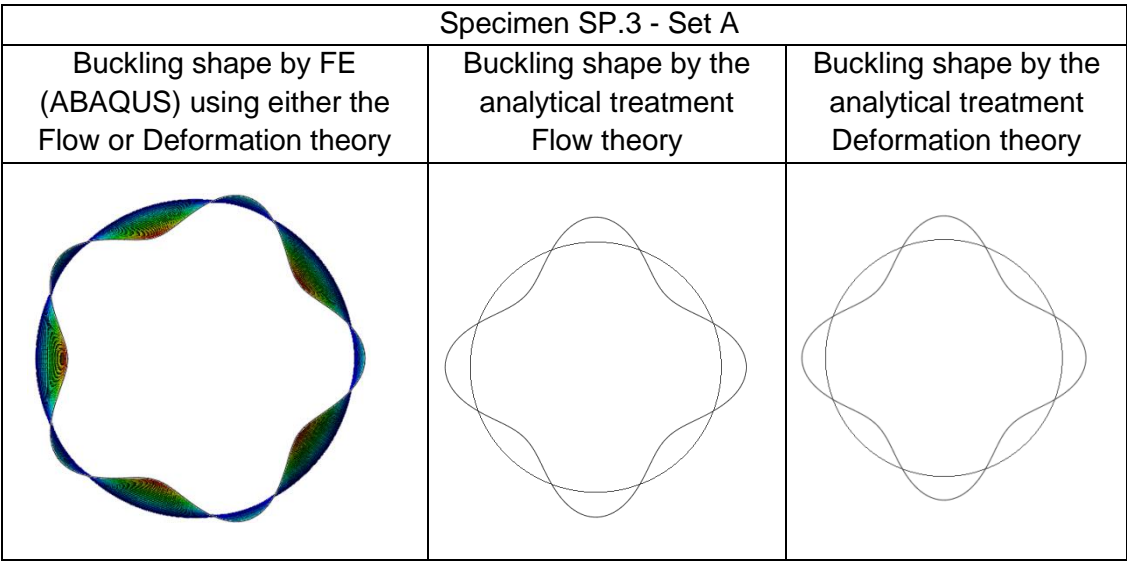
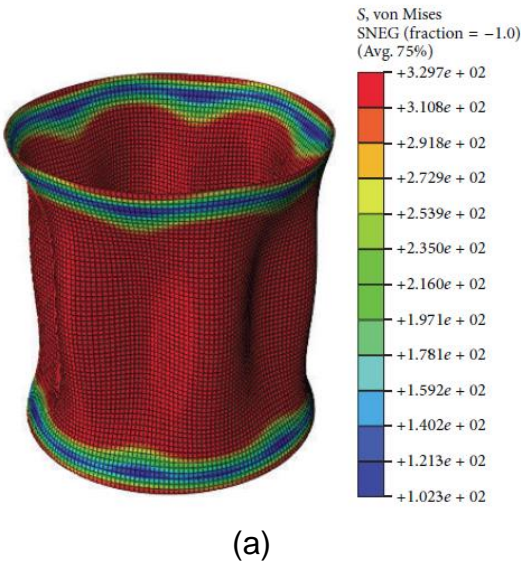


Figure 4.28: Specimen SP.3 - Set A (Giezen et al., 1991), Comparison between buckling shapes from different methods.



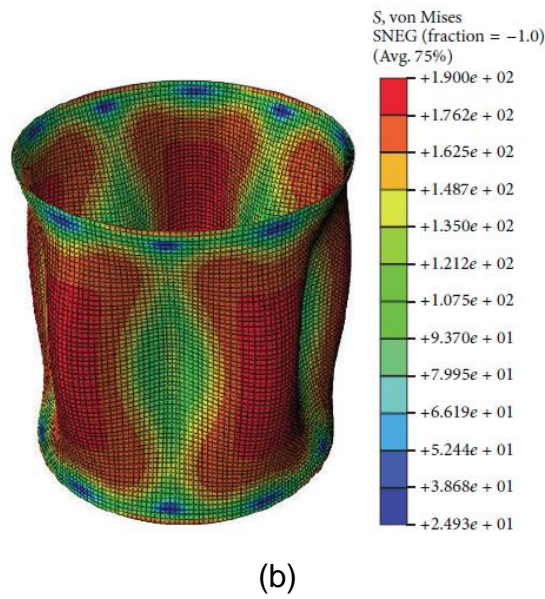


Figure 4.29: Von Mises stress contour at the ultimate pressure for: (a) Specimen S2 (Deformation is 50 times enlarged) and (b) Specimen SP.3-Set A (Deformation is 20 times enlarged).

Overall the presented investigation suggests that, also in the case of non-proportional loading, there is actually no plastic buckling paradox. In fact, when the buckling shapes coincide, the analytical treatment of the problem based on the flow theory of plasticity leads to predictions of the buckling load which are very close to the corresponding test results. This is again in contrast with the conclusions by other authors and with the widely accepted belief that the flow theory leads to a significant overestimation of the buckling stress while the deformation theory leads to much more accurate predictions. The discrepancy between the results from the analytical use of the deformation or of the flow theory of plasticity arises instead when the buckling modes do not coincide. This can be related to the phenomenon of change in buckle patterns in elastic structures studied by Chilver (1967), Supple (1968) and Guarracino and Walker (2008), among the others. The phenomenon can be attributed to an interference between the geometrical and material properties, which can induce a change of the collapsing modes. In such a case, it might happen that, adopting the deformation theory of plasticity compensates the over-stiffness of the cylinder induced by kinematically constraining the cylinders to follow predefined buckling modes, thus providing results that are only apparently more in line with the

experimental findings. However, the flow theory cannot compensate such over-stiffness and consequently the predicted buckling loads will be more than those predicted by the deformation theory.

Once again, this does not happen in the case of carefully constructed and validated nonlinear FE analyses in which the kinematic is free.

4.8. Interpretation of FEA results in the context of the plastic buckling paradox

The main findings from the numerical results presented in Sections 4.3, 4.4 and 4.5, and analytical results presented in Section 4.7 are the following:

1. When an accurate and consistent FE model is set up, both the flow and deformation theories can predict buckling loads within acceptable plastic strains for different values of the applied axial tensile load.
2. Buckling pressures calculated numerically by means of the flow theory are generally in better agreement with the experimental data.
3. Analytical analyses provide results which are very similar to those obtained by Blachut et al. (1996) and Giezen et al. (1991) using the code BOSOR5 for both flow and deformation theories. Such results lead to analogous conclusions as those by Blachut et al. (1996) and Giezen et al. (1991) in which the flow theory over-predicts buckling pressure for high value of tensile load while the deformation theory provides more accurate results.

The first two findings, discussed in Sections 4.3 and 4.4, are in contrast with the conclusions obtained by Blachut et al. (1996) and Giezen et al. (1991) by means of the code BOSOR5. In fact, according to BOSOR5 the flow theory tends to overpredict the values of the buckling pressure and of the plastic strains while the deformation theory results are more in line with the experimental results.

In general, it has been observed that BOSOR5 is not a very good predictor of non-axisymmetric buckling because it does not handle pre-buckling transverse shear deformation and non-axisymmetric initial imperfections (Bushnell, private communication). In fact, for a long time it was believed

that the difference in buckling predictions between flow versus deformation theory was entirely caused by the difference in the effective shear modulus used for the bifurcation buckling phase of the analysis (Onat and Drucker, 1953). However, Giezen (1988) showed, using the code BOSOR5, that in the case of cylinders under non-proportional loading the adoption of the effective shear modulus predicted by the deformation theory, \overline{G} , instead of the elastic one, G , in the flow theory does lead to a certain reduction in the value of the buckling load but not as much as to make it comparable with the predictions from the deformation theory, based on the secant modulus in shear.

Table 4.15 clearly shows that, although this modification is used in the BOSOR5 calculations based on the flow theory of plasticity (Bushnell, 1974), the results still overestimate the experimental buckling pressures or even fail to predict buckling at all. It is therefore clear that the difference in buckling predictions between flow versus deformation theory can be only partially attributed to the difference in the effective shear modulus used for the bifurcation buckling phase of the analysis.

The discrepancies between the numerical results from the presented study, particularly in terms of buckling pressure, and those obtained numerically using BOSOR5 can be explained by analysing the type of assumptions made in BOSOR5.

In fact, we already concluded in Section 3.5, in the case of proportional loading, that the simplifying assumptions on the buckling shape made in several analytical treatments, which result in a sort of kinematic constraint, lead to an excessive stiffness of the cylinders and, consequently, to an overestimation of the buckling stress for both the flow and deformation theories. However, the deformation theory tends to compensate this kinematic overstiffness and provides results that are more in line with the experimental ones. This fact seems confirmed also in the case of non-proportional loading by the presented comparison between the FE results and those obtained by Blachut et al. (1996) and Giezen et al. (1991) using BOSOR5. In fact, BOSOR5 assumes that the buckling shapes vary harmonically in the circumferential direction. Once again, this assumption

regarding the kinematics of the problem seems to be the main reason for the systematic discrepancies between the results from BOSOR5 based on the flow theory of plasticity and those from the numerical analyses performed in the present study, especially when a noticeable value of axial loading is applied.

4.9. Conclusions

An analytical and numerical analysis of the plastic buckling of cylinders subjected to non-proportional loading, i.e. axial tensile load and external pressure has been presented with the aim of providing further understanding of the apparent discrepancy between the predictions of the flow and deformation theories of plasticity. By comparing the analytical results with experimental and numerical results, the following conclusions may be drawn:

- the numerical FE predictions based on the flow theory of plasticity are once again in good agreement with the experimental results. This is in contrast to the conclusions by other authors that the flow theory, as in the case of BOSOR5 code results, leads to incorrect predictions of plastic strains and buckling pressures while the deformation theory leads to much more accurate predictions;
- the buckling loads calculated analytically using both the flow and deformation theories of plasticity often match those obtained numerically by using the code BOSOR5;
- the root of the apparent discrepancy seems to be a change in the buckling modes induced in some cases by the different material stiffness provided by the deformation and flow theories of plasticity. In such cases there is an apparent overestimation of the buckling loads by the flow theory while the deformation theory counterbalances the excessive kinematic stiffness of the cylinder due to a constrained kinematics.

The conclusion of the present investigation is that also in the case of cylinders subjected to non-proportional loading actually there seems to be no plastic buckling paradox when using detailed nonlinear finite element analysis models.

Chapter 5

On the Elastoplastic Buckling Analysis of Cylinders under Non-proportional Loadings via the Differential Quadrature Method

5.1. Introduction

There are many practical cases of buckling of shells involving various combinations of boundary conditions. Obtaining closed form solutions for different boundary conditions requires complex mathematics and is generally difficult or even impossible to obtain analytically. Therefore, many approximate numerical methods have been employed over the years for buckling problems, such as the finite difference (FD), the finite element (FE), the Rayleigh-Ritz and the Galerkin methods, etc. The differential quadrature method (DQM) may offer some advantages over some of these methods and at the same time a clearer insight into the mechanics of the problem under

analysis. For example, Wang (1982) employed the DQ method to study transient analysis of isothermal chemical reactors. He showed that the DQM can provide accurate results using only nine grid points while the FD method required 480 grid points to provide the same accuracy.

The Rayleigh-Ritz and Galerkin methods require less computational effort in comparison with the FE and FD methods but at the same time they require the selection of trial functions satisfying boundary conditions. This does not apply to the DQ method, which leaves a certain freedom in dealing with the boundary conditions of the problem. Therefore, the method has become quite popular in the numerical solution of some problems in engineering and physical science. For instance, the DQ method is routinely employed to provide solutions to partial differential equations arising in various simplified models of fluid flow, diffusion of neutrons through homogeneous media and one-dimensional nonlinear transient heat diffusion and conduction problems (Bert and Malik, 1996a). This technique has been applied in the simulation of fluid mechanics (Shu and Richards, 1992), heat transfer (Bert and Malik, 1996a), transport processes (Civan and Sliepcevich, 1983), chemical engineering (Civan, 1994), lubrication mechanics (Malik and Bert, 1994) and static aero-elasticity (Bert and Malik, 1996a). The method has also been used to analyse deflection, vibration and buckling of linear and nonlinear structural components (Nassar et al., 2013; Wang and Gu, 1997; Bert and Malik, 1996b, Bert et al., 1989).

The DQ method, first used by Bert et al. (1988) to solve structural problems of shell analysis, was successively used to analyse other linear and nonlinear structural problems. More recently, geometrically nonlinear transient analysis of moderately thick laminated composite shallow shells were studied using the DQ method (Kurtaran, 2015). At the date of writing, the DQ method has been applied to analyse elastic buckling of plates of different shapes such as rectangle, square, skew, circle and trapezoid with different boundary conditions (Civalek, 2004), elastic buckling of circular cylindrical shells (Mirfakhraei and Redekop, 1998), elastic buckling of one-dimensional composite laminated beam-plates (Moradi and Taheri, 1999), elastoplastic

buckling of thick rectangular plates under biaxial loadings (Wang and Huang, 2009; Zhang and Wang, 2011; Maarefdoust and Kadkhodayan, 2014b) and elastoplastic buckling of skew thin plates (Maarefdoust, and Kadkhodayan, 2014a).

It can be noticed that, so far, the DQ method has only been successfully used to obtain elastic buckling loads of plates and cylinders and plastic buckling loads of plates. The available analytical solutions of plastic buckling of cylindrical shells subjected to combined loadings are only for cylinders with one type of simply-supported boundary conditions (Chakrabarty, 2010). Thus, the DQ method is used herein for the first time for the elastoplastic buckling analysis of cylinders subjected to combined tensile stress and external pressure with different boundary conditions.

Moreover, Becque (2010) proposed a modification for the flow theory to overcome the plastic buckling paradox of plates by using a modified shear modulus at the onset of inelastic buckling.

This study assumes that the cylindrical shells are thin, homogeneous and isotropic. The Flugge stability equations, based on the assumption of infinitesimal deformations and moderate rotations, are used and a buckling mode varying harmonically in the circumferential direction of the cylinder is assumed, thus allowing using the one-dimensional version of the DQ method. Both the flow theory and deformation theory of plasticity are considered. The validated elastic and plastic buckling results obtained with the help of the DQ method are analysed to achieve the following objectives in the framework of the study of the so-called “plastic buckling paradox”:

- investigate the effect of different boundary conditions on the plastic buckling results and the discrepancies between predictions of the flow and deformation theories;
- investigate the effect of cylinder's geometries (thickness-to-radius t/R and length-to-diameter L/D ratios), material properties (Young's modulus-to-yield strength E/σ_y) and values of the applied tensile stress on the plastic buckling pressure and the discrepancy between the results of the flow and deformation theories;

- assess the proposed modifications of the flow theory by Becque (2010).
- compare the results of the DQM, which uses a bifurcation analysis approach, with those of nonlinear incremental FE analyses based on both the flow and the deformation theories of plasticity;
- point out once more the possible reasons of some large discrepancies in the predictions of buckling loads between the flow theory and the deformation theory of plasticity when the kinematics is not free, following work in Chapters 3 and 4.

The outline of the chapter is as follows. The main governing equations and related boundary conditions of the problems are derived in Section 5.2. In Section 5.3 a solution procedure for these equations, based on the DQ method, is described and results are presented and discussed together with a sensitivity analysis with respect to the boundary conditions and to some of the key input parameters. The results of nonlinear FE simulations are then presented in Section 5.4 and their comparison with those given by the DQM is discussed in Section 5.5, also within the framework of the plastic buckling paradox. Conclusions are then drawn in Section 5.6.

5.2. Flugge's differential equations for cylinders under combined loading

Consider a circular cylindrical shell of length L radius R and uniform thickness t and subjected to two different loads: a uniform normal pressure on its lateral surface, P , and an axial tensile stress, σ_t .

Let denote by x the axis of the shell and by r an axis orthogonal to x on a reference cross section, defining a radial direction. Introducing an angle $\theta \in [0, 2\pi]$, (x, θ, r) a set of cylindrical coordinates is set for the cylindrical shell, see Figure 4.26. At any point within the shell, let denote by z the distance of the point from the middle surface of the shell, taken positive if the point is on the outer side of the middle surface. Writing the governing equations in rate form, the components of the velocity vector may be written as follows (Flugge, 1960):

$$\begin{aligned}
v_x &= u - z \frac{\partial w}{\partial x} \\
v_\theta &= v - \frac{z}{R} \frac{\partial w}{\partial \theta}
\end{aligned} \tag{5. 1}$$

$$v_r = w$$

where u and v are the velocity components at the middle surface of the shell in the x and θ directions, respectively and w is the transverse velocity in the r direction.

5.2.1. Strain-displacement relations

Within the framework of the thin-shell theory, the through-thickness shear strain rates $\dot{\varepsilon}_{rx}$ and $\dot{\varepsilon}_{r\theta}$ are zero. The non-zero components of the strain rate associated with the velocity field in Eq. (5. 1) at an arbitrary point of the shell are related to the middle-surface strain-rate components $\dot{\lambda}_x, \dot{\lambda}_\theta$ and $\dot{\lambda}_{x\theta}$ and to the changes in the curvature and twist of the middle surface, $\dot{K}_x, \dot{K}_\theta$ and $\dot{K}_{x\theta}$, by the following three relations

$$\begin{aligned}
\dot{\varepsilon}_{xx} &= \dot{\lambda}_x - z \dot{K}_x \\
\dot{\varepsilon}_{\theta\theta} &= \dot{\lambda}_\theta - z \dot{K}_\theta \\
\dot{\varepsilon}_{x\theta} &= \dot{\lambda}_{x\theta} - z \dot{K}_{x\theta}
\end{aligned} \tag{5. 2}$$

The expressions of the strain rates of the middle surface, assuming a small displacement theory, may be written as

$$\begin{aligned}
\dot{\lambda}_x &= \frac{\partial u}{\partial x} \\
\dot{\lambda}_\theta &= \frac{1}{R} \left(\frac{\partial v}{\partial \theta} + w \right) \\
\dot{\lambda}_{x\theta} &= \frac{1}{2} \left(\frac{\partial v}{\partial x} + \frac{1}{R} \frac{\partial u}{\partial \theta} \right)
\end{aligned} \tag{5. 3}$$

while those for the changes in the curvature and twist of the middle surface are as follows

$$\begin{aligned}
\dot{K}_x &= \frac{\partial^2 w}{\partial x^2} \\
\dot{K}_\theta &= \frac{1}{R^2} \frac{\partial^2 w}{\partial \theta^2}
\end{aligned} \tag{5. 4}$$

$$K_{x\theta} = \frac{1}{R} \frac{\partial^2 w}{\partial \theta \partial x}$$

5.2.2. Stress-strain relations in plastic range

While strains are linearly related to stresses by Hooke's law in the elastic range, the relations between stresses and strains are nonlinear in the plastic range.

In this study, two plasticity theories, namely the flow and the deformation theories, are considered.

Since the stress rate through the thickness ($\dot{\sigma}_{rr}$) is identically zero in the thin-shell theory, the constitutive relations for a linearized elastic-plastic solid, in the assumption that that no unloading takes place (or that behaviour is identical under loading and unloading), are as follows (see Section 2.7.3)

$$\begin{aligned}\dot{\sigma}_{xx} &= \frac{E}{1+\nu} (\alpha \dot{\varepsilon}_{xx} + \beta \dot{\varepsilon}_{\theta\theta}) \\ \dot{\sigma}_{\theta\theta} &= \frac{E}{1+\nu} (\beta \dot{\varepsilon}_{xx} + \gamma \dot{\varepsilon}_{\theta\theta}) \\ \dot{\tau}_{x\theta} &= \frac{E}{1+\nu} \left(\frac{2+2\nu}{E} G \dot{\varepsilon}_{x\theta} \right)\end{aligned}\tag{5. 5}$$

where E is the elastic modulus, G is the effective shear modulus and ν is the Poisson's ratio for the material.

The expressions of α , β , γ and G are given in Eq. (2.53) for the case of the flow theory and in Eq. (2.70) for the case of the deformation theory.

For the case of elastic buckling, both the tangent modulus and the secant modulus at the point of bifurcation are equal to elastic moduli, i.e. $E_t = E_s = E$, then

$$\alpha = \gamma = \frac{1}{1-\nu}, \quad \beta = \frac{\nu}{1-\nu}\tag{5. 6}$$

Since the material obeys the von Mises yield criterion, the effective stress $\bar{\sigma}$ is written with the assumption of plane stress as follows

$$\bar{\sigma}^2 = \sigma_1^2 - \sigma_1 \sigma_2 + \sigma_2^2$$

Setting $\sigma_1 = \sigma_t$, that is the applied axial tensile stress, and $\sigma_2 = \frac{-P R}{t}$ at the point of bifurcation, one obtains

$$\bar{\sigma}^2 = \sigma_t^2 + \sigma_t \frac{P R}{t} + \left(\frac{P R}{t} \right)^2 \quad (5.7)$$

The Ramberg-Osgood relationship between the effective stress $\bar{\sigma}$ and the effective strain $\bar{\varepsilon}$ is used:

$$\bar{\varepsilon} = \frac{\bar{\sigma}}{E} \left[1 + \alpha \left(\frac{\bar{\sigma}}{\sigma_y} \right)^{n_p-1} \right] \quad (5.8)$$

where σ_y is the nominal yield strength, sometimes called ‘proof stress’, α is the ‘yield offset’ and n_p is the hardening parameter.

The material used in this study is aluminium alloy 6061-T4 that used in the tests carried out by Giezen et al (1991). The material constants were found in Section 4.2.2 by fitting the Ramberg-Osgood relation to the available data set. They are reported again in Table 5. 1:

E [MPa]	σ_y [MPa]	ν	n_p	α
65129.73	177.8	0.31	16	0.733

Table 5. 1: Ramberg-Osgood constants

The ratios of the elastic modulus E to the tangent modulus, E_t , and to the secant modulus, E_s , are expressed by the Ramberg and Osgood relationship as shown in Eqs. (4.5) and (4.6)

5.2.3. Governing differential equations

Assuming that u, v and w are the incremental velocity components at the middle surface of the shell when it buckles. The rate of change of the additional membrane forces and bending moments (stress resultants) per unit length of the middle surface, associated to a variation of the original state, are denoted by $\dot{N}_x, \dot{N}_\theta, \dot{N}_{\theta x}$ and $\dot{M}_x, \dot{M}_\theta, \dot{M}_{\theta x}$, respectively.

We also assume that no unloading occurs at the instant of the plastic buckling, an assumption normally made in the analytical or semi-analytical formulation of plastic buckling problems (Hutchinson, 1974). Then, based on Flugge’s theory, the rate form of the governing differential equations considering a membrane pre-buckling state for the case of cylinders

subjected to external pressure and axial tension can be formulated as (Flugge, 1960)

$$\begin{aligned}
R^2 \frac{\partial \dot{N}_x}{\partial x} + R \frac{\partial \dot{N}_{\theta x}}{\partial \theta} - P R \left(\frac{\partial^2 u}{\partial \theta^2} - R \frac{\partial w}{\partial x} \right) + R^2 t \sigma_t \frac{\partial^2 u}{\partial x^2} &= 0 \\
R \frac{\partial \dot{N}_\theta}{\partial \theta} + R^2 \frac{\partial \dot{N}_{x\theta}}{\partial x} - \frac{\partial \dot{M}_\theta}{\partial \theta} - R \frac{\partial \dot{M}_{x\theta}}{\partial x} - P R \left(\frac{\partial^2 v}{\partial \theta^2} + \frac{\partial w}{\partial \theta} \right) + t \sigma_t R^2 \frac{\partial^2 v}{\partial x^2} &= 0 \\
\frac{\partial^2 \dot{M}_\theta}{\partial \theta^2} + R \frac{\partial^2 \dot{M}_{x\theta}}{\partial x \partial \theta} + R \frac{\partial^2 \dot{M}_{\theta x}}{\partial x \partial \theta} + R^2 \frac{\partial^2 \dot{M}_x}{\partial x^2} + R \dot{N}_\theta + P R \left(R \frac{\partial u}{\partial x} - \frac{\partial v}{\partial \theta} + \right. & \\
\left. \frac{\partial^2 w}{\partial \theta^2} \right) - t \sigma_t R^2 \frac{\partial^2 w}{\partial x^2} &= 0
\end{aligned} \tag{5.9}$$

The stress rate resultants are related to the stress rate by

$$\begin{aligned}
\dot{N}_x &= \int_{-h/2}^{h/2} \dot{\sigma}_x dz \\
\dot{N}_\theta &= \int_{-h/2}^{h/2} \dot{\sigma}_\theta dz \\
\dot{N}_{x\theta} = \dot{N}_{\theta x} &= \int_{-h/2}^{h/2} \dot{\tau}_{x\theta} dz \\
\dot{M}_x &= - \int_{-h/2}^{h/2} z \dot{\sigma}_x dz \\
\dot{M}_\theta &= - \int_{-h/2}^{h/2} z \dot{\sigma}_\theta dz \\
\dot{M}_{x\theta} = \dot{M}_{\theta x} &= - \int_{-h/2}^{h/2} z \dot{\tau}_{x\theta} dz
\end{aligned} \tag{5.10}$$

Eq. (5.9) are supplemented by the conditions along the boundaries $x = 0$ and $x = L$. For simply-supported boundary conditions we have the following four possibilities (Ore and Durban, 1992)

$$\begin{aligned}
S1: w = v = \dot{N}_x = \dot{M}_x &= 0 \\
S2: w = \dot{M}_x = \dot{N}_x = \dot{N}_{x\theta} &= 0 \\
S3: w = u = \dot{M}_x = \dot{N}_{x\theta} &= 0 \\
S4: w = v = u = \dot{M}_x &= 0
\end{aligned} \tag{5.11}$$

while for clamped boundary conditions we have the following four possibilities (Ore and Durban, 1992)

$$\begin{aligned}
C1: w = v = \dot{N}_x = w' &= 0 \\
C2: w = w' = \dot{N}_x = \dot{N}_{x\theta} &= 0 \\
C3: w = u = w' = \dot{N}_{x\theta} &= 0 \\
C4: w = v = u = w' &= 0
\end{aligned} \tag{5.12}$$

In the numerical analyses described later for BOSOR5 and ABAQUS, the above boundary conditions are defined in Table 5.2, where δu , δv , δw and $\delta \beta$ are incremental displacements at the boundary.

Name	δu	δv	δw	$\delta \beta$	Name	δu	δv	δw	$\delta \beta$
S1	f	r	r	f	C1	f	r	r	r
S2	f	f	r	f	C2	f	f	r	r
S3	r	f	r	f	C3	r	f	r	r
S4	r	r	r	f	C4	r	r	r	r

Table 5. 2: Different boundary conditions terminology for cylindrical shells (f: free to displace during buckling; r: restrained displacement during buckling) (Teng and Rotter, 2004)

5.2.4. The rate of displacement function

At the onset of bifurcation, the variables u, v and w shown in the resulting governing Eqs. (5.9) are function of both coordinates x and θ . To solve the set of partial differential Eqs. (5.9), the separation method is used in which the dependent variables u, v and w can be expressed as a multiplication of two functions of independent variables x and θ . The key assumption here is that the buckling mode u, v and w is assumed to vary harmonically in the circumferential direction of the cylinder. Thus an analytically two-dimensional problem is reduced to a numerically one-dimensional model. This simplifying assumption with regards to assumed buckling modes is used in many analytical and numerical treatment such as BOSOR5 (Bushnell, 1976) and NAPAS (Teng and Rotter, 1989). Thus, displacements are therefore assumed to be expressed as follows:

$$\begin{aligned}
 u(x, \theta) &= u(x) \sin(n\theta) \\
 v(x, \theta) &= v(x) \cos(n\theta) \\
 w(x, \theta) &= w(x) \sin(n\theta)
 \end{aligned} \tag{5.13}$$

where n is the number of waves in the circumferential direction of the cylinder.

Substituting these expressions into Eqs. (5.3) and (5.4), then the resulting strain rate components from Eq. (5.2) are substituted into constitutive

equations (5.5). Integrating Eq. (5.10) and substituting the stress rate resultants into the governing equations of the eigenvalue problem (Eq. (5.9)) give:

$$\begin{aligned}
& u'' \left(R^2 t \sigma_t + \frac{R^2 E t \alpha}{1+\nu} \right) + u(x)(-G t n^2) + v' \left(-R G t n - \frac{R E t n \beta}{1+\nu} \right) + \\
& w' \left(\frac{R E t \beta}{1+\nu} \right) = P \left(-R n^2 u(x) - R^2 w' \right) \\
& u' \left(\frac{R E t n \beta}{1+\nu} + R G t n \right) + v'' (R^2 t \sigma_t + R^2 G t) + v(x) \left(\frac{-E t n^2 \gamma}{1+\nu} \right) + \\
& w'' \left(-\frac{1}{6} G t^3 n - \frac{E t^3 n \beta}{12(1+\nu)} \right) + w(x) \left(\frac{E t n \gamma}{1+\nu} + \frac{E t^3 n^3 \gamma}{12 R^2 (1+\nu)} \right) = P \left(R n w(x) - \right. \\
& \left. R n^2 v(x) \right) \\
& u' \left(\frac{R E t \beta}{1+\nu} \right) + v(x) \left(\frac{-E t n \gamma}{1+\nu} \right) + w'''' \left(\frac{R^2 E t^3 \alpha}{12 (1+\nu)} \right) + w'' \left(-\frac{1}{3} G t^3 n^2 - \right. \\
& \left. R^2 t \sigma_t - \frac{E t^3 n^2 \beta}{6(1+\nu)} \right) + w(x) \left(\frac{E t \gamma}{1+\nu} + \frac{E t^3 n^4 \gamma}{12 R^2 (1+\nu)} \right) = P \left(R n^2 w(x) - \right. \\
& \left. R n v(x) - R^2 u' \right)
\end{aligned} \tag{5.14}$$

or

$$\begin{aligned}
& A_1 u'' + A_2 u(x) + A_3 v' + A_4 w' = P \left(A_5 u(x) + A_6 w' \right) \\
& C_1 u' + C_2 v'' + C_3 v(x) + C_4 w'' + C_5 w(x) = P \left(C_6 w(x) + C_7 v(x) \right) \\
& D_1 u' + D_2 v(x) + D_3 w'''' + D_4 w'' + D_5 w(x) = P \left(D_6 w(x) + \right. \\
& \left. D_7 v(x) + D_8 u' \right)
\end{aligned} \tag{5.15}$$

The expressions of \dot{M}_x , \dot{N}_x and $\dot{N}_{x\theta}$ used for the boundary conditions become

$$\begin{aligned}
\dot{M}_x &= w'' + \left(\frac{-n^2 \beta}{R^2 \alpha} \right) w(x) = 0 \\
\dot{N}_x &= u' + \left(\frac{-n \beta}{R \alpha} \right) v(x) + \left(\frac{\beta}{R \alpha} \right) w(x) = 0 \\
\dot{N}_{x\theta} &= \left(\frac{n}{R} \right) u(x) + v' = 0
\end{aligned} \tag{5.16}$$

or

$$\begin{aligned}
\dot{M}_x &= w'' + B_1 w(x) = 0 \\
\dot{N}_x &= u' + B_2 v(x) + B_3 w(x) = 0 \\
\dot{N}_{x\theta} &= B_4 u(x) + v' = 0
\end{aligned} \tag{5.17}$$

where the primes indicate the derivatives with respect to the coordinate x .

5.3. Solution via the differential quadrature method

The differential quadrature (DQ) is an approximation method to calculate the k^{th} -order derivative of the solution function $f(x)$ at a grid point i . Consider firstly a one dimensional problem. The k^{th} -order derivative of a function $f(x)$ is given by a linear weighting of the function values at N points of the domain

$$\left. \frac{d^k f}{dx^k} \right|_{x=x_i} = \sum_{j=1}^N E_{ij}^k f(x_j) \quad i = 1, 2, \dots, N \quad (5.18)$$

Here E_{ij}^k are called the weighting coefficients of the k th-order derivative at the i^{th} point in the domain, N and $f(x_j)$ are the total number of grid points and the solution values at the grid point j , respectively. Denote A_{ij} , B_{ij} , C_{ij} and D_{ij} the weighting coefficients of the first-, second-, third- and fourth-order derivatives for the ordinary DQ method. The weighting coefficient A_{ij} can be computed explicitly by (Wang et al., 2005)

$$\begin{aligned} A_{ij} &= \frac{\omega'_N(x_i)}{(x_i - x_j) \omega'_N(x_j)} \quad i \neq j \\ A_{ii} &= \sum_{j=1, j \neq i}^N \frac{1}{(x_i - x_j)} \end{aligned} \quad (5.19)$$

where

$$\begin{aligned} \omega_N(x) &= (x - x_1)(x - x_2) \dots (x - x_{i-1})(x - x_i)(x - x_{i+1}) \dots (x - x_N) \\ \omega'_N(x) &= (x - x_1)(x - x_2) \dots (x - x_{i-1})(x - x_{i+1}) \dots (x - x_N) \end{aligned} \quad (5.20)$$

The weighting coefficients for higher order derivatives B_{ij} , C_{ij} and D_{ij} can be calculated through the following (Wang et al., 2005)

$$\begin{aligned} B_{ij} &= \sum_{k=1}^N A_{ik} A_{kj} \\ C_{ij} &= \sum_{k=1}^N A_{ik} B_{kj} \\ D_{ij} &= \sum_{k=1}^N B_{ik} B_{kj} \end{aligned} \quad (5.21)$$

It is worth pointing out that also the finite difference method (FD) discretizes the continuous domain into N discrete points. In the FD method, the approximation of the derivatives at one grid point is based on a low-order (linear or quadratic) interpolation of the function values over a small number of adjacent points. Instead, in the DQ method the derivatives at each point are based on the interpolation of the function over all the grid points, using

Lagrange polynomials. This normally increases the accuracy of the solution for a given number of grid points, although the method leads to a full matrix instead of the banded matrix obtained with the FD method. In other words, the DQ method can be considered as a higher-order finite difference method (Shu and Richards, 1992).

There are two main issues related to sampling points in the DQ method. The first one is the location of the sampling points, which can affect the accuracy of the solution of the differential equations. The simplest choice is to take them evenly spaced. However, in most cases, one can obtain better convergence and a more accurate solution by choosing unequally spaced sampling points (Bert and Malik, 1996a; Moradi and Taheri, 1999). The second issue is how to enforce the boundary conditions. Jang and his co-workers (Jang et al., 1989) propose the so-called δ -technique, in which additional points are located at a small distance ($\delta = 10^{-5}$) from the boundary points. Then the boundary conditions are applied at both the actual boundary points and the δ -points.

In this study, as already discussed, the buckling mode is assumed to follow a trigonometric curve in the circumferential direction. In this way, the problem is reduced to a one-dimensional one and the sampling points are only taken in the axial direction of the cylinder. The following relation for the grid spacing has been used:

$$\begin{aligned} x(1) &= 0, & x(2) &= \delta L, & x(N-1) &= L(1-\delta), & x(N) &= L \\ x(i) &= L \left(\frac{1 - \cos\left(\frac{\pi(i-2)}{N-3}\right)}{2} \right) & 3 < i < N-2 \end{aligned} \quad (5.22)$$

Figure 5.1 shows the position of the grid points along the axial direction of the cylinder for $N=15$.

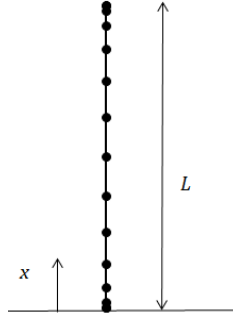


Figure 5. 1: Sketch of the axial direction of a cylinder with grid points

5.3.1. DQ approximation of the differential equations and solution procedure

Using the DQ method, the governing Eqs. (5.15) are expressed as

$$A_1 \sum_{j=1}^N B_{ij} u_j + A_2 u_i + A_3 \sum_{j=1}^N A_{ij} v_j + A_4 \sum_{j=1}^N A_{ij} w_j = P (A_5 u_i + A_6 \sum_{j=1}^N A_{ij} w_j) \quad (5. 23a)$$

$$C_1 \sum_{j=1}^N A_{ij} u_j + C_2 \sum_{j=1}^N B_{ij} v_j + C_3 v_i + C_4 \sum_{j=1}^N B_{ij} w_j + C_5 w_i = P (C_6 w_i + C_7 v_i) \quad (5. 23b)$$

$$D_1 \sum_{j=1}^N A_{ij} u_j + D_2 v_i + D_3 \sum_{j=1}^N D_{ij} w_j + D_4 \sum_{j=1}^N B_{ij} w_j + D_5 w_i = P (D_6 w_i + D_7 v_i + D_8 \sum_{j=1}^N A_{ij} u_j) \quad (5. 23c)$$

The boundary conditions (Eq. (5.12)) become

$$\begin{aligned} w_1 &= w_N = v_1 = v_N = 0 \\ \sum_{j=1}^N A_{1j} u_j + B_2 v_1 + B_3 w_1 &= 0 \\ \text{S1: } \sum_{j=1}^N A_{Nj} u_j + B_2 v_N + B_3 w_N &= 0 \\ \sum_{j=1}^N B_{1j} w_j + B_1 w_1 &= 0 \\ \sum_{j=1}^N B_{Nj} w_j + B_1 w_N &= 0 \\ w_1 &= w_N = 0 \\ \sum_{j=1}^N A_{1j} u_j + B_2 v_1 + B_3 w_1 &= 0 \\ \sum_{j=1}^N A_{Nj} u_j + B_2 v_N + B_3 w_N &= 0 \\ \text{S2: } \sum_{j=1}^N B_{1j} w_j + B_1 w_1 &= 0 \\ \sum_{j=1}^N B_{Nj} w_j + B_1 w_N &= 0 \\ B_4 u_1 + \sum_{j=1}^N A_{1j} v_j &= 0 \end{aligned} \quad (5. 24)$$

$$\begin{aligned}
& B_4 u_N + \sum_{j=1}^N A_{Nj} v_j = 0 \\
& w_1 = w_N = u_1 = u_N = 0 \\
& B_4 u_1 + \sum_{j=1}^N A_{1j} v_j = 0 \\
\text{S3: } & B_4 u_N + \sum_{j=1}^N A_{Nj} v_j = 0 \\
& \sum_{j=1}^N B_{1j} w_j + B_1 w_1 = 0 \\
& \sum_{j=1}^N B_{Nj} w_j + B_1 w_N = 0 \\
& w_1 = w_N = v_1 = v_N = u_1 = u_N = 0 \\
\text{S4: } & \sum_{j=1}^N B_{1j} w_j + B_1 w_1 = 0 \\
& \sum_{j=1}^N B_{Nj} w_j + B_1 w_N = 0
\end{aligned}$$

Similar expressions hold for the clamped boundaries except that $\dot{M}_x = 0$ is replaced by $w' = 0$. Thus they become

$$\begin{aligned}
& \sum_{j=1}^N A_{1j} w_j = 0 \\
& \sum_{j=1}^N A_{Nj} w_j = 0
\end{aligned} \tag{5. 25}$$

Imposing these boundary conditions makes some of the equations in (5.23) redundant. In order to eliminate such a redundancy, the numberings of the inner point are chosen as: $i = 2, 3, \dots, N - 1$ for the Eq. (5.23a), $i = 2, 3, \dots, N - 1$ for the Eq. (5.23b) and $i = 3, 4, \dots, N - 2$ for the Eq. (5.23c).

The combination of the governing equations written in differential quadrature form Eqs. (5.23) and of the boundary conditions yield a set of linear equations which can be written in the following partitioned matrix form

$$\begin{bmatrix} [ABB] & [ABI] \\ [AIB] & [AII] \end{bmatrix} \cdot \begin{Bmatrix} \{u_b\} \\ \{v_b\} \\ \{w_b\} \\ \{u_i\} \\ \{v_i\} \\ \{w_i\} \end{Bmatrix} = P \cdot \begin{bmatrix} [0] & [0] \\ [BIB] & [BII] \end{bmatrix} \cdot \begin{Bmatrix} \{u_b\} \\ \{v_b\} \\ \{w_b\} \\ \{u_i\} \\ \{v_i\} \\ \{w_i\} \end{Bmatrix} \tag{5. 26}$$

Sub-matrices $[ABB]_{8 \times 8}$, $[ABI]_{8 \times (3N-8)}$ stem from the boundary conditions while $[AIB]_{(3N-8) \times 8}$, $[AII]_{(3N-8) \times (3N-8)}$, $[BIB]_{(3N-8) \times 8}$, $[BII]_{(3N-8) \times (3N-8)}$ stem from the governing equations. b and i refer to the location of boundary and interior points, respectively.

$$\{u_b\} = \{u_1, u_N\}^T, \{v_b\} = \{v_1, v_N\}^T \text{ and } \{w_b\} = \{w_1, w_2, w_{N-1}, w_N\}^T$$

The above equation can be transformed into a general eigenvalue form

$$[A^*].\{W_i\} = P [B^*].\{W_i\} \quad \Leftrightarrow \quad [[B^*]^{-1}.[A^*] - P [I]].\{W_i\} = 0 \quad (5.27)$$

where

$$\begin{aligned} [A^*] &= [[A_{II}] - [A_{IB}].[ABB]^{-1}.[ABI]] \\ [B^*] &= [[B_{II}] - [B_{IB}].[ABB]^{-1}.[ABI]] \\ \{W_i\} &= \begin{Bmatrix} \{u_i\} \\ \{v_i\} \\ \{w_i\} \end{Bmatrix} \end{aligned} \quad (5.28)$$

By solving the eigenvalue problem represented by Eq. (5.27) with the help of a standard eigensolver, one can obtain the lowest eigenvalue (i.e., buckling pressure P) and corresponding eigenvector (i.e., the buckling mode $\{W_i\}$).

Since α, β, γ and G depend on the unknown load P , Eq. (5.27) defines a nonlinear problem. Thus an iterative method is needed for obtaining the solution of Eq. (5.27). The number of circumferential waves n varies between n_{min} and n_{max} . For each value of n , the buckling pressure is calculated. The smallest value of P and the corresponding determinations of n provide the buckling pressure P_{cr} and the corresponding buckling mode.

A computer program has been written in Matlab language for determining the plastic buckling pressure and buckling mode using both the flow and deformation theories of plasticity for the examined cylinders (Appendix A4). The flow chart of the algorithm implemented is illustrated in Figure 5.2.

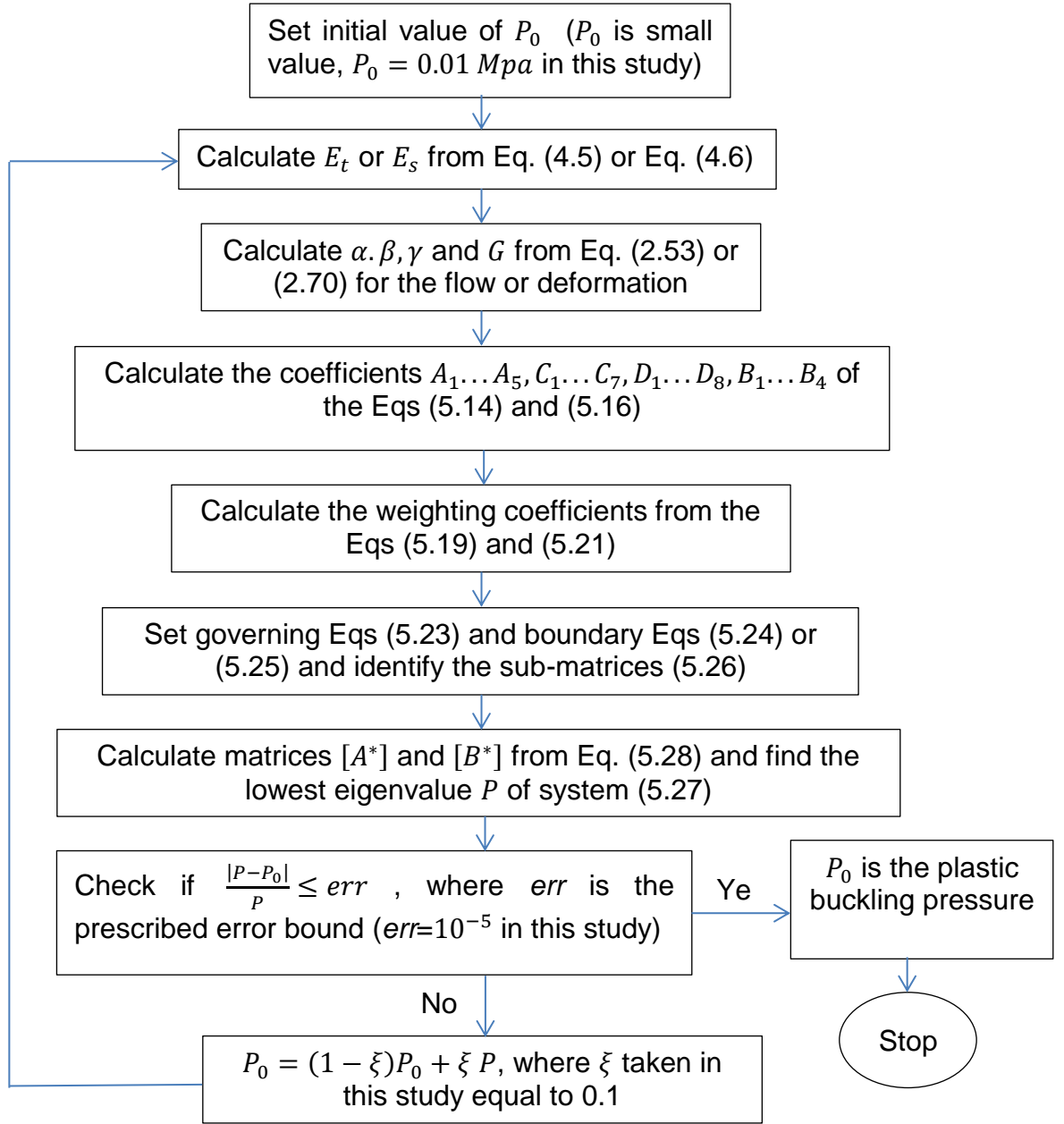


Figure 5. 2: Flow chart of the solution procedure

5.3.2. Verification with known solutions

In order to verify the solution procedure based on the DQ method has been correctly implemented in the written code, the obtained results in term of the buckling pressure of cylinders subjected to combined loading, are compared with those provided by the BOSOR5 code and with analytical solutions in Section 4.6, as shown in Tables 5.3 and 5.4.

For brevity, letter S is used for the case of simply-supported edge and letter C for that of a clamped edge. Two letters and numbers are used to represent the boundary conditions of the cylinder. For example, a S1-S1 cylinder will have a simply-supported edge of the type 1 at $x = 0$ and $x = L$.

Figure 5.3 shows the buckling pressures computed for a C4-C4 cylinder under constant tensile stress $\sigma_t = 82.7$ MPa by the DQ method with different numbers of grid points. The geometry of the cylinder is given by $L = 2R = 38.1$ mm and $t = 0.76$ mm. It can be seen that the DQ method with $N = 9$ can already yield accurate results for both the flow and deformation theory of plasticity. N is set to 15 for all DQ results presented in this paper.

Tables 5.3a-5.3b show the plastic buckling pressures and corresponding buckling modes calculated by DQ method for C3-C3 and C4-C4 cylinders with $L/D = 1$, $D = 38.1$ mm and $t = 0.76$ mm and subjected to increasing value of axial tensile stress, while Table 5.3c-5.3d show the plastic buckling pressures for S4-S4 and S1-S1 cylinders for increasing t/R ratios. The results are shown together with results calculated using BOSOR5. Here it should be noted that the flow theory employed in BOSOR5 uses the modified shear modulus which is the shear modulus predicted by the deformation theory (Bushnell, 1976). Therefore, for comparison purpose, the flow theory with the same modified shear modulus was used in the DQ method. The DQ plastic buckling pressures and corresponding buckling modes are in very good agreement with those obtained using BOSOR5 for all types of boundary conditions, loadings and cylinders' geometry.

The results for S1-S1 cylinders subjected to combined axial tensile stress and external pressure and bifurcated in plastic phase are shown in Table 5.4 for both the flow and deformation theory of plasticity. The results are shown together with plastic buckling pressures obtained using analytical solution in Section 4.6 (Eq. (4.11)), which assumes the S1-S1 type (simply-supported) of boundary condition. The geometry of the cylinder is defined by $L = 2R = 38.1$ mm and $t = 0.76$ mm. For all the cases of applied axial tension, the current buckling pressure results agree with those obtained analytically with errors varying in the range 0.7%-9% using the flow theory and 3.1%-3.7%

using the deformation theory. It should be noted that in some cases the buckling modes obtained here are different from those obtained analytically when the flow theory is used.

These examples serve as a check that both the formulations and the computer program are correct.

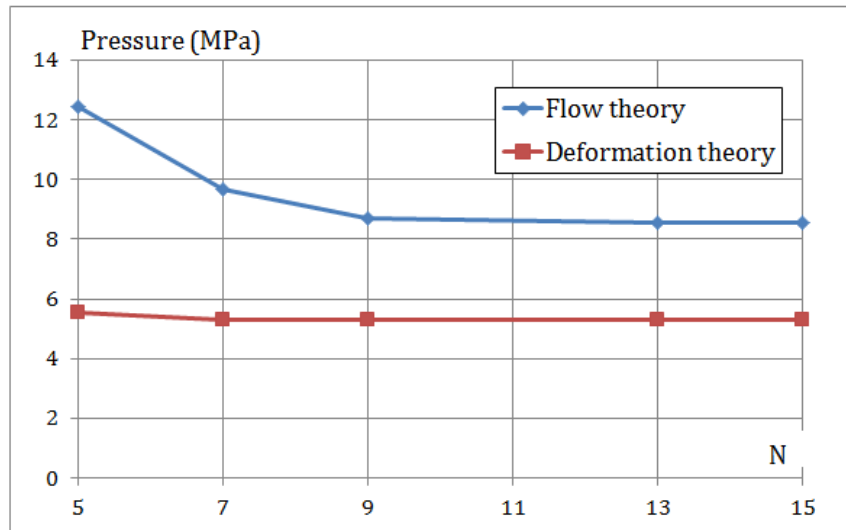


Figure 5. 3: Convergence study

Buckling pressure P_{cr} (MPa) and corresponding buckling mode n,m calculated from BOSOR5					Buckling pressure P_{cr} (MPa) and corresponding buckling mode n,m calculated from present study				Error - flow theory (%)	Error - deformation theory (%)
Tensile stress (MPa)	Flow theory		Deformation theory		Flow theory		Deformation theory			
	n,m	P_{cr}	n,m	P_{cr}	n,m	P_{cr}	n,m	P_{cr}		
0.00	5,1	7.24	5,1	7.07	5,1	7.149	5,1	6.91	-1.3	-2.2
13.79	5,1	7.16	5,1	6.9	5,1	7.06	5,1	6.72	-1.4	-2.5
27.58	5,1	7.07	5,1	6.64	5,1	6.96	5,1	6.50	-1.6	-2.1
55.16	4,1	6.9	5,1	6.12	4,1	6.87	5,1	5.96	-0.4	-2.6
82.74	4,1	6.55	5,1	5.52	4,1	6.62	5,1	5.30	1.1	-4.0
110.32	3,1	6.64	5,1	4.74	3,1	6.24	5,1	4.52	-6.0	-4.7
137.90	NB	NB	5,1	3.88	NB	5.73	5,1	3.63	NB	-6.5
165.47	NB	NB	5,1	3.02	8,2	5.07	5,1	2.68	NB	-11.4

(a)

Buckling pressure P_{cr} (MPa) and corresponding buckling mode n,m calculated from BOSOR5					Buckling pressure P_{cr} (MPa) and corresponding buckling mode n,m calculated from present study				error-flow theory (%)	error-deformation theory (%)
Tensile stress (MPa)	The flow theory		The deformation theory		The flow theory		The deformation theory			
	n,m	P_{cr}	n,m	P_{cr}	n,m	P_{cr}	n,m	P_{cr}		
0	5,1	7.24	5,1	7.07	5,1	7.15	5,1	6.92	-1.3	-2.1
13.79	5,1	7.16	5,1	6.90	5,1	7.05	5,1	6.73	-1.5	-2.5
27.58	5,1	7.07	5,1	6.72	5,1	6.97	5,1	6.5	-1.4	-3.3
55.16	5,1	6.98	5,1	6.13	4,1	6.88	5,1	6.0	-1.5	-2.1
82.74	NB	NB	5,1	5.52	4,1	6.64	5,1	5.3	NB	-4.0
110.32	NB	NB	5,1	4.75	NB	NB	5,1	4.52	NB	-4.8
137.9	NB	NB	5,1	3.96	NB	NB	5,1	3.63	NB	-8.4
165.48	NB	NB	5,1	3.02	NB	NB	5,1	2.67	NB	-12

(b)

Buckling pressure P_{cr} (MPa) and corresponding buckling mode n,m calculated from BOSOR5					Buckling pressure P_{cr} (MPa) and corresponding buckling mode n,m calculated from present study				error- flow theory (%)	error- deformation theory (%)
h/R	The flow theory		The deformation theory		The flow theory		The deformation theory			
	n,m	P_{cr}	n,m	P_{cr}	n,m	P_{cr}	n,m	P_{cr}		
0.0107	7,1	0.52	7,1	0.52	7,1	0.53	7,1	0.53	1.9	1.0
0.0160	6,1	1.24	6,1	1.22	6,1	1.18	6,1	1.14	-5.1	-6.7
0.0214	5,1	2.06	6,1	1.94	5,1	1.96	5,1	1.84	-4.9	-5.4
0.0321	4,1	4.05	5,1	3.4	4,1	3.9	5,1	3.24	-3.7	-4.7
0.0408	3,1	6.64	5,1	4.66	3,1	6.11	5,1	4.46	-8.0	-4.3
0.0428	3,1	7.15	5,1	5	3,1	6.59	5,1	4.75	-7.9	-5.0
0.0535	NB	NB	5,1	6.68	NB	NB	4,1	6.26	NB	-6.2
0.0749	NB	NB	4,1	10	NB	NB	4,1	9.46	NB	-5.4
0.0856	NB	NB	4,1	11.89	NB	NB	4,1	11.1 4	NB	-6.3

(c)

Buckling pressure P_{cr} (MPa) and corresponding buckling mode n,m calculated from BOSOR5					Buckling pressure P_{cr} (MPa) and corresponding buckling mode n,m calculated from present study				error-flow theory (%)	error-deformation theory (%)
h/R	The flow theory		The deformation theory		The flow theory		The deformation theory			
	n,m	P_{cr}	n,m	P_{cr}	n,m	P_{cr}	n,m	P_{cr}		
0.00802	6,1	0.21	7,1	0.18	6,1	0.212	7,1	0.17	1.0	-4.9
0.01070	6,1	0.35	6,1	0.31	5,1	0.37	6,1	0.29	5.7	-5.6
0.02140	4,1	1.64	5,1	1	4,1	1.588	5,1	0.96	-3.2	-3.6
0.03210	NB	NB	5,1	1.98	4,1	3.872	5,1	1.82	NB	-8.1
0.04076	NB	NB	4,1	2.8	NB	NB	4,1	2.59	NB	-7.4
0.04279	NB	NB	4,1	3.1	NB	NB	4,1	2.78	NB	-10.4
0.05349	NB	NB	4,1	4.3	8,3	6.659	4,1	3.80	NB	-11.6
0.07489	NB	NB	4,1	7.06	8,3	9.32	4,1	6.62	NB	-6.3

(d)

Table 5. 3: Comparison between plastic buckling pressures and corresponding buckling mode obtained using DQ method and BOSOR5 for: (a) C3-C3 cylinders, (b) C4-C4 cylinders, (c) S4-S4 cylinders with $\sigma_t = 110.3$ MPa, (d) S1-S1 cylinders with $\sigma_t = 165.5$ MPa (NB: No buckling)
(m : number of half waves in the longitudinal direction of the cylinder, n : number of half waves in the circumferential direction)

Tensile stress (MPa)	Buckling pressure P_{cr} (MPa) and corresponding buckling mode n,m calculated from present study				Buckling pressure P_{cr} (MPa) and corresponding buckling mode n,m calculated from Eq. (4.11)				error % - flow theory	error %-deformation theory
	The flow theory		The deformation theory		The flow theory		The deformation theory			
	n,m	P_{cr}	n,m	P_{cr}	n,m	P_{cr}	n,m	P_{cr}		
0.0	5,1	6.75	5,1	6.60	5,1	6.51	5,1	6.39	3.7	3.3
13.8	4,1	6.68	5,1	6.42	5,1	6.42	5,1	6.21	4.0	3.4
27.6	4,1	6.52	4,1	6.19	4,1	6.27	4,1	6.00	4.0	3.2
41.4	4,1	6.40	4,1	5.93	4,1	6.11	4,1	5.75	4.7	3.1
55.2	4,1	6.36	4,1	5.66	4,1	5.99	4,1	5.47	6.2	3.5
68.9	4,1	6.44	4,1	5.35	4,1	5.98	4,1	5.18	7.7	3.3
82.7	3,1	6.43	4,1	5.02	3,1	6.03	4,1	4.85	6.6	3.5
96.5	3,1	6.47	4,1	4.67	3,1	5.93	4,1	4.51	9.1	3.5
110.3	5,3	6.45	4,1	4.29	3,1	5.97	4,1	4.14	8.0	3.6
124.1	8,5	6.26	4,1	3.88	3,1	6.14	4,1	3.74	2.0	3.7
137.9	8,5	6.3	4,1	3.45	3,1	6.36	4,1	3.33	-0.9	3.6

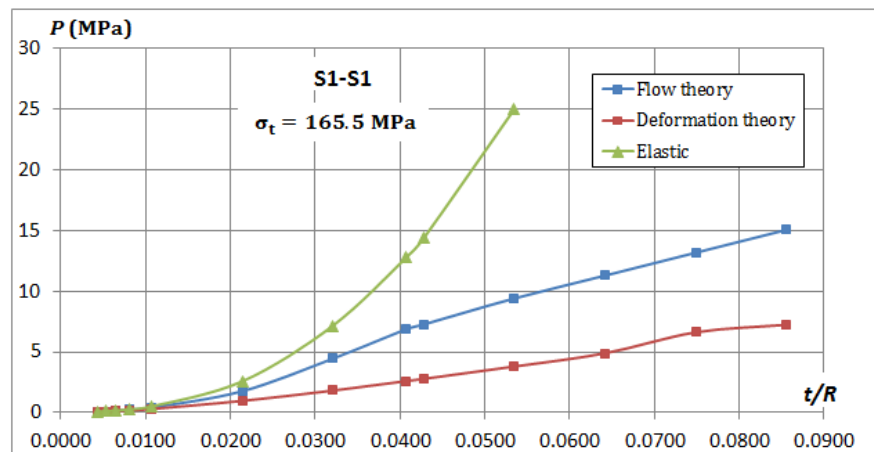
151.7	3,2	6.52	4,1	3.02	3,1	6.60	4,1	2.91	-1.2	3.8
165.5	3,2	6.89	4,1	2.59	3,1	6.84	4,1	2.50	0.7	3.6

Table 5. 4: Comparison of Eq. (4.11) with present study for both the flow and deformation theories.

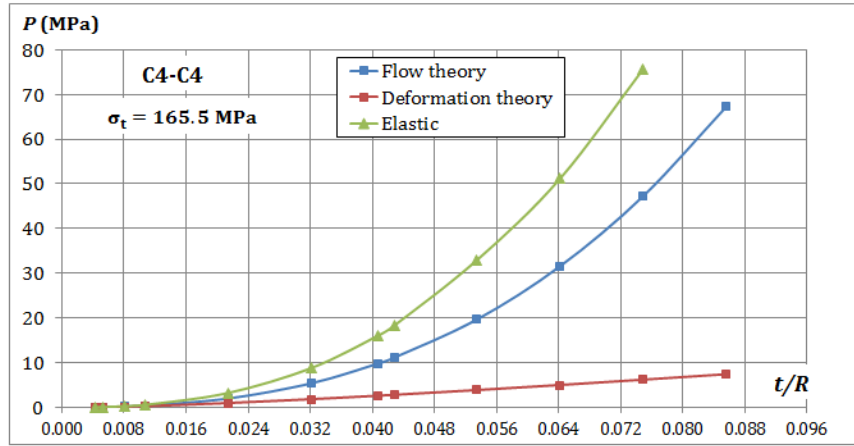
5.3.3. Effect of thickness ratio on the buckling pressure

The influence of the thickness-radius ratio t/R on the buckling pressure (P) for different values of applied tensile stresses, using both the flow and deformation theories, is presented in Figure 5.4. The elastic and plastic buckling results are also presented in the same figures. The length-diameter ratio is taken as $L/D = 1$. The results are calculated for three different values of the axial tensile stress and three cases of boundary conditions.

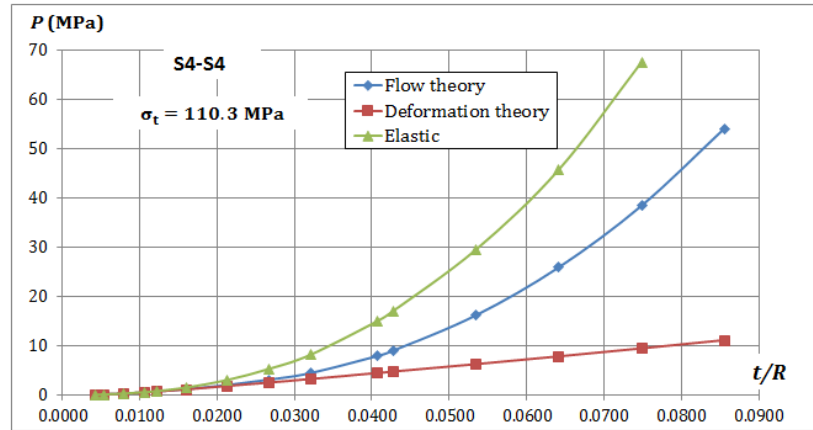
Figures 5.4a-5.4d show that, below a certain value of thickness-radius ratio t/R , i.e. 0.008, 0.008, 0.0214 and 0.0428, respectively, for the four considered cases, the plastic buckling results predicted using the flow and deformation theories are identical. When the thickness ratio is increased beyond these values, the differences in results between the two theories tend to increase and become extremely high for high thickness ratios. It is also observed that the deformation theory generally gives consistently lower buckling pressures than the flow theory. This confirms what is generally reported as the plastic buckling paradox.



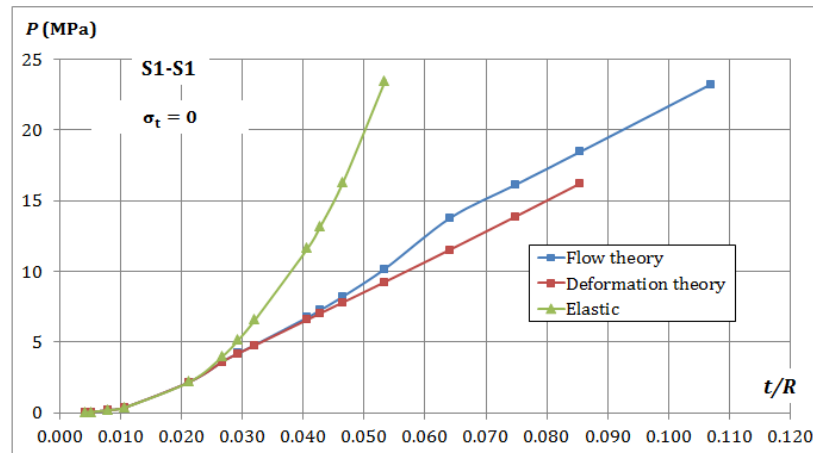
(a)



(b)



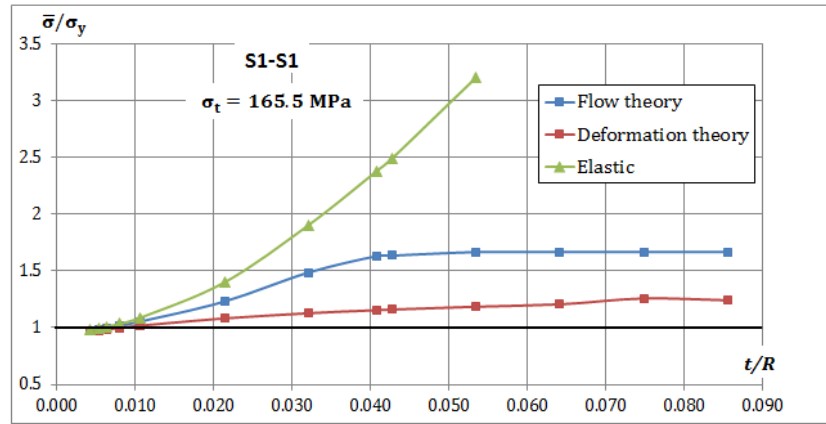
(c)



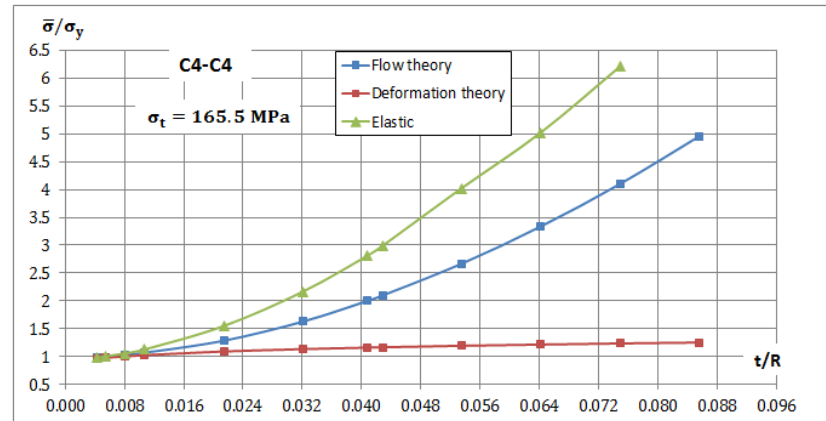
(d)

Figure 5. 4: Influence of thickness ratio t/R on the discrepancies between the buckling pressures P obtained using the flow and deformation theories

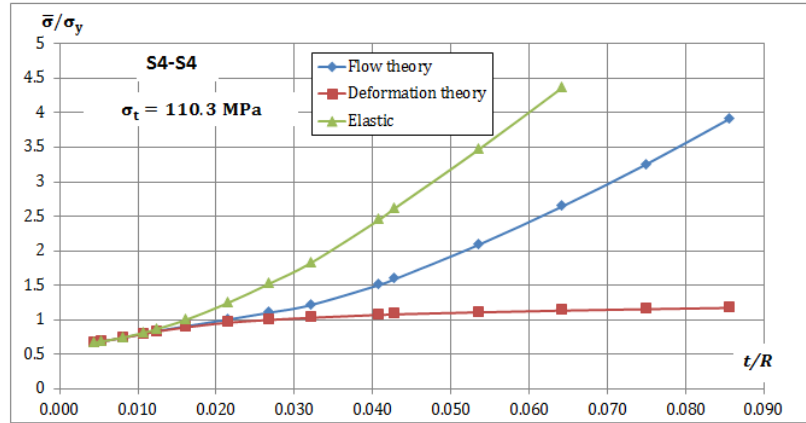
Figure 5.5 shows the influence of the thickness-radius ratio t/R on the ratio $\bar{\sigma}/\sigma_y$ calculated using the flow, the deformation and the elastic theory, where $\bar{\sigma}$ is the effective stress calculated from Eq. (5.7). When it is $\frac{\bar{\sigma}}{\sigma_y} > 1$, noticeable differences between buckling pressure obtained by the flow theory and the deformation theory are observed. Moreover, increasing the ratio $\frac{\bar{\sigma}}{\sigma_y}$, the discrepancies between the two plasticity theories also increase. Although both theories of plasticity could be expected to give approximately the same results for proportional loading (tensile stress equal to zero), Figure 5.4d shows that, also in this case, there are some differences in plastic buckling pressures predicted by the flow and deformation theories when the ratio t/R is high and Figure 5.5d shows the discrepancy in the calculated buckling pressure occurs when $\frac{\bar{\sigma}}{\sigma_y} > 1$.



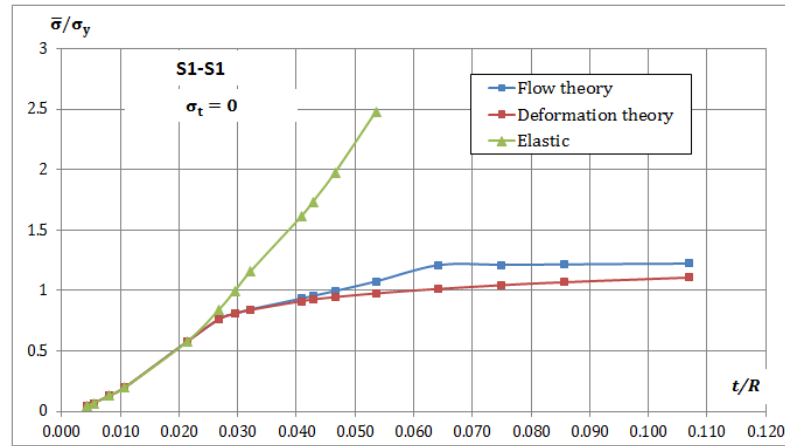
(a)



(b)



(c)



(d)

Figure 5. 5: Influence of thickness ratio t/R on the ratio $\bar{\sigma}/\sigma_y$

5.3.4. Effect of tensile stress and E/σ_y ratio on the buckling pressure

Figure 5.6 shows the plastic buckling pressures under various axial tensile stresses according to the flow and deformation theory for S3-S3 cylinders. Two thickness-radius ratios are considered. The length-diameter ratio is taken as $L/D = 1$. It is observed that the differences between the flow theory and deformation theory results are quite large when $t/R = 0.041$. In a certain loading range ($0 \leq \sigma_t \leq 70$ MPa) and when $t/R = 0.0214$, both plasticity results are identical while they are quite different when $t/R=0.041$.

Figure 5.7 shows the influence of the ratio E/σ_y on the buckling pressures using both the flow and deformation theories of plasticity for C4-C4 cylinders.

Again, the length-diameter ratio is taken as $L/D = 1$. It is seems that large a discrepancy in predictions between two theories exists for increasing E/σ_y ratio.

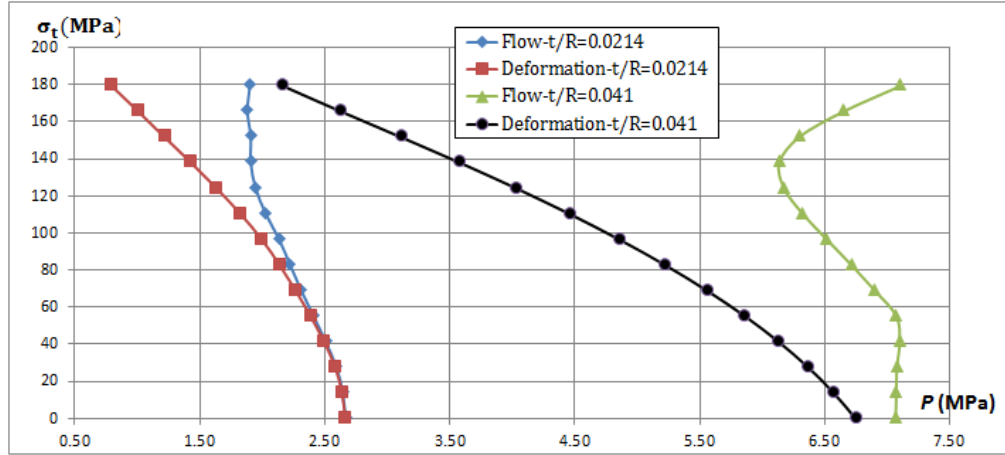


Figure 5. 6: Influence of tensile stress σ_t on the discrepancies between the buckling pressures P obtained using the flow and deformation theories for two thickness ratios

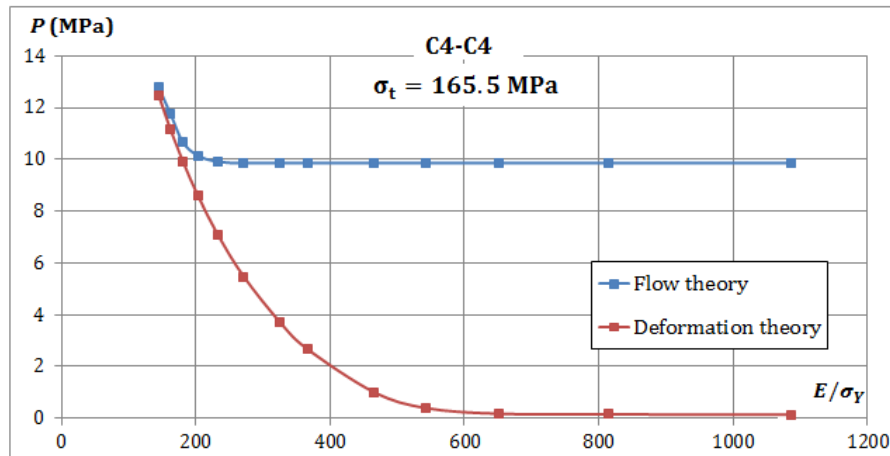


Figure 5. 7: Influence of E/σ_y ratio on the discrepancies between the buckling pressures P obtained using the flow and deformation theories

5.3.5. Effect of boundary conditions on the buckling pressure

Tables 5.5-5.8 show the buckling pressures and buckling modes of cylinders for eight sets of boundary conditions and for different values of axial tensile stress with $L/D = 1$, $D = 38.1$ mm and $t = 0.762$ mm. The plastic buckling results for clamped and simply-supported cylinders represented by the boundary conditions C4-C4 and S4-S4 indicate that clamping increases the

plastic buckling pressures predicted using the flow theory by 10%-15% when $\sigma_t \geq 82.7 \text{ MPa}$ while it has no influence on the plastic buckling pressures predicted by the deformation theory.

In the following a comparison between the plastic buckling pressures for additional sets of cylinders is presented. In the first set, the boundary condition is S1-S1 (or C1-C1), for which the edges are free to move axially. In the second set, the boundary condition is S4-S4 (or C4-C4), for which the incremental axial displacement u vanishes. It can be observed that the presence of the axial restraint at the boundaries increases the plastic buckling pressures calculated using the flow theory by 17%-22% when $\sigma_t \geq 96.5 \text{ MPa}$ and by 25%-32% when C1-C1 and C4-C4 cylinders are compared, while it has no significant influence on the plastic buckling pressures calculated using the deformation theory (the intensification is about 4%).

The influence of the incremental circumferential displacement v on the plastic buckling pressures can be investigated in two sets of boundary conditions, namely S3-S3 and S4-S4 (or C3-C3 and C4-C4). The incremental circumferential displacement v vanishes in the S4-S4 and C4-C4 cylinders. It seems that the circumferential restraint at the boundaries increases the plastic buckling pressures predicted using the flow theory by 20%-25% when $\sigma_t \geq 96.5 \text{ MPa}$ and by 25%-35% when C3-C3 and C4-C4 cylinders are compared, while it has no influence on the results calculated using the deformation theory for all values of tensile stresses.

It can be concluded that the presence of axial, circumferential and rotational restrains at the edges of the cylinders with increasing axial tensile stresses can significantly increase the discrepancies between the results of the flow and deformation theories in the range 8%-260%, as it is shown in Table 5.7 for cylinders C4-C4.

Constant axial tensile stress (MPa)	S1-S1				S2-S2			
	Buckling mode n,m	Buckling pressure-Flow	Buckling mode n,m	Buckling pressure-Deformation	Buckling mode n,m	Buckling pressure-Flow	Buckling mode n,m	Buckling pressure-Deformation
0.0	5,1	6.75	5,1	6.60	4,1	6.69	4,1	6.53
13.8	4,1	6.68	5,1	6.42	4,1	6.56	4,1	6.34
27.6	4,1	6.52	4,1	6.19	4,1	6.43	4,1	6.13
41.4	4,1	6.40	4,1	5.93	4,1	6.34	4,1	5.88
55.2	4,1	6.36	4,1	5.66	4,1	6.34	4,1	5.62
68.9	4,1	6.44	4,1	5.35	3,1	6.37	4,1	5.33
82.7	3,1	6.43	4,1	5.02	3,1	6.35	4,1	5.01
96.5	3,1	6.47	4,1	4.67	3,1	6.5	4,1	4.66
110.3	5,3	6.45	4,1	4.29	4,2	6.4	4,1	4.28
124.1	8,5	6.26	4,1	3.88	9,5	6.2	4,1	3.87
137.9	8,5	6.3	4,1	3.45	NB	NB	4,1	3.45
151.7	3,2	6.52	4,1	3.02	NB	NB	4,1	3.02
165.5	3,2	6.89	4,1	2.59	NB	NB	4,1	2.59

Table 5. 5: Plastic buckling pressures and corresponding buckling modes calculated using the DQ method and obtained by the flow theory and the deformation theory under different values of tensile stresses for S1-S1 and S2-S2 cylinders.

Constant axial tensile stress (MPa)	S3-S3				S4-S4			
	Buckling mode n,m	Buckling pressure-Flow	Buckling mode n,m	Buckling pressure-Deformation	Buckling mode n,m	Buckling pressure-Flow	Buckling mode n,m	Buckling pressure-Deformation
0.0	5,1	7.07	5,1	6.75	5,1	7.14	5,1	6.79
13.8	5,1	7.07	5,1	6.57	5,1	7.09	5,1	6.60
27.6	5,1	7.08	5,1	6.37	5,1	7.08	5,1	6.39
41.4	5,1	7.1	5,1	6.13	5,1	7.12	5,1	6.14
55.2	3,1	7.07	5,1	5.86	5,1	7.26	5,1	5.86
68.9	3,1	6.9	5,1	5.56	4,1	7.50	5,1	5.56
82.7	3,1	6.71	5,1	5.22	4,1	7.76	5,1	5.23
96.5	3,1	6.52	5,1	4.86	4,1	7.82	5,1	4.86
110.3	3,1	6.32	5,1	4.46	4,1	7.91	5,1	4.46
124.1	3,1	6.17	5,1	4.03	4,1	8.02	5,1	4.03
137.9	3,1	6.14	5,1	3.58	4,1	8.14	5,1	3.58
151.7	3,1	6.30	5,1	3.11	4,1	8.27	5,1	3.11
165.5	3,1	6.65	5,1	2.63	4,1	8.40	5,1	2.63

Table 5. 6: Plastic buckling pressures and corresponding buckling modes calculated using the DQ method and obtained by the flow theory and the deformation theory under different values of tensile stresses for S3-S3 and S4-S4 cylinders.

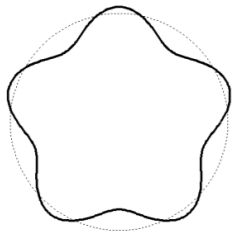
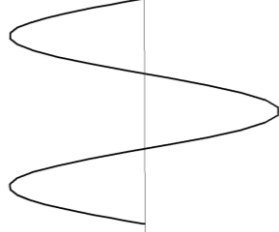
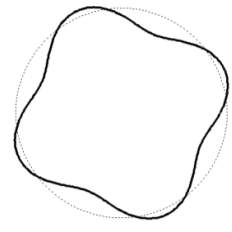
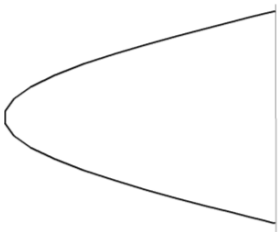
Constant axial tensile stress (MPa)	C1-C1				C2-C2			
	Buckling mode n,m	Buckling pressure-Flow	Buckling mode n,m	Buckling pressure-Deformation	Buckling mode n,m	Buckling pressure-Flow	Buckling mode n,m	Buckling pressure-Deformation
0.0	5,1	7.0	5,1	6.73	5,1	7.0	5,1	6.73
13.8	5,1	7.0	5,1	6.55	5,1	7.0	5,1	6.55
27.6	4,1	6.94	5,1	6.35	4,1	6.94	5,1	6.35
41.4	4,1	6.92	4,1	6.10	4,1	6.92	4,1	6.10
55.2	4,1	7.02	4,1	5.81	4,1	7.01	4,1	5.81
68.9	4,1	7.21	4,1	5.50	2,1	7.20	4,1	5.50
82.7	7,4	6.97	4,1	5.16	2,1	6.89	4,1	5.16
96.5	5,3	6.71	4,1	4.79	2,1	6.6	4,1	4.79
110.3	5,3	6.45	4,1	4.40	2,1	6.39	4,1	4.40
124.1	5,3	6.26	4,1	3.98	7,4	6.23	4,1	3.98
137.9	3,2	6.3	4,1	3.55	NB	NB	4,1	3.55
151.7	3,2	6.64	4,1	3.11	NB	NB	4,1	3.11
165.5	3,2	6.98	5,1	2.65	NB	NB	5,1	2.65

Table 5. 7: Plastic buckling pressures and corresponding buckling modes calculated using the DQ method and obtained by the flow theory and the deformation theory under different values of tensile stresses for C1-C1 and C2-C2 cylinders.

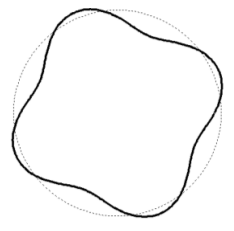
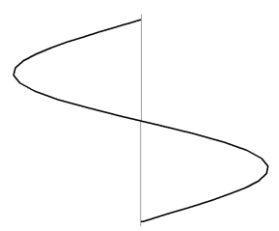
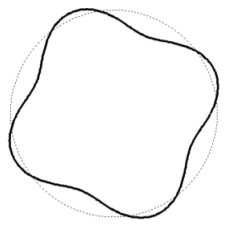
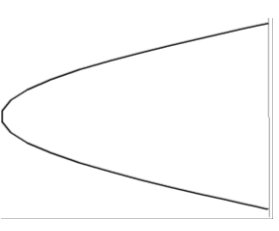
Constant axial tensile stress (MPa)	C3-C3				C4-C4			
	Buckling mode n,m	Buckling pressure-Flow	Buckling mode n,m	Buckling pressure-Deformation	Buckling mode n,m	Buckling pressure-Flow	Buckling mode n,m	Buckling pressure-Deformation
0.0	6,1	7.47	5,1	6.91	6,1	7.48	5,1	6.92
13.8	5,1	7.54	5,1	6.72	5,1	7.63	5,1	6.73
27.6	5,1	7.48	5,1	6.50	5,1	7.71	5,1	6.50
41.4	5,1	7.50	5,1	6.25	5,1	7.85	5,1	6.25
55.2	3,1	7.45	5,1	5.96	5,1	8.05	5,1	6.0
68.9	3,1	7.24	5,1	5.64	5,1	8.30	5,1	5.65
82.7	3,1	6.98	5,1	5.30	5,1	8.54	5,1	5.30
96.5	3,1	6.7	5,1	4.92	5,1	8.79	5,1	4.92
110.3	3,1	6.5	5,1	4.52	5,1	9.02	5,1	4.52
124.1	3,1	6.3	5,1	4.10	5,1	9.24	5,1	4.10
137.9	3,1	6.26	5,1	3.63	5,1	9.51	5,1	3.63
151.7	3,1	6.40	5,1	3.16	5,1	9.68	5,1	3.16
165.5	3,1	6.76	5,1	2.67	5,1	9.85	5,1	2.67

Table 5. 8: Plastic buckling pressures and corresponding buckling modes calculated using the DQ method and obtained by the flow theory and the deformation theory under different values of tensile stresses for C3-C3 and C4-C4 cylinders.

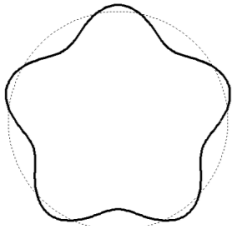
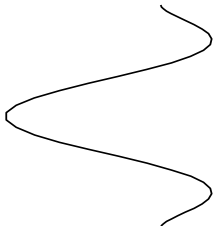
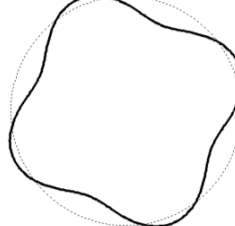
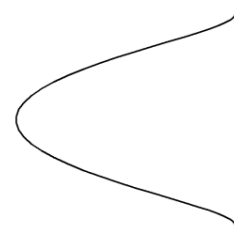
Tables 5.9a-5.9d show the computed buckling mode of cylinders subjected to constant axial tensile stress equals to 110.3 MPa and under different boundary conditions using both the flow and deformation theories. In these tables, the buckling shape in the circumferential direction of the cylinders is reported at the section in which the maximum radial displacement is observed. The buckling shape in the axial direction of the cylinders is reported for $\theta = 0$. It is interesting to observe from Tables 5.5 to 5.9 that for high values of applied axial tensile stress and for all types of boundary conditions except for C4-C4, the buckling modes observed using the flow theory differ from those obtained using the deformation theory of plasticity.

S1-S1			
Buckling shape in the circumferential direction using the flow theory	Buckling shape in the axial direction using the flow theory	Buckling shape in the circumferential direction using the deformation theory	Buckling shape in the axial direction using the deformation theory
			

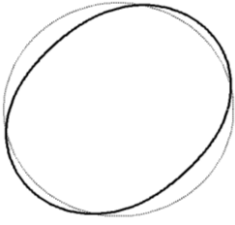
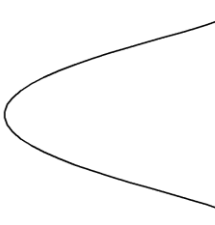
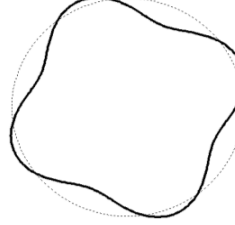
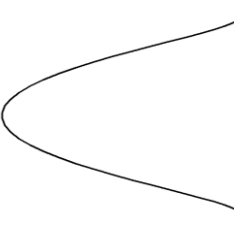
(a)

S2-S2			
Buckling shape in the circumferential direction using the flow theory	Buckling shape in the axial direction using the flow theory	Buckling shape in the circumferential direction using the deformation theory	Buckling shape in the axial direction using the deformation theory
			

(b)

C1-C1			
Buckling shape in the circumferential direction using the flow theory	Buckling shape in the axial direction using the flow theory	Buckling shape in the circumferential direction using the deformation theory	Buckling shape in the axial direction using the deformation theory
			

(c)

C2-C2			
Buckling shape in the circumferential direction using the flow theory	Buckling shape in the axial direction using the flow theory	Buckling shape in the circumferential direction using the deformation theory	Buckling shape in the axial direction using the deformation theory
			

(d)

Table 5. 9: Buckling mode shapes of cylindrical shells under proportional loading and various boundary conditions (the constant axial tensile stress is 110.3 MPa)

5.3.6. Effects of L/D ratio on the buckling pressure

The effects of length-diameter ratio L/D on the plastic buckling pressures of cylinders subjected to various values of axial tension using both the flow and deformation theories are presented in Figure 5.8. The results are relative to C4-C4 cylinders. It can be seen that, by decreasing the ratio L/D and increasing the tensile stress, the differences between the results obtained using the flow and the deformation theory increase significantly. It is clear that increasing L/D causes a significant reduction in plastic buckling pressures predicted using the flow theory and a slight reduction in critical pressures obtained using the deformation theory.

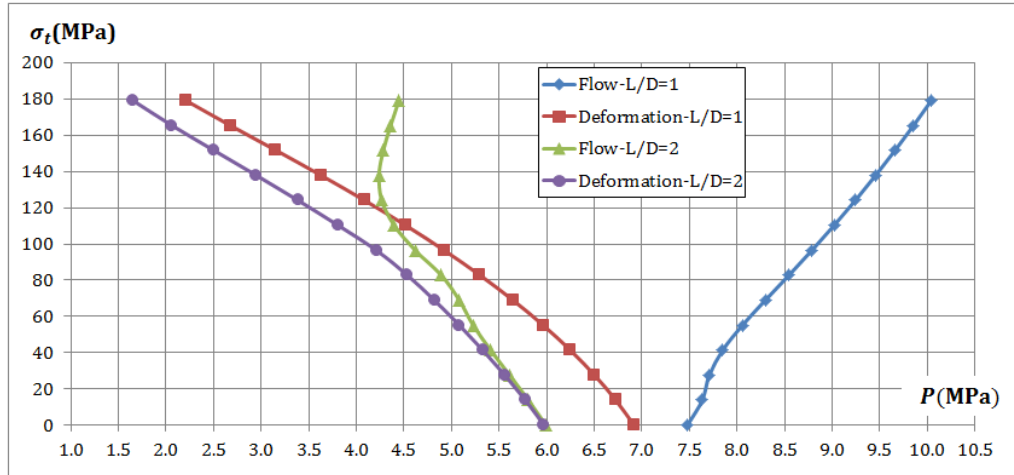


Figure 5. 8: Influence of L/D ratio on the discrepancies between the buckling pressures obtained using the flow and deformation theories

5.4. Effect of shear stiffness proposed by Becque (2010)

As discussed in Section 5.1, Becque (2010) proposed a modification to the J_2 flow theory which hinges on the determination of the shear stiffness from second-order considerations. The shear stiffness is taken as follows

$$G_{\text{Becque}} = \frac{E_t E}{(1 + \kappa + 2\nu)E_t + (1 - \kappa)E} \quad (5.29)$$

where parameter κ is the ratio of the plastic strain in the Principal 2 direction (y -direction) to the plastic strain in the Principal 1 direction (x -direction) at the point of local buckling. In case the von Mises yield surface is used $\kappa = -0.5$ for the plate studied by Beque. Eq. (5.29) therefore becomes

$$G_{\text{Becque}} = \frac{E_t E}{(0.5 + 2\nu)E_t + 1.5 E} \quad (5.30)$$

Eq. (5.30) is then substituted into Eq. (2.7) so that the shear stiffness G_{Becque} is adopted instead of the elastic one in the flow theory.

Moreover, it was discussed in Section 4.8 that Bushnell (1974) proposed adopting the effective shear modulus predicted by the deformation theory, \bar{G} , instead of the elastic one, G_{elastic} , in the flow theory. It was concluded that this modification in the flow theory does lead to a certain reduction in the

value of the buckling load but not as much as to make it comparable with the predictions from the deformation theory.

In order to assess the efficiency of Becque's proposed shear stiffness, a series of results are obtained for cylinders with boundary conditions S1-S1 and C4-C4, which have dimensions $L = 2R = 37.4\text{mm}$ and $h = 0.7\text{mm}$. The deformation theory and the flow theory adopting three shear modulus G_{elastic} , \bar{G} and G_{Becque} are employed. The results are shown in Table 5.10.

Constant axial tensile stress (MPa)	Deformation theory		G_{elastic} is used for the flow theory		G_{Becque} is used for the flow theory		\bar{G} is used for the flow theory	
	Buckling mode n,m	Buckling pressure-Deformation	Buckling mode n,m	Buckling pressure-Flow	Buckling mode n,m	Buckling pressure-Flow	Buckling mode n,m	Buckling pressure-Flow
0	5,1	6.6	5,1	6.75	4,1	6.5	5,1	6.68
13.8	5,1	6.42	4,1	6.68	4,1	6.3	4,1	6.55
27.6	4,1	6.19	4,1	6.52	4,1	6.1	4,1	6.4
41.4	4,1	5.93	4,1	6.4	4,1	5.9	4,1	6.17
55.2	4,1	5.66	4,1	6.36	4,1	5.75	4,1	6.0
68.9	4,1	5.35	4,1	6.44	4,1	5.65	4,1	5.87
82.7	4,1	5.02	3,1	6.43	3,1	5.61	4,1	5.83
96.5	4,1	4.67	3,1	6.47	3,1	5.5	3,1	5.72
110.3	4,1	4.29	5,3	6.45	3,1	5.53	3,1	5.67
124.1	4,1	3.88	8,5	6.26	2,1	5.38	3,1	5.76
137.9	4,1	3.45	8,5	6.3	2,1	4.88	2,1	5.69
151.7	4,1	3.02	3,2	6.52	2,1	4.36	2,1	5.36

(a)

Constant axial tensile stress (MPa)	Deformation theory		$G_{elastic}$ is used for the flow theory		G_{Becque} is used for the flow theory		\bar{G} is used for the flow theory	
	Buckling mode n,m	Buckling pressure-Deformation	Buckling mode n,m	Buckling pressure-Flow	Buckling mode n,m	Buckling pressure-Flow	Buckling mode n,m	Buckling pressure-Flow
0	5,1	6.92	6,1	7.48	5,1	6.78	5,1	7.15
13.8	5,1	6.73	5,1	7.63	5,1	6.66	5,1	7.06
27.6	5,1	6.5	5,1	7.71	4,1	6.55	5,1	6.97
41.4	5,1	6.25	5,1	7.85	4,1	6.4	5,1	6.91
55.2	5,1	6.0	5,1	8.05	4,1	6.26	4,1	6.88
68.9	5,1	5.65	5,1	8.3	4,1	6.22	4,1	6.73
82.7	5,1	5.3	5,1	8.54	4,1	6.28	4,1	6.64
96.5	5,1	4.92	5,1	8.79	NB	NB	NB	NB
110.3	5,1	4.52	5,1	9.02	NB	NB	NB	NB
124.1	5,1	4.1	5,1	9.24	NB	NB	NB	NB
137.9	5,1	3.63	5,1	9.51	NB	NB	NB	NB
151.7	5,1	3.16	5,1	9.68	NB	NB	NB	NB

(b)

Table 5. 10: Plastic buckling pressures and corresponding buckling modes calculated using the DQ method and obtained by the flow theory and the deformation theory under different values of tensile stresses for (a) S1-S1 and (b) C4-C4 cylinders.

For S1-S1 cylinders one can observe that employing the shear modulus G_{Becque} in the flow theory can reduce the buckling pressures calculated using the flow theory based on the elastic shear modulus $G_{elastic}$ by 3.7% to 12.7% for axial tensile stress ranging between 0- 82.7 MPa and by 14% -33% for higher values of tensile stresses (between 96.5 -151.7 MPa). Furthermore it can be noted that employing the effective shear modulus \bar{G} in the flow theory can reduce the buckling pressures calculated using the flow theory based on the elastic shear modulus $G_{elastic}$ by 2.7% to 4.7% for axial tensile stress ranging between 0- 82.7 MPa and by 3.8% to 18.7% for higher values of tensile stresses (between 96.5 - 151.7 MPa). The differences between the results obtained by the flow theory based on G_{Becque} and those obtained based on \bar{G} range between 2.5 % to 6.6% for axial tension ranging between 0 - 124.1 MPa and by 14.2% to 18.7% for higher values of tensile stresses

(between 137.9 - 151.7 MPa). Moreover, the flow theory based on G_{Becque} provides the same trend as the deformation theory, in which the buckling pressure reduces by increasing the axial tensile stress. Comparing with the deformation theory results, it can be seen that the discrepancy between the results obtained by the deformation theory and the flow theory based on G_{Becque} ranges between 0.5% to 11% for axial tension ranging between 0 - 82.7 MPa and 17% - 44% for higher values of axial tension (between 96.5 – 151.7 MPa).

For C4-C4 cylinders in which the degree of boundary clamping is higher, the flow theory based on G_{Becque} or \overline{G} does not predict buckling for axial tensile stress more than 96.7 MPa while the deformation theory can predict buckling. The differences between the results obtained by the flow theory based on G_{Becque} and those obtained based on \overline{G} range between 5.2% to 9%. Moreover, the discrepancy in the results between the results obtained by the deformation theory and the flow theory based on G_{Becque} ranges between 2% to 18.5%.

On the basis of these discussions and comparisons, it can be concluded that employing the shear modulus proposed by Becque (2010) in the flow theory does lead to a certain reduction in the value of the buckling pressure but not as much as to make it comparable with the predictions from the deformation theory for higher value of axial tensile stress. Moreover, by increasing the clamping of the cylinders, the flow theory failed to predict buckling at all. It is therefore clear that the difference in buckling predictions between flow theory and deformation theory can be only partially attributed to the difference in the shear modulus used for the bifurcation buckling analysis.

5.5. Finite-element modelling

The plastic buckling of imperfect cylinders subjected to constant axial tensile stress and increasing external pressure has been numerically simulated by means of the nonlinear FE commercial package ABAQUS, version 6.11-1 (Simulia, 2011), using both the flow and deformation theories of plasticity. The results of the analysis are compared with the current DQ results.

The FE simulations were conducted for cylinders of aluminum alloy 6061-T4. The plastic buckling pressures and the corresponding deformation shapes predicted by the flow theory and deformation theory were obtained for: a) C1-C1 cylinders subjected to various axial tensile stresses with $t/R = 0.0408$; b) S1-S1 cylinders with different values of thickness-radius ratios, t/R , and subjected to constant axial tensile stress; c) S2-S2 cylinders subjected to three different values of axial tensile stress with $t/R = 0.0408$. The chosen length-diameter ratio L/D was equal to one. For this value most of the buckling modes are symmetric with respect to the middle cross section. Therefore, half of the cylinder was modelled and symmetry boundary conditions were assigned to the symmetry plane of the cylinder, as shown in Figure 5.9. In the case of C1-C1 boundary conditions, nodes on the top edge of the shell were fixed except for the axial displacement (Table 5.1). In the case of S1-S1 boundary conditions, the rotations normal to the cylinder wall were allowed (Table 5.1). For cylinders S2-S2, the circumferential displacements were allowed (Table 5.1). Two types of loading were considered: axial tensile load applied at the top edge as a shell edge load in the longitudinal direction and external pressure applied normally to the surface of the shell elements (Figure 5.9). First the tensile load was applied and held constant. Successively, an increasing lateral pressure was applied.

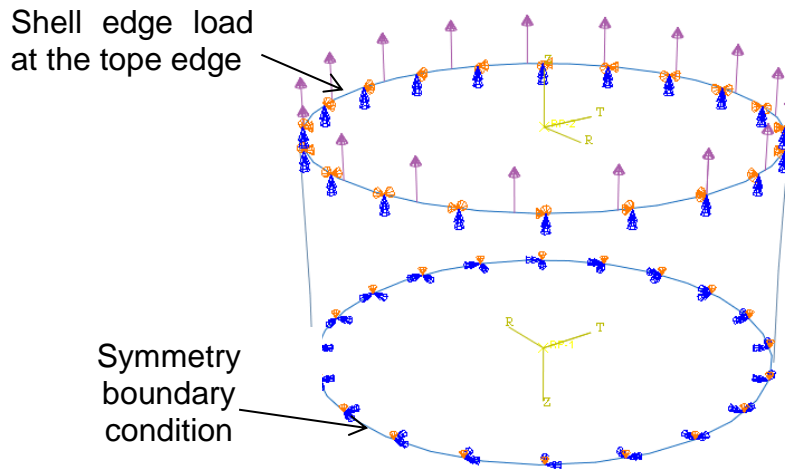
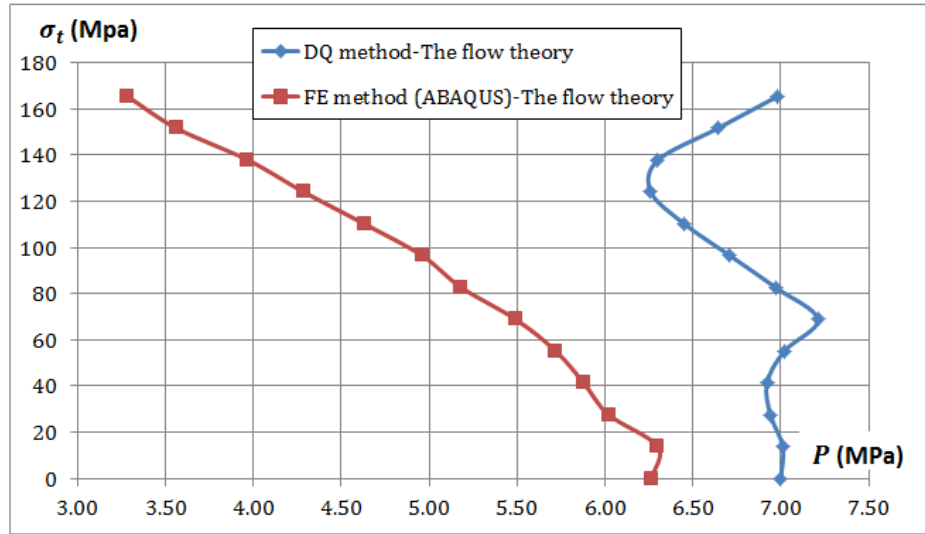


Figure 5. 9: Boundary conditions

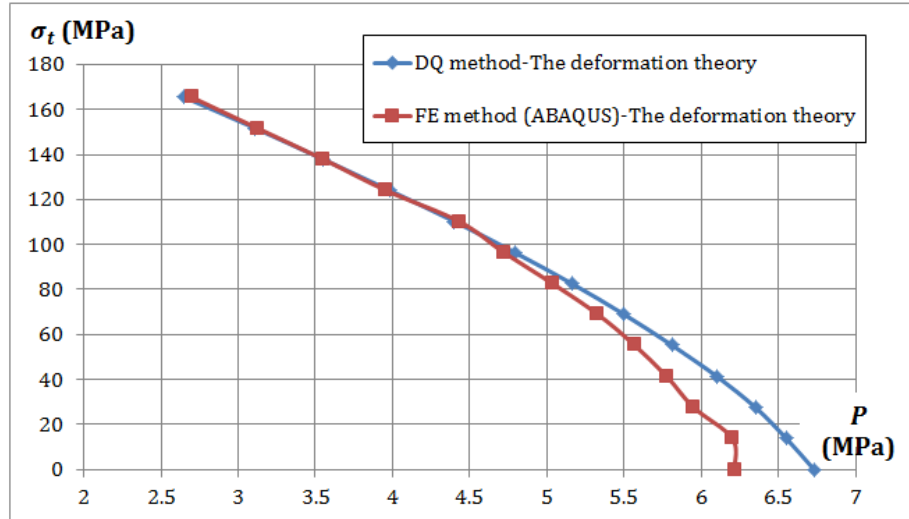
The cylinders were modelled using a general-purpose 4-noded fully integrated shell element, “S4” (Simulia, 2011). This element accounts for finite membrane strains and large rotations; therefore, it is suitable for large-strain analyses (Simulia, 2011). A structured mesh was used, made from a division of 150 and 50 elements along the circumference and the length, respectively. The Ramberg–Osgood input parameters used in the numerical simulations were reported in Table 5.1. Both the flow and deformation theories of plasticity have been employed. A detailed description of the implementation of the flow and deformation theories in the numerical analysis was given in Section 3.2.2. Initially, a linear buckling analysis was conducted assuming linear elastic material behavior and small displacements. The first 16 eigenmodes were used to seed the imperfection with maximum amplitude equal to 3% of the thickness. This strategy removes the presence of bifurcation point associated with primary and secondary paths (Falzon, 2006). The smallest buckling pressure predicted for all imperfection shapes, each one being proportional to one of the eigenmodes, was assumed to be the buckling pressure and its deformation shape was taken as the corresponding buckling mode. The Newton-Raphson scheme implemented in ABAQUS was used.

5.6. Comparison between the DQ and the FEA results

The plastic buckling pressures, based on the flow theory and deformation theory, were calculated numerically using ABAQUS and compared with the results by the DQ method. The results are presented in Figures 5.10 – 5.12 and Table 5.10. It can be observed that the flow theory employed in the DQ method gives consistently higher values of the buckling pressures than those calculated using deformation theory, as illustrated in Figures 5.10-5.11. Moreover, Table 5.11 shows that the equivalent strains (Eq. (5.8)) corresponding to the calculated buckling pressure for S1-S1 and C1-C1 cylinders on the basis of the flow theory are exceedingly large to be considered realistic, while the deformation theory provides physically more acceptable equivalent strains. However, Figures 5.12a-5.12b show that when conducting geometrically nonlinear finite-element calculations using the flow theory and the deformation theory of plasticity, the flow theory results become realistic and much closer to the results from the deformation theory. The differences in the results is in the range 0.7% - 15% for C1-C1 cylinders and -6% - 9.4% for S1-S1 cylinders. It is important to note that the plastic buckling pressures calculated analytically using the deformation theory are in very good agreement with those obtained numerically, as shown in Figures 5.10b- 5.11b. The discrepancy between the analytical and numerical results using the deformation theory ranges from -4.3% to 9.4% for S1-S1 cylinders, and from -1.7% to 8.2 % for C1-C1 cylinders. It is thus confirmed that, using the DQ method with a harmonic variation of the buckling mode assumed along the circumferential direction, the use of the flow theory of plasticity in the elastic-plastic bifurcation analysis may lead to unacceptable results and to over-estimate the buckling pressures when buckling occurs at an advanced plastic phase, while the deformation theory provides physically acceptable results within the same framework. However, the flow theory provides acceptable and reliable results in a nonlinear incremental analysis, which therefore does not give origin to any plastic buckling paradox

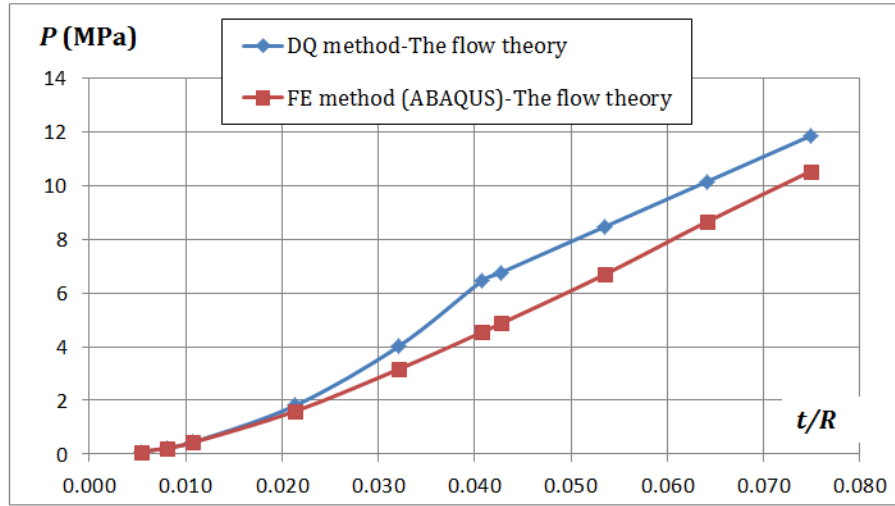


(a)

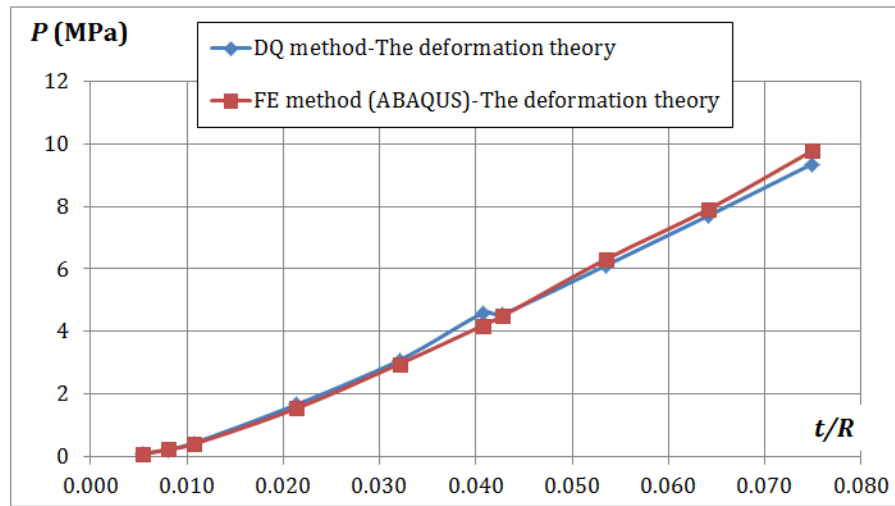


(b)

Figure 5. 10: Comparison between DQ method and numerical buckling pressure for C1-C1 cylinders with $h/R = 0.0408$, calculated using both the: (a) flow theory and (b) deformation theory

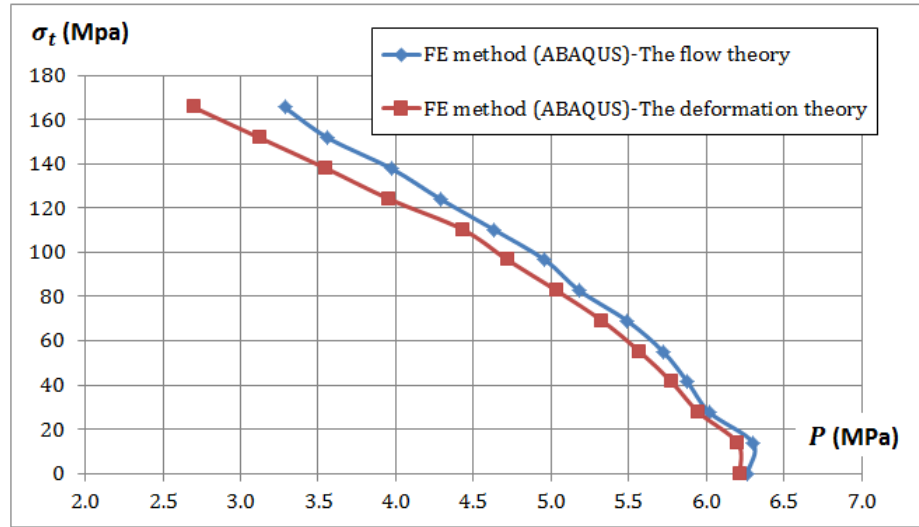


(a)

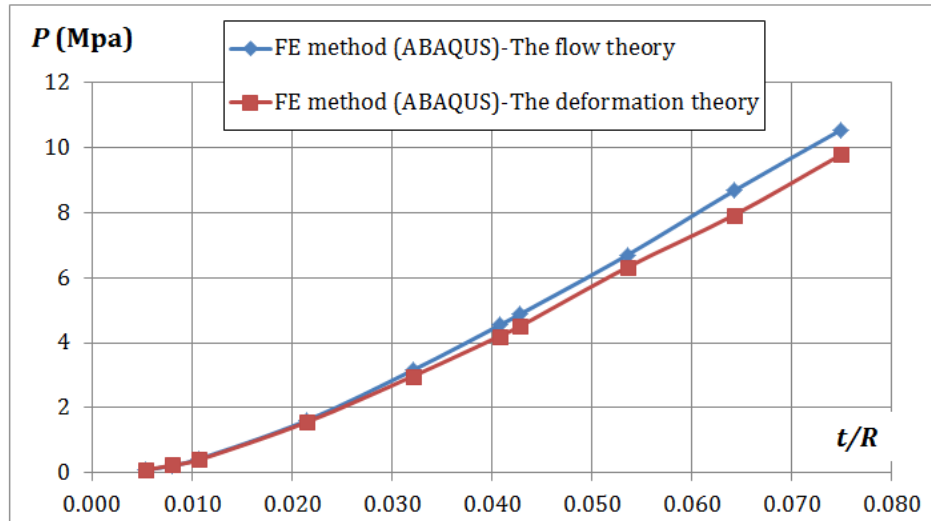


(b)

Figure 5. 11: Comparison between DQ method and numerical buckling pressure for S1-S1 cylinders with $\sigma_t = 110.5$ MPa, calculated using both the: (a) flow theory and (b) deformation theory



(a)



(b)

Figure 5. 12: Comparison between the flow and deformation theory buckling pressures calculated using ABAQUS for: (a) C1-C1 cylinders and (b) S1-S1 cylinders.

DQ results					
S1-S1 $\sigma t = 110.5$ Mpa			C1-C1 $t/R = 0.0408$		
t/R	Equivalent strain (%) - Flow	Equivalent strain (%) - Deformation	Tensile stress (Mpa)	Equivalent strain (%) - Flow	Equivalent strain (%) - Deformation
0.0053	0.185	0.19	0	0.379	0.31
0.0080	0.197	0.2	13.8	0.503	0.34
0.0107	0.212	0.21	27.6	0.685	0.37
0.0214	0.355	0.31	41.4	1.097	0.41
0.0321	2.13	0.51	55.2	2.329	0.45
0.0408	16.55	0.72	68.9	6.197	0.51
0.0428	16.56	0.79	82.7	8.607	0.59
0.0535	16.57	1.16	96.5	11.62	0.67
0.0642	16.57	1.60	110.3	16.48	0.82
0.0749	16.58	2.12	124.1	36.80	1.02
			137.9	83.98	1.29
			151.7	187.09	1.73
			165.5	549.19	2.40

Table 5. 11: Equivalent strain (%) of the cylinders S1-S1 and C1-C1

5.5.1. Interpretation of the presented and FE results in the context of the plastic buckling paradox

The main findings from the present study are the following:

- (1) when an accurate FE model is set up accounting for material and geometrical nonlinearity, the flow theory does not over-estimate plastic buckling pressures and the results obtained by the flow and deformation theories are similar and may occasionally differ by no more than 14%, a fact which has already been discussed in Chapter 4;
- (2) the discrepancy between the flow and deformation theories results arises when they are calculated in the framework of a buckling analysis, either analytically or by using the DQ method. The discrepancy increases significantly when the buckling occurs well within the plastic domain of the material. The deformation theory generally provides consistently lower buckling pressures than the flow theory;

(3) the discrepancy in the results between the flow theory and the deformation theory significantly increases, according to the presented procedure, with the stiffening of the cylinder, that is with the increase of the thickness ratio, the clamping of the boundaries and the ratio E/σ_y .

It has been already shown in Section 3.5 that a certain buckling shape determined by the simplified assumptions of the analytical treatments, which result in kinematic constraints, leads to an excessive stiffness of the cylinder and, consequently, an overestimation of the buckling stress for both the flow and deformation theories. However, the deformation theory compensates the over-stiffening of the shell, thus providing buckling stress results that are lower than those obtained by the flow theory. This fact is confirmed also by the DQ treatment presented here, in which the kinematic of the problem is approximated by assuming that the buckling mode varies harmonically in the circumferential directions, as shown in Eq. (5.13). Therefore, the implicit kinematic constraint, which derives from assuming a harmonic buckling shape, seems to be once again the main reason for the discrepancy between the flow theory and deformation theory results obtained analytically. This does not happen in the case of carefully constructed and validated nonlinear FE analyses in which the kinematics is far less constrained.

Table 5.12 shows the plastic buckling pressures and corresponding buckling modes obtained using the DQ method and geometrically nonlinear finite element method. It can be seen for all cases, as mentioned above, that the flow and the deformation theory results obtained by the FE method are similar, and the corresponding buckling modes predicted by both plasticity theories are identical. However, by using the DQ method, when large differences in the buckling pressures between the flow and deformation theories are observed, it is seen that the buckling modes are different. These buckling modes predicted by the flow theory are also different from those obtained by the FE method, see Tables 5.13-5.15.

Tensile stress (MPa)	Buckling pressure P_{cr} (MPa) and corresponding buckling mode n,m calculated from present study				Buckling pressure P_{cr} (MPa) and corresponding buckling mode n,m obtained from ABAQUS			
	The flow theory		The deformation theory		The flow theory		The deformation theory	
	n,m	P_{cr}	n,m	P_{cr}	n,m	P_{cr}	n,m	P_{cr}
0	5,1	7.00	5,1	6.73	5,1	6.26	5,1	6.22
13.8	5,1	7.01	5,1	6.55	5,1	6.30	5,1	6.20
27.6	4,1	6.94	5,1	6.35	5,1	6.02	5,1	5.95
41.4	4,1	6.92	4,1	6.1	5,1	5.88	5,1	5.78
55.2	4,1	7.02	4,1	5.81	5,1	5.72	5,1	5.57
68.9	4,1	7.21	4,1	5.5	5,1	5.49	5,1	5.33
82.7	7,4	6.97	4,1	5.16	4,1	5.18	4,1	5.04
96.5	5,3	6.71	4,1	4.79	4,1	4.96	5,1	4.72
110.3	5,3	6.45	4,1	4.4	4,1	4.63	4,1	4.43
124.1	5,3	6.26	4,1	3.98	4,1	4.29	4,1	3.96
137.9	3,2	6.3	4,1	3.55	4,1	3.97	4,1	3.55
151.7	3,2	6.64	4,1	3.11	4,1	3.56	5,1	3.13
165.5	3,2	6.98	5,1	2.65	5,1	3.28	5,1	2.70

(a)

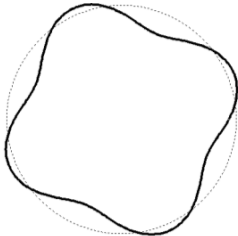
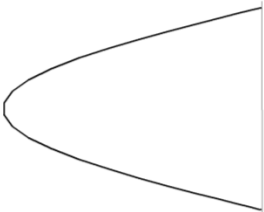
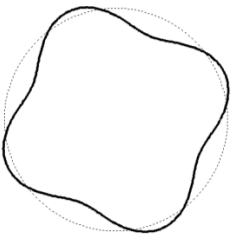
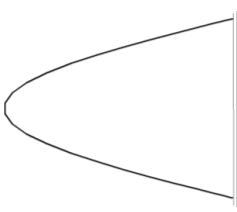
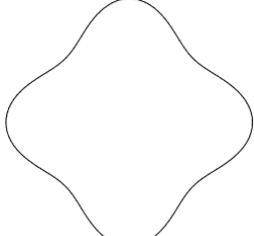

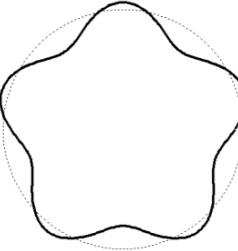
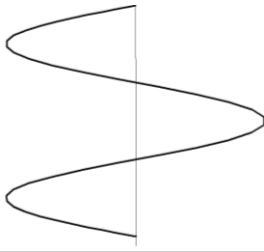
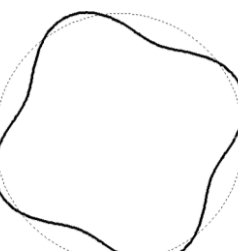
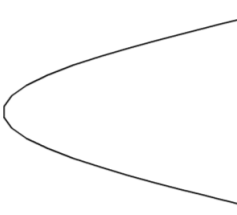
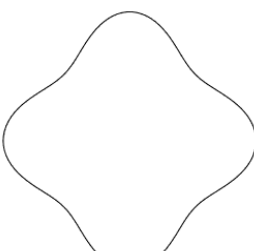

t/R	Buckling pressure P_{cr} (MPa) and corresponding buckling mode n,m calculated from present study				Buckling pressure P_{cr} (MPa) and corresponding buckling mode n,m obtained from ABAQUS			
	The flow theory		The deformation theory		The flow theory		The deformation theory	
	n,m	P_{cr}	n,m	P_{cr}	n,m	P_{cr}	n,m	P_{cr}
0.0053	8,1	0.092	8,1	0.092	7,1	0.092	7,1	0.092
0.0080	7,1	0.23	7,1	0.23	6,1	0.226	6,1	0.241
0.0107	6,1	0.44	6,1	0.44	7,1	0.43	7,1	0.41
0.0214	5,1	1.82	5,1	1.67	5,1	1.61	5,1	1.56
0.0321	4,1	4.01	4,1	3.09	4,1	3.16	4,1	2.98
0.0408	5,3	6.45	4,1	4.55	4,1	4.54	4,1	4.20
0.0428	5,3	6.77	4,1	4.57	4,1	4.88	4,1	4.51
0.0535	5,3	8.46	4,1	6.11	4,1	6.69	5,1	6.31
0.0642	5,3	10.16	4,1	7.71	4,1	8.66	4,1	7.92
0.0749	5,3	11.85	4,1	9.35	4,1	10.53	4,1	9.77

(b)

Tensile stress (MPa)	Buckling pressure P_{cr} (MPa) and corresponding buckling mode n,m calculated from present study				Buckling pressure P_{cr} (MPa) and corresponding buckling mode n,m obtained from ABAQUS			
	The flow theory		The deformation theory		The flow theory		The deformation theory	
	n,m	P_{cr}	n,m	P_{cr}	n,m	P_{cr}	n,m	P_{cr}
27.6	4,1	6.43	4,1	6.13	4,1	5.82	4,1	5.72
68.9	3,1	6.36	4,1	5.33	4,1	5.23	4,1	5.11
110.3	4,2	6.38	4,1	4.28	4,1	4.57	4,1	4.21

(c)

Table 5. 12: plastic buckling pressure and corresponding buckling mode obtained using the DQ and FE method: (a) C1-C1 cylinder; (b) S1-S1 cylinder and (c) S2-S2 cylinder.

t/R	The DQ results				The FE results (ABAQUS)	
	Buckling shape in the circumferential direction using the flow theory (n)	Buckling shape in the axial direction using the flow theory (m)	Buckling shape in the circumferential direction using the deformation theory (n)	Buckling shape in the axial direction using the deformation theory (m)	Buckling shape in the circumferential direction using either the flow theory or deformation theory	Buckling shape in the axial direction using either the flow theory or deformation theory
0.0321						
0.0408						

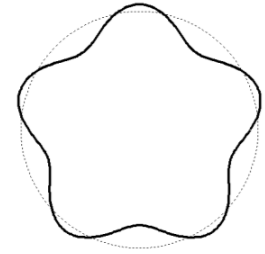
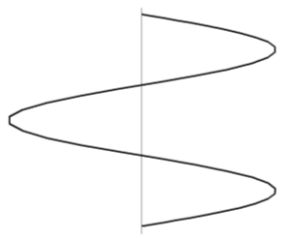
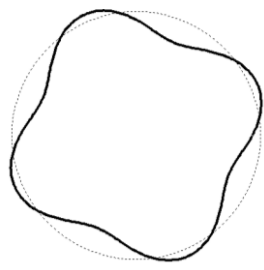
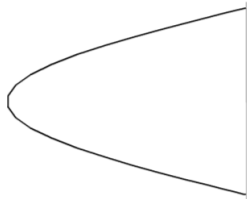
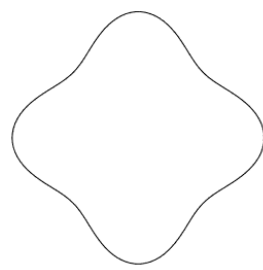

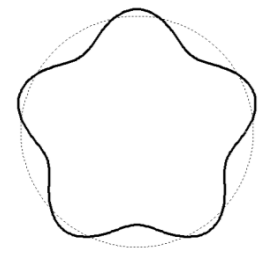
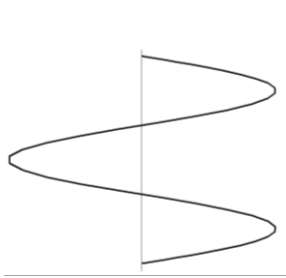
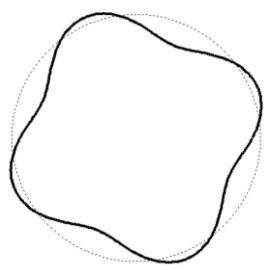
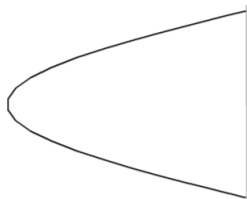
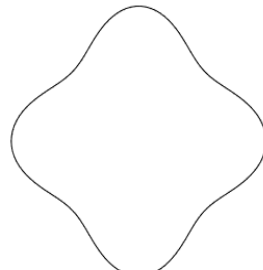

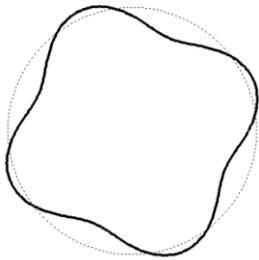
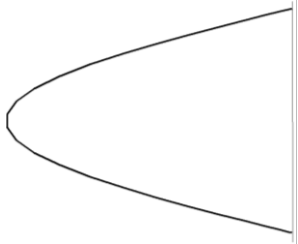
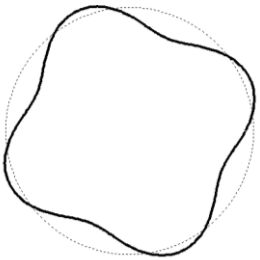
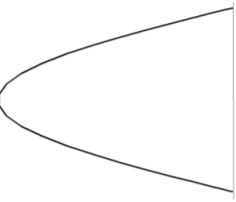
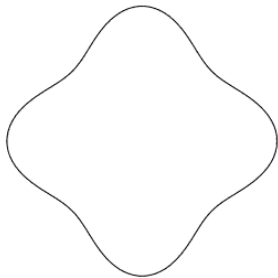

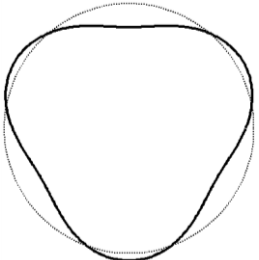
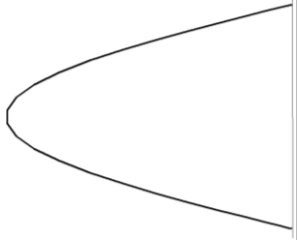
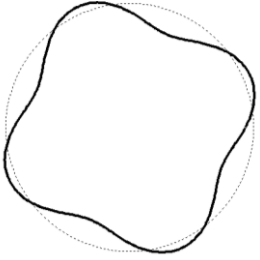
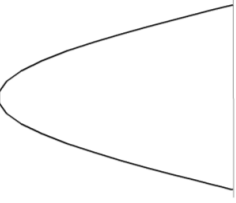
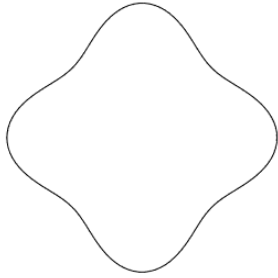

0.0642						
0.0749						

Table 5. 13: Comparison between buckling shapes from different methods for S1-S1 cylinders ($\sigma_t = 110.5$ MPa,)

σ_t (MPa)	The DQ results				The FE results (ABAQUS)	
	Buckling shape in the circumferential direction using the flow theory (n)	Buckling shape in the axial direction using the flow theory (m)	Buckling shape in the circumferential direction using the deformation theory (n)	Buckling shape in the axial direction using the deformation theory (m)	Buckling shape in the circumferential direction using either the flow theory or deformation theory	Buckling shape in the axial direction using either the flow theory or deformation theory
27.6						
68.9						

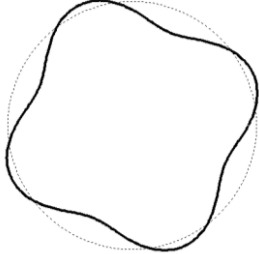
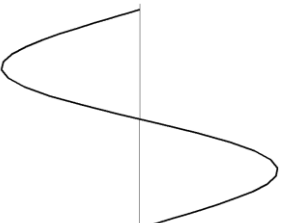
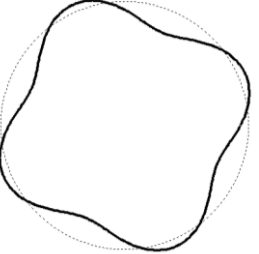
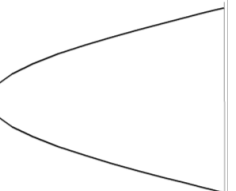
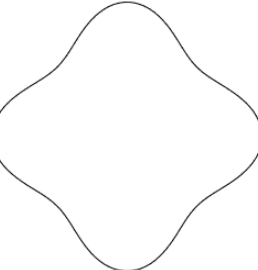

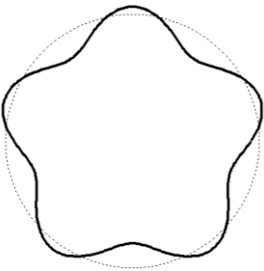
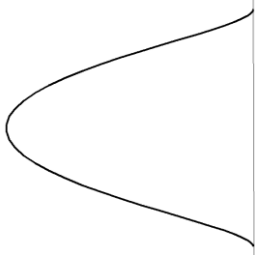
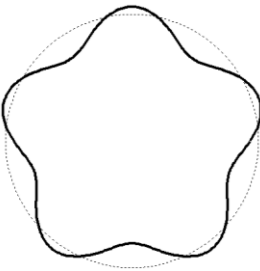
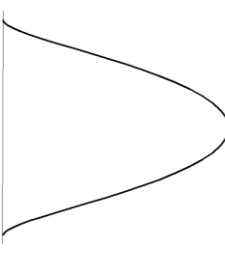
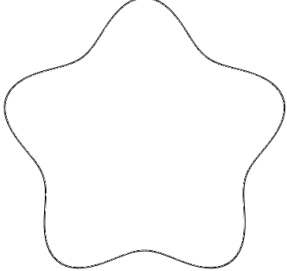

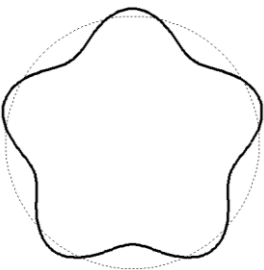
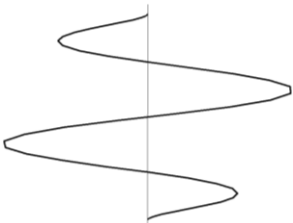
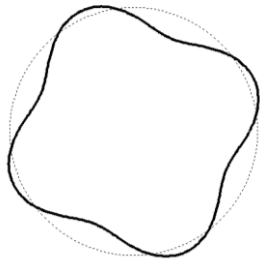
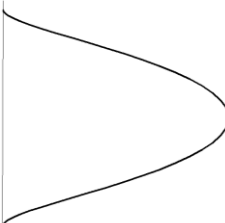
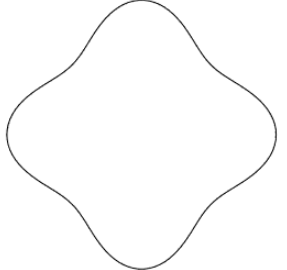

110.3						
-------	---	---	--	---	---	---

Table 5. 14: Comparison between buckling shapes from different methods for S2-S2 cylinders ($\frac{t}{R} = 0.0408$)

σ_t (MPa)	The DQ results				The FE results (ABAQUS)	
	Buckling shape in the circumferential direction using the flow theory (n)	Buckling shape in the axial direction using the flow theory (m)	Buckling shape in the circumferential direction using the deformation theory (n)	Buckling shape in the axial direction using the deformation theory (m)	Buckling shape in the circumferential direction using either the flow theory or deformation theory	Buckling shape in the axial direction using either the flow theory or deformation theory
13.8						
110.3						

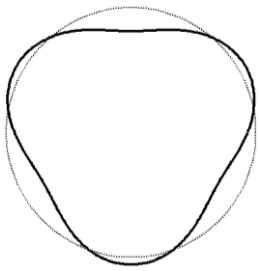
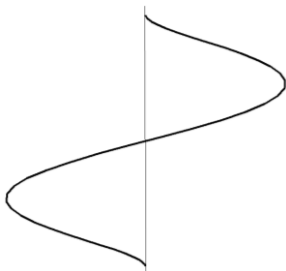
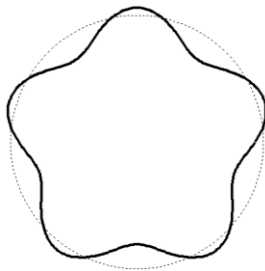
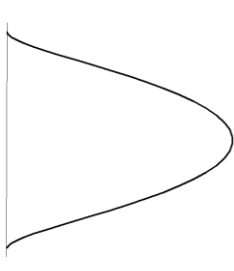
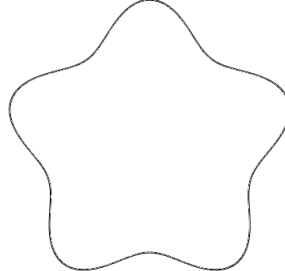

165.5						
-------	---	---	--	---	---	---

Table 5. 15: Comparison between buckling shapes from different methods for C1-C1 cylinders ($\frac{t}{R} = 0.0408$)

5.7. Conclusions

In this chapter, the DQ method has been used to obtain the elastic-plastic buckling pressures of cylinders under non-proportional loadings and various boundary conditions. The analysis has been based on Flugge stability equations. In the problem considered, the buckling mode was assumed to vary harmonically in the circumferential direction. The problem has thus been reduced to a one-dimensional one, and the sampling points had to be taken only in the axial direction of the shell. Buckling pressures were obtained using direct iterations with a standard eigenvalue solver.

Comparisons were made with some results given in the literature and results obtained using BOSOR5. The DQ results show good agreement with some of the known solutions. A parametric study was then performed to characterise the effect of the thickness-radius, t/R , length-diameter, L/D , material stiffness-strength, E/σ_y ratios, tensile stress and various boundary conditions on the discrepancies between the flow theory and deformation theory predictions.

Nonlinear finite-element (FE) analyses of cylindrical shells have also been carefully conducted using both the flow theory and the deformation theory of plasticity. Plastic buckling results were compared with the present DQ results for three types of boundary conditions, various values of thickness-radius h/R ratio and tensile stress.

The findings are:

- using the DQ method, the discrepancy between the buckling pressures predicted by the flow theory and the deformation theory increases with the increase in t/R , E/σ_y ratios and tensile stress and with the decrease in the L/D ratio;
- using the DQ method, both theories provide the same results when the buckling occurs in the elastic phase. When buckling occurs in plastic phase, the flow theory results deviate from those obtained using the deformation theory;

- preventing the edge rotation along of the generator and the presence of axial and circumferential restraint at the boundaries increase the plastic buckling pressures obtained using the flow theory while it has no or very little influence on the plastic buckling pressures calculated using the deformation theory for all values of the applied tensile stresses;
- by conducting geometrically nonlinear finite-element analyses, the flow theory provides physically reliable results, which are in accordance with the deformation theory ones. The large discrepancies between flow and deformation theories results observed with analytical solutions or using the DQ method vanish when using the flow theory in nonlinear incremental analysis;
- the root of the discrepancy can once again be attributed to the over-constrained assumed kinematics, i.e. harmonic buckling shapes in the circumferential direction. This fact leads to overestimate the buckling pressures when the flow theory of plasticity is used, while the deformation theory counterbalances the excessive kinematic stiffness and provides results which are much lower than the flow theory findings;
- in order to further verify that the assumption on the harmonic kinematics in Eq. (5.13) is the only origin of the unacceptable results for the DQ method, additional analytical investigations could be carried out by taking into consideration buckling modes different from the harmonic one and evaluate if this can deliver any improvement in the predictions based on the flow theory of plasticity. However, since the harmonic assumption is the standard approach in the DQ method, this would imply a modification of the whole procedure, which could become more complex and therefore offset many of its advantages;
- The proposed modifications of the flow theory by Becque (2010) or Bushnell (1974), which hinge on the use of a shear stiffness different from the elastic one, do lead to a certain reduction in the buckling pressure but not as much as to make it comparable with the

predictions from the deformation theory for higher value of axial tensile stress. Moreover, the flow theory failed to predict buckling for cylinders with higher clamping condition.

- it is recommended that a geometrically nonlinear finite-element formulation for imperfect shells is used, with carefully determined and validated constitutive laws, to avoid the discrepancies between the two plasticity theories, and that accurate post-buckling curves are tracked using the physically more sound flow theory of plasticity.

Chapter 6

Conclusions and Recommendations

6.1. Conclusions

The research work presented in this thesis generally achieved its objectives as stated in the introduction. More in detail it managed to:

- *clarify whether the paradox really exists for cylindrical shells subjected to axial compression or combined axial tension and external pressure.*

This has been achieved to a good extent in Chapters 3 and 4. It was found that by conducting accurate geometrically nonlinear FE analysis using both the flow and the deformation theories of plasticity, the flow theory of plasticity led to predictions of buckling load and pressure that were in better agreement with the corresponding experimental results than those provided by the deformation theory. Moreover, the flow theory of plasticity succeeds in predicting buckling with physically acceptable plastic strains. Additionally the discrepancies between the flow and deformation theories results in terms of plastic buckling stress for both perfect and imperfect cylinders were quite small for both thick and thin cylinders.

- *provide possible explanation of the plastic buckling paradox and a critical revision of the results obtained by many authors in the literature, which led to the definition of the paradox.*

This was achieved and discussed in Chapters 3, 4. In Chapter 3, for the case of cylinders subjected to axial compression, many analytical equations used in the literature to determine the plastic buckling and corresponding buckling mode were derived from the assumption of harmonic expression of buckling shape. It was found that imposing a constrained kinematics on the FE model in order to produce the buckling shape of the analytical solution made the buckling stresses predicted by the flow theory well in excess of those obtained by the deformation theory of plasticity. When no kinematic constraints were used, the results of the flow theory were in much better agreement with the test results than those of the deformation theory. This led to conclude that the roots of the discrepancy for the case of cylinders subjected to axial compression are found in the simplifying assumptions regarding the buckling modes used as the basis of many analytical investigations. The deformation theory of plasticity counterbalances the excessive stiffness induced by kinematically constraining the cylinders to follow predefined buckling modes, thus providing results that are only apparently more in line with the experimental findings.

In Chapter 4, for cylinders subjected to non-proportional loading, consisting of combined external pressure and axial tensile stress, an analytical formulation was established employing both the flow and deformation theories. The analytical results were compared with those provided by the code BOSOR5 and with those provided by nonlinear FE analyses, for a vast range of boundary conditions, geometries and loadings. It was found that the plastic buckling pressures calculated analytically using both the flow and the deformation theories closely matched those obtained numerically by use of the code BOSOR5. The proposed analytical findings and BOSOR5 results confirm that the flow theory over-predicts plastic buckling pressure for high values of applied axial tensile stress and for thick cylinders while the deformation theory provides results in better agreement with test results. It was noted that both analytical and BOSOR5 treatments

used the same simplifying assumption in which the kinematics of the problem was constrained to follow harmonic expressions in the circumferential direction while the kinematics in the current FE approach was free. Therefore, the discrepancy between the FE predictions, the analytical solutions and the numerical results computed by BOSOR5 could be attributed to the simplifying assumptions on the buckling shape used in BOSOR5 and in the analytical treatment. These result in a kinematic constraint which lead to an excessive stiffness of the cylinders and, ultimately, to an overestimation of the buckling stress for both the flow and deformation theories. However, the deformation theory tends to compensate this kinematic over-stiffness and provides results that are more in line with the experimental ones. Given that the kinematics in the FE approach is far less constrained than that in the analytical one, the flow theory provides results more in line with the tests results.

- *assess the imperfection sensitivity of shells buckling in the plastic domain.*

This has been achieved in Chapters 3 and 4. For cylinders subjected to axial compression, it was found that the plastic buckling stresses obtained using the flow and deformation theories showed low sensitivity to the imperfection for shells with $10 \leq R/t \leq 45$ while both theories showed imperfection sensitivity for R/t over 45. For cylinders subjected to non-proportional loading, it was found that the discrepancies in the predictions of buckling pressure between the two plasticity theories increase as the imperfection ratios decrease but significantly less than observed in other previous numerical treatments in the literature.

- *establish new analytical solutions for plastic buckling of cylindrical shells in order to investigate the effect the boundary conditions, material parameters and geometry of the cylinders on the discrepancies in the results obtained using the flow and deformation theories.*

This has been achieved in Chapter 5. The governing equations of buckling analysis of cylindrical shells derived by Flugge (1960) served as the basis of the analysis, conducted for both the flow theory and the deformation theory of plasticity. The plastic buckling results were obtained by means of the differential quadrature method (DQM), which has been successfully used in the literature to analyse the elastic buckling of plates and cylinders and the plastic buckling of plates. It was found that the DQ results obtained from the flow and deformation theories confirm that, using over-constrained kinematics for the buckling shape in the circumferential direction, the deformation theory tends to provide lower values of buckling pressure and the discrepancies in the results from the two plasticity theories increase with increasing thickness-to-radius ratio, tensile stresses, boundary clamping and material stiffness-to-strength, E/σ_y , ratio. Moreover, it is concluded that the difference in buckling pressure between flow theory and deformation theory can be only partially attributed to the difference in the shear modulus proposed by Becque (2010) or Bushnell (1974) used for the bifurcation buckling analysis.

6.2. Recommendations for further work

This thesis focuses on the plastic buckling paradox for cylinders subjected to two loading cases, i.e. simple axial compression and combined external pressure and axial tensile stress. Other load patterns, such as combined tensile load, external pressure and bending, could be explored in further studies. These loadings are induced in pipelines during installation in deep water.

The geometric imperfection in the cylinders studied in Chapter 4 was assumed to have the shape of a single mode, i.e. the first, third and fifth, and of a linear combination of such modes. If the maximum value of imperfection is known, the question will be what the critical imperfection shape which leads to lowest buckling load is. Further work could consider a larger number of single modes and combinations of such modes.

Chapter 5 shows that DQ method can yield accurate results using less number of grid points than for the finite-difference method. Therefore, a possible area for future work is the extension of DQ method to nonlinear analysis, accounting for the effect of imperfections. Chapter 5 mainly focused on the plastic buckling analysis in the case of small deflections. Therefore, the effect of initial imperfections cannot be taken into consideration in the present study. In order to include the effect of imperfections, a nonlinear analysis with large deflection needs to be conducted. Therefore, the application of the DQ method to the nonlinear analysis of cylindrical shells, including the effects of imperfections and plasticity, could be considered in future.

BOSOR5 takes in considerations the effect of pre-buckling stresses by conducting a nonlinear analysis which accounts for large deformation and material nonlinearity. Then an eigenvalue analysis is carried out to calculate the buckling load and corresponding buckling mode. The equations that describe the pre-buckling and plastic eigenvalue analyses are derived from the finite difference method. The DQ method used in Chapter 5 provides results in very good agreements with BOSOR5 results. However, the DQ method presented in this thesis assumes linear pre-buckling and therefore small differences in the results between the DQ results and BOSOR5 results are due to the effect of pre-buckling. It is reasonable to extend the DQ method in the elastoplastic buckling and include the effect of nonlinear pre-buckling.

References

- Allen, H.G. and Bulson, P.S. (1980) *Background to Buckling*. McGraw-Hill, England.
- Ambartsumjan, S.A. (1963) 'On the stability of inelastic plates with consideration of shear deformation', *PMM: Prikladnaya Matematika I Mekhanika* (in Russian), 27(4), pp. 753-757.
- Asadzadeh, E. and Alam, M. (2014) 'A Survey On Hyperbolic Cooling Towers', *International Journal Of Civil, Structural, Construction And Architectural Engineering*, 8(10), pp.1027-1039.
- Batdorf, S.B and Budiansky, B. (1949) 'A mathematical theory of plasticity based on the concept of slip', *National Advisory Committee for Aeronautics Technical Note- 1871*, pp. 1-36.
- Bathe, K.J. (1982) *Finite element procedures in engineering analysis*. Prentice-Hall, Inc., Englewood Cliffs, New Jersey.
- Batterman, S.C. (1965) 'Plastic buckling of axially compressed cylindrical shells', *AIAA Journal*, 3(2), pp. 316-325.
- Bardi, F.C. and Kyriakides, S. (2006) 'Plastic buckling of circular tubes under axial compression - Part I: Experiments', *International Journal of Mechanical Sciences*, 48(8), pp. 830-841.
- Bell, J., (1984) *Mechanics of Solids. Vol. 1: The Experimental Foundations of Solid Mechanics*. Springer-Verlag.
- Bert, C. W., Jang, S. K. and Striz, A. G. (1988) 'Two new approximate methods for analyzing free vibration of structural components', *AIAA journal*, 26(5), pp. 612-618.
- Bert, C. W., Jang, S. K. and Striz, A. G. (1989) 'Nonlinear bending analysis of orthotropic rectangular plates by the method of differential quadrature', *Computational Mechanics*, 5(2-3), pp. 217-226.
- Bert, C. W. and Malik, M. (1996a) 'Differential quadrature method in computational mechanics: a review', *Applied Mechanics Reviews*, 49(1), pp.1-28.
- Bert, C. W. and Malik, M. (1996b) 'Free vibration analysis of thin cylindrical shells by the differential quadrature method', *Journal of pressure vessel technology*, 118(1), pp. 1-12.
- Becque, J. (2010) 'Inelastic plate buckling', *Journal of Engineering Mechanics*, 136(9), pp. 1123-1130.
- Biezeno, C.B. and Hencky, H. (1928) 'On the general theory of elastic stability', *Proceeding Academy of Arts Sciences in Amsterdam*, 31, pp. 569-578.

Blachut, J., Galletly, G.D and James, S. (1996) 'On the plastic buckling paradox for cylindrical shells', *Proceedings of the Institution of Mechanical Engineers, Part C*, 210(5), pp. 477-488.

Blachut, J. and Galletly, G. D. (1993) 'Influence of local imperfections on the collapse strength of domed end closures', *Proceedings of the Institution of Mechanical Engineers, Part C Journal of Mechanical Engineering Science*, 207, pp. 197-207.

Boeing (2014). Non-Normal Landing Service Experience. Available at: http://www.boeing.com/commercial/aeromagazine/aero_14/nonnormal_landing.html (Accessed: 7 December 2015)

Boit, M. (1938) 'Theory of elastic with large displacements and rotations', *Proceeding of the fifth International Congress of Applied Mechanics*. pp. 117-122.

Brush, D. O. and Almroth, B. O. (1975) *Buckling of Bars, Plates and Shells*. New York: McGraw-Hill.

Bryan, G.H. (1890) 'On the stability of elastic systems', *Proceedings of the Cambridge Philosophical Society*, 4, pp. 199-286.

Budiansky, B. (1959) 'A reassessment of deformation theory of plasticity', *Journal of Applied Mechanics*, 26, pp. 259-264.

Bushnell, D. (1974) 'Bifurcation Buckling Of Shells of Revolution Including Large Deflections, Plasticity and Creep' *International Journal of Solids and Structures*, California, 10, pp. 1287-1305.

Bushnell, D. (1981) 'Computerized Buckling Analysis of Shells,' Air Force Wright Aeronautical Laboratories, Report No. AFWAL-TR-81-3049

Bushnell, D. (1982) 'Plastic Buckling', *In Pressure Vessels and Piping: Design Technology – 1982, A Decade of Progress*, edited by Zamrik, S. Y. and Dietrich, D. American Society of Mechanical Engineers, New York, pp. 47-117.

Bushnell, D. (1984) 'Computerized Analysis of Shells-Governing Equations', *Computers and Structures*, California, 18, pp. 471-536.

Bushnell, D. (1986) 'BOSOR5 – Program for Buckling of Complex, Branched Shells of Revolution Including Large Deflections, Plasticity and Creep', *In Structural Analysis Systems – 2*, edited by Niku-Lari, A. Pergamon, pp. 25-54.

Bushnell, D., and Bushnell, B. Shell Buckling (2005). Available at: <http://shellbuckling.com/shellBuckling.php> (Accessed: 24/08/2014)

Bushnell, D. (2015) Private communication.

Chakrabarty, J. (2010) *Applied Plasticity*, 2nd edition. Springer, New York, USA.

- Chilver, A.H. (1967) 'Coupled modes in elastic buckling', *Journal of the Mechanics and Physics of Solids*, 15, pp. 15-28.
- Civalek, Ö. (2004) 'Application of differential quadrature (DQ) and harmonic differential quadrature (HDQ) for buckling analysis of thin isotropic plates and elastic columns', *Engineering Structures*, 26(2), pp. 171-186.
- Civan, F. (1994) 'Rapid and accurate solution of reactor models by the quadrature method', *Computers and chemical engineering*, 18(10), pp.1005-1009.
- Civan, F. and Sliepcevich, C. M. (1983) 'Application of differential quadrature to transport processes', *Journal of Mathematical Analysis and Applications*, 93(1), pp. 206-221.
- Drucker, D. C. (1949) 'A discussion of theories of plasticity', *Journal of Aerospace Science*, 16, pp. 567.
- Duberg, L. E. and Wilder, T. W. (1952) 'Inelastic column behaviour', *National Advisory Committee for Aeronautics Report-1072*
- Durban, D. and Zuckerman, Z. (1999) 'Elastoplastic buckling of rectangular plates in biaxial compression/tension', *International Journal of Mechanical Sciences*, 15(7), pp. 751-765.
- Euler, L. (1757) 'Methodus inveniendi lineas curvas maximi minimive proprietate gaudentes (appendix, de curvis elasticis)', *Lausanne und Genf*, 1744.
- Falzon, B.G. and Hitchings, D. (2006) *An Introduction to Modelling Buckling and Collapse*. Glasgow, UK, NAFEMS Ltd
- Falzon B.G. and Aliabadi M. H. (2008) *Buckling and Postbuckling Structures: Experimental, Analytical and Numerical Studies*. Imperial College Press.
- Flügge, W. (1960) *Stresses in Shells*. Springer-Verlag, Berlin, Germany.
- Galletly G.D., Blachut, J., and Moreton, D.N. (1990) 'Internally pressurized machined domed ends - a comparison of the plastic buckling predictions of the deformation and flow theories', *Proceedings of the Institution of Mechanical Engineers, Part C*, 204(2), pp. 169-186.
- Giezen, J.J. (1988) 'Plastic buckling of cylinders under biaxial loading', (Ph.D. thesis), *California Institute of Technology, Pasadena, CA*, February.
- Giezen, J.J, Babcock, C. D. and Singer, J.(1991) 'Plastic buckling of cylindrical shells under biaxial loading', *Experimental Mechanics journal*, 31(4), pp. 337-343
- Guarracino, F. and Walker, A.C. (2008) 'Some comments on the numerical analysis of plates and thin-walled structures', *Thin-Walled Structures*, 46, pp. 975-980.

- Hencky, H.Z. (1924) 'Theorie Plastischer Deformationen und der hierdurch im Material hervorgerufenen Nachspannungen', *Zeitschrift für Angewandte Mathematik und Mechanik (Journal of Applied Mathematics and Mechanics)*, 4, pp. 323-334.
- Hilberink, A., Gresnigt, A.M. and Sluys, L.J. 'Liner wrinkling of lined pipe under compression. A numerical and experimental investigation' *In: Proceedings of the ASME 29th International Conference on Ocean, Offshore and Arctic Engineering OMAE 2012* Shanghai, China, June 6-11, 2010.
- Hill, R. (1950) *The mathematical theory of plasticity*. Oxford university press Inc., New York.
- Hill, R. (1956) 'On the problem of uniqueness in the theory of a rigid-plastic solid—1', *Journal of the Mechanics and Physics of Solids*, 4(4), pp. 247-255.
- Hill, R. (1958) 'A general theory of uniqueness and stability in elastic-plastic solids', *Journal of the Mechanics and Physics of Solids*, 6(3), pp. 236-249.
- Hutchinson, J.W. and Koiter, W.T. (1970) 'Postbuckling Theory', *Applied Mechanics Reviews*, 23, pp. 1353-1366.
- Hutchinson, J.W. (1972) 'On the postbuckling behavior of imperfection-sensitive structures in the plastic range', *Journal of Applied Mechanics – Transactions of ASME*, 39, pp. 155–162.
- Hutchinson, J. W. (1974) 'Plastic Buckling', *Advances in Applied Mechanics*, 14(67).
- Hutchinson, J., Budiansky, B. (1976) 'Analytical and numerical study of the effects of initial imperfections on the inelastic buckling of a cruciform column', *In: Budiansky, B. (Ed.), Proceedings of IUTAM Symposium on Buckling of Structures*. Springer, pp. 98-105.
- Jahed H, Lambert S.B. and Dubey R.N. (1998) 'Total deformation theory for non-proportional loading', *International Journal of Pressure Vessels Piping*, 75(8), pp. 633–42.
- Jang, S. K., Bert, C. W. and Striz, A. G. (1989) 'Application of differential quadrature to static analysis of structural components', *International Journal for Numerical Methods in Engineering*, 28(3), pp. 561-577.
- Jones, R. M. (2006) *Buckling of bars, plates, and shells*. Bull Ridge Corporation.
- Jones, R. M. (2009) *Deformation theory of plasticity*. Bull Ridge Corporation.
- Kadkhodayan, M. and Maarefdoust, M. (2014) 'Elastic/plastic buckling of isotropic thin plates subjected to uniform and linearly varying in-plane loading using incremental and deformation theories', *Aerospace Science and Technology*, 32(1), pp. 66-83.

Karman, T. V. and Tsien, H. S., (1939) 'The buckling of spherical shells by external pressure', *Journal of the Aeronautical Sciences*, 7(2), pp. 43-50.

Kashani, M., and Young, R. (2005) 'Installation load consideration in ultra-deepwater pipeline sizing', *Journal of Transportation Engineering*, 131(8), pp. 632-639.

Kyriakides, S. and Corona, E. (2007). *Mechanics of offshore pipelines: volume 1 buckling and collapse*. Elsevier, UK.

Koiter, W. T., (1945) 'On stability of elastic equilibrium', (Ph.D. thesis), *Technical Sciences at the Technische Hooge School*.

Kurtaran, H. (2015) 'Geometrically nonlinear transient analysis of moderately thick laminated composite shallow shells with generalized differential quadrature method', *Composite Structures*, 125, pp. 605-614.

Lay, M.G. (1965) 'Flange local buckling in wide-flange shapes', *Journal of the Structural Division*, 91(6), pp. 95-116.

Lee, L. (1962) 'Inelastic buckling of initially imperfect cylindrical shells subjected to axial compression', *Journal of Aerospace Science*, 29, pp. 87-95.

Maarefdoust, M. and Kadkhodayan, M. (2014a) 'Elastic/plastic buckling analysis of skew thin plates based on incremental and deformation theories of plasticity using generalized differential quadrature method', *International Journal of Engineering-Transactions B: Applications*, 27(8), pp. 1277-1286.

Maarefdoust, M., and Kadkhodayan, M. (2014b) 'Elastoplastic buckling analysis of rectangular thick plates by incremental and deformation theories of plasticity', *Proceedings of the Institution of Mechanical Engineers, Part G: Journal of Aerospace Engineering*, 0954410014550047.

Malik, M. and Bert, C. W. (1994) 'Differential quadrature solutions for steady-state incompressible and compressible lubrication problems', *Journal of Tribology*, 116(2), pp. 296-302.

Maltby, T. C. and Calladine, C. R. (1995). 'An investigation into upheaval buckling of buried pipelines—I. Experimental apparatus and some observations', *International Journal of Mechanical Sciences*, 37(9), pp. 943-963.

Mao, R. and Lu, G. (1999) 'Plastic buckling of circular cylindrical shells under combined in-plane loads', *International Journal of Solids and Structures*, 38(5), pp. 741-757.

Mao, R. and Lu, G. (2001) 'A study of the plastic buckling of axially compressed cylindrical shells with a thick-shell theory', *International Journal of Mechanical Sciences*, 43(10), pp. 2319-2330.

Mao, R. and Lu, G. (2002) 'A study of elastic-plastic buckling of cylindrical shells under torsion', *Thin-Walled Structures*, 40(12), pp. 1051-1071.

Marcal, P.V., King, I.P., (1967) 'Elastic-plastic analysis of two-dimensional stress systems by the finite element method', *International Journal of Mechanical Science*, 9(3), pp. 143–145.

McMeeking, R.M. and Rice, J.R. (1975) 'Finite-element formulations for problems of large elastic-plastic deformation', *International Journal of Solid and Structures* 11(5), pp. 601–616.

Mendelson, A. (1968) *Plasticity: Theory and Application*. Macmillan Company, New York, USA.

Mirfakhraei, P. and Redekop, D. (1998) 'Buckling of circular cylindrical shells by the differential quadrature method', *International Journal of Pressure Vessels and Piping*, 75(4), pp. 347-353.

Moradi, S. and Taheri, F. (1999) 'Delamination buckling analysis of general laminated composite beams by differential quadrature method', *Composites Part B: Engineering*, 30(5), pp. 503-511.

Nassar, M., Matbul, M. S. and Ragb, O. (2013) 'Vibration analysis of structural elements using differential quadrature method', *Journal of advanced research*, 4(1), pp. 93-102.

NASA (2013). NASA Engineers Crush Giant Fuel Tank to Improve Rocket Designs. Available at: <http://www.nasa.gov/exploration/systems/sls/shell-buckling-test.html> (Accessed: 7 December 2015)

Onat, E. T. and Drucker, D. C. (1953) 'Inelastic instability and incremental theories of plasticity', *Journal of the Aeronautical Sciences*, 20(3), pp. 181-186.

Ore, E. and Durban, D. (1989) 'Elastoplastic buckling of annular plates in pure shear', *Journal of applied mechanics*, 56(3), pp. 644-651.

Ore, E. and Durban, D. (1992) 'Elastoplastic buckling of axially compressed circular cylindrical shells', *International Journal of Mechanical Sciences*, 34(9), pp. 727-742.

Osakada, K. (2010) 'History of plasticity and metal forming analysis', *Journal of Materials Processing Technology*, 210(11), pp. 1436-1454.

Peek, R. (2000) 'An incrementally continuous deformation theory of plasticity with unloading', *International Journal of Solids and Structures*, 37(36), pp. 5009–32.

Rees, D. (2006) *Basic engineering plasticity: an introduction with engineering and manufacturing applications*. Butterworth-heinemann, Oxford, UK.

Riks, E. (1979) 'An incremental approach to the solution of snapping and buckling problems', *International Journal of Solids and Structures*, 15(7), pp. 529-551.

Sewell, M. J. (1963) 'A general theory of elastic and inelastic plate failure', *International Journal of the Mechanics and Physics of Solids*, 11, pp. 377-393.

Sewell, M. J. (1973) 'A yield-surface corner lowers the buckling stress of an elastic-plastic plate under compression', *Journal of the Mechanics and Physics of Solids*, 21, pp. 19-45.

Shanley, F. R. (1947) 'Inelastic column theory', *Journal of the Aeronautical Science*, 14, pp. 261-267.

Shu, C. and Richards, B. E. (1992) 'Application of generalized differential quadrature to solve two-dimensional incompressible Navier-Stokes equations', *International Journal for Numerical Methods in Fluids*, 15(7), pp. 791-798.

Simo J.C. and Hughes T.J.R. (1998) *Computational Inelasticity*. Springer.

Simulia (2011). *ABAQUS Theory Manual*. Version 6.11-1. Dassault Systems.

Southwell, R.V. (1913) 'On the general theory of elastic stability', *Philosophical Transactions of the Royal Society of London. Series A*, 213, pp. 187-244.

Supple, W.J. (1968) 'On the change in buckle pattern in elastic structures', *International Journal of Mechanical Sciences*, 10, pp. 737-745.

Teng, J. G. (1996) 'Buckling of thin shells: recent advances and trends', *Applied Mechanics Reviews*, 49(4), pp. 263-274.

Teng, J. G. and Rotter, J. M. (1989) 'Non-symmetric bifurcation of geometrically nonlinear elastic-plastic axisymmetric shells under combined loads including torsion', *Computers and structures*, 32(2), pp. 453-475.

Teng J.G. and Rotter J.M. (2004). *Buckling of thin metal shells*. Spon press, London.

Timoshenko, S.P. (1953) *History of Strength of Materials*. Dover Publication, New York.

Timoshenko, S.P. and Gere, J.M. (1961) *Theory of elastic stability*. 2nd edition, McGraw-Hill, London.

Timoshenko, S.P. (1983) *History of strength of material*. Courier Dover Publications, Toronto.

Trefftz, E. (1933) 'Zur theorie der stabilität des elastischen gleichgewichts', *ZAMM-Journal of Applied Mathematics and Mechanics*, 13(2), pp. 160-165.

Tuğcu, P. (1991a) 'Plate buckling in the plastic range', *International Journal of Mechanical Sciences*, 33(1), pp. 1-11.

Tuğcu, P. (1991b) 'On plastic buckling predictions', *International Journal of Mechanical Sciences*, 33(7), pp. 529-539.

- Tuğcu, P. (1998) 'Effect of axial loading on plastic buckling of long strips under pure shear', *Computers and Structures*, 66(2), pp. 155-161.
- Von Karman, Th. and Tsien (1939) 'The buckling of spherical shells by external pressure', *Journal Of Aerosol Science.*, 7, pp. 43-50.
- Von Karman, Th., 1925 'Beitrag zur Theorie des Walzvorges', *Zeitschrift für Angewandte Mathematik und Mechanik (Journal of Applied Mathematics and Mechanics)* 5, pp. 139–141.
- Wang, K. M. (1982) 'Solving the model of isothermal reactors with axial mixing by the differential quadrature method', *International Journal for Numerical Methods in Engineering*, 18(1), pp. 111-118.
- Wang, X. and Gu, H. (1997) 'Static analysis of frame structures by the differential quadrature element method', *International Journal for Numerical Methods in Engineering*, 40(4), pp. 759-772.
- Wang, X. and Huang, J. (2009) 'Elastoplastic buckling analyses of rectangular plates under biaxial loadings by the differential quadrature method', *Thin-Walled Structures*, 47(1), pp. 14-20.
- Wang, X., Liu, F., Wang, X. and Gan, L. (2005) 'New approaches in application of differential quadrature method to fourth-order differential equations', *Communications in Numerical Methods in Engineering*, 21(2), pp. 61-71.
- Wang, C.M., Xiang, Y. and Chakrabarty, J. (2001) 'Elastic/plastic buckling of thick plates', *International Journal of Solids and Structures*, 38(48), pp. 8617-8640.
- Yamada, Y., Yoshimura, N., Sakurai, T. (1968) 'Plastic stress–strain matrix and its application for the solution of elastic-plastic problems by finite element method', *International Journal of Mechanical Science*. 10(5), pp. 343–354.
- Yoo, C. H., and Lee, S. (2011). *Stability of structures: principles and applications*. Elsevier.
- Yun, H. and Kyriakides, S. (1990) 'On the beam and shell modes of buckling of buried pipelines', *Soil Dynamics and Earthquake Engineering*, 9(4), pp. 179-193.
- Zhang, W. and Wang, X. (2011) 'Elastoplastic buckling analysis of thick rectangular plates by using the differential quadrature method', *Computers and Mathematics with Applications*, 61(1), pp. 44-61.
- Zhang, Y., Huang, H. and Han, Q. (2015) 'Buckling of elastoplastic functionally graded cylindrical shells under combined compression and pressure', *Composites Part B: Engineering*, 69, pp. 120-126.
- Zienkiewicz, O. C. and Taylor, R. L. (2005) *The finite element method for solid and structural mechanics*. Butterworth-heinemann, Oxford, UK.

Appendix

A1. Equations used for the flow theory of plasticity employed in ABAQUS

The J_2 flow theory of plasticity theory (Simo and Hughes, 1998; Simulia, 2011), available in ABAQUS and used in the numerical simulations, is based on the additive decomposition of the spatial rate of the deformation tensor $\dot{\epsilon}$ into its elastic and plastic parts $\dot{\epsilon}_e$ and $\dot{\epsilon}_p$, respectively,

$$\dot{\epsilon} = \dot{\epsilon}_e + \dot{\epsilon}_p \quad \text{A.5}$$

The rate of the Cauchy stress tensor $\dot{\sigma}$ is obtained from the elastic part of the strain tensor through the isotropic linear elastic relation

$$\dot{\sigma} = 2G\dot{\epsilon}_e + \mu \text{tr } \dot{\epsilon}_e \mathbf{I} \quad \text{A.6}$$

where G and μ are Lamé's elastic constants and \mathbf{I} is the rank-2 identity tensor.

The von Mises yield function f is

$$f(\sigma, \epsilon_p^{eq}) = \|\text{dev } \sigma\| - \sqrt{\frac{2}{3}} \bar{\sigma}(\epsilon_p^{eq}) \quad \text{A.7}$$

where $\bar{\sigma}$ represents the uniaxial yield strength which, in order to model nonlinear isotropic hardening, is assumed to be an increasing function of the equivalent plastic strain ϵ_p^{eq} , defined at time t as follows

$$\epsilon_p^{eq}(t) = \int_{-\infty}^t \|\dot{\epsilon}_p(\tau)\| d\tau \quad \text{A.8}$$

The evolution of the plastic strain is given by the associated flow rule:

$$\dot{\epsilon}_p = \dot{\lambda} \left(\frac{\partial f}{\partial s} \right)_{s=\text{dev } \sigma} \quad \text{A.9}$$

where $\dot{\lambda}$ is a plastic multiplier which must satisfy the complementarity conditions:

$$\dot{\lambda} \geq 0 \quad f(\sigma, \epsilon_p^{eq}) \leq 0 \quad \dot{\lambda} f(\sigma, \epsilon_p^{eq}) = 0 \quad \text{A.10}$$

A2. Analytically derived buckling formulas derived by Batterman

The buckling stresses were analytically derived by Batterman (1965) in the following manner. In the case of the flow theory of plasticity the buckling stress is denoted by σ_f and the following expression was obtained:

$$\sigma_f = \frac{k (A + B - C)}{D} \quad \text{A.1}$$

with

$$\begin{aligned} k &= L^4(\lambda(5 - 4\nu) - (1 - 2\nu)^2) & A &= \frac{4E^2 t^2 m^2 \pi^2 \lambda(3 + \lambda)}{L^2 R^2 (\lambda(5 - 4\nu) - (1 - 2\nu)^2)^2} \\ B &= \frac{E^2 t^4 m^6 \pi^6 (3 + \lambda)^2}{12 L^6 (\lambda(5 - 4\nu) - (1 - 2\nu)^2)^2} & C &= \frac{4E^2 t^2 m^2 \pi^2 (-1 + \lambda + 2\nu)^2}{L^2 R^2 (\lambda(5 - 4\nu) - (1 - 2\nu)^2)^2} \\ D &= E t^2 m^4 \pi^4 (3 + \lambda) \end{aligned} \quad \text{A.2}$$

where t, R, L, m are the thickness, radius, length of the cylinder and number of half waves, respectively, $\lambda = E/E_t$, E_t being tangent modulus of the material evaluated at stress level σ on a uniaxial stress-strain test curve and E being the elastic Young's modulus.

In the case of the deformation theory of plasticity the buckling stress is denoted by σ_d and the following expression was obtained:

$$\sigma_d = \frac{\bar{k} (\bar{A} + \bar{B} - \bar{C})}{\bar{D}} \quad \text{A.3}$$

with

$$\begin{aligned} \bar{k} &= L^4(-(1 - 2\nu)^2 + \lambda(2 - 4\nu + 3\psi)) \\ \bar{A} &= \frac{E^2 t^4 m^6 \pi^6 (\lambda + 3\psi)^2}{12 L^6 (-(1 - 2\nu)^2 + \lambda(2 - 4\nu + 3\psi))^2} \\ \bar{B} &= \frac{4E^2 t^2 m^2 \pi^2 \lambda(\lambda + 3\psi)}{L^2 R^2 (-(1 - 2\nu)^2 + \lambda(2 - 4\nu + 3\psi))^2} & \bar{C} &= \frac{4E^2 t^2 m^2 \pi^2 (-1 + \lambda + 2\nu)^2}{L^2 R^2 (-(1 - 2\nu)^2 + \lambda(2 - 4\nu + 3\psi))^2} \\ \bar{D} &= E t^2 m^4 \pi^4 (\lambda + 3\psi) \end{aligned} \quad \text{A.4}$$

where $\Psi = E/E_s$, E_s being the secant modulus of the material evaluated at stress level σ on a uniaxial stress-strain test curve.

A3. FORTRAN code for the semi-analytical model in Chapter 3

```

program BLASTICBUCKLING
  implicit none
  integer n,mode,itheory,nmax,nout,idummy
  real*8 a1,a2,b1,b2,vmax,theta
  real*8 EE,sigy,tau,Et,hh,dd,aa,ecc,beta
  real*8 vv,dv,sig,sig1,sig2,sig1tr,sig2tr,
        eps1,eps2,eps1new,eps2new,xx,uu  !(vv=Delta,Deflection)
c-----
c  Assign input parameters
  EE=70000d0
  sigy=100d0
  tau=0.5d0
  hh=5d0
  dd=15d0
  aa=250d0
  ecc=0.5d0
  beta=10d0
  itheory=1  !itheory=1 -> flow theory / itheory=2 -> def theory
c  Assign algorithm parameters
  nmax=10000
  vmax=10d0
  dv=vmax/nmax
  nout=10
c  Initialise
  Et=tau*EE
  vv=0d0
  a1=0d0
  a2=0d0
  b1=EE
  b2=EE
  sig1=0d0
  sig2=0d0
  eps1new=0d0
  eps2new=0d0
  mode=1  !Both bars elastic
c
c  For flow theory
c  mode=2 -> bar1 elastic loading / bar 2 plastic loading
c  mode=3 -> bar1 plastic loading / bar 2 plastic loading
c  mode=4 -> bar1 elastic unloading / bar 2 plastic loading
c  mode=5 -> bar1 plastic re-loading (tension) / bar 2 plastic loading
c-----
c  Create the output file (overwrite it if already existing)
  OPEN(UNIT=1,FILE="load-disp.txt",STATUS='UNKNOWN')
  OPEN(UNIT=2,FILE="switches.txt",STATUS='UNKNOWN')
  WRITE(1,*) ' Deflection      Load'
  WRITE(1,1)0d0,0d0,0d0,0d0
c-----
do n=1,nmax
  xx=vv*dd/((aa-hh)*hh)
  sig=((a2*b1-a1*b2+b1*b2*xx)*dd*dd-
        (aa-hh)*(b1+b2)*(2d0*beta*vv*vv))
        /(dd*(b2*(-dd+2d0*(ecc+vv))+b1*(dd+2d0*(ecc+vv))))
  eps1new=(-b2*xx-a1-a2+2d0*sig)/(b1+b2)

```

```

eps2new=( b1*xx-a1-a2+2d0*sig)/(b1+b2)
sig1tr=a1+b1*eps1new
sig2tr=a2+b2*eps2new
c  decide if mode to be increased
  if(itheory.eq.1)then
c    flow theory
    if(mode.eq.1)then
      if(sig2tr.gt.sigy)then
        mode=2
        a2=(1d0-tau)*sigy
        b2=Et
        sig1=sig1tr
        sig2=a2+b2*eps2new
c    Mark swithing point in the output,mode 1 to mode 2
        WRITE(2,1)'1->2 ',vv,sig,uu,sig
        WRITE(2,*)' '
      else
        sig1=sig1tr
        sig2=sig2tr
      endif
    elseif(mode.eq.2)then
      if(sig1tr.gt.sigy)then
        mode=3
        a1=(1d0-tau)*sigy
        b1=Et
        sig1=a1+b1*eps1new
        sig2=sig2tr
c    Mark swithing point in the output,mode 2 to mode 3
        WRITE(2,1)'2->3 ',vv,sig,uu,sig
        WRITE(2,*)' '
      else
        sig1=sig1tr
        sig2=sig2tr
      endif
    elseif(mode.eq.3)then
      if(sig1tr.lt.sig1)then
        mode=4
        sigy=sig1tr
        b1=Et
        a1=sig1-Et*eps1new
        sig1=a1+b1*eps1new
        sig2=sig2tr
c    Mark swithing point in the output,mode 3 to mode 4
        WRITE(2,1)'3->4 ',vv,sig,uu,sig
        WRITE(2,*)' '
      else
        sig1=sig1tr
        sig2=sig2tr
      endif

    endif
  else
c -----
c    deformation theory
    if(mode.eq.1)then
      if(sig2tr.gt.sigy)then
        mode=2
        a2=(1d0-tau)*sigy
        b2=Et

```

```

sig1=sig1tr
sig2=a2+b2*eps2new
c Mark swithing point in the output,mode 1 to mode 2
WRITE(2,1)'1->2 ',vv,sig,uu,sig
else
sig1=sig1tr
sig2=sig2tr
endif
elseif(mode.eq.2)then
if(sig1tr.gt.sigy)then
mode=3
a1=(1d0-tau)*sigy
b1=Et
sig1=a1+b1*eps1new
sig2=sig2tr
c Mark swithing point in the output,mode 2 to mode 3
WRITE(2,1)'2->3 ',vv,sig,uu,sig
else
sig1=sig1tr
sig2=sig2tr
endif
elseif(mode.eq.3)then
if(sig1tr.lt.sig1)then
mode=4
b1=Et
a1=sig1-Et*eps1new
sig1=a1+b1*eps1new
sig2=sig2tr
c Mark swithing point in the output,mode 3 to mode 4
WRITE(2,1)'3->4 ',vv,sig,uu,sig
else
sig1=sig1tr
sig2=sig2tr
endif
elseif(mode.eq.4)then
if(sig1tr.lt.sigy)then
mode=5
b1=Ee
a1=0
sig1=a1+b1*eps1new
sig2=sig2tr
c Mark swithing point in the output,mode 4 to mode 5
WRITE(2,1)'4->5 ',vv,sig,uu,sig
else
sig1=sig1tr
sig2=sig2tr
endif
elseif(mode.eq.5)then
if(sig1tr.lt.-sigy) then
mode=6
b1=Et
a1=sig1-Et*eps1new
sig1=a1+b1*eps1new
sig2=sig2tr
c Mark swithing point in the output,mode 5 to mode 6
WRITE(2,1)'5->6 ',vv,sig,uu,sig
else
sig1=sig1tr
sig2=sig2tr

```

```

        endif
        elseif(mode.eq.6)then
            sig1=sig1tr
            sig2=sig2tr
        endif
    endif

C-----
C    Update strains
    eps1=eps1new
    eps2=eps2new
C    Get horizontal displacement
    theta=atan((eps2-eps1)*hh/dd)
    uu=(eps1+eps2)/2d0*hh+theta*ecc+aa*(1d0-cos(theta))
C-----
C    Write output
    if(vv.gt.4.359d0)then
        idummy=0
    endif
    if(mod(n,nout).eq.0)then
        WRITE(1,1)vv,sig,uu,sig
    endif
C-----
C    Increase applied deflection
    vv=vv+dv
end do
close(1)
close(2)
C-----Format statements
1  FORMAT(6(2X,G13.5))
end

```

A4. Matlab code for determining the plastic buckling pressure and buckling mode using the DQ method based on both the flow and deformation theories of plasticity

For the case of the flow theory

```

clc
clear
disp('Wait Please')
nmax=4;
eta=0.1;
%data input
Di=37.388; %diameter
h=0.762; %Thickness
L=38.1; %Length
a=Di/2; %Radius
%----material -----
EE=65129.73;
nue=0.3;
np=16;
alphap=0.733;
sigmay=177.75;
%-----
Axial_tensile_stress=165.5;
Ft= Axial_tensile_stress*(Di*h*pi);
Pa=Ft/(3.14*Di);
%-----number of points-----
N=15;
%-----
for n=2:nmax
Po=0.01;
for ii=1:200
Pa=Ft/(3.14*Di);
%Flow theory equations
P=Po;
sigmat=Ft/(Di*pi*h);
sigma1=sigmat;
sigma2=-a*P/h;
sigmaeff=(sigma1^2+sigma2^2-sigma1*sigma2)^0.5;
lambda=1/(1+alphap*np*sigmaeff^(np-1)*sigmay^(1-np));
roh=5-((3*(1-lambda)*sigma1*sigma2*(1-2*nue))/sigmaeff^2)-lambda*(1-2*nue)^2-4*nue;
alpha=((1+nue)/roh)*(4-(3-3*lambda)*sigma1^2/sigmaeff^2);
beta=((1+nue)/roh)*(2-((3-3*lambda)*sigma1*sigma2/sigmaeff^2)-2*lambda*(1-2*nue));
gama=((1+nue)/roh)*(4-(3-3*lambda)*sigma2^2/sigmaeff^2);
G=EE/(2+2*nue);
%-----A1,A2...A6,C1,C2...C7,D1,D2,...D8,B1,B2,B3-----
A1=a^2*Pa+a*a*EE*h*alpha/(1+nue);
A2=-G*h*n^2;
A3=(-a*G*h*n)-(a*EE*h*n*beta/(1+nue));
A4=a*EE*h*beta/(1+nue);
A5=-a*n;
A6=-a*a;

```

```

C1=(a*EE*h*n*beta/(1+nue))+a*G*h*n;
C2=a^2*Pa+a*a*G*h;
C3=-EE*h*n*n*gama/(1+nue);
C4=(-G*h^3*n/6)-(EE*h^3*n*beta/(12+12*nue));
C5=(EE*h*n*gama/(nue+1))+(EE*h^3*n^3*gama/(12*a^2*(nue+1)));
C6=a*n;
C7=-a*n^2;
D1=(a*EE*h*beta/(nue+1));
D2=-EE*h*n*gama/(nue+1);
D3=a^2*EE*h^3*alpha/(12*(1+nue));
D4=(-G*h^3*n^2/3)-(EE*h^3*n^2*beta/(6*(1+nue)))-a^2*Pa;
D5=(EE*h*gama/(nue+1))+(EE*h^3*n^4*gama/(12*a^2*(nue+1)));
D6=a*n^2;
D7=-a*n;
D8=-a^2;
B1=-n^2*beta/(a^2*alpha);
B2=-n*beta/(a*alpha);
B3=beta/(a*alpha);

```

```

% claculate Xi

```

```

X(1)=0;
X(2)=0.00001*L;
X(N-1)=(1-0.00001)*L;
X(N)=L;
for i=3:N-2
    X(i)=L*(1-cos(pi*(i-2)/(N-3)))/2;
end

```

```

% Calculate omegai

```

```

for i=1:N
    for j=1:N
        if i~=j
            M(j)=X(i)-X(j);
        else
            M(j)=1;
        end
    end
    omega(i)= prod(M);
end

```

```

% Calculate A,B,C,D

```

```

for i=1:N
    for j=1:N
        if i~=j
            A(i,j)=omega(i)/((X(i)-X(j))*omega(j));
        else
            for v=1:N
                if v~=i
                    P(v)=1/(X(i)-X(v));
                else
                    P(v)=0;
                end
            end
            A(i,j)=sum(P);
        end
    end
end
for i=1:N
    for j=1:N

```

```

    for k=1:N
        BB(k)=A(i,k)*A(k,j);
    end
    B(i,j)=sum(BB);
end
end

```

```

for i=1:N
    for j=1:N
        for k=1:N
            CC(k)=A(i,k)*B(k,j);
        end
        C(i,j)=sum(CC);
    end
end

```

```

for i=1:N
    for j=1:N
        for k=1:N
            DD(k)=B(i,k)*B(k,j);
        end
        D(i,j)=sum(DD);
    end
end

```

%Caculate Astar (Boundary conditions is C1-C1)

%-----Abb-----

```

Abb(1,1)=0;
Abb(1,2)=0;
Abb(1,3)=0;
Abb(1,4)=0;
Abb(1,5)=1;
Abb(1,6)=0;
Abb(1,7)=0;
Abb(1,8)=0;

```

```

Abb(2,1)=0;
Abb(2,2)=0;
Abb(2,3)=0;
Abb(2,4)=0;
Abb(2,5)=0;
Abb(2,6)=1;
Abb(2,7)=0;
Abb(2,8)=0;

```

```

Abb(3,1)=0;
Abb(3,2)=0;
Abb(3,3)=1;
Abb(3,4)=0;
Abb(3,5)=0;
Abb(3,6)=0;
Abb(3,7)=0;
Abb(3,8)=0;

```

```

Abb(4,1)=0;
Abb(4,2)=0;
Abb(4,3)=0;
Abb(4,4)=1;

```

```

Abb(4,5)=0;
Abb(4,6)=0;
Abb(4,7)=0;
Abb(4,8)=0;

```

```

Abb(5,1)=A(1,1);
Abb(5,2)=A(1,N);
Abb(5,3)=B2;
Abb(5,4)=0;
Abb(5,5)=B3;
Abb(5,6)=0;
Abb(5,7)=0;
Abb(5,8)=0;

```

```

Abb(6,1)=A(N,1);
Abb(6,2)=A(N,N);
Abb(6,3)=0;
Abb(6,4)=B2;
Abb(6,5)=0;
Abb(6,6)=B3;
Abb(6,7)=0;
Abb(6,8)=0;

```

```

Abb(7,1)=0;
Abb(7,2)=0;
Abb(7,3)=0;
Abb(7,4)=0;
Abb(7,5)=A(1,1);
Abb(7,6)=A(1,N);
Abb(7,7)=A(1,2);
Abb(7,8)=A(1,N-1);

```

```

Abb(8,1)=0;
Abb(8,2)=0;
Abb(8,3)=0;
Abb(8,4)=0;
Abb(8,5)=A(N,1);
Abb(8,6)=A(N,N);
Abb(8,7)=A(N,2);
Abb(8,8)=A(N,N-1);

```

```

%-----Aib (1)-----
%-----u1 uN-----
for i=2:(N-1)
Aib(i-1,1)=A1*B(i,1);
end
for i=2:(N-1)
Aib(i-1,2)=A1*B(i,N);
end

```

```

%-----v1 vN-----
for i=2:(N-1)
Aib(i-1,3)=A3*A(i,1);
end
for i=2:(N-1)
Aib(i-1,4)=A3*A(i,N);
end

```



```

%-----w1 wN-----
for i=2:(N-1)
Aib(i-1,5)=A4*A(i,1);
end
for i=2:(N-1)
Aib(i-1,6)=A4*A(i,N);
end

%-----w2 wN-1-----
for i=2:(N-1)
Aib(i-1,7)=A4*A(i,2);
end
for i=2:(N-1)
Aib(i-1,8)=A4*A(i,N-1);
end

%-----Aib (2)-----
%-----u1 uN-----
for i=2:(N-1)
Aib(i-1+N-2,1)=C1*A(i,1);
end
for i=2:(N-1)
Aib(i-1+N-2,2)=C1*A(i,N);
end

%-----v1 vN-----
for i=2:(N-1)
Aib(i-1+N-2,3)=C2*B(i,1);
end
for i=2:(N-1)
Aib(i-1+N-2,4)=C2*B(i,N);
end

%-----w1 wN-----
for i=2:(N-1)
Aib(i-1+N-2,5)=C4*B(i,1);
end
for i=2:(N-1)
Aib(i-1+N-2,6)=C4*B(i,N);
end

%-----w2 wN-1-----
for i=2:(N-1)
Aib(i-1+N-2,7)=C4*B(i,2);
end
for i=2:(N-1)
Aib(i-1+N-2,8)=C4*B(i,N-1);
end

%-----Aib (3)-----
%-----u1 uN-----
for i=3:(N-2)
Aib(i-2+(N-2)+(N-2),1)=D1*A(i,1);
end
for i=3:(N-2)
Aib(i-2+(N-2)+(N-2),2)=D1*A(i,N);
end

```

```

%-----v1 vN-----
for i=3:(N-2)
Aib(i-2+(N-2)+(N-2),3)=0;
end
for i=3:(N-2)
Aib(i-2+(N-2)+(N-2),4)=0;
end

%-----w1 wN-----
for i=3:(N-2)
Aib(i-2+(N-2)+(N-2),5)=D3*D(i,1)+D4*B(i,1);
end
for i=3:(N-2)
Aib(i-2+(N-2)+(N-2),6)=D3*D(i,N)+D4*B(i,N);
end

%-----w2 wN-1-----
for i=3:(N-2)
Aib(i-2+(N-2)+(N-2),7)=D3*D(i,2)+D4*B(i,2);
end
for i=3:(N-2)
Aib(i-2+(N-2)+(N-2),8)=D3*D(i,N-1)+D4*B(i,N-1);
end

%-----Abi-----
for j=1:((N-2)+(N-2)+(N-4))
Abi(1,j)=0;
end

for j=1:((N-2)+(N-2)+(N-4))
Abi(2,j)=0;
end

for j=1:((N-2)+(N-2)+(N-4))
Abi(3,j)=0;
end

for j=1:((N-2)+(N-2)+(N-4))
Abi(4,j)=0;
end

for j=2:(N-1)
Abi(5,j-1)=A(1,j);
end
for j=1:((N-2)+(N-4))
Abi(5,j+(N-2))=0;
end

for j=2:(N-1)
Abi(6,j-1)=A(N,j);
end
for j=1:((N-2)+(N-4))
Abi(6,j+(N-2))=0;
end

for j=1:((N-2)+(N-2))
Abi(7,j)=0;
end

```

```

end
for j=3:(N-2)
Abi(7,j-2+(N-2)+(N-2))=A(1,j);
end

```

```

for j=1:((N-2)+(N-2))
Abi(8,j)=0;
end
for j=3:(N-2)
Abi(8,j-2+(N-2)+(N-2))=A(N,j);
end

```

```

%-----Aii (1)-----
for i=2:(N-1)
    for j=2:N-1
        if i==j
Aii(i-1,j-1)=A1*B(i,j)+A2;
        else
            Aii(i-1,j-1)=A1*B(i,j) ;
        end
    end
end
end

```

```

for i=2:(N-1)
    for j=2:(N-1)
Aii(i-1,j-1+N-2)=A3*A(i,j);
    end
end

```

```

for i=2:(N-1)
    for j=3:(N-2)
Aii(i-1,j-2+N-2+N-2)=A4*A(i,j);
    end
end

```

```

%_____Aii (2) _____

```

```

for i=2:(N-1)
    for j=2:N-1
Aii(i-1+N-2,j-1)=C1*A(i,j);
    end
end

```

```

for i=2:(N-1)
    for j=2:(N-1)
        if i==j
Aii(i-1+N-2,j-1+N-2)=C2*B(i,j)+C3;
        else
            Aii(i-1+N-2,j-1+N-2)=C2*B(i,j);
        end
    end
end
end

```

```

for i=2:(N-1)
    for j=3:(N-2)
        if i==j

```

```

Aii(i-1+N-2,j-2+N-2+N-2)=C4*B(i,j)+C5;
    else
        Aii(i-1+N-2,j-2+N-2+N-2)=C4*B(i,j);
    end
end
end
%-----Aii (3)-----
for i=3:(N-2)
    for j=2:N-1
        Aii(i-2+N-2+N-2,j-1)=D1*A(i,j);
    end
end

for i=3:(N-2)
    for j=2:(N-1)
        if i==j
            Aii(i-2+N-2+N-2,j-1+N-2)=D2;
        else
            Aii(i-2+N-2+N-2,j-1+N-2)=0;
        end
    end
end

for i=3:(N-2)
    for j=3:(N-2)
        if i==j
            Aii(i-2+N-2+N-2,j-2+N-2+N-2)=D4*B(i,j)+D3*D(i,j)+D5;
        else
            Aii(i-2+N-2+N-2,j-2+N-2+N-2)=D4*B(i,j)+D3*D(i,j);
        end
    end
end

%-----Bib(1)-----
%-----u1 uN-----
for i=2:(N-1)
    Bib(i-1,1)=0;
end
for i=2:(N-1)
    Bib(i-1,2)=0;
end

%-----v1 vN-----
for i=2:(N-1)
    Bib(i-1,3)=0;
end
for i=2:(N-1)
    Bib(i-1,4)=0;
end

%-----w1 wN-----
for i=2:(N-1)
    Bib(i-1,5)=A6*A(i,1);
end
for i=2:(N-1)
    Bib(i-1,6)=A6*A(i,N);
end

```

```

%-----w2 wN-1-----
for i=2:(N-1)
Bib(i-1,7)=A6*A(i,2);
end
for i=2:(N-1)
Bib(i-1,8)=A6*A(i,N-1);
end

%-----Bib (2)-----
%-----u1 uN-----
for i=2:(N-1)
Bib(i-1+N-2,1)=0;
end
for i=2:(N-1)
Bib(i-1+N-2,2)=0;
end

%-----v1 vN-----
for i=2:(N-1)
Bib(i-1+N-2,3)=0;
end
for i=2:(N-1)
Bib(i-1+N-2,4)=0;
end

%-----w1 wN-----
for i=2:(N-1)
Bib(i-1+N-2,5)=0;
end
for i=2:(N-1)
Bib(i-1+N-2,6)=0;
end

%-----w2 wN-1-----
for i=2:(N-1)
    if i==2
Bib(i-1+N-2,7)=C6;
    else
        Bib(i-1+N-2,7)=0;
    end
end
for i=2:(N-1)
    if i==N-1
Bib(i-1+N-2,8)=C6;
    else
        Bib(i-1+N-2,8)=0;
    end
end

%-----Bib (3)-----
%-----u1 uN-----
for i=3:(N-2)
Bib(i-2+(N-2)+(N-2),1)=D8*A(i,1);
end
for i=3:(N-2)
Bib(i-2+(N-2)+(N-2),2)=D8*A(i,N);
end

```

```

%-----v1 vN-----
for i=3:(N-2)
Bib(i-2+(N-2)+(N-2),3)=0;
end
for i=3:(N-2)
Bib(i-2+(N-2)+(N-2),4)=0;
end
%-----w1 wN-----
for i=3:(N-2)
Bib(i-2+(N-2)+(N-2),5)=0;
end
for i=3:(N-2)
Bib(i-2+(N-2)+(N-2),6)=0;
end

%-----w2 wN-1-----
for i=3:(N-2)
Bib(i-2+(N-2)+(N-2),7)=0;
end
for i=3:(N-2)
Bib(i-2+(N-2)+(N-2),8)=0;
end

%-----Bii (1)-----
for i=2:(N-1)
    for j=2:N-1
        if i==j
            Bii(i-1,j-1)=A5;
        else
            Bii(i-1,j-1)=0;
        end
    end
end

for i=2:(N-1)
    for j=2:(N-1)
        Bii(i-1,j-1+N-2)=0;
    end
end

for i=2:(N-1)
    for j=3:(N-2)
        Bii(i-1,j-2+N-2+N-2)=A6*A(i,j);
    end
end

%-----Bii (2)-----

for i=2:(N-1)
    for j=2:N-1

        Bii(i-1+N-2,j-1)=0;
    end
end

for i=2:(N-1)

```

```

for j=2:(N-1)
    if i==j
        Bii(i-1+N-2,j-1+N-2)=C7;
    else
        Bii(i-1+N-2,j-1+N-2)=0;
    end
end
end

for i=2:(N-1)
    for j=3:(N-2)
        if i==j
            Bii(i-1+N-2,j-2+N-2+N-2)=C6;
        else
            Bii(i-1+N-2,j-2+N-2+N-2)=0;
        end
    end
end
end
%-----Bii (3)-----
for i=3:(N-2)
    for j=2:N-1
        Bii(i-2+N-2+N-2,j-1)=D8*A(i,j);
    end
end

for i=3:(N-2)
    for j=2:(N-1)
        if i==j
            Bii(i-2+N-2+N-2,j-1+N-2)=D7;
        else
            Bii(i-2+N-2+N-2,j-1+N-2)=0;
        end
    end
end

for i=3:(N-2)
    for j=3:(N-2)
        if i==j
            Bii(i-2+N-2+N-2,j-2+N-2+N-2)=D6;
        else
            Bii(i-2+N-2+N-2,j-2+N-2+N-2)=0;
        end
    end
end
%-----

Astar=Aii-Aib*inv(Abb)*Abi;
Bstar=Bii-Bib*inv(Abb)*Abi;

% find the eigenvalue and vectors

Mat=inv(Bstar)*Astar;
[Eigen_vector,All_Eigen_value]=eig(Mat);

for i=1:3*N-8
    for j=1:3*N-8
        if All_Eigen_value(i,j)>0;

```

```

        Eigen_value2(i,j)=All_Eigen_value(i,j);
    else
    end
end
end
end

Eigen_value_positive=nonzeros(Eigen_value2);

min_Eigen_value=min(Eigen_value_positive);
if (abs(P-min_Eigen_value)/min_Eigen_value) <= 0.000001
    Pfinal_buckling_pressure(n-1)=min_Eigen_value;
    break
else
    clearvars -except ii P min_Eigen_value eta n nmax Pfinal_buckling_pressure Di h a EE
    nue np alphap sigmay Ft N L
    Po=(1-eta)*P+eta*min_Eigen_value;
    clearvars P min_Eigen_value
    end
end
end
buckling_pressure=min(Pfinal_buckling_pressure)
for i=2:nmax
    if Pfinal_buckling_pressure(i-1)==buckling_pressure
        number_of_wave_n=i
    else
    end
end
end

%-----
clearvars -except buckling_pressure number_of_wave_n Di h a EE nue np alphap sigmay Ft
N L
n=number_of_wave_n;

%FLOW THEORY EQUATIONS

P=buckling_pressure;
Pa=Ft/(3.14*Di);
sigmat=Ft/(Di*pi*h);
sigma1=sigmat;
sigma2=-a*P/h;
sigmaeff=(sigma1^2+sigma2^2-sigma1*sigma2)^0.5;
lambda=1/(1+alphap*np*sigmaeff^(np-1)*sigmay^(1-np));
roh=5-((3*(1-lambda)*sigma1*sigma2*(1-2*nue))/sigmaeff^2)-lambda*(1-2*nue)^2-4*nue;

alpha=((1+nue)/roh)*(4-(3-3*lambda)*sigma1^2/sigmaeff^2);
beta=((1+nue)/roh)*(2-((3-3*lambda)*sigma1*sigma2/sigmaeff^2)-2*lambda*(1-2*nue));
gama=((1+nue)/roh)*(4-(3-3*lambda)*sigma2^2/sigmaeff^2);
G=EE/(2+2*nue);

A1=a^2*Pa+a*a*EE*h*alpha/(1+nue);
A2=-G*h*n^2;
A3=(-a*G*h*n)-(a*EE*h*n*beta/(1+nue));
A4=a*EE*h*beta/(1+nue);
A5=-a*n*n;
A6=-a*a;

C1=(a*EE*h*n*beta/(1+nue))+(a*G*h*n);
C2=a^2*Pa+a*a*G*h;

```



```

C3=-EE*h*n*gama/(1+nue);
C4=(-G*h^3*n/6)-(EE*h^3*n*beta/(12+12*nue));
C5=(EE*h*n*gama/(nue+1))+(EE*h^3*n^3*gama/(12*a^2*(nue+1)));
C6=a*n;
C7=-a*n^2;

```

```

D1=(a*EE*h*beta/(nue+1));
D2=-EE*h*n*gama/(nue+1);
D3=a^2*EE*h^3*alpha/(12*(1+nue));
D4=(-G*h^3*n^2/3)-(EE*h^3*n^2*beta/(6*(1+nue)))-a^2*Pa;
D5=(EE*h*gama/(nue+1))+(EE*h^3*n^4*gama/(12*a^2*(nue+1)));
D6=a*n^2;
D7=-a*n;
D8=-a^2;

```

```

B1=-n^2*beta/(a^2*alpha);
B2=-n*beta/(a*alpha);
B3=beta/(a*alpha);

```

```
% claculate Xi
```

```

X(1)=0;
X(2)=0.00001;
X(N-1)=L-0.00001;
X(N)=L;
for i=3:N-2
    X(i)=L*(1-cos(pi*(i-2)/(N-3)))/2;
end

```

```
% Calculate omegai
```

```

for i=1:N
    for j=1:N
        if i~=j
            M(j)=X(i)-X(j);
        else
            M(j)=1;
        end
    end
    omega(i)= prod(M);
end

```

```
% Calculate A,B,C,D
```

```

for i=1:N
    for j=1:N
        if i~=j
            A(i,j)=omega(i)/((X(i)-X(j))*omega(j));
        else
            for v=1:N
                if v~=i
                    P(v)=1/(X(i)-X(v));
                else
                    P(v)=0;
                end
            end
            A(i,j)=sum(P);
        end
    end
end

```

```

for i=1:N
    for j=1:N
        for k=1:N
            BB(k)=A(i,k)*A(k,j);
        end
        B(i,j)=sum(BB);
    end
end

```

```

for i=1:N
    for j=1:N
        for k=1:N
            CC(k)=A(i,k)*B(k,j);
        end
        C(i,j)=sum(CC);
    end
end

```

```

for i=1:N
    for j=1:N
        for k=1:N
            DD(k)=B(i,k)*B(k,j);
        end
        D(i,j)=sum(DD);
    end
end

```

```

%Calculate Astar
%-----Abb-----
Abb(1,1)=0;
Abb(1,2)=0;
Abb(1,3)=0;
Abb(1,4)=0;
Abb(1,5)=1;
Abb(1,6)=0;
Abb(1,7)=0;
Abb(1,8)=0;

Abb(2,1)=0;
Abb(2,2)=0;
Abb(2,3)=0;
Abb(2,4)=0;
Abb(2,5)=0;
Abb(2,6)=1;
Abb(2,7)=0;
Abb(2,8)=0;

Abb(3,1)=0;
Abb(3,2)=0;
Abb(3,3)=1;
Abb(3,4)=0;
Abb(3,5)=0;
Abb(3,6)=0;
Abb(3,7)=0;
Abb(3,8)=0;

Abb(4,1)=0;

```

```

Abb(4,2)=0;
Abb(4,3)=0;
Abb(4,4)=1;
Abb(4,5)=0;
Abb(4,6)=0;
Abb(4,7)=0;
Abb(4,8)=0;

```

```

Abb(5,1)=A(1,1);
Abb(5,2)=A(1,N);
Abb(5,3)=B2;
Abb(5,4)=0;
Abb(5,5)=B3;
Abb(5,6)=0;
Abb(5,7)=0;
Abb(5,8)=0;

```

```

Abb(6,1)=A(N,1);
Abb(6,2)=A(N,N);
Abb(6,3)=0;
Abb(6,4)=B2;
Abb(6,5)=0;
Abb(6,6)=B3;
Abb(6,7)=0;
Abb(6,8)=0;

```

```

Abb(7,1)=0;
Abb(7,2)=0;
Abb(7,3)=0;
Abb(7,4)=0;
Abb(7,5)=A(1,1);
Abb(7,6)=A(1,N);
Abb(7,7)=A(1,2);
Abb(7,8)=A(1,N-1);

```

```

Abb(8,1)=0;
Abb(8,2)=0;
Abb(8,3)=0;
Abb(8,4)=0;
Abb(8,5)=A(N,1);
Abb(8,6)=A(N,N);
Abb(8,7)=A(N,2);
Abb(8,8)=A(N,N-1);

```

```

%-----
%-----Aib (1)-----
%-----u1 uN-----
for i=2:(N-1)
    Aib(i-1,1)=A1*B(i,1);
end
for i=2:(N-1)
    Aib(i-1,2)=A1*B(i,N);
end

%-----v1 vN-----
for i=2:(N-1)
    Aib(i-1,3)=A3*A(i,1);
end

```

```

for i=2:(N-1)
Aib(i-1,4)=A3*A(i,N);
end

%-----w1 wN-----
for i=2:(N-1)
Aib(i-1,5)=A4*A(i,1);
end
for i=2:(N-1)
Aib(i-1,6)=A4*A(i,N);
end

%-----w2 wN-1-----
for i=2:(N-1)
Aib(i-1,7)=A4*A(i,2);
end
for i=2:(N-1)
Aib(i-1,8)=A4*A(i,N-1);
end

%-----Aib (2)-----
%-----u1 uN-----
for i=2:(N-1)
Aib(i-1+N-2,1)=C1*A(i,1);
end
for i=2:(N-1)
Aib(i-1+N-2,2)=C1*A(i,N);
end

%-----v1 vN-----
for i=2:(N-1)
Aib(i-1+N-2,3)=C2*B(i,1);
end
for i=2:(N-1)
Aib(i-1+N-2,4)=C2*B(i,N);
end

%-----w1 wN-----
for i=2:(N-1)
Aib(i-1+N-2,5)=C4*B(i,1);
end
for i=2:(N-1)
Aib(i-1+N-2,6)=C4*B(i,N);
end

%-----w2 wN-1-----
for i=2:(N-1)
Aib(i-1+N-2,7)=C4*B(i,2);
end
for i=2:(N-1)
Aib(i-1+N-2,8)=C4*B(i,N-1);
end

%-----Aib (3)-----
%-----u1 uN-----
for i=3:(N-2)
Aib(i-2+(N-2)+(N-2),1)=D1*A(i,1);
end

```

```

for i=3:(N-2)
Aib(i-2+(N-2)+(N-2),2)=D1*A(i,N);
end

%-----v1 vN-----
for i=3:(N-2)
Aib(i-2+(N-2)+(N-2),3)=0;
end
for i=3:(N-2)
Aib(i-2+(N-2)+(N-2),4)=0;
end

%-----w1 wN-----
for i=3:(N-2)
Aib(i-2+(N-2)+(N-2),5)=D3*D(i,1)+D4*B(i,1);
end
for i=3:(N-2)
Aib(i-2+(N-2)+(N-2),6)=D3*D(i,N)+D4*B(i,N);
end

%-----w2 wN-1-----
for i=3:(N-2)
Aib(i-2+(N-2)+(N-2),7)=D3*D(i,2)+D4*B(i,2);
end
for i=3:(N-2)
Aib(i-2+(N-2)+(N-2),8)=D3*D(i,N-1)+D4*B(i,N-1);
end

%-----Abi-----
for j=1:((N-2)+(N-2)+(N-4))
Abi(1,j)=0;
end

for j=1:((N-2)+(N-2)+(N-4))
Abi(2,j)=0;
end

for j=1:((N-2)+(N-2)+(N-4))
Abi(3,j)=0;
end

for j=1:((N-2)+(N-2)+(N-4))
Abi(4,j)=0;
end

for j=2:(N-1)
Abi(5,j-1)=A(1,j);
end
for j=1:((N-2)+(N-4))
Abi(5,j+(N-2))=0;
end

for j=2:(N-1)
Abi(6,j-1)=A(N,j);
end
for j=1:((N-2)+(N-4))
Abi(6,j+(N-2))=0;
end

```

```

end

for j=1:((N-2)+(N-2))
    Abi(7,j)=0;
end
for j=3:(N-2)
    Abi(7,j-2+(N-2)+(N-2))=A(1,j);
end

for j=1:((N-2)+(N-2))
    Abi(8,j)=0;
end
for j=3:(N-2)
    Abi(8,j-2+(N-2)+(N-2))=A(N,j);
end

%-----Aii (1)-----
for i=2:(N-1)
    for j=2:N-1
        if i==j
            Aii(i-1,j-1)=A1*B(i,j)+A2;
        else
            Aii(i-1,j-1)=A1*B(i,j) ;
        end
    end
end

for i=2:(N-1)
    for j=2:(N-1)
        Aii(i-1,j-1+N-2)=A3*A(i,j);
    end
end

for i=2:(N-1)
    for j=3:(N-2)
        Aii(i-1,j-2+N-2+N-2)=A4*A(i,j);
    end
end

%_____Aii (2) _____

for i=2:(N-1)
    for j=2:N-1
        Aii(i-1+N-2,j-1)=C1*A(i,j);
    end
end

for i=2:(N-1)
    for j=2:(N-1)
        if i==j
            Aii(i-1+N-2,j-1+N-2)=C2*B(i,j)+C3;
        else
            Aii(i-1+N-2,j-1+N-2)=C2*B(i,j);
        end
    end
end

```

```

for i=2:(N-1)
    for j=3:(N-2)
        if i==j
            Aii(i-1+N-2,j-2+N-2+N-2)=C4*B(i,j)+C5;
        else
            Aii(i-1+N-2,j-2+N-2+N-2)=C4*B(i,j);
        end
    end
end
%-----Aii (3)-----
for i=3:(N-2)
    for j=2:N-1
        Aii(i-2+N-2+N-2,j-1)=D1*A(i,j);
    end
end

for i=3:(N-2)
    for j=2:(N-1)
        if i==j
            Aii(i-2+N-2+N-2,j-1+N-2)=D2;
        else
            Aii(i-2+N-2+N-2,j-1+N-2)=0;
        end
    end
end

for i=3:(N-2)
    for j=3:(N-2)
        if i==j
            Aii(i-2+N-2+N-2,j-2+N-2+N-2)=D4*B(i,j)+D3*D(i,j)+D5;
        else
            Aii(i-2+N-2+N-2,j-2+N-2+N-2)=D4*B(i,j)+D3*D(i,j);
        end
    end
end

%-----Bib-(1)-----
%-----u1 uN-----
for i=2:(N-1)
    Bib(i-1,1)=0;
end
for i=2:(N-1)
    Bib(i-1,2)=0;
end

%-----v1 vN-----
for i=2:(N-1)
    Bib(i-1,3)=0;
end
for i=2:(N-1)
    Bib(i-1,4)=0;
end

%-----w1 wN-----
for i=2:(N-1)
    Bib(i-1,5)=A6*A(i,1);
end

```

```

for i=2:(N-1)
Bib(i-1,6)=A6*A(i,N);
end

%-----w2 wN-1-----
for i=2:(N-1)
Bib(i-1,7)=A6*A(i,2);
end
for i=2:(N-1)
Bib(i-1,8)=A6*A(i,N-1);
end

%-----Bib (2)-----
%-----u1 uN-----
for i=2:(N-1)
Bib(i-1+N-2,1)=0;
end
for i=2:(N-1)
Bib(i-1+N-2,2)=0;
end

%-----v1 vN-----
for i=2:(N-1)
Bib(i-1+N-2,3)=0;
end
for i=2:(N-1)
Bib(i-1+N-2,4)=0;
end

%-----w1 wN-----
for i=2:(N-1)
Bib(i-1+N-2,5)=0;
end
for i=2:(N-1)
Bib(i-1+N-2,6)=0;
end

%-----w2 wN-1-----
for i=2:(N-1)
    if i==2
Bib(i-1+N-2,7)=C6;
    else
        Bib(i-1+N-2,7)=0;
    end
end
for i=2:(N-1)
    if i==N-1
Bib(i-1+N-2,8)=C6;
    else
        Bib(i-1+N-2,8)=0;
    end
end

%-----Bib (3)-----
%-----u1 uN-----
for i=3:(N-2)
Bib(i-2+(N-2)+(N-2),1)=D8*A(i,1);
end

```



```

for i=3:(N-2)
Bib(i-2+(N-2)+(N-2),2)=D8*A(i,N);
end

```

```

%-----v1 vN-----
for i=3:(N-2)
Bib(i-2+(N-2)+(N-2),3)=0;
end
for i=3:(N-2)
Bib(i-2+(N-2)+(N-2),4)=0;
end

```

```

%-----w1 wN-----
for i=3:(N-2)
Bib(i-2+(N-2)+(N-2),5)=0;
end
for i=3:(N-2)
Bib(i-2+(N-2)+(N-2),6)=0;
end

```

```

%-----w2 wN-1-----
for i=3:(N-2)
Bib(i-2+(N-2)+(N-2),7)=0;
end
for i=3:(N-2)
Bib(i-2+(N-2)+(N-2),8)=0;
end

```

```

%-----Bii (1)-----
for i=2:(N-1)
    for j=2:N-1
        if i==j
            Bii(i-1,j-1)=A5;
        else
            Bii(i-1,j-1)=0;
        end
    end
end

```

```

for i=2:(N-1)
    for j=2:(N-1)
        Bii(i-1,j-1+N-2)=0;
    end
end

```

```

for i=2:(N-1)
    for j=3:(N-2)
        Bii(i-1,j-2+N-2+N-2)=A6*A(i,j);
    end
end

```

```

%_____Bii (2)_____

```

```

for i=2:(N-1)
    for j=2:N-1

        Bii(i-1+N-2,j-1)=0;
    end
end

```

```

    end
end

for i=2:(N-1)
    for j=2:(N-1)
        if i==j
            Bii(i-1+N-2,j-1+N-2)=C7;
        else
            Bii(i-1+N-2,j-1+N-2)=0;
        end
    end
end

for i=2:(N-1)
    for j=3:(N-2)
        if i==j
            Bii(i-1+N-2,j-2+N-2+N-2)=C6;
        else
            Bii(i-1+N-2,j-2+N-2+N-2)=0;
        end
    end
end
%-----Bii (3)-----
for i=3:(N-2)
    for j=2:N-1
        Bii(i-2+N-2+N-2,j-1)=D8*A(i,j);
    end
end

for i=3:(N-2)
    for j=2:(N-1)
        if i==j
            Bii(i-2+N-2+N-2,j-1+N-2)=D7;
        else
            Bii(i-2+N-2+N-2,j-1+N-2)=0;
        end
    end
end

for i=3:(N-2)
    for j=3:(N-2)
        if i==j
            Bii(i-2+N-2+N-2,j-2+N-2+N-2)=D6;
        else
            Bii(i-2+N-2+N-2,j-2+N-2+N-2)=0;
        end
    end
end
%-----

Astar=Aii-Aib*inv(Abb)*Abi;
Bstar=Bii-Bib*inv(Abb)*Abi;

% find the eigenvalue and vectors

Mat=inv(Bstar)*Astar;
[Eigen_vector,All_Eigen_value]=eig(Mat);

```

```

for i=1:3*N-8
    for j=1:3*N-8
        if All_Eigen_value(i,j)>0;
            Eigen_value2(i,j)=All_Eigen_value(i,j);
        else
            end
        end
    end
end

Eigen_value_positive=nonzeros(Eigen_value2);
min_Eigen_value=min(Eigen_value_positive);

%-----
for i=1:3*N-8
    for j=1:3*N-8
        if All_Eigen_value(i,j)== min_Eigen_value
            kk=j;
            Vector=Eigen_vector(:,kk);
        else
            end
        end
    end
end
Fianl_Eigen_verctor=Vector;

for i=2:N-1
    u(i)=Fianl_Eigen_verctor(i-1);
end
for i=2:N-1
    v(i)=Fianl_Eigen_verctor(i-1+N-2);
end
for i=3:N-2
    w(i)=Fianl_Eigen_verctor(i-2+N-2+N-2);
end
u(1)=u(2);
u(N)=u(N-1);
v(1)=v(2);
v(N)=v(N-1);
w(1)=0;
w(2)=0;
w(N)=0;
w(N-1)=0;
Eigen_verctor_x_u_v_w=[transpose(X) transpose(u) transpose(v) transpose(w)];
plot(w,X,'-o')
plot(w,X)
ylabel('Axial coordinates')
legend('Buckling shape in axial direction')

for t=0:360
    theata(t+1)=t*pi/180;

    ww(t+1)=sin(n*theata(t+1))+Di/5;
end

polar(theata,ww)
ylabel('circumferential coordinates')
legend('Buckling shape in circumferential direction')

```

```
eps_eff=(sigmaeff+alphap*sigmaeff^(np-1)*sigmay^(1-np)*sigmaeff)/EE*100
sigma_eff=sigmaeff
```

For the case of the deformation theory

It is the same previous code. However, the deformation theory equations are:

```
% deformation theory equations
```

```
P=Po;
sigmat=Ft/(Di*3.14*h);
sigma1=sigmat;
sigma2=-a*P/h;
sigmaeff=(sigma1^2+sigma2^2-sigma1*sigma2)^0.5;

lambda=1/(1+alphap*np*sigmaeff^(np-1)*sigmay^(1-np));
psai=1/(1+alphap*sigmaeff^(np-1)*sigmay^(1-np));
roh=(3/psai)+(1-2*nue)*(2-lambda*(1-2*nue)-(3*sigma1*sigma2*(1-
lambda/psai)/sigmaeff^2));
alpha=((1+nue)/roh)*(4-(3-3*lambda/psai)*sigma1^2/sigmaeff^2);
beta=((1+nue)/roh)*(2-((3-3*lambda/psai)*sigma1*sigma2/sigmaeff^2)-2*lambda*(1-2*nue));
gama=((1+nue)/roh)*(4-(3-3*lambda/psai)*sigma2^2/sigmaeff^2);
G=EE/(-1+2*nue+3/psai);
```

